BIOCHEMICAL AND PHARMACOLOGICAL CHARACTERIZATION OF THE ATG8 CONJUGATION SYSTEM IN *TOXOPLASMA GONDII*

Joseph M. Varberg

Submitted to the faculty of the University Graduate School
in partial fulfillment of the requirements
for the degree
Doctor of Philosophy
in the Department of Pharmacology & Toxicology
Indiana University

October 2017

Accepted by the Graduate Faculty of Indiana University, in partial fulfillment of the requirements for the degree of Doctor of Philosophy.

Doctoral Committee

Gustavo Arrizabalaga, PhD, Co-Chair

William J. Sullivan, Jr., PhD, Co-Chair

Amber Mosley, PhD

June 28, 2017

Ahmad Safa, PhD

Michael R. Vasko, PhD

Dedication

In loving memory of Linda Varberg

"Awakening"

It's not that I consider myself
invincible
or that I don't know what it is
to wander, lost and alone,
for decades at a time.

It's simply that one morning
I heard the aching
blessing-call of geese,
headed due north
and more than once now
I have been
baptized
by a gentle summer rain.

So can you blame me when I tell you
how I long to taste
my own sweet desire,
swallow it whole,
and follow it home?

-lrv
July 19, 2008

Acknowledgements

I am very grateful for the many teachers and mentors I have had during my education for their investment in my development as a student and scientist. I am especially thankful for the mentorship and training of Dr. Petia Bobadova-Parvanova, who gave me my first opportunity to engage in scientific research and encouraged me to pursue graduate education in the sciences. I am also extremely thankful for the early guidance and mentorship of Dr. Chris Elles, and Dr. Ali Shilatifard, as my time in their laboratories provided me with skills and experiences that were critical to my success in graduate training. In particular, Dr. Edwin Smith provided fundamental training in molecular biology techniques and laboratory skills for which I am incredibly grateful.

I would also like to thank my two graduate mentors, Dr. Gustavo Arrizabalaga and Dr. Bill Sullivan, for providing me the opportunity to develop my own project and giving me all of the tools and resources needed to succeed in my graduate training. I appreciate your commitment to the development of students and trainees in your labs, and am grateful to have had opportunities to attend various conferences and workshops during my training to engage with the international research community. I am also thankful for the opportunities you have provided to develop my scientific writing and communication skills that will be invaluable as I move forward in my career. I would also like to thank all of the members of my thesis committee; Dr. Amber Mosley, Dr. Ahmad Safa, and Dr. Michael Vasko. Thank you all for the time and effort you have given to help guide my graduate training over the last four years. Your support, mentorship and helpful feedback have made important contributions to my personal and professional development.

During my graduate training I have had the great pleasure of working with many amazing co-workers and labmates. Their friendship and support made it possible to make it through even the hardest times during the last four years. I would like to especially thank Tamila Garbuz and Vicki Jeffers for the time they invested in training me in microscopy and working with *Toxoplasma*. I would also like to personally thank Leah Padgett, Kaice LaFavers, Raj Gaji and Vicki Jeffers, and Irene Heredero Bermejo, with whom I've worked closely on collaborative projects during my training. The successes of these collaborations are some of my fondest memories, and were a great source of support and motivation when I was experiencing challenges and difficulties in my personal projects. To all my lab mates - I am thankful for all of the memories and

friendships that were made both in and outside of lab, and look forward to celebrating all of your future successes with you in the years to come.

I would like to thank my family for being an amazing source of love and support over the last five years. To my parents – thank you for teaching me the value of hard work, persistence and humility, and for giving me every opportunity to succeed in life. I hope I have made you proud. Finally, I would like to thank my wife Kaela for being an amazing source of support and encouragement, and for inspiring me to be a better person every day. While the last four years brought times of great stress and many new challenges, I am so proud of all that we have accomplished individually and together during our PhD training.

Joseph M. Varberg

BIOCHEMICAL AND PHARMACOLOGICAL CHARACTERIZATION OF THE ATG8 CONJUGATION SYSTEM IN *TOXOPLASMA GONDII*

Toxoplasma gondii is an important human pathogen that infects millions of people worldwide and causing severe and potentially lethal disease in immunocompromised individuals. Recently, a homologue for the autophagy protein Atg8 (TgAtg8) was identified in *Toxoplasma* that is required for both canonical and non-canonical processes essential for parasite viability. Importantly, TgAtg8 functionality requires its conjugation to phosphatidylethanolamine through the activity of the Atg8 conjugation system. In this thesis, we characterized the proteins that interact with TgAtg8 and TgAtg3, a component of the Atg8 conjugation system, to further define their functions in *Toxoplasma* and identify opportunities for targeted inhibition of Atg8-related processes.

We previously identified that TgAtg8 is acetylated at lysine 23 (K23) and assessed the role of this modification in this thesis. Using mutagenesis, we showed that K23 acetylation did not modulate the interaction with TgAtg3, but appeared to promote TgAtg8 protein stability. Additionally, endogenous mutation of K23 to the non-acetylatable amino acid arginine resulted in severe impairment of parasite replication and spontaneous differentiation into bradyzoites.

To gain insight into the role of TgAtg8 in *Toxoplasma* biology, we next characterized TgAtg8 and TgAtg3 interacting proteins using affinity purification and mass spectrometry. We identified a novel group of interacting proteins that are unique to *Toxoplasma,* including the dynamin-related protein DrpC. Functional characterization of DrpC identified a potential role of TgAtg8 in trafficking of membrane from the Golgi to the nascent daughter parasites during replication.

Lastly, we examined a group of small molecules recently identified as Atg3-Atg8 inhibitors in *Plasmodium falciparum* and assessed their activity against *Toxoplasma*. Although the compounds effectively inhibited *Toxoplasma* replication, they did so through novel mechanisms of action unrelated to the disruption of the TgAtg3-Atg8 interaction. Together, this work provides insight into the function of the Atg8 conjugation

system in *Toxoplasma* that will help guide the future development of novel therapeutics targeting Atg8-related processes.

Gustavo Arrizabalaga, PhD, Co-Chair

William J. Sullivan, Jr., PhD, Co-Chair

Table of Contents

List of Tables

List of Figures

List of Abbreviations

3-MA	3-methyladenine
aa	amino acid
ADP	adenosine diphosphate
AIDS	acquired immune deficiency syndrome
AIM	Atg8 Interacting Motif
AMP	adenosine monophosphate
AMPK	AMP-activated protein kinase
ATG	autophagy
ATP	adenosine triphosphate
BLAST	basic local alignment search tool
BME	beta-mercaptoethanol
bp	base pairs
BSA	bovine serum albumin
cDNA	complementary DNA
cGMP	cyclic guanosine monophosphate
CPRG	chlorophenol red β-D-galactopyranoside
CT	C-terminus
DAPI	4',6-diamidino-2-phylindole
DD	destabilization domain
DHFR	dihydrofolate reductase
DHFR-TS	dihydrofolate reductase-thymidylate synthase
DMEM	Dulbecco's Modified Eagle Medium
DNA	deoxyribonucleic acid
EDTA	ethylenediaminetetraacetic acid
FBS	fetal bovine serum
GABA	gamma-Aminobutyric acid
GABARAP	GABA-receptor associated protein
GATE-16	Golgi-associated ATPase Enhancer of 16 kDa
GFP	green fluorescent protein
HA	hemagglutinin
HBSS	Hank's buffered saline solution
HDAC	histone deacetylase

HEPES	4-(2-hydroxyethyl)-1-piperazineethanesulfonic acid
HFF	human foreskin fibroblast
His	Histidine
HRP	horseradish peroxidase
HXGPRT	hypoxanthine-xanthine-guanine phosphoribosyl transferase
IFA	immunofluorescence assay
IgG	immunoglobulin G
IMPDH	Inosine monophosphate dehydrogenase
IB	Immunoblot
IP	immunoprecipitation
IPTG	isopropyl β-D-1-thiogalactopyranoside
kDa	kilodalton
LDH	lactate dehydrogenase
LIR	LC3 Interacting Region
MPA	mycophenolic acid
mRNA	messenger RNA
mTOR	mammalian target of rapamycin
MW	molecular weight
NAD	nicotinamide adenine dinucleotide
NCBI	National Center for Biotechnology Information
nm	nanometers
nM	nanomolar
NSF	N-ethylmaleimide-sensitive factor
NT	N-terminus
PAGE	polyacrylamide gel electrophoresis
PBS	phosphate buffered saline
PBST	phosphate buffered saline with Tween-20 detergent
PCR	polymerase chain reaction
PDB	protein data bank
PE	phosphatidyl ethanolamine
pH	potential of hydrogen
PI3K	Phosphatidylinositol-4,5-bisphosphate 3-kinase
qPCR	quantitative polymerase chain reaction
rcf	relative centrifugal force

RIPA	radio immunoprecipitation assay
RNA	ribonucleic acid
rpm	revolutions per minute
SDS	sodium dodecyl sulfate
SNAP	Soluble NSF Attachment Protein
SNARE	Soluble NSF-attachment protein receptor
spp.	species
TBE	Tris/Borate/EDTA
TBS	Tris buffered saline
TBST	Tris buffered saline with Triton-X 100 detergent
U	unit
ULK	Unc-like kinase
UTR	untranslated region
V	volts
WT	wild-type
XAN	xanthine
Ω	Ohms
β-gal	β-galactosidase
μM	micromolar

Chapter 1: Introduction

1.1 *Toxoplasma gondii*, a model apicomplexan

Toxoplasma gondii is an obligate, intracellular protozoan pathogen, and a member of the phylum Apicomplexa. This group contains over 6000 known species that collectively parasitize virtually all known animals [1]. Felids are the definitive host for *Toxoplasma*, and the parasite can only undergo sexual reproduction in the endothelial cells lining the cat small intestine. However, among the apicomplexans, *Toxoplasma gondii* exhibits a uniquely broad range of intermediate hosts due to its ability to infect any nucleated cell in all warm-blooded animals [2]. As a result, *Toxoplasma* is considered by many to be the world's most successful parasite, and is of significant veterinary and medical importance for the disease it causes (toxoplasmosis) in its intermediate hosts. In addition to *Toxoplasma*, the phylum Apicomplexa contains other notable human parasites including *Plasmodium* spp., *Cryptosporidium* spp., and *Babesia* spp., the causative agents of malaria, cryptosporidiosis, and babesiosis, respectively. Together, the apicomplexans represent a group of extremely successful pathogens with significant impacts on global economics and human health.

As a single cell, eukaryotic organism, *Toxoplasma* contains a full collection of standard eukaryotic organelles, including a nucleus, endoplasmic reticulum, Golgi apparatus and a single mitochondrion (**Figure 1**). In addition to these standard eukaryotic features, the apicomplexans all share a characteristic structure called the apical complex, from which the phylum derives its name. This complex includes cytoskeletal structures, such as the conoid and apical polar rings, as well as secretory organelles that facilitate host cell attachment and invasion, including the micronemes, rhoptries and dense granules [3,4]. Other parasite specific organelles include the plant-like vacuole (PLV), acidocalcisomes, and a non-photosynthetic plastid organelle, termed the apicoplast. The apicoplast is thought to be a vestigial plastid of green algae origin acquired by endosymbiosis and is found in all apicomplexans, with the notable exception of *Cryptosporidium* spp. [5,6]. It contains its own 35-kb circular genome that encodes for transfer RNAs and ribosomal genes, allowing for translation of protein-coding gene present in the apicoplast genome. The apicoplast is also the site of important metabolic processes, and is essential for parasite viability [7,8].

In addition to these organelles, *Toxoplasma* has unique cytoskeletal features that collectively form a structure known as the pellicle. Like other alveolates, *Toxoplasma* contains a collection of alveolar sacs, which are flattened vesicles derived from the

ER/Golgi compartment [9]. In *Toxoplasma,* these vesicles are referred to as the Inner Membrane Complex (IMC), and are located between the parasite plasma membrane and the cortical microtubules (also referred to as the subpellicular microtubules). This set of 22 cortical microtubules emanates from the apical polar ring and are tethered to the IMC in a highly ordered fashion, providing structural support to maintain the characteristic crescent shape and apically polarized cell morphology [10]. Unlike other eukaryotes, the cortical microtubules in *Toxoplasma* are non-dynamic, and remain attached to the IMC throughout interphase.

Toxoplasma gondii was first described in two papers published in 1908; one by Alfonso Splendore, who discovered the parasite while working with rabbits in Brazil [11], and another by Charles Nicolle and Louis Manceaux [12], who were conducting research on leishmaniasis in the North African rodent *Ctenodactylus gundi* [13]. Both groups initially mistook the parasite for *Leishmania*, however Nicolle and Manceaux realized soon after that they had discovered a new species of protozoan, which they named *Toxoplasma gondii*, in reference to the parasite's crescent-shaped morphology (modified from the Latin word for arc or bow, *toxon*) and the host it was found in (*gundi)* [14]. In the following decades, numerous species of *Toxoplasma* were named according to the host species in which they were identified. However, advancements in biological and immunological techniques soon provided evidence that all of the various isolates collected from humans and animals were actually *Toxoplasma gondii* [2]. Currently, *Toxoplasma gondii* is thought to be the only species of the genus *Toxoplasma,* with most strains falling into one of three dominant clonal subtypes, referred to as types I, II and III [15–17]. This unique clonal structure is attributed to a genetic bottleneck event that occurred approximately 10,000 years ago, in which a single genetic cross was followed by a rapid expansion that produced the three clonal lineages observed today [18,19].

Most cases of human toxoplasmosis are caused by infection with strains of the type II genotype. This is particularly true in Europe and North America, where 80-90% of human infections have been attributed to type II strains [17,20]. It is important to note that additional subtypes that do not fall into the traditional three clonal lineages have been reported in other continents, including South America, Africa and Asia [21–23]. These atypical strains display a wide range of virulence, however some have been shown to be hypervirulent and capable of causing lethal acute infections in immunocompetent individuals [24].

In addition to these differences in human toxoplasmosis, the three major subtypes display dramatic differences in virulence in laboratory mice (type I LD_{100} ~ 1 parasite, type II $LD_{100} \geq 10^3$, type III $LD_{100} \geq 10^5$) [25], which has been attributed to variability of gene loci that encode two kinases secreted by the parasite into the host cell [26,27]. Another major difference between the three lineages is that the commonly-studied type I RH strain parasites have lost the ability to form orally infective bradyzoite tissue cysts [28,29]. Additionally, type I parasites have a short doubling time, can be maintained indefinitely in tissue culture, and can be genetically manipulated using a variety of techniques [30].This is in contrast to technical challenges observed for many fellow apicomplexans with regards to culture maintenance and genetic tractability [31,32]. As a result, *Toxoplasma* type I strains have been established as a model organism for dissecting the molecular mechanisms behind many processes of zoite-stage apicomplexan biology, including attachment, invasion, egress and motility [33].

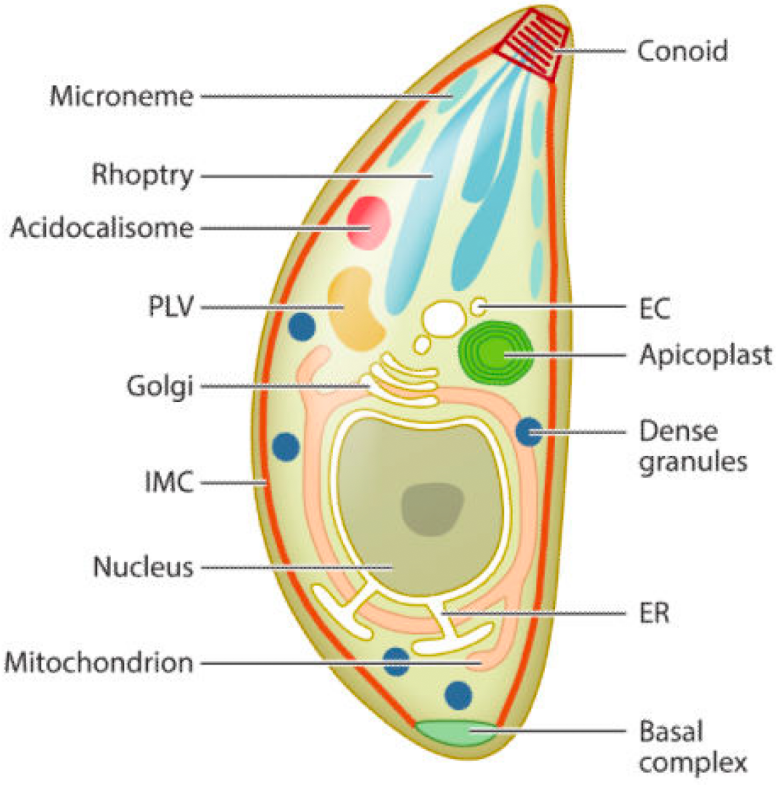

Figure 1: *Toxoplasma* tachyzoite organelles.
Adapted from Blader *et al.*, Annu Rev Microbiol, 2015. Schematic representation of a *Toxoplasma gondii* tachyzoite. EC, endosomal compartment, ER, endoplasmic reticulum, IMC, inner membrane complex, PLV, plant-like vacuole.

1.2 *Toxoplasma* life cycle and modes of transmission

Throughout its complex life cycle, *Toxoplasma* differentiates between numerous stages (**Figure 2)** [34,35]. Of these different stages, three are infective, including the tachyzoite stage, the bradyzoite stage, and the sporozoite stage shed by cats in the form of oocysts. Within the intermediate host, *Toxoplasma* persists as highly proliferative tachyzoites that are responsible for acute toxoplasmosis and bradyzoites that form latent tissue cysts that persist during chronic toxoplasmosis. Upon invasion of the host cell, *Toxoplasma* establishes residence within the parasitophorous vacuole (PV), a membrane structure formed during the invasion process that is devoid of host membrane proteins and is protected from fusion with host lysosomes [36]. Within the PV, *Toxoplasma* replicates through a form of asexual reproduction known as endodyogeny, in which two daughter parasites form within the growing mother parasite [37]. In endodyogeny, the mother parasite divides using closed mitosis, in which the nuclear envelope remains intact. During this process, some organelles are partitioned into each nascent daughter parasite (nucleus, Golgi, ER, mitochondrion, apicoplast), while some are formed *de novo* (rhoptries and micronemes [38]). Additionally, the IMC and cytoskeleton are formed *de novo* in each daughter parasite, while the plasma membrane is derived from the mother plasma membrane material. Multiple rounds of division continue until the PV contains 64-128 parasites, at which point the parasites actively egress from the vacuole, resulting in lysis of the host cell [39].

Tachyzoite replication is thought to be responsible for the initial expansion and dissemination of parasites throughout the host following primary infection [40]. After establishing infection in an intermediate host, the fast-replicating tachyzoites undergo differentiation into the slow-growing bradyzoite form, mediated at least in part by the elevated production of interferon gamma as part of the host immune response [41]. These bradyzoites form latent tissue cysts that are most commonly found in striated muscle fibers of the heart and in the central nervous system. Importantly, tissue cysts persist throughout the life of the infected host, and can reactivate back to tachyzoites in the absence of immune pressure. In addition to their role in establishing chronic infection, bradyzoite tissue cysts play a central role in the *Toxoplasma* transmission, as they can establish infection in both intermediate and definitive hosts upon ingestion of cysts present in tissues from infected animals.

Toxoplasma can only enter its sexual stage of replication in the small intestine of its definitive host, the cat [42]. Felids can become infected by *Toxoplasma* either by

direct ingestion of infectious oocysts deposited into the environment by other cats, or by ingesting tissue cysts from chronically infected intermediate hosts. After an unknown number of rounds of asexual replication in the enterocytes lining the small intestine, *Toxoplasma* undergoes differentiation into gametocytes, termed microgametocytes (male) and macrogametocytes (female). These in turn produce the micro- and macrogametes that ultimately fuse together during fertilization to form the oocyst. Following fertilization, the oocysts are released into the lumen of the small intestine and shed into the environment in the cat's feces. Within 1-5 days of excretion, the oocyst undergoes sporulation and are only then considered infectious. After sporulation, infectious oocysts are highly stable and are resistant to many chemical and physical disinfectants [43–45]. Additionally, each infected cat sheds tens of millions of oocysts into the environment, which then persist in both soil and water for years while maintaining their infectivity [46,47]. Upon ingestion of sporulated oocysts by an intermediate or definitive host, the sporozoites undergo an excystation process that is stimulated by bile salts and digestive enzymes present in the host stomach. The released sporozoites can then infect the epithelium of the host and differentiate into tachyzoites (if infecting an intermediate host) or merozoites/shizonts (upon infection of the definitive host), thus restarting the cycles of asexual or sexual replication as described above.

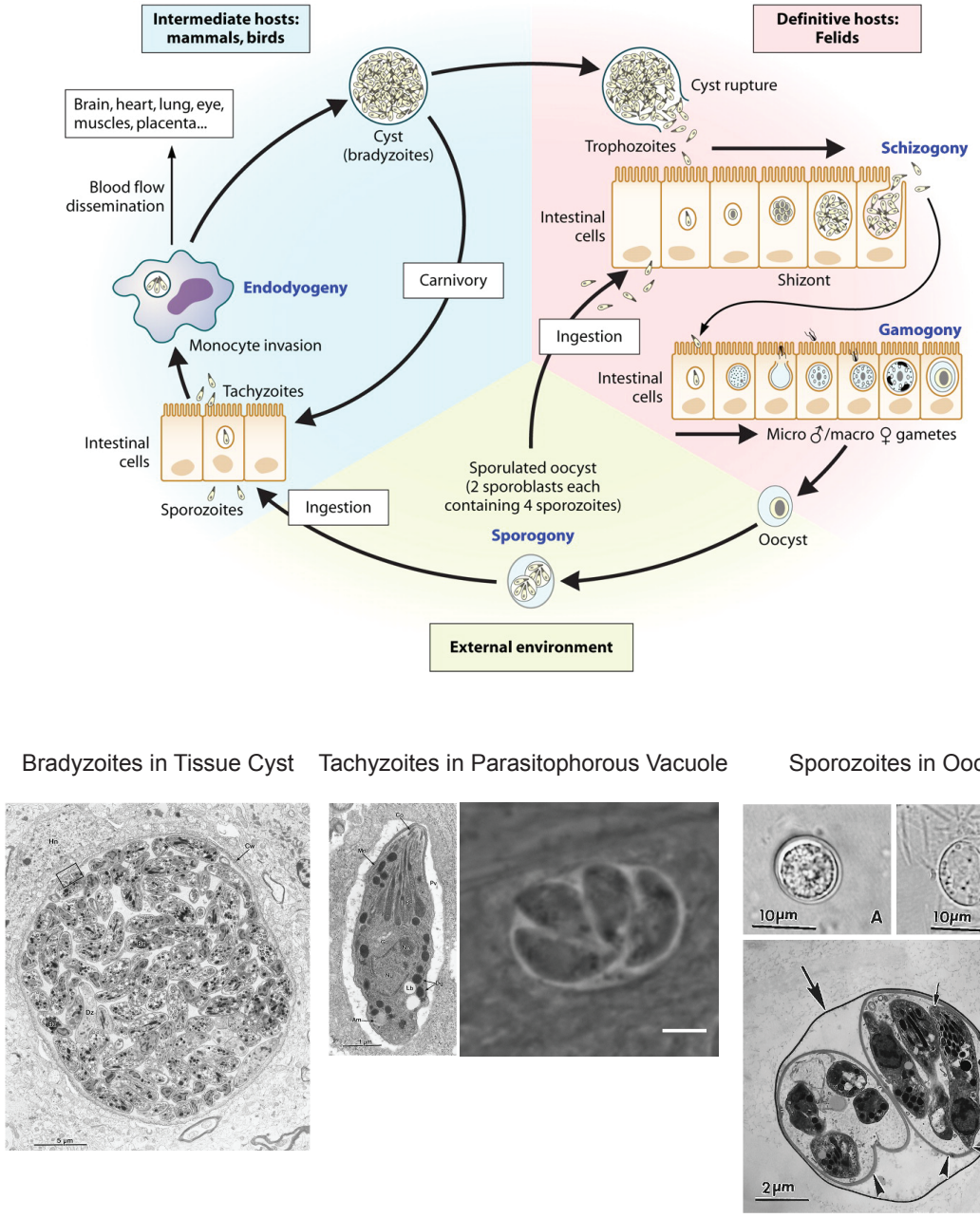

Figure 2: Life cycle of *Toxoplasma gondii*.
(*Top*) Schematic representation of the *Toxoplasma* life cycle in intermediate and definitive hosts (from Florence Robert-Gangneux, and Marie-Laure Dardé Clin. Microbiol. Rev. 2012;25:264-296). (*Bottom*) Ultrastructures of the three infectious stages of *Toxoplasma.* (*left*) Tissue cyst that was isolated from the brain of a chronically infected mouse. Hn, host nuclei, Cw, cyst wall, Bz, bradyzoite, Dz, dead zoite. (*center*) Transmission electron micrograph (TEM) of a single tachyzoite residing in the parasitophorous vacuole (Pv). Organelles are labeled, including the conoid (Co), dense granule (Dg), the Golgi apparatus (Go), micronemes (Mn), nucleus (Nu), nucleolus (No)

and rhoptries (Rh). Also shown is a light microscopy image of a parasitophorous vacuole containing four tachyzoites. Scale bar = 3 μm. (*right*) Images of *Toxoplasma* oocysts. (A) Unsporulated oocyst; (B) Sporulated oocyst. Note four sporozoites (arrows) that are visible in the right sporocyst. (C) Transmission electron micrograph of a sporulated oocyst. The oocyst wall (large arrow) surrounds two sporocysts (arrowheads), each of which contain four sporozoites (small arrows). Images of bradyzoite tissue cysts, TEM of tachyzoite, and oocysts all used from J.P. Dubey, D.S. Lindsay, and C. A. Speer, Clin. Microbiol. Rev 1998; 11:267-299.

1.3 Clinical toxoplasmosis: disease manifestations and current therapeutics

Toxoplasmosis is one of the most prevalent parasitic infections in humans, infecting an estimated 30 percent of the world's population [2]. In the United States alone, more than 60 million people are infected with *Toxoplasma,* costing an estimated 3.3 billion dollars annually for medical treatment and the economic impact caused by loss of productivity [48]. Additionally, toxoplasmosis is widespread in agricultural livestock used for meat production, particularly in sheep and pigs, costing an estimated 445 million dollars annually in the US [49]. For all hosts, infection with *Toxoplasma* can occur in one of three ways: ingestion of infectious sporozoites shed by cats in the form of oocysts, ingestion of bradyzoite tissue cysts through carnivorism of infected animals, or congenital transmission from an infected mother to the developing fetus. All three routes of infection have been observed in both intermediate and definitive hosts, however, the exact contribution that each route plays epidemiologically is still a matter of investigation [50,51].

Postnatally acquired toxoplasmosis results in an acute infection that later resolves to chronic disease upon conversion of the parasite to bradyzoites and the formation of tissue cysts. In immunocompetent hosts, symptoms are typically mild and can include headache, fever, and swelling of the lymph nodes [52]. However, the reactivation of latent infections or primary infection of immunocompromised patients often leads to the development of severe toxoplasmic encephalitis and pulmonary disease. As an opportunistic pathogen, *Toxoplasma* causes severe encephalitis in an estimated 40% of AIDS patients, with 10-30% of cases resulting in fatality [53–55]. In addition to AIDS patients, patients receiving immunosuppressive therapy for organ transplantation or receiving antineoplastic chemotherapeutics are also at risk for developing severe toxoplasmosis [56–58].

Congenitally acquired toxoplasmosis occurs following vertical transmission of the parasite from a pregnant mother to the fetus. This typically occurs if the woman is

infected for the first time during pregnancy, however cases of vertical transmission following reactivation of chronic infection have been reported [59]. Generally, the risk of vertical transmission and the severity of the effects on the fetus depends on the immunological competence of the mother, and the age of the fetus when transmission occurs. The most severe forms of congenital disease occur when transmission happens early during fetal development, often resulting in encephalomyelitis and causing neonatal death in approximately 10% of cases [60]. Infants that survive prenatal infection display a variety of symptoms, often including intracranial calcifications, hydrocephalus and retinochoroiditis. These can lead to development of mental retardation and neurological deficiencies that severely impair quality of life for those who survive past infancy. In cases when transmission occurs during the third trimester of pregnancy, the infants are often asymptomatic at birth. However, congenital toxoplasmosis often leads to the development of clinical symptoms later in life, the most common of which is retinochoroiditis caused by reactivation of latent infections in the eye [61]. Indeed, toxoplasmosis accounts for 30-55% of all cases of infectious posterior uveitis, resulting in loss of visual acuity and frequently leading to bilateral blindness [62,63].

Acute toxoplasmosis typically is treated by administration of a combination of pyrimethamine and sulfadiazine. These two compounds work to inhibit the enzymes dihydrofolate reductase (DHFR) and dihydropterate synthetase (DHPS), respectively, resulting in the inhibition of the folate synthesis pathway (**Figure 3**). This leads to a decreased availability of tetrahydrofolic acid, a cofactor that is required for the synthesis of thymidine and purines required for nucleic acid synthesis and for the synthesis of the amino acid methionine. Although humans do not have a homologue of the DHPS enzyme, a DHFR homologue does exist and also is inhibited by treatment with pyrimethamine. As a result, patients undergoing treatment with pyrimethamine often experience toxic side effects including bone marrow suppression. Accordingly, patients are often co-administered folinic acid (leucovorin), which can rescue bone marrow cells from the effects of pyrimethamine to prevent hemotoxicity. In patients who experience adverse side effects due to sulfa allergies, sulfadiazine can be replaced with the antibiotic clindamycin. In place of pyrimethamine and sulfadiazine, which can both cross the placental barrier, mothers infected with *Toxoplasma* during the first 18 weeks of pregnancy are treated with the macrolide antibiotic spiramycin [64,65]. The proposed mechanism of action for spiramycin and other antibiotics shown to have activity against *Toxoplasma* (clindamycin, azithromycin) is the inhibition of protein synthesis. This is

thought to result from the inhibition of bacterial-like ribosomes present at the apicoplast due to the endosymbiotic origin of this organelle [8,66,67]. Although drug treatments can clear the acute stage of toxoplasmosis, no therapies currently exist that are able to target the latent tissue cysts present in the chronic stage of infection. Additionally, the development of resistance to pyrimethamine-based treatments in *Plasmodium falciparum* highlights the need for the identification of novel drug targets to treat *Toxoplasma* and related parasitic infections [68].

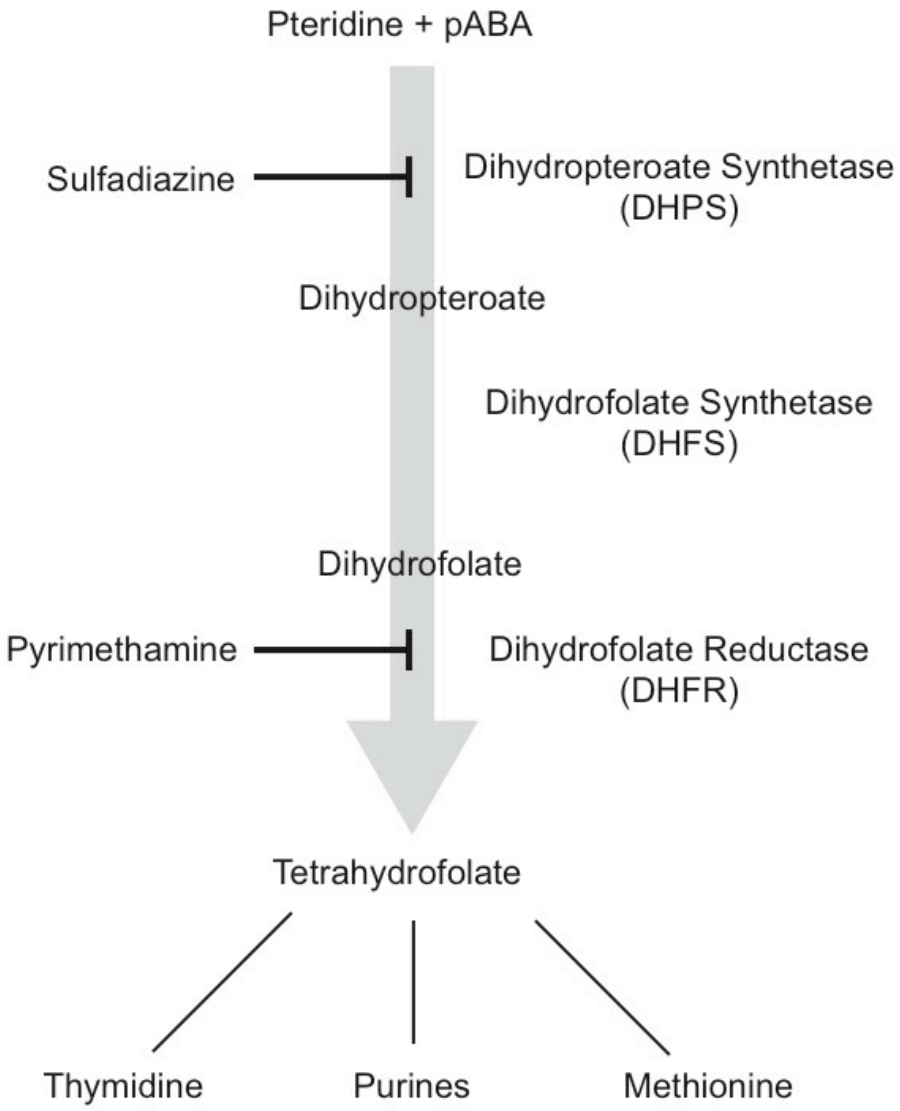

Figure 3: Mechanism of action for antiparasitics targeting the folate synthesis pathway.
Current first-line therapies to treat toxoplasmosis involve inhibition of folate synthesis by

a combination of pyrimethamine and sulfadiazine. These drugs target the dihydrofolate reductase (DHFR) and dihydropteroate syntehtase (DHPS) enzymes, respectively. This treatment often is poorly tolerated because of patient allergies to sulfa compounds and side effects caused by the inhibition of host DHFR.

1.4 Autophagy in eukaryotes: molecular machinery and cellular functions

The identification of new and selective drug targets to treat toxoplasmosis and other parasitic infections relies on the identification of cellular processes that are either absent or sufficiently divergent from similar processes in the eukaryotic host to allow for specific targeting of the parasite. Identifying selective targets is complicated by the fact that many aspects of *Toxoplasma* biology rely on the function of standard eukaryotic organelles, including the Golgi apparatus, endoplasmic reticulum and mitochondrion. One approach to identify opportunities for therapeutic intervention is to target parasite-specific proteins, biological processes or organelles. In the following section, we will introduce aspects of the eukaryotic autophagy pathway, for which a subset of homologues has recently been identified in *Toxoplasma* and other protozoan parasites. We will first outline the core components of the autophagy pathway and their canonical functions in higher eukaryotes. We will then identify aspects of these complexes that are absent or divergent in function in *Toxoplasma* and may represent possible targets for the development of new antiparasitics.

In eukaryotic cells, macroautophagy (referred to hereafter as autophagy) is a catabolic process in which components of the cytoplasm are engulfed by an elongating membrane structure called the phagophore. This vesicle matures into an enclosed, dual-membrane vesicle termed the autophagosome and is trafficked to the lysosome/vacuole where the engulfed material is degraded [69]. This process is induced in response to nutrient starvation [70,71], but also plays a significant role in cellular development and differentiation [72], proteostasis [73], clearance of damaged organelles and as a defense mechanism against invading pathogens [74,75]. While over 30 autophagy-related (ATG) genes have been identified, a subset of these genes comprise the “core” autophagy machinery, representing the genes that are required for *de novo* autophagosome formation and are especially well conserved across eukaryotic organisms [76]. The core ATG proteins separate into functional subgroups as depicted in **Table 1**.

The first set of core ATG proteins is the Atg1/ULK1 kinase complex. In yeast, Atg1 activity is regulated by the formation of a complex containing Atg1, Atg13 and the scaffolding complex consisting of Atg17, Atg29 and Atg31 [77,78]. Atg1 is a

serine/threonine kinase, and its role in the initiation of autophagy lies downstream of the target of rapamycin kinase (TOR1). Under nutrient replete conditions, TOR phosphorylates Atg13 at multiple residues, reducing its affinity for Atg1 and preventing formation of the functional Atg1 complex [79]. Under starvation conditions, TOR kinase is inactivated, resulting in hypophosphorylation of Atg13. This allows for the formation of the pentameric Atg1 complex containing Atg1, Atg13, and the Atg17/29/31 complex [80]. Once formed, the active Atg1/ULK1 complex localizes to the preautophagosomal assembly site (PAS), where it serves as a docking site for vesicles containing the integral membrane protein Atg9 [81]. Recent studies have shown that in yeast, an average of three Atg9-containing vesicles coalesce at the PAS and initiate autophagosome biogenesis by facilitating the recruitment of ATG proteins Atg8 and Atg18 [78,81,82].

The second core group comprises the PI3-Kinase complex, and includes the class-III PI3-kinase Vps34 and its associated proteins. The kinase activity of Vps34 is required for the production of phosphatidylinositol (3)-phosphate (PI3P) at the membrane of the PAS and is regulated by phosphorylation by Vps15 [83,84]. Atg14 is recruited to the PAS independently of Vps34, and is thought to be important for proper localization of Vps34 to the autophagosome membrane [83]. Additionally, Atg14 has been shown to stimulate the kinase activity of Vps34. Activation of Vps34 leads to increased production of PI3P and recruitment of PI3P-effector proteins, such as Atg18 and Atg2, which are required for autophagosome formation [83,85]. The functional role of Atg6 in this complex is less defined, but it appears to be able to associate directly with the PAS membrane and regulate autophagosome size and number [86].

The third and fourth core autophagy groups are conjugation systems for the two ubiquitin-like proteins Atg12 and Atg8. The first system is responsible for conjugation of Atg12 to Atg5, via the activity of the E1-like enzyme Atg7 and the E2-like enzyme Atg10, and without the activity of an E3-like enzyme [87]. The Atg5-Atg12 complex then forms a hetrotrimeric complex with Atg16, which homodimerizes to generate the functional Atg16-complex. The second conjugation system facilitates the conjugation of the cytosolic ubiquitin-like protein Atg8 (LC3/GABARAP/GATE-16 in mammals) to phosphatidylethanolamine (PE) present in the phagophore membrane. At the membrane, Atg8 plays important roles in the elongation and fusion of the phagophore membrane, and can also bind with substrate and adapter proteins containing the Atg8-interacting motif (AIM) to selectively recruit proteins to the autophagosome for

degradation [88,89]. Conjugation of Atg8 to PE is carried out via the E1-like enzyme Atg7 and the E2-like enzyme Atg3, with the oligomeric Atg5-Atg12-Atg16 complex providing E3-like enzymatic function to stimulate transfer of Atg8 from Atg3 to PE [90,91]. Additionally, the cysteine proteinase Atg4 is responsible for both the pre-processing of Atg8 to expose the C-terminal glycine for lipidation. Atg4 is also required for the cleavage of the amide bond between Atg8 and PE to liberate Atg8 from the autophagosomal outer membrane during autophagosome maturation [90,92].

Table 1: Conservation of core ATG proteins in *Toxoplasma gondii*

S. cerevisiae	*H. sapiens*	*T. gondii*	*Subgroup and Function*
Atg1	ULK1/2	*Atg1*	*Atg1/ULK1 kinase and its regulators*
Atg13	Atg13	---	Through Atg1/ULK1 kinase activity, triggers formation of the early autophagosome and recruitment of downstream Atg proteins
Atg17	FIP200	---	
Atg29	Atg101	---	
Atg31		---	
Atg9	Atg9A/B	Atg9	*Integral Membrane Protein* Phosphorylated by Atg1/ULK1, recruits Atg8 and Atg18 to autophagosome
Vps34	Vps34	Vps34	*PI3-Kinase Complex*
Vps15	Vps15	*Vps15*	Produces PIP3 at the autophagosome membrane and recruits Atg proteins to membrane structure
Vps30/Atg6	Beclin1	*Atg6*	
Atg14	Atg14(L)	---	
---	AMBRA1	---	
Atg12	Atg12	*Atg12*	*Atg 12 Ubiquitin-like Conjugation System*
Atg7	Atg7	*Atg7*	Autophagy-related membrane biogenesis and stimulation of Atg8 lipidation
Atg10	Atg10	---	
Atg5	Atg5	*Atg5*	
Atg16	Atg16L1	---	
Atg3	Atg3	Atg3	*Atg8 Ubiquitin-like Conjugation System*
Atg4	Atg4A/B/C/D	Atg4	Regulates Atg8 lipidation, coordinates membrane tethering, expansion and hemifusion of nascent autophagosomes, recruitment of cargo to autophagosomes for degradation
Atg7	Atg7	Atg7	
Atg8	LC3A1/A2/B/C GABARAP/L1 GATE-16	Atg8	

*Genes in italics represent putative *Toxoplasma* homologues identified based on sequence homology but have not been functionally characterized

Conservation in *Toxoplasma:*

Atg1/ULK complex – No components of the Atg1/ULK complex or their upstream regulator TOR have been functionally characterized in *Toxoplasma*. Bioinformatics searches for homologues of the Atg1/ULK complex members identify putative TOR and Atg1 proteins in *Toxoplasma,* (TgTOR, TGGT1_316430; TgAtg1, TGGT1_316150). Importantly, when compared to the human and yeast mTOR/TOR1 proteins, the putative TgTOR protein is missing a significant portion of the kinase domain and has a large (~3 kb) N-terminal extension with no identifiable domains. This divergence could explain the reduced sensitivity of *Toxoplasma* to the TOR inhibitor rapamaycin [93,94]. *Toxoplasma* lacks all components of the Atg17/29/31 scaffolding complex required for recruitment of the Atg1 complex to the PAS in higher eukaryotes, as well as an Atg13 homologue. Homologues to Atg18 and Atg9 are present, however their role in autophagy remains unclear, and in the case of Atg18, have not been studied. Recent studies characterizing the function of TgAtg9 showed that parasites lacking this protein had a reduced ability to survive prolonged periods of extracellular stress and had attenuated virulence in mice [95].

PI3K Complex – The *Toxoplasma* genome encodes a single class-III PI3K, TgPI3K (TGGT1_215700), which shares strong sequence homology with Vps34 (47% identity, 67% similarity). TgPI3K localizes to the parasite cytoplasm, and conditional knock-down results in significant enlargement and subsequent loss of the apicoplast, suggesting a role for this kinase in apicoplast homeostasis [96]. Visualization of the Vps34 product, PI3P, shows that this lipid is enriched in the plant-like vacuole, a lysosome-like vacuolar compartment that contains the cathepsin proteases TgCPB and TgCPL [97,98]. *Toxoplasma* also has putative homologues of the regulatory kinase Vps15 (TGGT1_310190) and Atg6 (TGGT1_221360). However, the function of these proteins in parasite biology remains unexplored. No homologue for Atg14 is present in *Toxoplasma.*

Ubiquitin-like Conjugation Systems – A clear homologue of Atg7, the E1 enzyme for both Atg12 and Atg8, is present in *Toxoplasma* (TGGT1_229690). Although its localization and biological function remains unknown in *Toxoplasma*, it has been shown to localize to the mitochondrion in *Plasmodium falciparum*, and is essential for *P. falciparum* viability [99]. A putative Atg12 homologue is identified based on sequence homology (TGGT1_321300), and although there is significant homology to human and yeast Atg12 proteins in the TgAtg12 C-terminus, the protein contains a large N-terminal

extension of unknown function. This results in a predicted protein size of 681 amino acids, as compared to 186 amino acids in higher eukaryotes. Additionally, the predicted TgAtg12 protein lacks the C-terminal glycine residue that is required for the formation of the thioester bond between Atg12 and Atg7 [100]. The putative *Toxoplasma* homologue of Atg5 is even more divergent, containing a ~375 bp N-terminal extension and a ~350 bp insertion that divides the conserved Atg5 domain into N-terminal and C-terminal fragments. Further, sequence alignments with human Atg5 show that the putative TgAtg5 lacks the conserved lysine residue that forms an isopeptide bond with Atg12 [101]. Together, these differences suggest that *Toxoplasma* (and other apicomplexans) may lack a functional Atg5-12 complex, unlike other protozoans in which Atg5-12 activity appears conserved [102].

Unlike the Atg5-12 conjugation system, all components of the Atg8 conjugation system are conserved and functional in *Toxoplasma* [94,103,104]. *Toxoplasma* homologues of TgAtg4 and TgAtg3 have been shown to coordinate TgAtg8 lipidation in similar manner to higher eukaryotes. Like PfAtg7, *Plasmodium* Atg3 orthologues localize to the parasite mitochondrion, while *Toxoplasma* Atg3 resides in the cytoplasm [94,105]. Although TgAtg7 has not been characterized in *Toxoplasma,* both TgAtg3 and TgAtg4 are essential for parasite viability [94,104]. Conditional knock-down of either gene resulted in fragmentation of the parasite mitochondrion, suggesting that the Atg8 conjugation pathway may be required for maintenance of this organelle. Functional homologues of Atg8 have also been found in both *Toxoplasma* and *Plasmodium*, and localize to the outer membrane of the apicoplast. The ability for apicomplexan Atg8 homologues to complement *Saccharomyces cerevisiae* Atg8 knock-outs varies across species: *Plasmodium falciparum* Atg8 could recue ScAtg8 knock-out strain function while *Plasmodium berghei* Atg8 was unable to do so [105,106]. These differences may be attributable to variations in the amino acid composition across apicomplexans in regions of Atg8 that coordinate protein-protein interactions [107].

Functional differences are also observed for apicomplexan Atg8 proteins as compared to yeast and mammalian systems. First, components of the Atg8 conjugation pathway appear to be essential for parasite viability under all conditions. This is in contrast to yeast, where ATG knock-outs are viable and can be maintained in the absence of autophagy-inducing stimuli [108]. This difference is likely attributed to the recently identified non-canonical functions that Atg8 proteins have in organelle maintenance and division in apicomplexans [103]. Additionally, in higher eukaryotes,

Atg8 is translated as a pro-peptide that must undergo C-terminal cleavage by Atg4 to expose the C-terminal glycine residue required for interaction with the Atg8 conjugation system machinery and ultimately for conjugation to PE. As a result, in the absence of autophagy inducing stresses, Atg8 exists predominantly in its unlipidated form. In contrast, apicomplexan Atg8 proteins lack the C-terminal extension and are therefore available to undergo lipidation without pre-processing by Atg4. Accordingly, a significant portion of Atg8 is found to be lipidated under basal conditions in both *Plasmodium* and *Toxoplasma* [94,106]. In addition to these differences, other unique aspects of the apicomplexan Atg8 conjugation system will be further discussed in Section 1.6, as this system is the major focus of the work presented in this thesis.

1.5 The Atg8 family of proteins: autophagy and beyond

Among the core ATG proteins, the members of the Atg8 conjugation pathway are uniquely well conserved across eukaryotes. Interestingly, the number of Atg8 orthologues present varies widely across species, ranging from a single Atg8 protein in yeast to 25 Atg8 orthologues in *Leishmania major* [109]. In mammals, there are at least six Atg8 proteins comprising three subfamilies: the Golgi-associated ATPase enhancer of 16 kDa (GATE-16), the gamma-aminobutyric acid receptor associated protein family (GABARAP), and the microtubule-associated protein 1 light chain 3 family (MAP1LC3, referred to hereafter as LC3). LC3B is the best studied human Atg8 protein with respect to canonical autophagy. In contrast, the biological functions of other Atg8 orthologues remains less clear and their potential contributions to both canonical and non-canonical processes are underappreciated. In the following section, we will discuss in detail members of each of the three Atg8 families of proteins in mammals, providing historical context and recent advancements that shed light on the various biological functions these proteins possess in higher eukaryotes. This information will be valuable as we examine the potential functions of Atg8 proteins in early-branching eukaryotes, including *Toxoplasma* and other protozoan pathogens.

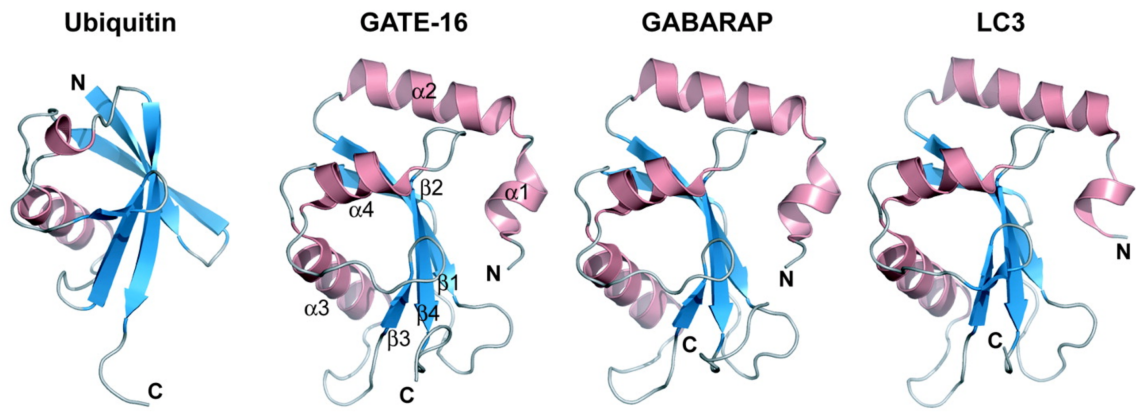

Figure 4: Structures of Atg8 family proteins.
Ribbon structure representations of ubiquitin, and the mammalian Atg8 family proteins GATE-16, GABARAP, and LC3B. Alpha helices are shown in pink, beta-strands are shown in cyan. From Noda N, Ohsumi Y, Inagaki F, Chem. Rev., 2009; 109:4:1587-1598.

Golgi-associated ATPase enhancer of 16 kDa (GATE-16) – GATE-16 was the first of the Atg8 proteins to be crystalized and its resolved structure is highly conserved across all Atg8 orthologues [110–113]. The GATE-16 protein consists of a ubiquitin-like core domain that is preceded by two N-terminal alpha-helices. The GATE-16 and GABARAP family proteins are both able to undergo conformational changes between an “open” and “closed” state, which can be mediated by protein interactions [114]. In the “open” state, the N-terminal helices adopt an extended position that enables penetration into membranes mediated by hydrophobic interactions between the N-terminal helices and the hydrophobic center of the lipid bilayer [89]. This contrasts with the mechanism of interaction between LC3 proteins and the membrane, which are facilitated by interaction with the lipid head groups. With regard to canonical autophagy, GATE-16 appears to have specific function in membrane fusion events required for late steps of autophagosome biogenesis [89,115].

Whereas LC3 proteins are ubiquitously expressed, GATE-16 is predominantly expressed in the brain [116]. Prior to being implicated in autophagy, GATE-16 was originally identified as being involved in ER-to-Golgi and intra-Golgi vesicular transport processes. Purified GATE-16 (then called p16) from bovine brains was found to stimulate intra-Golgi trafficking in an *in vitro* system and its activity was dependent on the presence of *N*-ethylmaleimide-sensitive factor (NSF) and soluble NSF attachment (SNAP) proteins [117]. It was later determined that GATE-16 binds directly to NSF and stimulates its ATPase activity to promote the disassembly of SNARE complexes formed

upon completion of vesicle fusion [118]. NSF and GATE-16 have since been shown to function outside of intra-Golgi transportation where they are required for homotypic fusion events in the post-mitotic Golgi [119–121]. In contrast to their function in intra-Golgi transport, the role of GATE-16 and NSF in post-mitotic fusion is independent of NSF ATPase activity [121,122].

GABARAP Family – The two GABARAP family proteins, GABARAP and GABARAPL1, share many structural similarities to GATE-16, including containing acidic residues in the N-terminal alpha helices [114]. GABARAPL1 shares a similar expression profile as GATE-16, being highly expressed in the central nervous system, while GABARAP is predominantly expressed in the endocrine glands and in distinct sub-regions of the brain [116,123]. GABARAP was originally described in the intracellular transport of the GABA (A) receptor (GABAAR), and was later found to mediate the membrane expression of the human kappa opioid receptor and the transient receptor potential cation channel V member TRPV-1 [124–127]. GABARAP proteins bind to these receptors to ensure their sequestration from the Golgi network into the appropriate transport vesicles [124]. Additionally, GABARAP proteins located on the surface of the transport vesicles can interact directly with kinesin family proteins to facilitate the anterograde transport of the GABAAR-containing vesicles to the plasma membrane along microtubules [128,129]. Recent studies suggest that in addition to binding with kinesin proteins, all members of the LC3/GABARAP/GATE-16 family proteins can directly interact with the microtubules through their N-terminus [130,131]. Lastly, GABARAP can also interact with the endocytosis-associated protein clathrin, suggesting a role for GABARAP proteins in receptor internalization and recycling [127,132].

LC3 Family – LC3 was originally identified in rats as a component of the microtubule associated protein MAP1A and MAP1B complexes [133]. MAP1A/B are microtubule stabilizing proteins that associate with microtubule lattices and are predominantly expressed in the brain. The MAP1A/B complex is composed of heavy and light chain subunits which are translated as polypeptides and processed by proteolytic cleavage near the C-terminus to generate the heavy and light chains [134]. In contrast, LC3 is an accessory protein that is found in complex with MAP1A/B heavy and light chains in a ratio of 1:2:0.2, and is transcribed from its own gene [135]. The human genome encodes for four members of the LC3 family: LC3A (for which two isoforms exist due to alternative splicing), LC3B and LC3C [115,136].

Structural studies have revealed that the C-terminal ubiquitin-like core is well conserved between LC3 and GABARAP/GATE-16 proteins, wherease variability is present in the N-terminal alpha-helices [112]. While these regions are acidic in GABARAP and GATE-16 proteins, they are highly basic in LC3 members. These differences have been proposed as a potential mechanism by which Atg8 orthologues interact with distinct subgroups of interacting proteins [137]. Most members of the LC3 family are ubiquitously expressed, however the LC3C protein is present at much lower levels than other members, and is only highly expressed in the lungs [136]. Loss of LC3 family proteins resulted in a specific impairment in the autophagosome biogenesis process, with cells producing significantly smaller autophagosomes [138]. The main function of LC3 members is in expansion and elongation of the phagophore membrane, while GABARAP and GATE-16 proteins are required at later stages to mediate autophagosome membrane hemifusion.

Of the LC3 family members, LC3B is the most studied and as a result more is known about its functional role in autophagy. It is the only member of the Atg8 proteins that can recruit p62/SQSTM1, an adapter protein that specifically targets polyubiquitinated proteins for degradation by autophagy. This interaction recruits p62/SQstm1 to the autophagosomal membrane [139] and is mediated by interaction of the LC3 Interacting Region (LIR) on p62/SQSTM with LC3B. This forms a bridge between membrane-bound, lipidated LC3 and the polyubiquitinated cargo proteins being targeted for degradation [140]. Although p62/SQSTM1 can interact with all Atg8 family proteins in their unlipidated state, p62/SQSTM1 is unable to interact with GABARAP/GATE-16 proteins following their lipidation [139]. LC3 proteins also interact with other cargo-recruiting proteins in a similar manner, including neighbor of Brca1 (NBR1, [141]), the mitophagy-related proteins BNIP3 and Nix [142–144], and autophagy-linked FYVE protein (Alfy) [145,146] . Thus, despite their overall similarity in structure to other Atg8 proteins, LC3 proteins have family-specific functionality in autophagosome biogenesis and cargo recruitment processes.

1.6 The apicomplexan Atg8 conjugation system: conserved and unique features

Autophagy was originally discovered in mammalian cells, but much of the work identifying the genes involved in autophagy and their functions has been done in the budding yeast *Saccharomyces cerevisae* [79,92]. However, phylogenomic studies have since identified orthologues of many of the autophagy-related genes in a wide range of

species, including plants and protozoans [109,147]. Among the core autophagy proteins identified, Atg8 and the members of the Atg8 conjugation system appear to be the most highly conserved. Functional characterization of Atg8 homologues in multiple protozoan parasites has revealed that this protein is required for multiple aspects of parasite biology, including stage conversion and differentiation. Atg8 homologues are also important for surviving the various environmental stresses that the parasites encounter as they complete their complex life cycles. For example, in *Trypanosoma cruzi* (the causative agent of Chagas disease), Atg8 is implicated in the delivery of proteins to the reservosome, an endocytic compartment rich in enzymes associated with proteolysis and lipid metabolism [148]. This allows for their degradation in response to changes in nutrient availability during transition from the vertebrate to invertebrate host [149]. Similarly, in *Trypanosoma brucei* (African sleeping sickness), autophagy is involved in the degradation of glycosomes during the transition from the bloodstream to the midgut of the tsetse fly [150]. In *Leishmania major* (the causative agent of cutaneous leishmaniasis), autophagy is required for cellular remodeling that occurs during differentiation into infective metacyclics [151]. Many of these processes depend on the canonical function of Atg8 and related autophagy proteins in the degradation of cellular components by autophagy. However, characterization of Atg8 proteins in other parasitic species, including the apicomplexans, has revealed that Atg8 and the Atg8 conjugation machinery also have functions in non-canonical processes that are specific to parasite biology.

Characterization of Atg8 homologues in the apicomplexan parasites *Plasmodium spp.* and *Toxoplasma gondii* revealed that in both species Atg8 localizes to the outer membrane of the apicoplast [94,106,152], a non-photosynthetic plastid organelle that plays an essential role in fatty acid metabolism [153]. In *Toxoplasma,* TgAtg8 tethers the apicoplast to centrosomes, either directly or indirectly, to ensure proper division of this organelle during parasite replication [103]. Conditional knock-down of TgAtg8 resulted in the failure of apicoplasts to be properly segregated into daughter parasites during replication and subsequent loss of parasite viability. The localization of TgAtg8 to the apicoplast is dependent on its conjugation to PE, which is facilitated by *Toxoplasma* homologues of Atg3 and Atg4. Both of these proteins, which localize to the parasite cytoplasm, are essential for parasite viability [94,104]. Conditional knock-down of either TgAtg3 or TgAtg4 resulted in fragmentation of the mitochondrion, suggesting that a

functional Atg8 conjugation pathway may be required for the maintenance of both apicoplast and mitochondrion organelles.

Two important structural features have been identified in apicomplexan Atg8 proteins that differentiate them from homologues found in higher eukaryotes. First, apicomplexan Atg8 proteins contain a nine amino acid insertion that forms an apicomplexan-specific loop structure. Studies in *Plasmodium falciparum* have shown that this loop is critically important for the interaction between PfAtg8 and PfAtg3 [107]. Although the role of this structure has not yet been explored for TgAtg8, it is likely to play a similar role in regulating protein-protein interactions in *Toxoplasma*. Second, apicomplexan Atg8 proteins lack the C-terminal extension present in mammalian Atg8 proteins that requires pre-processing by Atg4 to expose the C-terminal glycine residue for conjugation to PE. As a result, Atg8 proteins in *Toxoplasma* and *Plasmodium* are able to undergo constitutive lipidation, whereas yeast and mammalian Atg8 proteins are only lipidated upon induction of autophagy. However, it is worth noting that a portion of Atg8 is observed in the non-lipidated state under basal conditions. This suggests that despite not requiring pre-processing by Atg4, TgAtg8 lipidation does appear to be under some form of regulation that is currently unidentified.

Despite basal levels of Atg8 lipidation in *Toxoplasma*, Atg8 lipidation is induced in response to starvation or drug treatment. This can be visualized by the formation of Atg8-containing double membrane vesicles and/or GFP-TgAtg8 punctae that resemble putative autophagosomes [94,154]. It is possible that this apparent induction of autophagy may represent a cytoprotective mechanism that allows the parasite to mitigate the effects of cytotoxic stimuli. However prolonged exposure to autophagy-inducing stressors results in a loss of parasite viability with features resembling autophagic cell death [93,154]. Interestingly, mutations in putative ATG proteins were shown to contribute to the development of chloroquine resistance in *Plasmodium falciparum*, lending further support for an autophagic cell death pathway in apicomplexans [155].

In higher eukaryotes, the induction of autophagy and Atg8 lipidation is regulated through the posttranslational modification of ATG proteins [156,157]. For example, acetylation of Atg1/Ulk1 increases its kinase activity and promotes autophagy induction, while acetylation of Atg3 by p300 promotes its interaction with Atg8 and induces Atg8 lipidation [158,159]. Additionally, acetylation of LC3B at K49 and K51 regulates its subcellular localization, requiring deacetylation by SIRT1 to translocate from the nucleus

to the cytoplasm for incorporation into nascent autophagosomes [160]. Interestingly, TgAtg8 was found to be acetylated in extracellular parasites [161], however the role of this modification in regulating TgAtg8 function remains unknown. The signaling pathways and enzymes that add or remove these PTMs to control autophagy have been well characterized in yeast and humans. In contrast, the analogous regulatory pathways remain largely undefined in *Toxoplasma. Toxoplasma* appears to have homologues to some of the kinases known to regulate autophagy in other systems (Atg1, TOR, PI3K), however these proteins remain poorly characterized in the parasite. Attempts to manipulate these pathways pharmacologically with compounds known to induce or inhibit autophagy in higher eukaryotes have been largely ineffective in *Toxoplasma* [93,94]. These findings illustrate the need to characterize the pathways that regulate the *Toxoplasma* autophagy pathway to allow for the future development of novel compounds to disrupt these pathways for therapeutic benefit.

Recent structural characterization of the *P. falciparum* Atg8 W- and L-site binding pockets identified differences in the electrostatic surface potential and amino acid composition between PfAtg8 and human Atg8 homologues LC3 and GATE-16 [107]. These differences were significant enough to result in a ~30-fold preference for the binding of small molecule inhibitors to PfAtg8 as compared to human LC3 [162]. Moreover, high-throughput screens have identified numerous compounds that bind within the PfAtg8 W- and L-site pockets and inhibit the interaction between recombinant PfAtg3 and PfAtg8 *in vitro*. These include multiple compounds from the Medicines for Malaria Venture “Malaria Box” that have anti-malarial activity in tissue culture [107,162]. An additional group of small molecules has been identified that bind to the PfAtg8 apicomplexan loop and prevent its interaction with PfAtg3 [163]. Although these compounds have not yet been tested in other apicomplexans, they have been proposed as novel compounds with potential broad-spectrum use therapeutically, and as tools to study the autophagy pathway in these parasites [164]

1.7 Summary and Aims

As introduced in the preceding sections, *Toxoplasma* and related apicomplexan parasites are important pathogens for which novel therapeutics are needed. These parasites contain a functional Atg8 conjugation system that is structurally unique from human Atg8 proteins and is essential for parasite-specific biological processes. Therefore, this pathway may be an ideal new target for the development of novel therapeutics to treat these parasitic infections. Further, the identification of specific Atg3-

Atg8 inhibitors in *Plasmodium falciparum* provides proof-of-concept for the development of new anti-parasitic compounds that target Atg8 protein-protein interactions. However, our current understanding of how TgAtg8 coordinates both canonical and non-canonical processes in apicomplexan biology is limited do to the lack of understanding regarding which proteins TgAtg8 interacts with, and how these interactions are regulated.

With the work presented in this thesis, we sought to characterize the proteins that interact with members of the *Toxoplasma* Atg8 conjugation system to identify novel interactions that could be targeted pharmacologically. *We hypothesized that in addition to interacting with homologues of the canonical eukaryotic Atg8 conjugation machinery, TgAtg8 interacts with novel proteins to facilitate its functions in parasite-specific processes. Additionally, we hypothesized that these protein interactions were subject to regulation by post-translational modifications, and that they could be pharmacologically disrupted by the recently identified PfAtg3-Atg8 interaction inhibitors.* We addressed these hypotheses with the following three aims: 1) Determine the functional consequences of TgAtg8 lysine-23 acetylation on the TgAtg3-TgAtg8 interaction; 2) Characterize the TgAtg8 interactome to identify novel TgAtg8 interacting proteins, and 3) Determine whether TgAtg8 lipidation could be pharmacologically inhibited by treatment with Atg3-Atg8 interaction inhibitors recently identified in *Plasmodium*.

Chapter 2: Materials and Methods

2.1 Tissue culture

Parasites were maintained in culture by continuous passage through human foreskin fibroblasts (HFFs). HFFs were grown to confluency in Dulbecco's Modified Eagle Medium (DMEM) supplemented with 10% heat-inactivated fetal bovine serum (FBS), 1% PenStrep (100 U/mL Penicillin and 100 µg/mL streptomycin) and 2 mM L-glutamine, in a humidified incubator at 37°C and 5% CO_2. Confluent HFF monolayers were inoculated with parasites and maintained until the parasites had completed sufficient rounds of replication to completely lyse the HFF monolayer, at which point the parasites were transferred to a new flask of confluent HFFs.

The parasites used in this study were all generated in a modified type I RH background in which the hypoxanthine-xanthine-guanine phosphoribosyl transferase (HXGPRT) gene has been knocked-out [165]. This strain allows for drug selection with mycophenolic acid (details of drug selection described in Section 2.3), and will be referred to as RHΔ*hx*gprt. Additionally, a derivative of the RHΔ*hxgprt* strain in which the DNA-repair enzyme ku80 has also been disrupted (RHΔ*hxgprt*Δ*ku80*) was used for tagging of genes at their endogenous locus, as the lack of ku80 greatly improves the efficiency of integration of transfected plasmid DNA by homologous recombination [166].

2.2 Molecular cloning techniques

For the isolation of genomic DNA, freshly lysed parasites were passed through a 3 µm polycarbonate filter to remove host cell material, and were centrifuged for 10 minutes at 1000 relative centrifugal force (rcf). The parasite pellet was washed once with PBS and centrifuged as before. Genomic DNA was isolated using the DNeasy Blood and Tissue kit (Qiagen), and the recovered DNA was used as template for PCR. Amplification of DNA sequences by polymerase chain reaction (PCR) was done using the Phusion® High Fidelity DNA polymerase (Thermo Scientific) according to manufacturers' guidelines. All PCR primers used in my studies are listed in **Appendix 1**.

For generation of constructs using coding sequences (CDS), parasite cDNA was prepared as follows and was used as template for PCR. First, parasites were harvested as described before, and total RNA was isolated from the pellet using the RNeasy kit (Qiagen) according to the manufacturers' protocol. The collected RNA was analyzed on the NanoDrop One spectrophotometer (Thermo Scientific) to determine RNA concentration, and 2 µg of total RNA was reverse-transcribed (RT) into cDNA using the

Omniscript RT kit (Qiagen). The resulting cDNA was then used as template for PCR or was stored at -20°C for later use.

Unless otherwise specified, all amplicons were cloned into their respective vectors using the In-Fusion® HD Cloning Kit (Clontech). This approach utilizes a proprietary DNA recombinase to seamlessly insert amplicons into linearized vectors in a single, 15-minute reaction. To allow for insertion, 15-bp sequences are included in the sense and anti-sense primers used for the initial PCR amplification that are homologous to the sequence 15-bp up- and down-stream of the intended insertion site in the vector. In-Fusion® cloning reaction products were transformed into Stellar™ competent cells (Clontech) according to manufacturers' protocol, plated on LB-agar plates containing 100 µg/mL ampicillin and incubated at 37°C overnight. Single bacterial colonies were picked and used to inoculate 3 mL cultures grown overnight at 37°C, 250 RPM. One-third of the culture was pelleted by centrifugation at 10,000 rcf for 1 minute, and plasmid DNA was isolated using the QuickLyse Miniprep Kit (Qiagen). All plasmids were confirmed by sequencing prior to further use in downstream applications.

Endogenous C-terminal epitope tagging of genes of interest was performed using the cloning approach and pLIC-3xHA-DHFR tagging construct described in [167]. Briefly, a fragment of the 3' end of the gene of interest was amplified by PCR from genomic DNA and inserted into PacI-digested pLIC-3xHA-DHFR using Infusion cloning. The Infusion reaction was transformed into Stellar™ competent cells and plasmid DNA from recovered bacterial colonies was collected as described above. Presence of the insert was first confirmed by restriction digestion with PacI and visualization of the digestion products by electrophoresis on a 1% agarose/TBE gel containing 1:40,000 GelRed DNA stain (Biotium). Plasmids found to contain bands corresponding to the insert were further analyzed by sequencing to confirm that the insert was in frame with downstream epitope tags. Modified versions of the plasmid described in [167] containing various C-terminal epitope tags (cMyc, Strep-TY, 2xHA-DD) were used with a similar cloning approach to introduce various epitope tags at genomic loci in these studies.

2.3 Transfection, drug selection, and isolation of clones

The plasmid DNA to be used for transfection was first linearized by restriction digestion overnight, and purified by phenol:chloroform extraction [168]. The purified DNA was isolated by ethanol precipitation [169], and was collected by centrifugation for 10 minutes at 4°C at 10,000 rcf. The pelleted DNA was left uncapped in the tissue culture hood for at least 1 hour to air dry, and was then dissolved in 400 µL of Cytomix buffer

(10 mM KPO_4, 120 mM KCl, 150 μM $CaCl_2$, 5 mM $MgCl_2$, 25mM Hepes, 2mM EDTA). To prepare parasites for transfection, freshly lysed parasites were pelleted by centrifugation for 10 minutes at 1000 rcf, washed with 10 mL of Cytomix buffer, and pelleted with an additional 10-minute spin at 1000 rcf. Parasites were then resuspended in Cytomix buffer to yield $3x10^7$ parasites in 400 μL of buffer. The resuspended parasites and DNA were combined and transferred to a 4 mm gap BTX disposable electroporation cuvette, and electroporated at 1500 V, 25 Ω. Transfected parasites were then transferred to tissue culture flasks with confluent HFF monolayer, incubated overnight, and the next day media was replaced with media containing drug for selection.

Two drug selection approaches were used to generate stable parasite strains. Parasites lacking the HXGPRT rely on the function of inosine-monophosphate dehydrogenase (IMPDH) to generate guanosine monophosphate (GMP) required for purine biosynthesis. Therefore, inhibition of IMPDH by mycophenolic acid (MPA) kills parasites lacking HXGPRT. This allows for positive selection for parasites that have integrated plasmids containing the HXGPRT minigene cassette by treatment with 25 μg/mL MPA and 25 μg/mL xanthine [170]. Parasites containing the HXGPRT gene are able to survive MPA treatment when supplemented with xanthine, which can be used to generate GMP through the activities of HXGPRT and GMP synthestase. A second selection approach utilizes a mutated dihydrofolate reductase-thymidlate synthase selection (DHFR-TS) cassette that produces a DHFR-TS enzyme that is resistant to the drug pyrimethamine [171]. Parasites transfected with plasmids containing the mutant DHFR-TS minigene were therefore selected by treatment with 1μM pyrimethamine.

Regardless of selection approach, parasites were maintained under drug for at least 3 passages, and were then cloned into 96-well plates by limiting dilution to isolate single parasite clones. Recovered parasite clones were screened for proper integration by PCR, immunofluorescence microscopy (IFA) and immunoblotting to confirm expression of tagged protein.

2.4 Immunoblotting

Parasites that had been harvested intracellularly by syringe lysis, or that were freshly egressed, were pelleted by centrifugation for 10 minutes at 1000 rcf. The collected parasite pellet was then washed once with cold PBS, and pelleted by centrifugation as before. The pellet was lysed in ice-cold radio immunoprecipitation assay (RIPA) buffer for 30 minutes at 4°C with gentle mixing. The lysate was then centrifuged for 10 minutes at 13,000 rcf at 4°C to pellet insoluble debris, and the cleared

supernatant was transferred to a new Eppendorf tube. A 1:10 dilution of cleared lysate in water was prepared and used to quantitate total protein concentration using a bicinchoninic acid (BCA) assay (Pierce) according to manufacturers' protocol. An equal amount of total protein for each strain or condition was separated by SDS-PAGE, with total protein loadings between 20 and 100 µg, depending on the experimental conditions. Alternatively, parasite lysates were normalized to parasite number by counting using a haemocytometer and resuspending the pellet in a volume of RIPA to yield 10^6 parasites per µL.

Unless otherwise specified, all SDS-PAGE assays were performed using 4-20% gradient gels (Bio-Rad, Mini-PROTEAN® TGX™) in a Tris/Glycine/SDS running buffer (25mM Tris, 192 mM glycine, 0.1% SDS, pH 8.3), and were electrophoresed at 100 V for 1 hour and 35 minutes. Gels were then electrotransferred to a nitrocellulose membrane in a Tris/Glycine/methanol buffer (25 mM Tris, 192 mM glycine, 20% methanol) for 1 hour at 100 V, or for 12-16 hours at 24 V, 4°C. Nitrocellulose membranes were rinsed once with water and the transfer was visually inspected for air bubbles or irregularities by staining with Ponceau S Staining Solution (1 mg/mL Ponceau S, 5% acetic acid) for 5 minutes. The blot was then washed with Tris buffered saline with 0.1% Tween-20 (TBST) for 30 minutes to remove Ponceau S Stain, and was blocked for 30 minutes in and 5% (w/v) dry milk in TBST. Primary antibodies diluted in milk/TBST were incubated for 1.5 hours at room temperature, or overnight at 4°C on a rocker. Primary antibodies used in these studies are listed in **Appendix 2**. Blots were washed three times for 10 minutes with TBST, and incubated with horseradish peroxidase (HRP)-conjugated secondary antibodies for 45 minutes at room temperature in milk/TBST. The membrane was then washed three times with TBST for 10 minutes, and proteins were detected with SuperSignal West Femto substrate (Thermo Fisher) and visualized with a FluorChem R imager (Bio-Techne).

2.5 Immunofluorescence assays

For immunofluorescence (IFA) assays of intracellular parasites, parasites were inoculated into a confluent HFF monolayer grown on a glass coverslip in a 12-well tissue culture plate and incubated at 37°C, 5% CO_2. The infected monolayer was then fixed for 15 minutes with 4% paraformaldehyde in phosphate buffered saline (PBS). The fixed coverslips were washed twice with PBS, blocked in PBS with 3% bovine serum albumin (BSA) for 15 minutes, and permeablized with 3% BSA/PBS with 0.2% Triton X-100 for 30 minutes. Primary antibodies were incubated in 3% BSA/PBS + Triton X-100 for 1.5

hours at room temperature, or overnight at 4°C. Coverslips were then washed three times for 15 minutes with PBS, and incubated with 3% BSA/PBS containing fluorophore-conjugated secondary antibodies for 45 minutes at room temperature. After an additional three 15 minute PBS washes, coverslips were stained with DAPI in PBS for 5 minutes, followed by three 5 minute washes, and were mounted onto slides using Vecta Shield mounting media. Primary antibodies used for IFA in this study are listed in **Appendix 2**.

For extracellular IFAs, coverslips were placed in a 12-well plate and were incubated in a 0.01% Poly-L-lysine solution for 30 minutes in the tissue culture hood. Coated coverslips were then washed three times with PBS, and were allowed to air dry for at least 1 hour prior to use. Extracellular parasites, either freshly lysed or syringe lysed and filtered, were washed as described previously, added to the Poly-L-lysine-coated coverslips and were placed in a 4°C refrigerator for 15-30 minutes to allow parasites to settle and attach to the coverslip. The coverslips were then processed for IFA as described above for intracellular IFA analyses.

2.6 Doubling Assays

Intracellular parasites were manually released from host cells by passage through a 27-gauge needle, and were filtered through a 3 µm filter to remove host cell debris. Filtered parasites were then pelleted by centrifugation for 10 minutes at 1000 rcf, and were resuspended in media for counting using a haemocytometer. A total of 100,000 parasites were used to infect a confluent HFF monolayer in a 12-well plate. Two-hours after infection, the monolayers were washed three times with media to remove any parasites that remained extracellular, and the media was replaced and stored in an incubator at 37°C, 5% CO_2. At either 24 or 48 hours post infection, cells were fixed with ice-cold methanol for 30 seconds, allowed to dry, and stained using Differential Quik Stain kit (Polysciences, Inc.). At least 100 vacuoles for each well were scored for the number of parasites per vacuole, and the raw counts were converted to percentages. Graphs represent the average of three independent experiments unless otherwise specified.

2.7 Plaque assays

Intracellular parasites were harvested as described in Section 2.6, and 500 parasites were used to infect a confluent HFF monolayer in 12-well plates. Infected plates were incubated at 37°C, 5% CO_2 and were left undisturbed for 5 days. The monolayer was then fixed with cold methanol, allowed to air dry, and stained with Crystal Violet dye solution (Sigma Aldrich). After rinsing with PBS, stained plates were allowed

to dry and were imaged on a FluorChem R imager (Bio-Techne). Plaque number was scored by manually counting the number of plaques in each well, while calculation of area of host cell lysis was done using the ColonyArea plug-in in ImageJ [172].

2.8 Egress assays

Freshly lysed parasites were used to inoculate confluent HFF monolayers in 12-well plates and incubated for 24-30 hours at 37°C, 5% CO_2. Media was then aspirated and monolayers were washed twice with HBSS pre-warmed to 37°C. Following the second wash, the HBSS was replaced with HBSS containing drug or vehicle, and plates were incubated for 2 minutes at 37°C, 5% CO_2. The monolayers were then fixed with methanol, stained with Differential Quik Stain, and a minimum of 100 vacuoles per condition were scored as intracellular or egressed to determine percent egress.

Egress was also quantitatively assessed using the CytoTox-ONE™ Homogenous Membrane Integrity Assay (Promega) to measure lactate dehydrogenase (LDH) released from host cells as a result of parasite egress as described in [173]. Confluent HFF monolayers were infected with 5 x 10^4 RHΔ*hxgprt* parasites per well in 96-well format. Twenty-four hours post infection, the monolayers were washed with DMEM supplemented with 1% FBS, and were incubated in the same media with drug in a two-fold serial dilution, or vehicle, with each treatment done in technical triplicate. After a 15-minute incubation at 37°C, 50 μL of CytoxONE Assay Buffer with substrate was added to each well and incubated 5 minutes at 25°C. The reaction was stopped by addition of 25 μL stop solution to each well, and plates were read on a plate reader at 560nm excitation and 590nm emission.

2.9 Co-immunoprecipitation assays

Co-immunoprecipitation (co-IP) assays in which the precipitated protein was visualized by immunoblotting used approximately 5 x 10^7 freshly egressed parasites. To identify interacting proteins by mass spectrometry, approximately 10^9 freshly egressed parasites were used. For both approaches, the extracellular parasites were collected by centrifugation for 10 minutes at 1000 rcf and 4°C, and the pellet was washed once with cold PBS. The pellet was then re-suspended in 150 μL (small-scale co-IP) or 500 μL (co-IP for mass spectrometry) of ice-cold Pierce Co-IP Lysis Buffer supplemented with protease and phosphatase inhibitor cocktail (CST). The pellet was lysed for 30 minutes at 4°C with gentle mixing, and was sonicated for 10 seconds using a microtip sonicator. The lysates were centrifuged for 10 minutes at 13,000 rcf and 4°C to remove insoluble debris, and the soluble fraction was transferred to a new 1.5 mL microfuge tube. Lysates

were first incubated for 30 minutes at 4°C with mouse IgG-conjugated magnetic beads (CST) to remove proteins that bound non-specifically to the beads. Following this incubation, the beads were collected on a magnet, and the pre-cleared lysate was transferred to a new 1.5 mL microfuge tube and incubated for 1 hour at 4°C with magnetic beads pre-conjugated with antibodies against the epitope tag on the target protein (either HA or cMyc). The beads were then collected on a magnet and washed three times with Co-IP Lysis Buffer, and twice with PBS. For detection of immunoprecipitated proteins by immunoblotting, the precipitated proteins were eluted off of the magnetic beads by the addition of 30 μL 2xSDS-PAGE buffer containing 5% β -mercaptoethanol and boiled for 5 minutes at 95°C.

Alternatively, the washed beads were submitted to the Indiana University School of Medicine Proteomics Core facility for protein identification by mass spectrometry. The on-bead samples were first dentatured in 8M urea, reduced with 5 mM (tris(2-carboxyethyl)phosphine), and alkylated with 10 mM chloroacetamide. Alkylated samples were then digested with 0.3 μg endoproteinase LysC (sequencing grade, Roche Diagnostics) overnight at 37°C. The samples were then diluted to a final concentration of 2M urea using 100 mM Tris-HCl, pH 8.5, and digested with 0.5 μg trypsin (Promega Gold) overnight at 37°C. Digested peptides were injected onto a 15 cm C18 column (PepMap, 3μm) on a Thermo Dionex UltiMate 3000 RSLCnano chromatography system, and eluted with a linear gradient from 3 to 40% acetonitrile (in water with 0.1% formic acid) over 120 min room temperature at a flow rate of 700 nL/min. Effluent was electrosprayed into a Orbitrap Velos Pro (Thermo-Fisher Scientific) mass spectrometer for analysis. Data analysis was performed using SEQUEST HT within Proteome Discoverer 2.1 (Thermo) and searched against the *Toxoplasma gondii* database (www.toxodb.org, TgondiiGT1_AnnotatedProteins version 29) with common contaminants using SEQUEST HT with an FDR of ≤1%. Results were imported into Scaffold 4 Q+ (Proteome Software) for additional analysis.

2.10 Bioinformatics: sequence alignments, structural modeling and virtual docking

Databases used for the retrieval and analysis of gene and protein sequences include the *Toxoplasma* database (ToxoDB, www.toxodb.org) [174], the National Center for Biotechnology Information database (www.ncbi.nlm.nih.gov) [175–177], and the Eukaryotic Pathogens database (EupathDB, www.eupathdb.org) [178]. Alignment of amino acid sequences and generation of phylogenetic trees was performed using

Clustal Omega [179]. Phylogenetic analyses were done using the PhyML 3.0 webserver (http://www.atgc-montpellier.fr/phyml/) using all default settings and with bootstrapping set at 100 [180]. The I-TASSER server [181] was used to generate the predicted TgAtg8 protein structure, supplying the full TgAtg8 protein sequence as input and without any modifications to default settings. Docking simulations were done using the SwissDock server [182] providing the solved PfAtg8 (PDB code 4EOY, [107]) structure or the output of the I-TASSER TgAtg8 model as input for the target, and the ZINC accession numbers for the MMV compounds as input for the ligands. All docking was done using the default/accurate specifications and without defining a region of interest. Docking results were visualized and screened using the ViewDock tool in UCSF Chimera [183,184]. Modeling of the K23 mutations and their effect on surface potential was done using SwissPDB Viewer [185].

2.14 Quantitative real-time PCR

Quantitative assessment of mRNA transcript levels was done using the Fast SYBR® Green Master Mix kit (ThermoFisher) according to the protocol provided by the manufacturer. These reactions were performed using cDNA prepared as described in section 2.2. Relative quantification of transcript levels was performed using the $2^{-\Delta\Delta Ct}$ methodology as described in [186], using alpha-tubulin (TUBA1) as the reference gene for normalization. Primers for qPCR were designed using the online software tool Primer3 (v. 0.4.0) [187] that selects for primer pairs with optimal thermodynamic properties to avoid hairpin formation and primer dimerization, and are listed in **Appendix 1**.

2.15 Expression and purification of recombinant TgAtg8

Recombinant, N-terminally 6xHis tagged TgAtg8 was generated by cloning the TgAtg8 coding sequence into NdeI/BamHI linearized pET19b expression plasmid using the In-Fusion® HD Cloning Kit (Clontech). The final construct was confirmed by sequencing and was transformed into Rosetta™ competent cells (Novagen), a derivative of BL21 DE3 pLysS cells that allows for expression of eukaryotic proteins containing codons rarely used in *E. coli* by supplying additional tRNAs on a secondary plasmid. Large (250 mL) bacterial cultures were grown in LB containing 100 µg/mL ampicillin at 250 rpm, 37°C, and the growth was monitored by measurement of OD_{600} using a NanoDrop One spectrophotometer. When the cultures reached an optical density of 0.6 – 0.8, protein expression was induced by addition of IPTG to a final concentration of 1 mM. Induction of 6xHis TgAtg8 was confirmed by SDS-PAGE analysis of bacterial

lysates before and after IPTG induction as shown by Coomassie or silver staining. After a 2 hour incubation following induction, bacterial pellets were collected by centrifugation at 4000 rcf for 20 minutes at 4°C, and the pellets were processed for purification using the TALON Metal Affinity Resin kit (Clontech) according to the manufacturer's protocol. Eluted proteins were concentrated using Vivaspin columns (GE Life Sciences) with a molecular weight cut-off of 3 kDa. Protein concentrations were determined using a NanoDrop One spectrophotometer and were further confirmed by BCA assay (Pierce). The purified TgAtg8 protein was analyzed by SDS-PAGE and silver staining, and was found to be >90% pure as determined by densitometry analysis using ImageJ [188,189].

2.16 Acetyl-TgAtg8-K23 antibody production and analysis

In an attempt to generate an Atg8 K23-acetyl specific antibody, two rabbits were immunized with a peptide corresponding to amino acids 18-32 of TgAtg8, containing acetylated-K23 [HRIRA-K(Acetyl)-YPNRIPVIC]. Four immunizations with the acetyl-K23 peptide were given over 13-weeks, and at the conclusion the sera were collected from both animals and were pooled for affinity purification. The serum was first purified over a column containing the non-acetyl-K23 peptide to remove any antibodies that recognized TgAtg8 independently of its acetylation status. The flow through was then purified over an affinity column containing the acetyl-K23 peptide. Pacific Immunology Corporation (Ramona, CA) performed all steps of the antibody production, including peptide synthesis, and confirmed the specificity of the affinity purified acetyl-K23 antibody by ELISA.

Upon the receipt of the affinity-purified antibodies, both antibodies were tested for their reactivity to additional peptides containing K23 mutants used in our studies (K23R, K23A, K23Q). To this end, 20 µg of each peptide was spotted onto a nitrocellulose membrane and allowed to air dry for 1.5 hours. The membrane was then blocked for 1hr in 5% milk/TBST, and was probed with both affinity purified antibodies diluted 1:1000 in milk/TBST for 1.5 hours. The membranes were then washed for 30 minutes in TBST, and probed with HRP-conjugated goat anti-rabbit secondary antibodies for 45 minutes. The membrane was washed for an additional 30 minutes and detected using SuperSignal West Femto substrate and visualized with a FluorChem R imager.

2.17 Methods of autophagy induction

The two previously established methods used to induce autophagy in these studies were treatment of intracellular parasites with the ionophore monensin [154], and starvation of extracellular parasites by incubation in HBSS [94]. For monensin treatment,

confluent monolayers of HFFs in tissue culture flasks (immunoblotting) or grown on glass coverslips in 12-well plates (IFA) were infected with freshly lysed parasites. For IFA experiments, the infected monolayers were washed twice with 1% FBS media 24 hours after infection, and was incubated in media supplemented with monensin at 1 ng/mL or vehicle (ethanol) for 6-24 hours. In some experiments, the autophagy inhibitor 3-methyladenine was included during monensin treatment at a final concentration of 10 mM. For monitoring of TgAtg8 lipidation following monensin treatment, 75 cm^2 tissue culture flasks containing confluent HFFs were infected with 10^7 freshly lysed parasites. After a 36-hour incubation, the monolayer was washed twice with 1% FBS media, and incubated in media containing monensin or vehicle for 6 hours. The monolayer was then processed for immunoblotting as described in section 2.4.

Alternatively, intracellular parasites were syringe lysed from the host cells, centrifuged for 10 minutes at 1000 rcf, and washed twice with HBSS. The pellet was then resuspended in HBSS and incubated in 15 mL polypropylene tubes, loosely capped, for 8 hours in a 37°C, 5% CO_2 tissue culture incubator. For visualization of GFP-Atg8 punctae following HBSS starvation, parasites were processed for extracellular IFA as described in section 2.5. Alternatively, parasites were pelleted by centrifugation for 10 minutes at 1000 rcf and processed to visualize TgAtg8 lipidation status by immoblotting as described in section 2.4.

2.18 CPRG assay for generation of growth inhibition curves

To generate growth inhibition curves to determine EC_{50} values for various compounds, HFF monolayers in 96-well plates were inoculated with 100 manually released β-galactosidase expressing parasites [190]. Four days after inoculation, chlorophenol red-β-D-galactopyranoside (CPRG) was added to each well at a final concentration of 100 μM. Plates were read 24 hours after addition of CPRG on a Synergy H1 (BioTek) plate reader at 570 nm excitation and 630 nm emission. Averages from three biological replicates were used to generate growth inhibition curves using Prism (GraphPad v 7.0a), normalizing to uninfected HFF (100% inhibition) and dimethylsulfoxide (DMSO) vehicle (0% inhibition) wells. Results from three independent replicates were plotted in Prism, and curves were fit to the log-transformed (x-axis) data by non-linear regression, using the four-parameter, variable slope settings.

2.19 Differential Scanning Fluorimetry

Differential scanning fluorimetry analyses (also referred to as thermal shift assays) were preformed to assess the effects of TgAtg8 K23 mutations on intrinsic

protein stability and interaction with the TgAtg3 AIM peptide. This assay measures the fluorescence of a SYPRO Orange thermofluor that binds nonspecifically to hydrophobic surfaces exposed during protein unfolding [191]. Assays were conducted in a 96-well plate in 100 mM HEPES (pH 7.0) buffer containing 150 mM NaCl and 5x SYPRO orange dye (Invitrogen) at a final volume of 20 μl per well. Each reaction mixture contained purified recombinant Atg8 at a final concentration of 8 μM, in the presence or absence of TgAtg3 AIM peptide (corresponding to residues 160-176) or cMyc control peptide. All reactions were heated from 25°C to 95°C at a ramp rate of 1°C/min on a StepOne Plus RT-PCR machine. SYPRO Orange fluorescence was measured at each temperature (StepOne Plus Filter 4; 488 nm/610 nm excitation and emission wavelengths), and the obtained values were plotted against temperature. The melting temperature (T_m) was obtained by taking the first derivative of this graph using Prism, and T_m values from triplicate experiments were used to calculate the T_m for each condition. Raw fluorescence values were normalized using Prism (minimum value set to 0%, maximum value set to 100%) and plotted as "Percent Unfolded".

2.20 Cytosolic Ca^{2+} Measurements

Freshly egressed parasites were passed through a 3 μm filter to remove host cell debris, and were washed once with Intracellular Buffer (IB) (5 mm NaCl, 144 mm KCl, 5.6 mm D-glucose, 1 mm $MgCl_2$, 2 mm EGTA, 25 mm HEPES, pH 7.4). The parasites were then loaded with 2.5 μM Fluo-4 AM calcium indicator dye (ThermoFisher) in IB for 1 hour at room temperature. Following a 30-minute wash with IB to remove extracellular dye, the parasites were resuspended in IB to a final concentration of 10^7 parasites per mL, and 100 μL were transferred to each well in a 96-well plate. A Synergy H1 (BioTek) plate reader was used to monitor Fluo-4 AM fluorescence at 488 nm excitation and 524 nm emission wavelengths. Each treatment condition was performed in triplicate, with measurements taken every 5 seconds. After a 1 minute period to establish baseline fluorescence levels, 10 μL of Hanks' Balanced Salt Solution (calcium and magnesium-free) containing DMSO vehicle, A23187, or MMV1 was added to each well using the Synergy H1 injectors and measurements were taken every 5 seconds for 10 minutes. Data were analyzed using Prism, with graphs representing the Fluo4-AM fluorescence intensities after DMSO subtraction.

2.21 Statistical Analyses

All statistical analysis performed in this study were conducted using Prism (GraphPad v 7.0a). All normalization and linear or non-linear regression techniques used

are described in their respective Methods sections. All graphs containing asterisks to denote significance contain information regarding p-value cut-off and statistical test used to determin significance in the respective figure legends. Statistical analysis of mass spectrometry results for TgAtg8 and TgAtg3 interactomes were conducted using the SAINTExpress [192,193] program with default settings (www.crapome.org). Raw total spectrum counts were supplied in list or matrix format according to guidelines. Proteins were considered significant if they were present in at least 2 out of 3 IPs, and had a fold-change (FC-B) value greater than 2.0 and SAINT Probability (SP) score ≥ 0.75.

Chapter 3: Results

Aim 1: Determine the functional consequences of TgAtg8 lysine-23 acetylation on the TgAtg3-TgAtg8 interaction

Acetylation of autophagy proteins is emerging as a major mechanism by which the autophagy pathway is regulated in eukaryotes. In particular, acetylation has been shown to regulate the Atg3-Atg8 interaction, and the subcellular localization of Atg8 family proteins. We had previously identified that autophagy was induced in response to drug treatment [154]. Additionally, we discovered that TgAtg8 was acetylated at lysine-23 [161]. Therefore, we sought to determine whether acetylation of TgAtg8 at lysine-23 regulated TgAtg8 localization or function. Our studies focused primarily on the effects of this modification on the interaction of TgAtg8 with TgAtg3, because this was the only proposed TgAtg8 interacting protein identified in *Toxoplasma* at the time. Using a combination of genetic and biochemical approaches, we determined that TgAtg8 acetylation is not likely to alter the TgAtg3-TgAtg8 interaction. However, our results suggest that this modification may affect TgAtg8 protein stability, potentially through regulation of TgAtg8 protein-protein interactions.

3.1 *Toxoplasma* Atg8 acetylation occurs on a conserved lysine residue near the TgAtg8 W-site binding pocket

Characterization of global protein acetylation in *Toxoplasma* tachyzoites identified that the parasite Atg8 homologue is acetylated at lysine 23 (K23) [161]. K23 acetylation on TgAtg8 was found only in extracellular parasites, leading us to hypothesize that this PTM might be involved in regulating TgAtg8 function in response to extracellular stress. Bioinformatics analyses showed that lysine-23 was conserved in numerous Atg8 homologues in higher eukaryotes, including *P. falciparum* Atg8, and 4 of the 6 human Atg8 proteins (**Figure 5**). Importantly, the analogous lysine residue (K24) in the human Atg8 homologue HsGABARAPL2 (also known as GATE-16) was identified as acetylated by two different proteomics studies looking at global protein acetylation [194,195]. Although the conservation of this PTM across eukaryotes is intriguing and may represent a conserved functional role of this modification, the biological significance of GABARAPL2/GATE-16 K24 acetylation remains unknown.

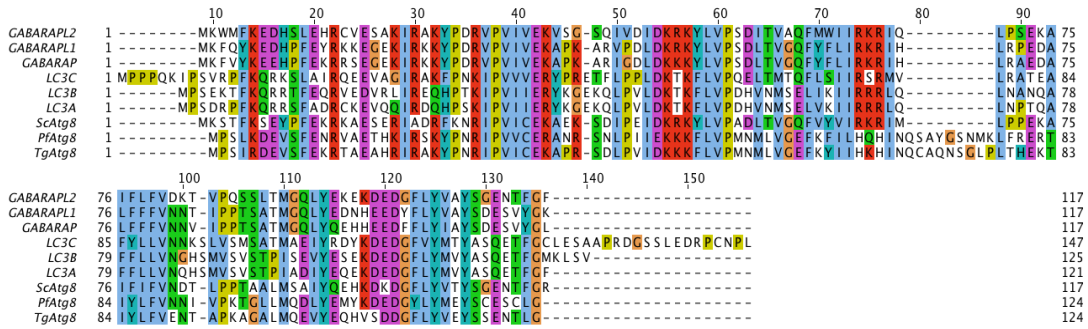

Figure 5: Amino acid sequence alignment of eukaryotic Atg8 homologues. ClustalOmega was used to align the amino acid sequences of Atg8 proteins from *Toxoplasma* (TgAtg8), *Plasmodium falciparum* (PfAtg8), *Saccharomyces cerevisiae* (ScAtg8), and the six human Atg8 homologues LC3A/B/C, GABARAP, and GABARAPL1/2.

Acetylation of lysine residues can alter many aspects of protein function, including protein stability, subcellular localization, protein-protein interactions, and enzymatic activity [195–197]. Additionally, the acetylation status of the human Atg8 protein LC3B regulates its localization by modulating its interaction with the protein DOR [160]. While acetylated, LC3B resides in the nucleus. However, upon deacetylation by Sirt1 LC3B interacts with DOR and translocates to the cytoplasm where it is utilized for autophagosome biogenesis. To gain insight into how acetylation of TgAtg8 at K23 might affect TgAtg8 function, we performed structural modeling using the I-TASSER server to develop a predicted model of TgAtg8 and determine where K23 localized within the TgAtg8 structure (**Figure 6A**). This modeling revealed that K23 localizes on the second alpha-helix in the N-terminus of TgAtg8 (**Figure 6B**). Additionally, this residue was localized adjacent to the W- and L-site binding pockets that facilitate protein-protein interactions between Atg8 and proteins that contain the consensus WXXL Atg8 Interacting Motif (AIM), also referred to as LC3 Interacting Motif (LIR) [198,199]. We therefore hypothesized that acetylation of TgAtg8 at K23 can reversibly neutralize the positive charge on K23, and in doing so, alter TgAtg8 protein-protein interactions.

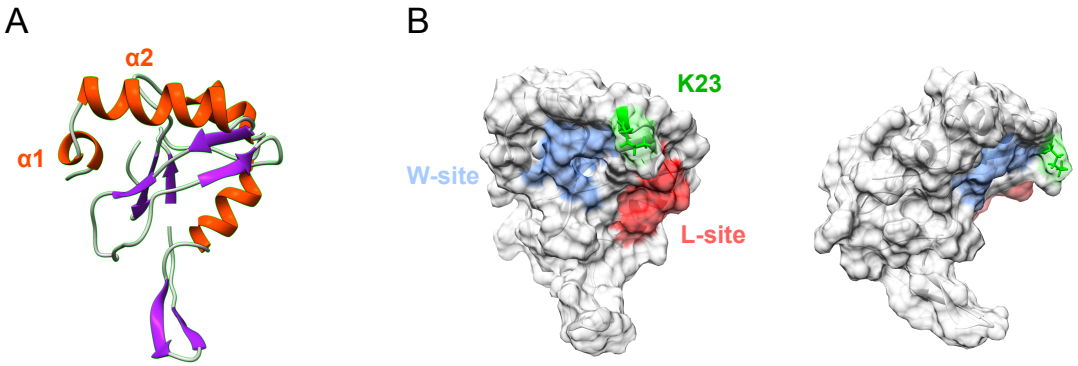

Figure 6: Structural modeling of TgAtg8.
The TgAtg8 amino acid sequence was submitted to the I-TASSER server to predict the three-dimensional protein structure. The predicted model is shown in (A) and is colored according to secondary structure (alpha helices in red, coils in grey, and beta sheets in purple). B) Visualization of the TgAtg8 W-site (blue) and L-site (red) binding pockets that are the sites of interaction with AIM motifs on Atg8 interacting proteins, with relation to the acetylated lysine residue K23, highlighted in green

The functional significance of specific acetylation events is typically determined using site-directed mutagenesis to mutate the acetylated lysine residue to arginine (R) that retains the charge of an unmodified lysine residue while preventing acetylation, glutamine (Q), which is routinely used as an acetyl-lysine mimic and can functionally mimic acetylated lysine residues in a variety of proteins, or alanine (A) to neutralize charge and prevent acetylation [200–203]. We therefore used these established methods to attempt to characterize the effects of K23 acetylation on TgAtg8 function. The effects of these mutations on the TgAtg8 electrostatic surface potential were visualized using the SwissPDB Viewer software program to model the K23R, K23Q, and K23A mutations to the predicted TgAtg8 protein structure. As shown in **Figure 7**, the K23R mutation maintains the positive charge of the alpha-2 helix on which K23 resides, while mutation to glutamine and alanine neutralizes this charge.

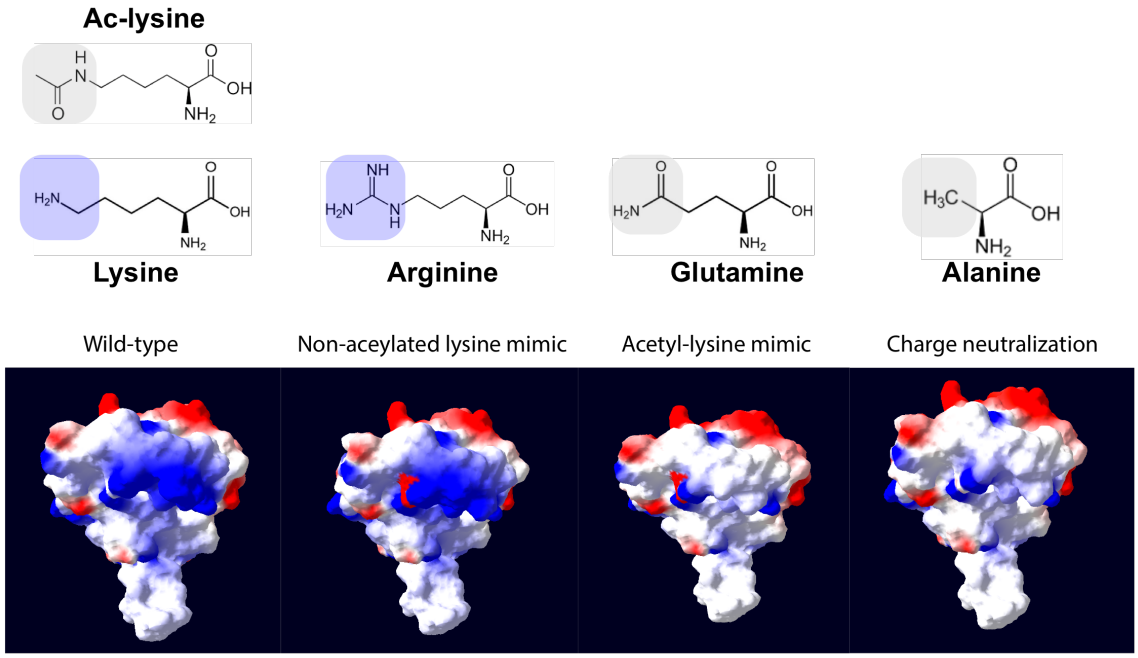

Figure 7: Modeling of K23 mutations and effects on surface potential.
(*top*) Chemical structures of lysine, acetylated lysine, and amino acids used to mimic acetylated and non-acetylated lysine by mutagenesis. Blue box illustrates positively charged side-chains, while gray box represents neutral side-chains. (*bottom*) Modeling of predicted TgAtg8 structure to visualize the effects of each K23 mutation on electrostatic surface potential.

3.2 Ectopic expression of K23 mutants does not affect parasite fitness

We next performed site-directed mutagenesis to introduce the K23R, K23Q, and K23A mutations into an expression plasmid containing a GFP-TgAtg8 fusion protein that was previously developed for use in monitoring TgAtg8 localization in *Toxoplasma* [94]. Each of these constructs was transfected into RHΔ*hxgprt* parasites and single-parasite clones for each were obtained. The expression of each GFP-TgAtg8 K23 mutant protein was confirmed by immunofluorescence assay and immunoblotting. Interestingly, both methods revealed differences in total protein levels, with K23R and K23A mutant proteins showing slightly lower expression, while K23Q mutant GFP-TgAtg8 was slightly higher as compared to wild-type K23K controls (**Figure 8A-B**). Importantly, a similar trend was observed in parasites obtained from multiple, independent transfections, suggesting that the observed differences were not likely due to differences in the genomic location of plasmid integration or number of integrations. Despite these differences in protein levels, the ectopic expression of GFP-Atg8 K23 mutants had no

observable impact on parasite fitness as demonstrated by equivalent rates of replication (**Figure 8C**).

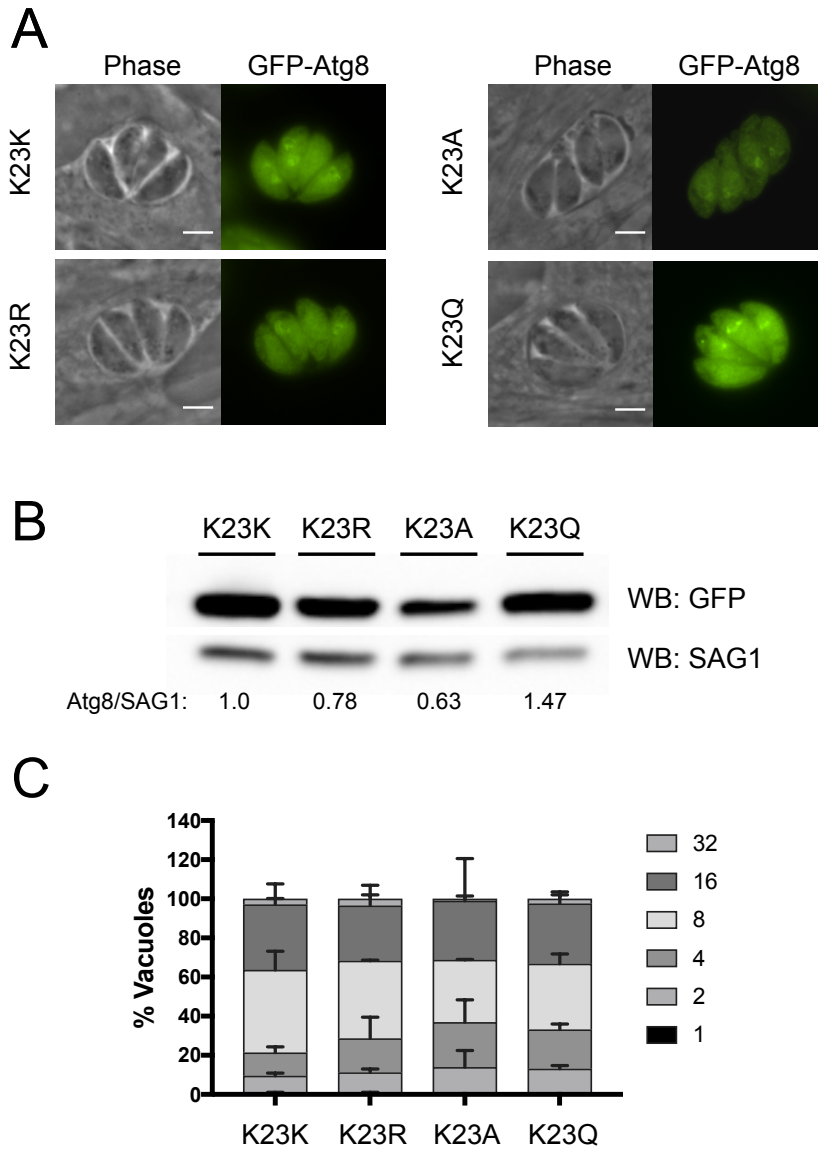

Figure 8: Ectopic expression of GFP-TgAtg8 K23 mutants does not impair parasite viability.
A) Representative IFA images of parasites expressing wild-type K23K or K23 mutant proteins, as visualizes using the GFP epitope tag. All proteins were found to localize predominantly to the cytosol, with additional signal enrichment at the parasite apicoplast. Scale bar represents 3 μm. B) Representative immunoblot of GFP-TgAtg8 proteins stained for anti-GFP or anti-SAG1 (loading control). Values below lanes represent densitometry values for this representative blot as calculated using ImageJ, and are normalized to K23K. C) Doubling assays of parasites ectopically expressing wild-type (K23K) or mutant GFP-Atg8 proteins. Parasites were allowed to replicate for 24 hours, at which point the number of parasites per vacuole was enumerated. Expression of K23 mutant proteins did not alter parasite replication rate (n=3, ± SEM).

3.3 GFP-TgAtg8 WT and K23 mutants localize to the daughter parasite pellicle during division

Previous studies characterizing GFP-TgAtg8 showed that this protein localizes predominantly in the cytoplasm, and is occasionally found to localize to bright punctae that co-localize with the apicoplast [94]. Further studies showed that this localization to the apicoplast increases during parasite division [103]. While characterizing our GFP-TgAtg8 K23 mutant, we observed that in addition to the apicoplast, GFP-TgAtg8 was also enriched at the daughter parasite pellicle during mitosis (**Figure 9**). We confirmed that this localization was TgAtg8 dependent by monitoring the localization of cytosolic GFP (not fused to TgAtg8). Immunofluorescence analyses of parasites expressing cytosolic GFP showed that this protein failed to localize to the daughter pellicle during mitosis (**Figure 10**). As Atg8 is known to interact with membranes through hydrophobic interactions with its N-terminal helices, we tested whether the alteration of charge by mutation of K23 affected the ability of GFP-TgAtg8 to localize to the daughter buds. Mutation of K23 to non-acetylated lysine mimic (K23R) or acetylated-lysine mimic (K23Q) residues did not prevent localization of GFP-TgAtg8 to daughter parasite pellicles during mitosis (**Figure 10**). These studies suggest that TgAtg8 localizes to the daughter parasite pellicle during division independently of its acetylation status.

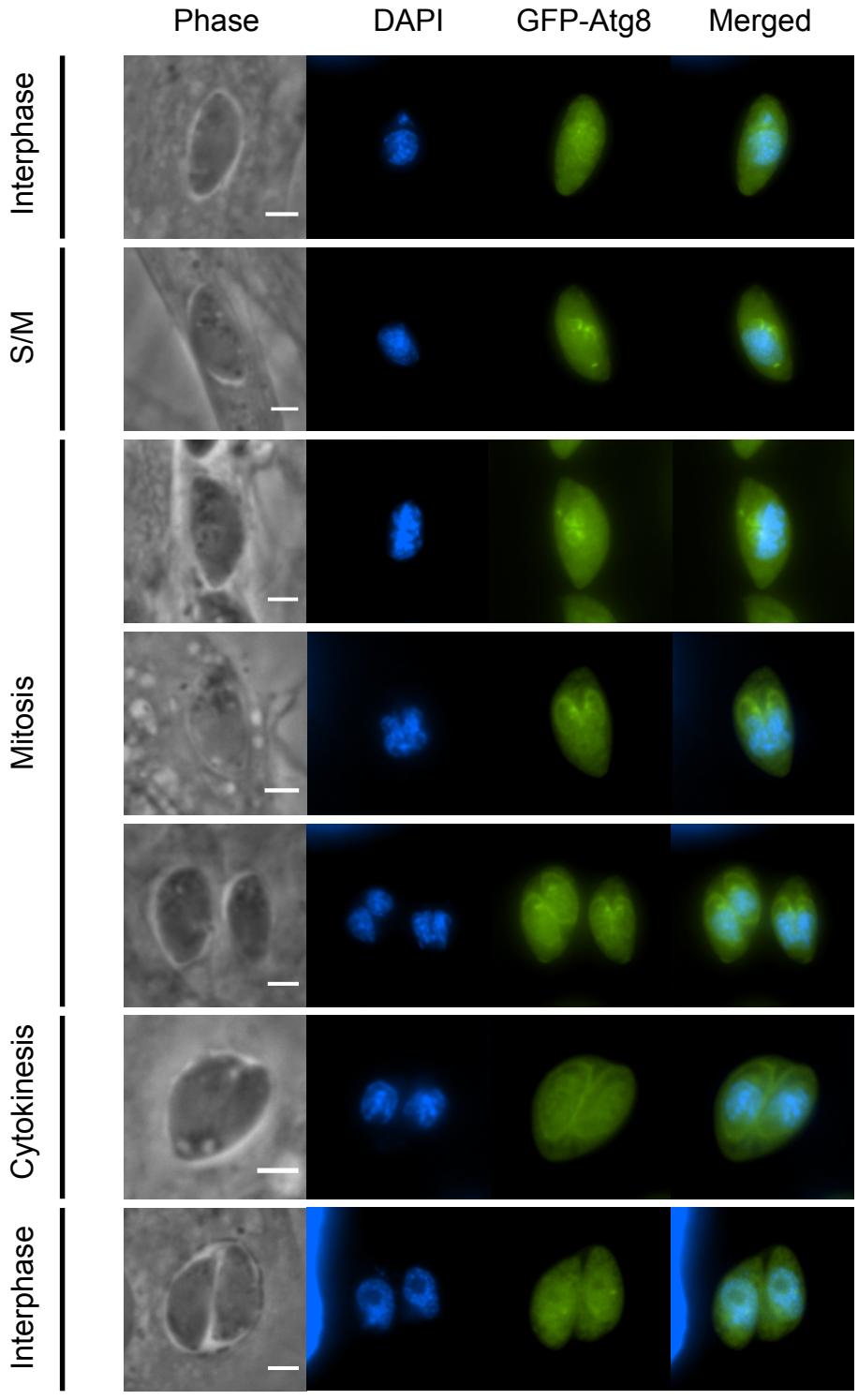

Figure 9: GFP-TgAtg8 is enriched at daughter parasite pellicle during mitosis.
A) IFA analysis of GFP-TgAtg8 during replication revealed that TgAtg8 localizes to the daughter parasite early during division and remains enriched at the daughter pellicle through completion of cytokinesis. GFP-TgAtg8 visualized in green, DAPI staining to visualize nuclei are shown in blue.

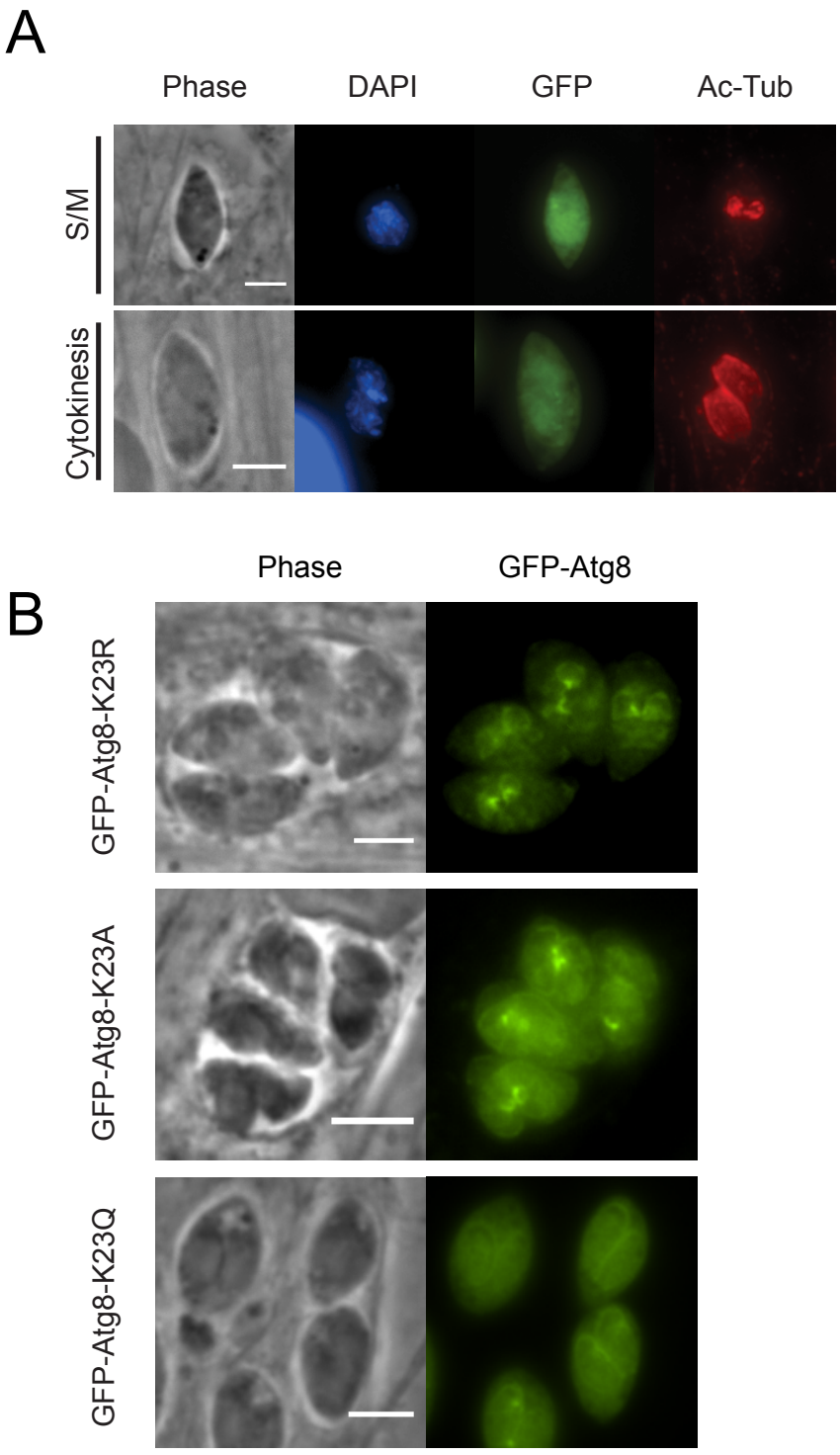

Figure 10: Localization of GFP-TgAtg8 to dividing parasites is not altered by mutation of K23.
A) Parasites expressing cytosolic GFP (green) failed to show enrichment of GFP at the daughter parasites during division. Daughter parasites were visualized by co-staining with acetyl-tubulin (red) to delineate daughter parasite cytoskeleton. B) IFA of GFP-TgAtg8 K23 mutant parasites, showing that all three K23 mutants were found to localize to the daughter parasites during division.

We next attempted to resolve whether mutation of K23 altered the ability of GFP-TgAtg8 proteins to undergo lipidation. Previous studies characterizing GFP-Atg8 in *Toxoplasma* showed that lipidation of the fusion protein is only visible by immunoblotting following extracellular starvation treatment [94]. Therefore, we conducted extracellular starvation assays in HBSS for each of the GFP-TgAtg8 K23 mutant proteins and sought to determine whether each of these proteins was lipidated. We were unable to resolve the two bands corresponding to GFP-TgAtg8 and GFP-TgAtg8-PE by SDS-PAGE using 4-20% gradient gels followed by immunoblotting for GFP (**Figure 11A**). For endogenous Atg8, resolution of the lipidated and unlipidated band is often improved by SDS-PAGE using gels containing 6 M Urea [204]. We also attempted to assess GFP-Atg8 lipidation status using this approach, but were once again unable to resolve the two bands (**Figure 11B**). Therefore, we were unable to assess the effect of TgAtg8 K23 acetylation on lipidation using the GFP-TgAtg8 strains.

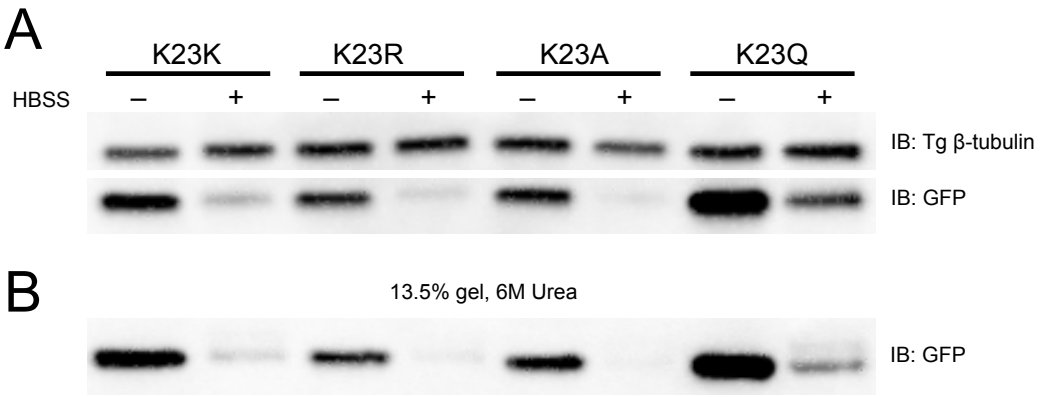

Figure 11: Assessment of GFP-Atg8 K23 mutant lipidation.
A) Immunoblot of GFP-TgAtg8 proteins attempting to visualize GFP-TgAtg8 lipidation after 8 hours of extracellular starvation (HBSS). Proteins were resolved using standard 4-20% Tris/Glycine SDS-PAGE gels, and transferred proteins were visualized with antibodies against GFP (TgAtg8) or *Toxoplasma* beta-tubulin as a loading control. B) Immunoblot of the same samples shown in (A) resolved by SDS-PAGE using a 13.5% separating gel containing 6M urea.

3.4 Generation of endogenously-tagged cMyc-Atg8 K23K and K23R parasite strains

Although parasite fitness did not appear to be altered when GFP-TgAtg8 K23 mutant proteins were ectopically expressed, we hypothesized that the lack of phenotype could be due to the presence of the endogenous TgAtg8 protein in these parasites. We therefore attempted to introduce these K23 mutations at the endogenous *TgAtg8* locus

using double-homologous recombination to replace the *TgAtg8* genomic sequence with a cDNA copy of *TgAtg8* containing wild-type K23K or K23R, A or Q mutations (**Figure 12A**). A cMyc-epitope tag was also introduced at the N-terminus of each of these constructs to allow for subcellular localization by IFA and to assess protein expression, stability and lipidation competence for the K23 mutant proteins.

Viable transfectants were recovered following transfection with the wild-type cMyc-TgAtg8-K23K control plasmid, and proper integration was confirmed by PCR of the *TgAtg8* locus (**Figure 12**). The endogenously tagged cMyc-TgAtg8-K23K protein resolved as two bands by SDS-PAGE and immunoblotting, representing unlipidated TgAtg8 and lipidated TgAtg8 (Atg8-PE). Additionally, cMyc-TgAtg8-K23K correctly localized to the parasite apicoplast, suggesting that the endogenously tagged cMyc-TgAtg8 retained all functionality previously reported for TgAtg8 and GFP-TgAtg8 fusion proteins. Although we easily obtained K23K wild-type cMyc-TgAtg8 parasites, we were unable to recover K23Q or K23A mutant parasites despite numerous attempts, suggesting that these mutations have deleterious effects on tachyzoite viability. We were, however, successful in recovering K23R mutants in one out of six independent transfections, and confirmed the proper integration by PCR (**Figure 13A**).

We next sought to determine the effects of ablation of K23 acetylation on TgAtg8 localization and lipidation by comparing the cMyc-Atg8-K23K and cMyc-Atg8-K23R parasites. Immunofluorescence assays showed that like K23K, the K23R mutant protein predominantly localized to the apicoplast (**Figure 13B**). This was further confirmed by immunoblotting which revealed that the cMyc-Atg8-K23R mutant protein migrated as two bands, representing unlipidated and lipidated TgAtg8 (**Figure 13C**). Interestingly, we observed that the endogenous K23R mutant protein also displayed lower levels of total protein as compared to K23K wild-type, similar to our observations with ectopic GFP-Atg8 K23K and K23R proteins.

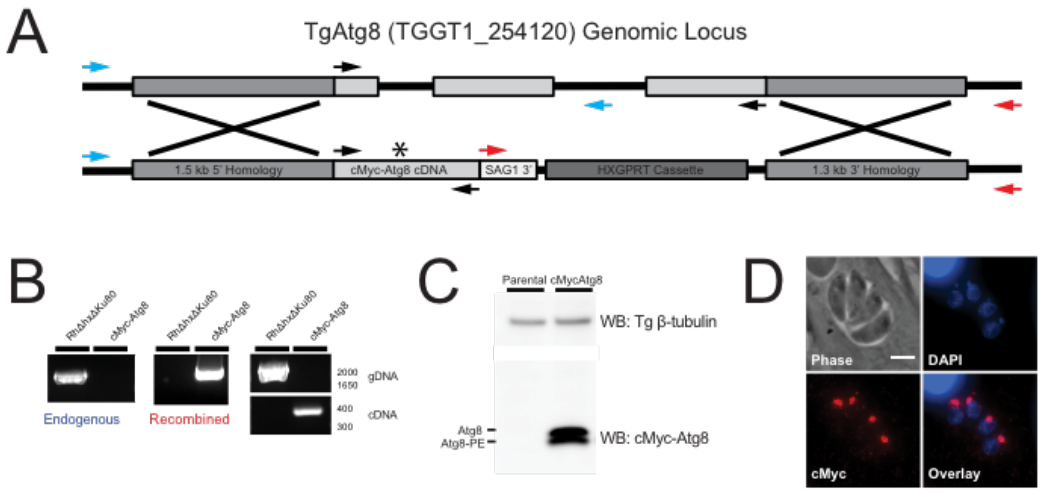

Figure 12: Generation of endogenous cMyc-Atg8 K23K parasites.
A) Diagram of the construct used to target the TgAtg8 genomic locus for replacement with a cMyc-epitope tagged TgAtg8 cDNA sequence. Arrows indicate primer pairs used to confirm proper integration at the endogenous TgAtg8 locus. The blue primer pair amplifies a fragment unique to parental strain, the red pair amplifies unique fragment in recombined strain, and the black pair amplifies a 1791 bp fragment in parental strain and a 372 bp fragment in recombined strain. Asterisks indicates site of K23 mutations. B) PCR products from genomic DNA isolated from cMyc-TgAtg8 and parental (RHΔ*hx*Δ*ku80*) parasites. Blue, red and black arrows refer to the primer pairs described in (A). C) Western blot of lysates from freshly egressed parental RHΔ*hxgprt*Δ*ku80* and cMyc-TgAtg8 parasites, probed with antibodies recognizing the cMyc epitope, and *Toxoplasma* β-tubulin as a loading control. Two bands are observed for cMyc-TgAtg8, representing unmodified (Atg8) and lipidated (Atg8-PE) forms of TgAtg8. D) IFA of cMyc-TgAtg8 parasites stained with DAPI (blue), and for cMyc (red), showing that cMyc-TgAtg8 localizes predominantly to the apicoplast. Scale bar = 3μm.

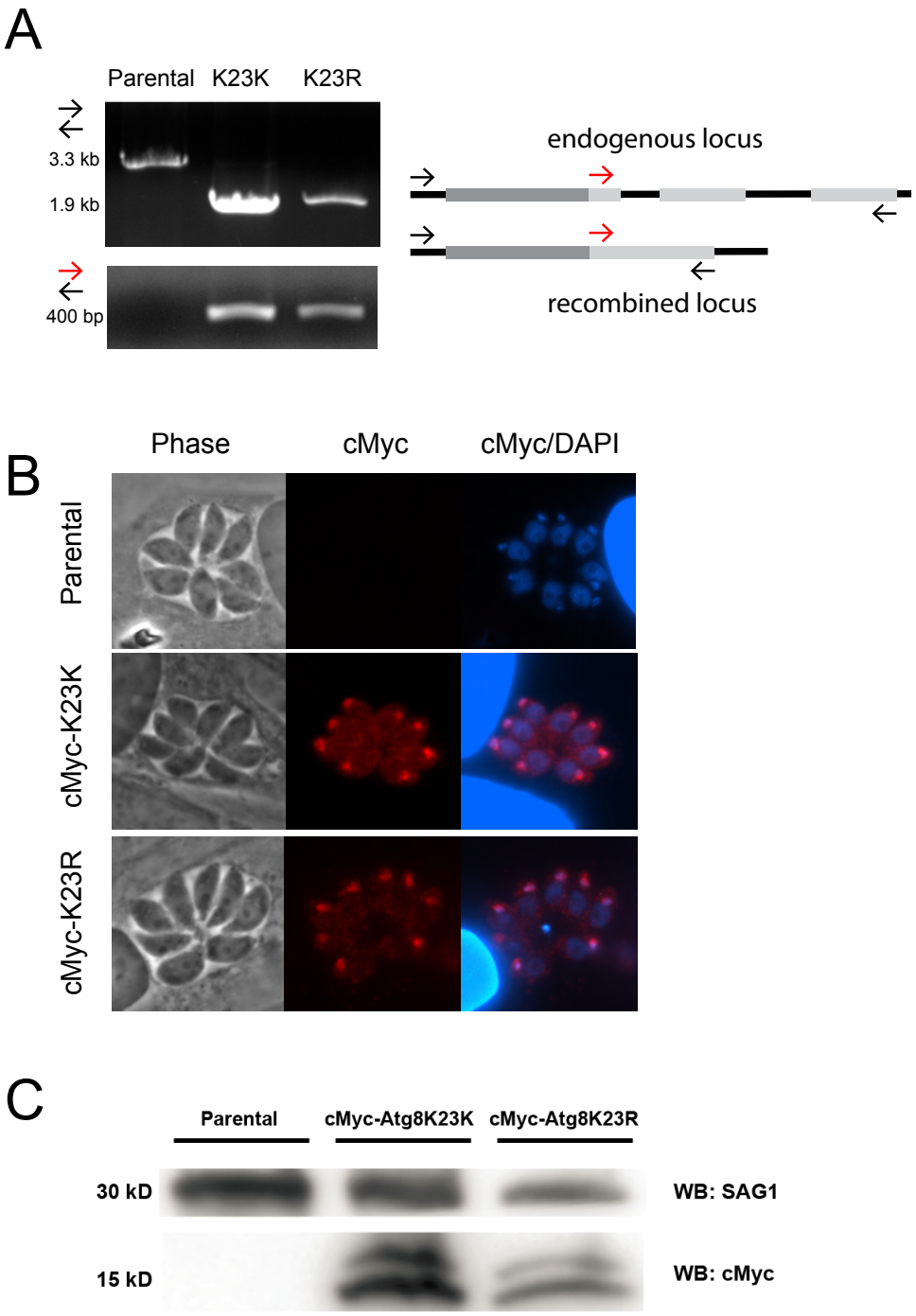

Figure 13: Endogenous K23R mutation does not alter localization to apicoplast or prevent lipidation.
A) PCR of the genomic Atg8 locus in RHΔ*hx*gprtΔ*ku80* parental, wild-type cMyc-Atg8 K23K, or cMyc-Atg8 K23R mutant parasites. Black arrows designate primer pair with forward primer upstream of 5' homology region used for recombination, and reverse primer that binds to 3' end of TgAtg8 CDS. This primer set produces a 3.3 kb amplicon in parental, and a 1.9 kb amplicon in recombined parasites. PCR using a forward primer that binds to the 5' of the TgAtg8 CDS (red) with the reverse TgAtg8 CDS primer (black)

generates a 400 bp amplicon in the recombined TgAtg8 locus. B) IFA analysis staining for cMyc revealed that both K23K and K23R proteins correctly localize to the apicoplast, visualized as the bright foci oriented immediately apical of DAPI-stained nuclei. C) Immunoblot with anti-cMyc showed that both K23K and K23R are present as unlipidated (top band in cMyc blot) and lipidated (bottom band in cMyc blot) forms. The *Toxoplasma* surface antigen SAG1 was used as a loading control.

3.5 Endogenous mutation of K23 to arginine impairs parasite replication and promotes spontaneous differentiation to bradyzoites

While characterizing the localization and lipidation status of cMyc-TgAtg8 K23R, we noticed that the K23R mutant parasites grew significantly slower than the parental and K23K wild-type control parasites. To assess their growth defects, we performed plaque assays to monitor parasite growth over a 5-day period. This assay showed that while the K23K parasites grew similarly to the parental strain, K23R mutants had a severe growth defect, as shown by the reduction in both number and area of plaques that represent destruction of the host cell monolayer as the result of parasite propagation and egress (**Figure 14**). The reduction in the size of plaques observed in the K23R mutant parasites suggested that the rate of intracellular replication was significantly slower than that of K23K and parental parasites. To test this, we performed a doubling assay to determine the number of rounds of division that parasites underwent in a 24-hour period. After allowing the parasites to replicate for 24 hours, the cells were fixed and the number of parasites per vacuole were counted. For both parental and K23K parasites, over half of the vacuoles contained 8 or 16 parasites, indicating that parasites had undergone 3 or 4 rounds of replication (**Figure 14**). In contrast, over 80 percent of the vacuoles for K23R parasites contained 4 or fewer parasites. This data shows that the endogenous mutation of Atg8K23 to arginine significantly impairs tachyzoite replication.

While assessing the growth defects in the K23R mutant parasite strain, we observed that these parasites remained intracellular for over 7 days, forming large, rounded vacuoles with features resembling bradyzoite tissue cysts formed *in vitro*. To determine whether the K23R parasites were undergoing differentiation into bradyzoites, we preformed immunofluorescence assays at 7 days post-infection to visualize two established markers of bradyzoite cysts: staining of the cyst wall glycoproteins using fluorophore-conjugated *Dolichos biflorus* lectin [205], and reactivity with antibodies against the bradyzoite-specific protein BAG1 [206]. Indeed, these analyses revealed at day 7 post infection, over 80% of the vacuoles stained positive with both markers of bradyzoite cysts (**Figure 15A-B**). This was specific to the K23R mutant parasites, as no

vacuoles stained positive for either marker in parental or K23K parasite strains. This observation was further confirmed by performing qPCR for genes specifically expressed during tachyzoite (SAG1) or bradyzoite (BAG1, ENO1, LDH2) stages, which showed that K23R parasites showed a down-regulation of tachyzoite gene markers and significantly higher expression level for bradyzoite specific genes (**Figure 15C**). The ability of the K23R parasites to differentiate into bradyzoites was remarkable, as they were generated in the Type I RHΔ*hxgprt*Δ*ku80* background strain that has a significantly lower ability to differentiate to bradyzoites. Additionally, bradyzoite differentiation *in vitro* in HFFs typically requires exogenous stress, usually in the form of altering pH stress [207,208]; however, the K23R parasites differentiated under normal tissue culture conditions without any such additional stress.

While attempting to further characterize this phenotype, we observed that the K23R mutant parasites lost both their replication defect and bradyzoite differentiation phenotype over the course of 3-4 months in culture. These phenotypes were retained in freshly-thawed stocks of the original parasite clone, but were subsequently and repeatedly lost following 4-5 passages. This adaptation prevented us from conducting complementation assays to determine whether the growth phenotypes could be corrected by complementation with a wild-type copy of TgAtg8, as the cloning procedure requires multiple rounds of passage over the course of multiple weeks. We also attempted to confirm the K23R mutant phenotype by isolating parasite clones from independent transfections, however these attempts were unsuccessful.

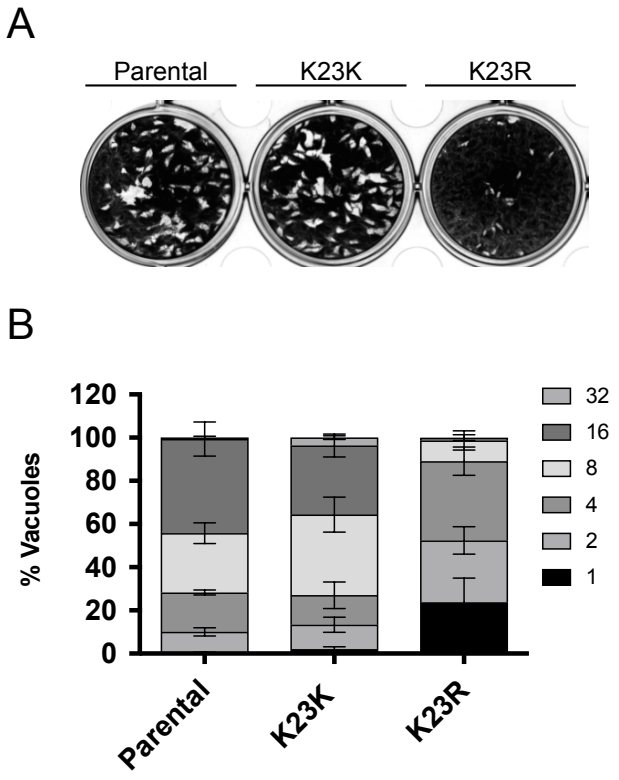

Figure 14: Parasite replication is significantly impaired in K23R endogenous mutant parasites.
A) Representative plaque assay of parental RHΔ*hx*gprtΔ*ku80*, cMyc-Atg8 K23K and cMyc-Atg8 K23R parasites. K23R mutant parasites showed a significant reduction in plaque number and area of host cell lysis indicating impairment of progression through the lytic cycle. B) Doubling assays of parental, K23K and K23R parasites assessing the number of parasites per vacuole at 24 hours post infection. While the majority of parental and K23K vacuoles contained 8 or more parasites, most K23R vacuoles contained 4 or fewer, indicating impairment of parasite replication.

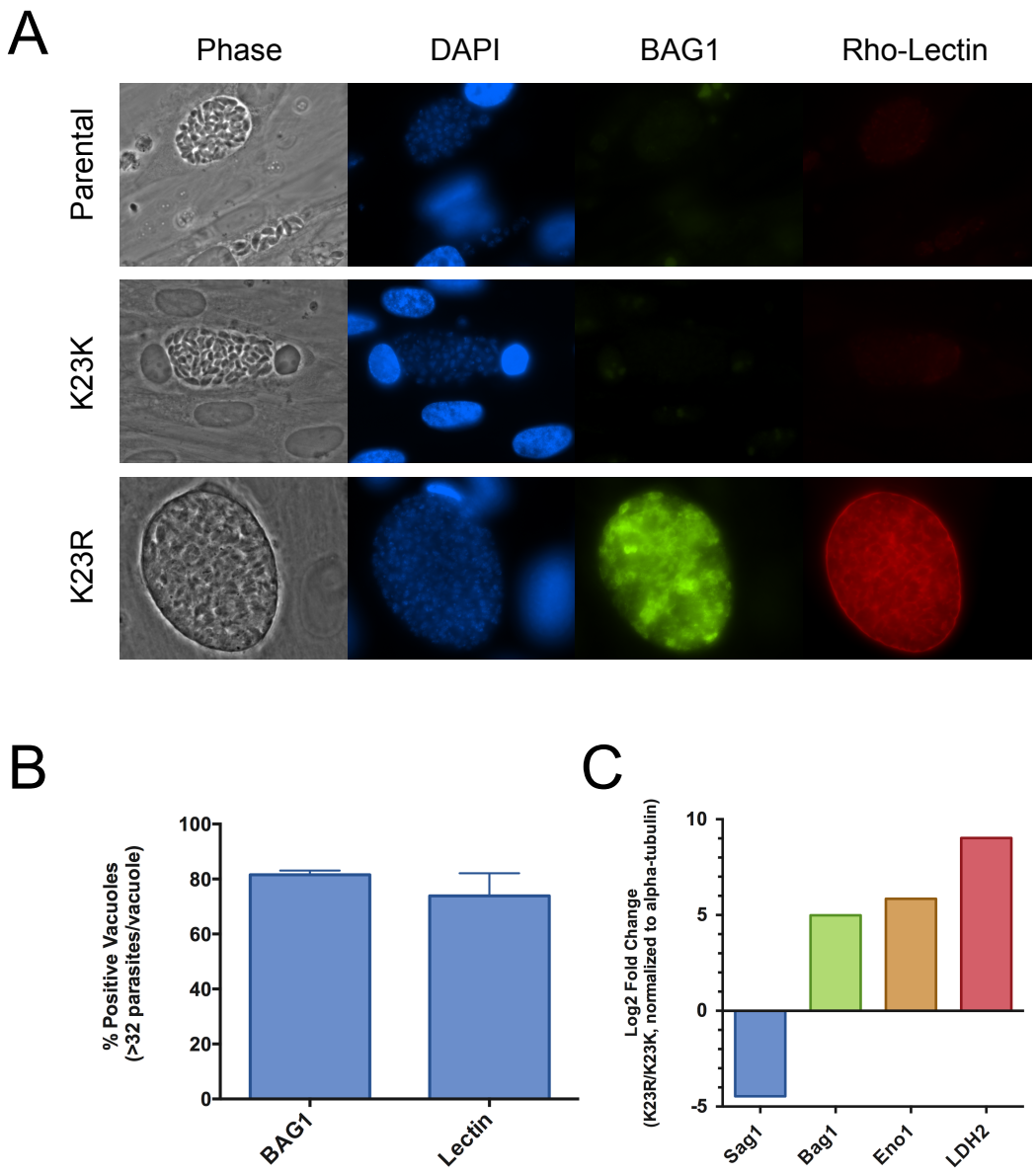

Figure 15: K23R mutant parasites undergo spontaneous differentiation into bradyzoites and form cysts *in vitro*.
A) Representative IFAs of RHΔ*hx*gprtΔ*ku80* parental strain, cMyc-TgAtg8 K23K and K23R parasites, stained with DAPI (blue), bradyzoite-specific chaperone protein BAG1 (green) and rhodamine-conjugated *Dolichos biflorus* lectin (red), which binds to glycoproteins in the bradyzoite tissue cyst wall. Parental and K23K vacuoles were imaged at 66 hours post infection, when vacuoles contained >32 parasites and prior to lysis of the host cell monolayer. K23R vacuoles were imaged Day 7 post-infection. B) Quantitation of percentage of K23R vacuoles that stained positive for BAG1 and lectin (n=3, ± SEM). C) Representative qPCR analysis of tachyzoite specific transcripts (SAG1) and bradyzoite-specific transcripts (BAG1, ENO1, LDH2). Values represent $\log_2$ fold-change in K23R parasites relative to K23K parasites (normalized to alpha-tubulin).

3.6 Attempt to generate a TgAtg8 K23-acetyl specific antibody

To overcome the difficulties encountered in dissecting the role of TgAtg8 K23-acetylation using a mutagenesis-based approach, we attempted to generate an antibody that specifically recognized the acetylated form of TgAtg8 to allow us to characterize TgAtg8 K23-acetylation under various conditions and treatments. To this end, two rabbits were immunized with a synthetic peptide containing acetylated K23. The sera from the two rabbits were pooled and affinity purified to isolate an antibody that specifically recognized K23-acetylated TgAtg8. We assessed the specificity of the affinity purified antibody by preforming dot blots with the acetylated K23 peptide, an unacetylated K23 peptide, and peptides containing each of the mutations used in our previous studies (K23R/A/Q). As shown in **Figure 16**, the acetyl-K23 specific antibody showed strong specificity in this assay, and recognized only the acetylated peptide. We next attempted to use this reagent to visualize TgAtg8 K23 acetylation by immunoblotting on parasite lysates. As a control, we included lysates from the GFP-TgAtg8 K23 mutant strains. We expected that given the specificity of the acetyl-K23 antibody as seen by dot blot, this antibody should not be able to bind to the K23 mutant proteins. However, while the antibody was specific for the acetylated peptide, we observed equivalent reactivity against K23K and K23 mutant proteins (**Figure 16C**). Due to a lack of specificity of this antibody at the protein level, we were unable to use this reagent for further characterization of TgAtg8 K23 acetylation in the parasite.

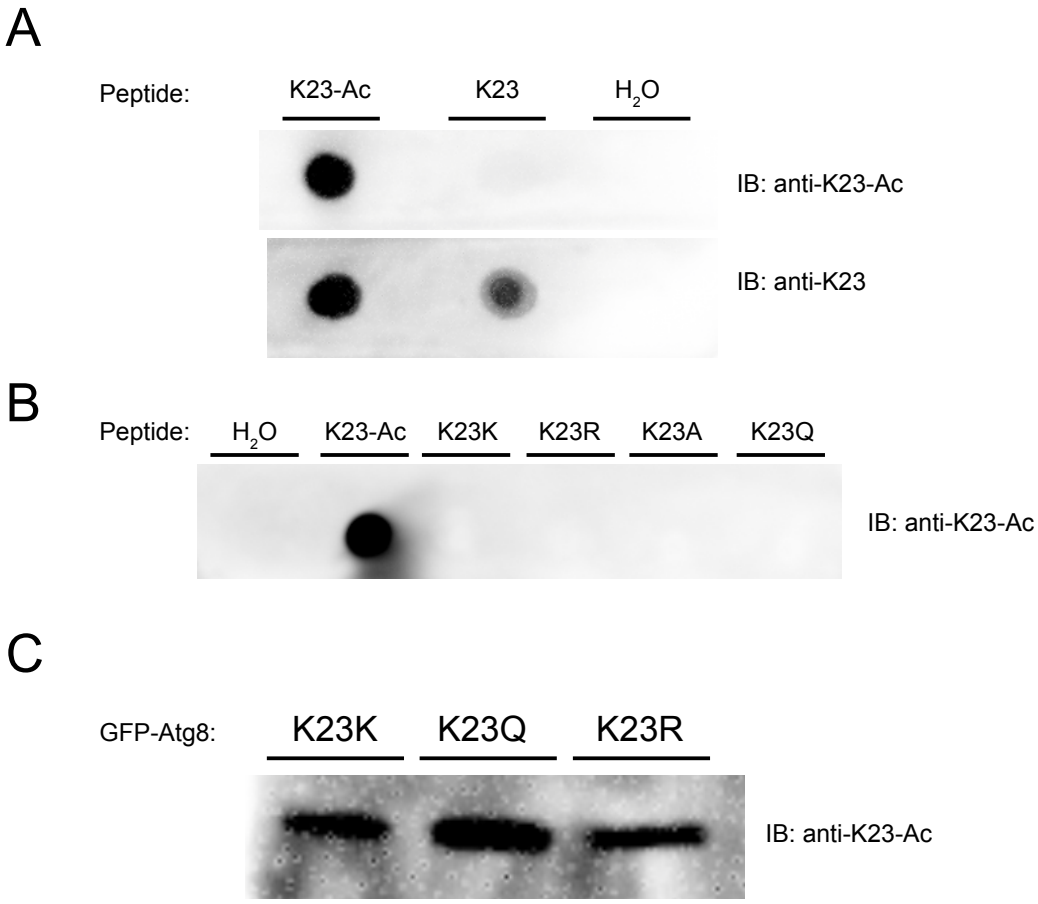

Figure 16: Acetyl-K23 non-specifically recognizes TgAtg8 K23 mutant proteins. A) Dot blot of K23-acetyl and K23-non-acetyl peptides (20μg each), probed with anti-K23-Acetyl antibody and non-acetyl specific antibodies. Water was used as a negative control. B) Dot blot of K23-acetyl and peptides containing each of the K23 mutations used in our study, probed with anti-K23-Acetyl antibody. C) Immunoblot of lysates from K23K, K23Q and K23R parasites probed with anti-K23-Acetyl antibody, showing that the antibody lacks specificity at the protein level.

3.7 Atg8 K23 mutations do not prevent binding with Atg3 AIM or alter protein thermal stability

In *Plasmodium falciparum*, structural characterization of the PfAtg3-Atg8 interaction showed that PfAtg3 contained a consensus AIM (Atg8 Interacting Motif) that binds within the W- and L-site pockets on PfAtg8 [107]. As the TgAtg8 acetylated lysine residue (K23) is located near these binding pockets, we hypothesized that this modification (and the mutations used to mimic this modification) may alter interaction between TgAtg8 and AIM-containing proteins, including TgAtg3. Although TgAtg3 and

TgAtg8 are assumed to interact in a similar manner as observed in other systems, this interaction has never been confirmed, and no AIM in TgAtg3 had been proposed or validated. Based on the identified PfAtg3 AIM sequence, we identified a similar putative AIM sequence in TgAtg3 (**Figure 18**). We therefore sought to confirm the ability of this predicted AIM sequence to bind to TgAtg8 and determine whether mutation of K23 altered this interaction.

As previously described, we encountered many difficulties in directly assessing the lipidation of the GFP-Atg8 proteins and were unable to generate an endogenous K23Q mutant parasite strain mimicking K23 acetylation. Therefore, we chose to examine the TgAtg3 AIM-TgAtg8 interaction using thermal shift assays. This assay measures the ability for a ligand to bind to a target protein by quantifying the resulting shift in melting temperature (T_m, the temperature at which half of the target protein is denatured) caused by ligand binding [209,210]. To conduct these assays, we expressed recombinant 6xHis-tagged TgAtg8 K23K, K23R, K23A and K23Q proteins in *E. coli*, which were purified using TALON cobalt affinity resins (**Figure 17**). Additionally, we synthesized a peptide corresponding to TgAtg3 amino acids 160-176 that contains the putative AIM sequence (VGHDVEGG**WMLP**LLNDE). These reagents were then used to perform thermal shift assays in the presence of the thermofluor dye SYPRO Orange, that fluoresces upon binding to hydrophobic surfaces exposed following protein denaturation [209,211]. Thermal unfolding curves were obtained for each TgAtg8 K23 mutant protein, and the T_m was determined (**Figure 18**). We observed a concentration-dependent increase in T_m in the presence of the TgAtg3 AIM peptide (**Figure 18A**). No increase in T_m was observed with equal concentrations of a control cMyc peptide, suggesting that the increased thermal stability was due to the interaction between the TgAtg3 AIM peptide and TgAtg8 (**Figure 18B**). Importantly, all K23 mutant proteins showed a similar increase in T_m in the presence of TgAtg3 AIM peptide, suggesting that none of the TgAtg8 K23 mutations altered the interaction between the TgAtg3 AIM peptide and TgAtg8.

In addition to being used to monitor protein-ligand interactions, thermal shift assays can be used to assess the effect of point mutations on protein thermal stability, with single mutations being able to alter thermal stability by as much as 10°C [212]. To determine whether the apparent effects of K23 mutations on protein stability were the result of alterations in the intrinsic protein stability, we preformed thermal shift assays in the absence of peptide ligands. We observed a similar trend in protein thermal stability as we saw with protein levels in the parasite, with K23R and K23A mutations having

decreased T_m values, and K23Q having a slightly increased T_m (**Figure 19**). However, these changes in T_m were less than 2°C as compared to K23K, suggesting that the observed differences in protein levels in the parasite are unlikely solely due to effects of these mutations on intrinsic protein stability.

The interaction between TgAtg3 and TgAtg8 was further confirmed by tagging the endogenous TgAtg3 locus with a C-terminal 3xHA epitope tag in the cMyc-TgAtg8-K23K and K23R background strains (**Figure 20**). This allowed for direct assessment of the interaction between full-length TgAtg3 and TgAtg8 proteins by co-immunoprecipitation and immunoblotting. We observed that TgAtg3 localized to the cytoplasm, and that the tagged protein resolved as two bands, correspond to the two previously reported splice variants observed for TgAtg3 [94]. In agreement with our previous findings, both K23K and K23R proteins were co-precipitated by immunoprecipitation of TgAtg3 using HA affinity resin (**Figure 20**). Reciprocal co-immunoprecipitations using anti-cMyc conjugated magnetic beads further demonstrated that both K23K and K23R proteins interact with TgAtg3 (**Figure 20**). These results show that mutation of Atg8 K23 to arginine (K23R) does not prevent interaction with the AIM motif present in TgAtg3.

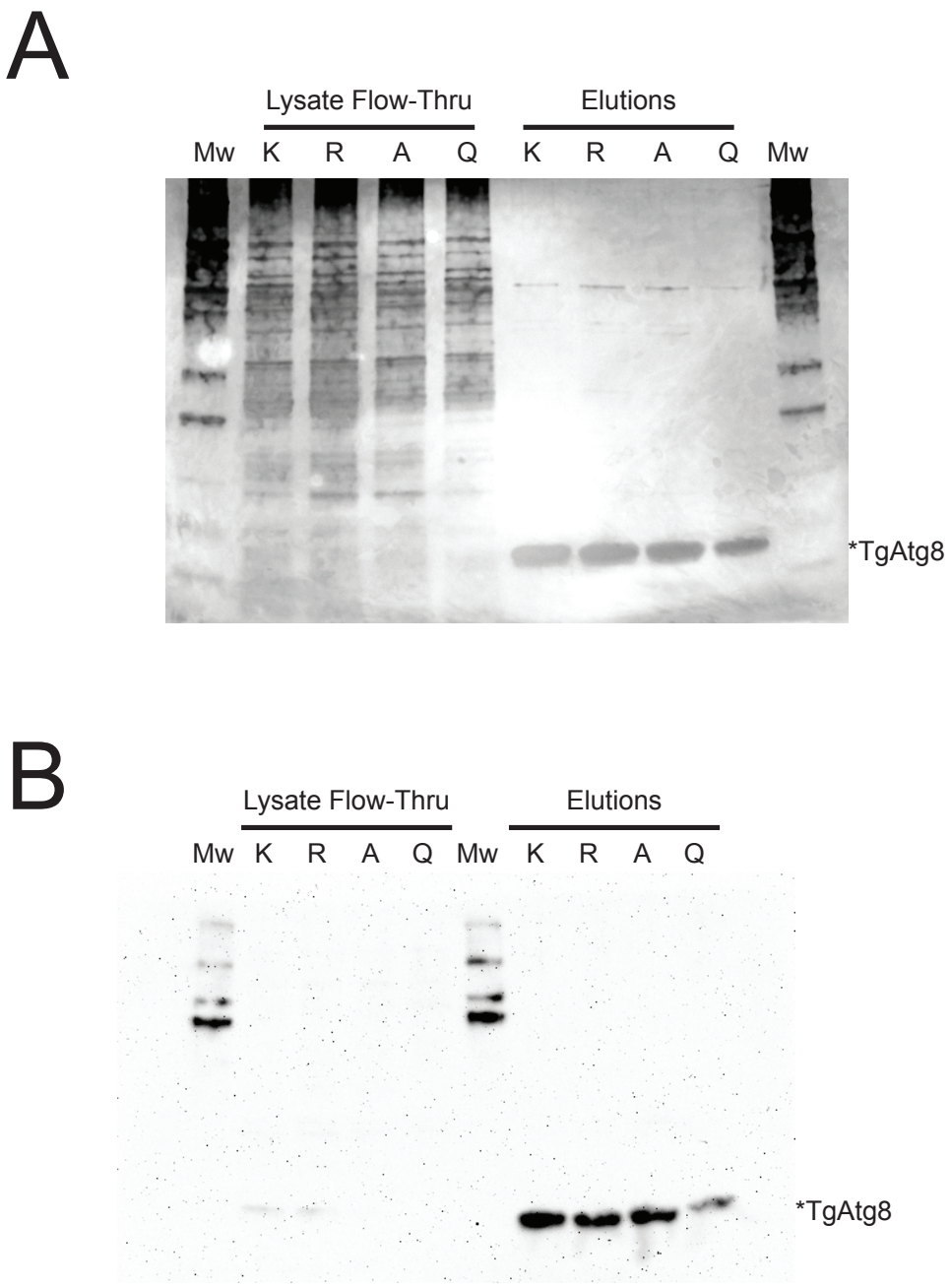

Figure 17: Purification of recombinant TgAtg8 K23 WT and mutant proteins.
A) Silver stained SDS-PAGE gel of recombinant 6xHIS-Atg8 K23K, K23R, K23A, and K23Q proteins. Proteins were purified using TALON Cobalt resin and the flow-through lysate (unbound) and recovered purified proteins (elutions) were subjected to SDS-PAGE. All Atg8 K23 proteins were found to be >90% purity as determined by densitometry analysis using ImageJ. B) Immunoblot of samples in (A) probing with an anti-HIS tag antibody.

PfAtg3 AIM: DNDWLLPSY

TgAtg3 AIM: EGGWMLPLL

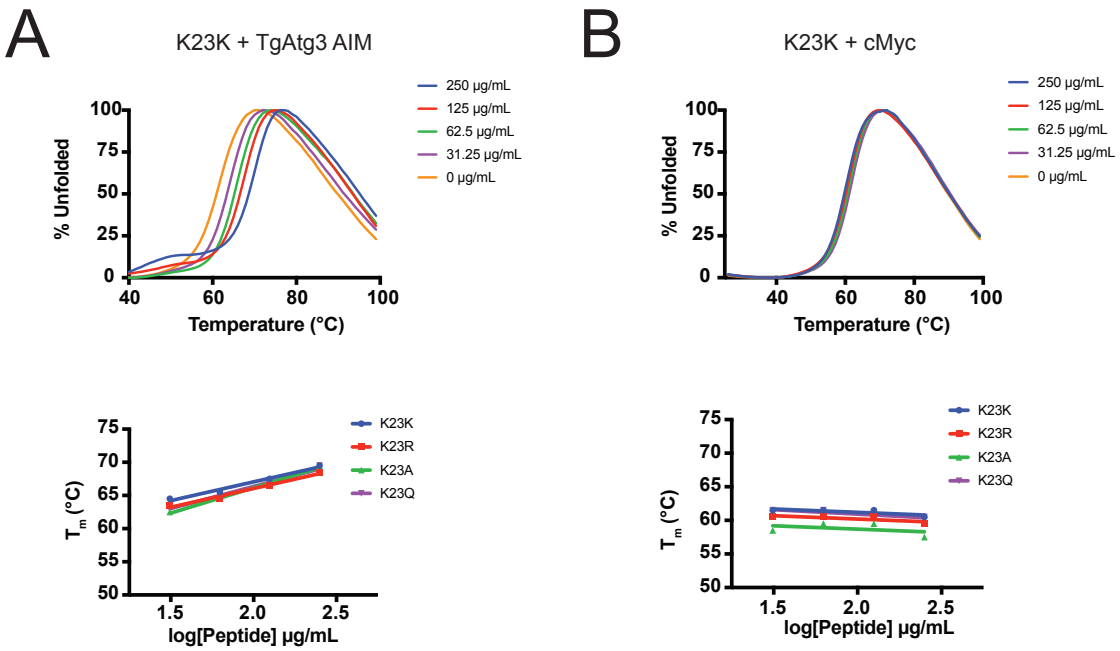

Figure 18: Mutation of K23 does not alter ability to bind to putative TgAtg3 AIM peptide.

A) (*top*) Representative plot for Atg8-K23K showing rightward-shift of melting temperature in response to increasing concentrations of TgAtg3 AIM peptide (sequence of TgAtg3 AIM aligned with PfAtg3 AIM shown above graph). (*bottom*) Melting temperature increases in presence of Atg3 AIM peptide for all K23 mutant proteins. B) Representative plot for TgAtg8-K23K in presence of cMyc control peptide that fails to alter melting temperature.

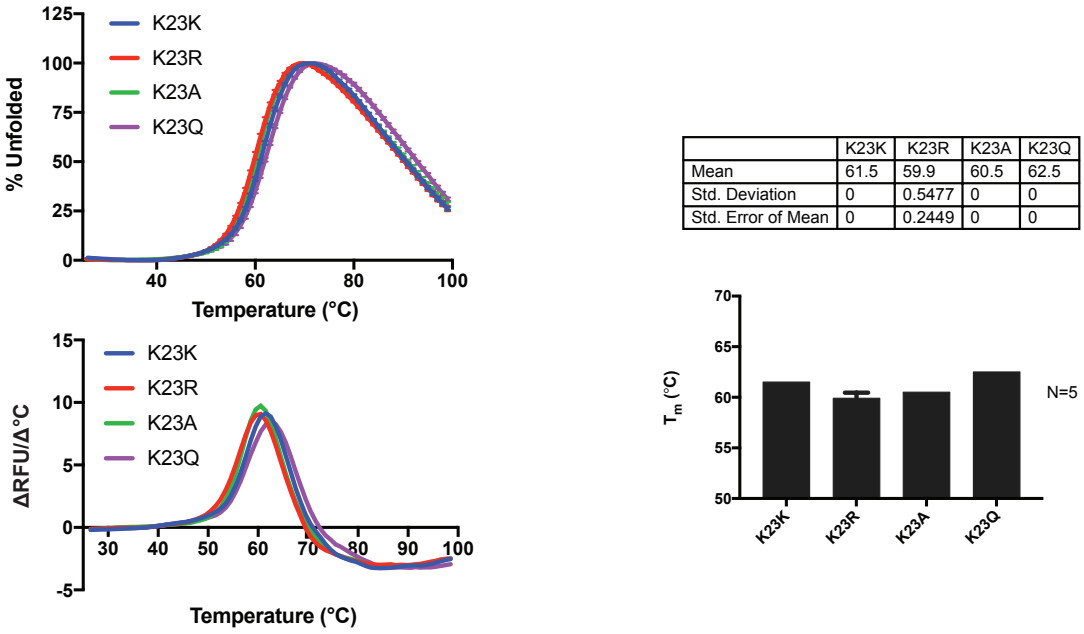

	K23K	K23R	K23A	K23Q
Mean	61.5	59.9	60.5	62.5
Std. Deviation	0	0.5477	0	0
Std. Error of Mean	0	0.2449	0	0

Figure 19: Mutation of K23 does not alter intrinsic protein thermal stability. Representative plot of Atg8-K23K and K23 mutant proteins, in the absence of peptide ligands. Quantitation of melting temperature for Atg8-K23K and K23 mutant proteins revealed minimal effects of K23 mutation on protein thermal stability, n=5, ± SEM.

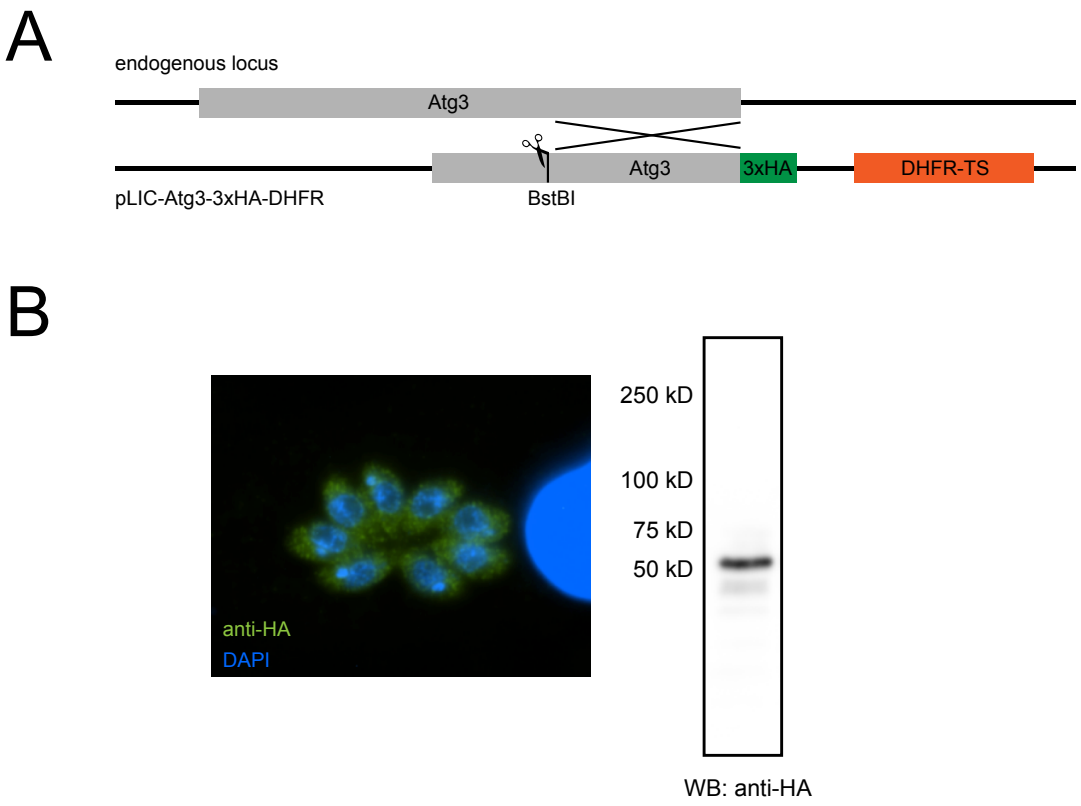

Figure 20: Endogenously-tagged TgAtg3-HA co-immunoprecipitates with both K23K and K23R proteins.
A) Schematic of cloning approach used to introduce a 3xHA epitope tag at the C-terminus of the endogenous TgAtg3 gene. Prior to transfection, the plasmid used for tagging was linearized by digestion with BstBI to allow for integration at the endogenous TgAtg3 locus. B) Representative IFA and immunoblotting analyses of recovered TgAtg3-

HA parasites. TgAtg3 (green) localizes to the cytoplasm and resolved as two bands, corresponding to two forms that arise by processing of the TgAtg3 N-terminus. C) Representative immunoblots (IB) probing for Atg3-HA and cMyc-Atg8 following immunoprecipitation (IP) with anti-HA (top) or anti-cMyc (bottom) resin. Both K23K and K23R proteins co-precipitate with TgAtg3, suggesting that acetylation of K23 is not required for their interaction.

Summary Aim 1:

To address our first aim, we used a combination of bioinformatics, structural modeling, mutational analyses and biophysical approaches to assess the effect of K23 acetylation TgAtg8 localization, interaction with TgAtg3 and on parasite fitness. We presented evidence that this modification may regulate TgAtg8 protein stability, potentially through altering TgAtg8 protein-protein interactions, as these mutations did not alter intrinsic protein thermal stability. Ablation of this modification at the endogenous gene locus is not well-tolerated; it impairs parasite replication and promotes spontaneous differentiation from tachyzoites to bradyzoite tissue cysts. However, our data collectively suggest that these observed phenotypes are not due to alterations of the interaction between TgAtg8 and TgAtg3. Our characterization of the endogenous K23R mutant parasites also suggests that this mutation is unlikely to prevent TgAtg8 interaction with other components of the Atg8 conjugation system (TgAtg7 and TgAtg4), as TgAtg8 lipidation and localization to the apicoplast was not affected in these mutants. This suggests that the phenotypes observed are likely due to altered TgAtg8 functions outside of its established role in autophagy and apicoplast maintenance. However, these potential alternative functions remain unknown, in large part due to our lack of understanding regarding which proteins TgAtg8 interacts with in *Toxoplasma*. Accordingly, in our second aim we sought to characterize the TgAtg8 interactome to identify novel interacting proteins and shed light on potential new functional roles for TgAg8 in parasite biology.

Aim 2: Characterization of the TgAtg8 interactome to identify TgAtg8 interacting proteins

The function of Atg8 in *Toxoplasma* has largely focused on its role in canonical autophagy-related processes in response to drug treatment or starvation. However, it is now apparent that TgAtg8 also exhibits non-canonical functions including but not limited to coordinating apicoplast division by tethering this organelle to the centrosomes [103]. The mechanism by which TgAtg8 exerts this function is unclear as is whether TgAtg8

directly tethers the apicoplast to the centrosome or indirectly through protein-protein interactions. Additionally, Atg8 proteins have diverse functions in higher eukaryotes, including in protein sorting, vesicle trafficking, and targeted degradation of organelles and proteins. Importantly, all of these processes rely on interactions between Atg8 and other proteins, and have not been explored in *Toxoplasma*. We hypothesized that TgAtg8 was also involved in diverse biological processes in *Toxoplasma* that are important for parasite viability. Further, we proposed that these unexplored functions may be identified by characterization of TgAtg8 interacting proteins. With our second aim, we used affinity purification and mass spectrometry to identify proteins that interact with TgAtg8 in tachyzoites. We present evidence supporting a functional role of TgAtg8 in trafficking of vesicles throughout the Golgi network, and characterize a novel dynamin-related protein identified in the TgAtg8 interactome. These results expand our understanding of the function of TgAtg8 in *Toxoplasma* biology and identify potential interactions that could be further explored as novel pharmacological targets.

3.8 Identification of TgAtg8 interacting proteins by affinity purification and mass spectrometry

Our results from the mutagenesis-based studies to assess K23 acetylation suggest that this modification does not alter the interaction between TgAtg8 and TgAtg3. However, Atg8 proteins interact with numerous proteins outside of the Atg8 conjugation machinery, and many of these interactions are dependent upon the electrostatic interactions with the Atg8 N-terminal helices where K23 acetylation is predicted to occur. We therefore hypothesized that the effects on protein stability and the phenotypes observed in the endogenous cMyc-Atg8 K23R parasites were due to alterations in the interaction of TgAtg8 with other AIM-containing proteins. We used a proteomics approach to identify proteins that interact with TgAtg8 by immunoprecipitation of TgAtg8 from the cMyc-Atg8 K23K parasite strain previously described (**Figure 12**). We hypothesized that the identification of TgAtg8 interacting proteins would inform future studies assessing the role of K23 acetylation on TgAtg8 protein-protein interactions, and provide insight into the potential mechanisms underlying the non-canonical functions of TgAtg8 in parasite biology.

Initially, we hoped to characterize the TgAtg8 interacting proteins from intracellular and extracellular tachyzoites, as well as following induction of autophagy. However, while preforming these assays, we observed that TgAtg8 protein levels were significantly lower in intracellular parasites than in extracellular parasites (**Figure 21**). As

a result, the TgAtg8 protein levels were often below the limit of detection by immunoblotting in lysates from intracellular parasites. The difference in TgAtg8 expression was also seen by qPCR from intracellular and extracellular parasites, which showed a ~2.5-fold increase in mRNA levels in freshly lysed parasites (**Figure 21**). Additionally, although we were able to immunoprecipitate TgAtg8 from extracellular parasites, induction of autophagy by extracellular HBSS starvation resulted in the retention of TgAtg8 in an insoluble fraction, thus preventing its immunoprecipitation (**Figure 21**). Therefore, we were only able to characterize the TgAtg8 interactome from freshly egressed, extracellular parasites.

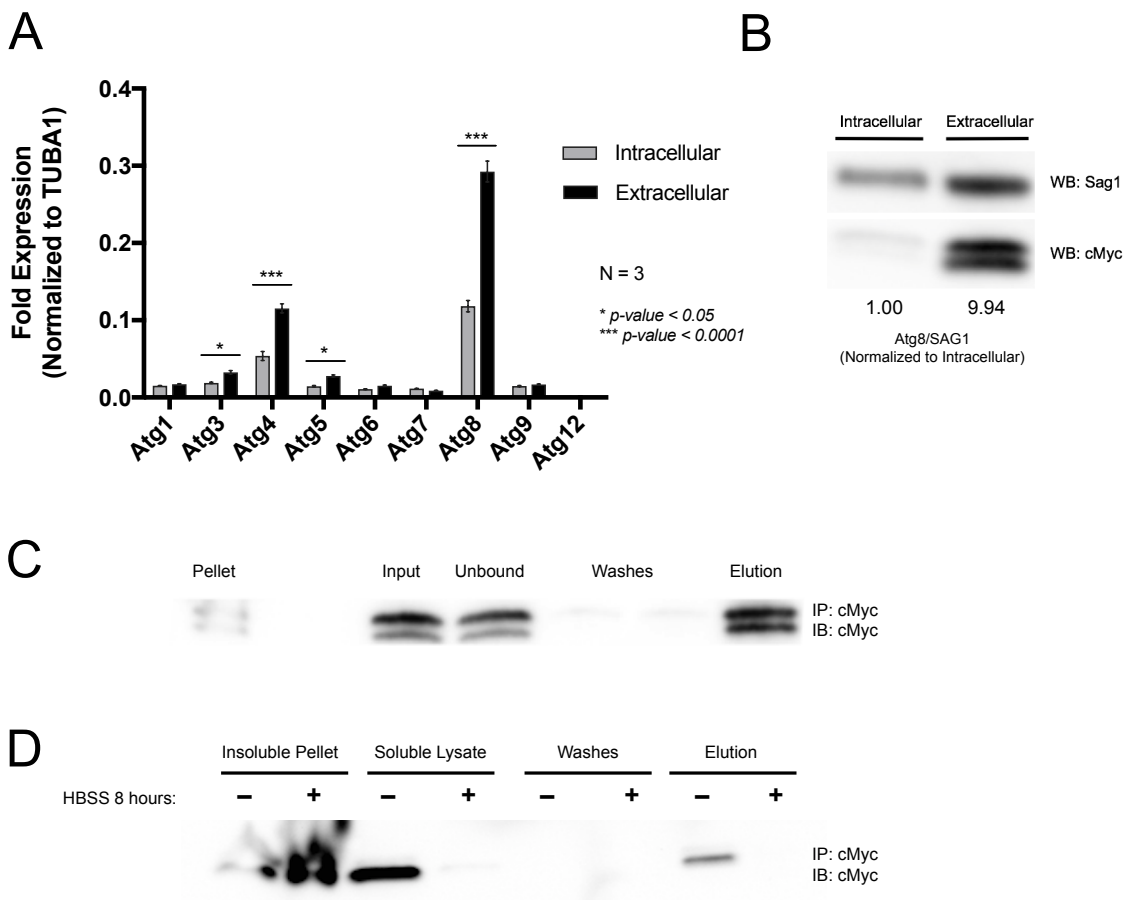

Figure 21: TgAtg8 expression increases in extracellular and remains insoluble upon HBSS starvation.

A) Quantitative RT-PCR of transcript levels for putative *Toxoplasma* ATG genes from intracellular and freshly egressed, extracellular parasites. Members of the Atg8 conjugation system, including TgAtg3, TgAtg4, and TgAtg8 show significantly increased expression levels in extracellular parasites. B) Representative immunoblot from cMyc-TgAtg8 parasite lysates harvested from intracellular and extracellular parasites. Blots were probed with anti-cMyc and with SAG1 as a loading control. Values below lanes indicate values of TgAtg8/SAG1 protein levels for each condition, as determined by densitometry using ImageJ. C) Representative immunoblot of lysates prepared for immunoprecipitation of cMyc-TgAtg8 from freshly egressed parasites. Pellets were lysed in RIPA buffer, and cMyc-TgAtg8 was found predominantly in the soluble lysate (Input) with minimal protein remaining in the insoluble pellet (pellet). Immunoprecipitation with anti-cMyc magnetic beads shows ability to IP both lipidated and unlipidated forms of cMyc-TgAtg8. D) Immunoblot of lysates prepared as described in (C) prior to and following 8 hours of extracellular HBSS starvation. Starvation prevents the liberation of cMyc-TgAtg8 from the insoluble fraction.

To identify TgAtg8 interacting proteins, we incubated lysate from 10^9 freshly egressed cMyc-Atg8 parasites with magnetic beads conjugated with non-specific mouse IgG (negative control) or with anti-cMyc antibodies. Mass spectrometry from three independent biological replicates identified proteins that were specifically enriched by immunoprecipitation with the anti-cMyc beads, likely representing TgAtg8 interacting proteins. The raw spectral counts from each biological replicate were used for statistical analysis using SAINT (Significance Analysis of INTeractome) to assign probability scores to each interaction (**Table 2, Appendix 3**). This analysis returned a list of twelve proteins with high-confidence enrichment values (SAINT Probability > 0.75), including the E1-like component of the Atg8 conjugation system TgAtg7 (**Table 2**). Many of the identified interacting proteins were also found to contain putative AIM sequences that could facilitate their interaction with TgAtg8, and have been implicated as important for tachyzoite viability based on a genome-wide CRISPR knockout study [213].

In addition to identifying homologues of Atg8 conjugation machinery, we identified homologues to the mammalian NSF and SNAP proteins (Sec18p and Sec17p in yeast), which are known interacting proteins of the Atg8 family protein GATE-16. We also found a significant enrichment of components of the branched chain ketodehydrogenase complex (BCKDH). In *Toxoplasma,* the primary function of this complex is the conversion of pyruvate to acetyl-CoA in the mitochondrion, as the *Toxoplasma* pyruvate dehydrogenase complex localizes to the apicoplast [7,214]. The BCKDH is a multi-subunit complex consisting of E1 alpha, E1 beta, E2, and E3 subunits, three of which were identified in our TgAtg8 interactome (**Table 2**). We also identified a putative thiamine pyrophosphokinase (TPP), which localizes to the mitochondrial matrix in higher eukaryotes and phosphorylates thiamine to generate TPP, an essential co-factor for the E1 subunits of 2-oxo acid dehydrogenase complexes including PDH and BCKDH [215,216].

A number of parasite-specific proteins of unknown function, annotated as “hypothetical proteins”, were also enriched in our dataset. Although these proteins lack conserved domains as identified by amino acid sequence, some insight on potential protein function was provided by analysis with HHpred [217], which identifies proteins with similar predicted tertiary structure. One of the identified hypothetical proteins, TGGT1_ 268430 had a predicted Golgi-localized gamma adaptin ear-containing, ARF-binding (GGA1) domain, found in clathrin adapter proteins involved in protein trafficking from the trans-Golgi network and from the Golgi to the lysosome [218]. Additionally, the

second hypothetical protein, TGGT1_ 247300, contained structural similarities to the Armadillo repeat proteins beta-catenin and kinesin-associated protein 3. Beta-catenin is a multifunctional protein implicated in cell-cell adhesion and the Wnt signaling pathway. However, it also plays a critical role in promoting mitotic progression, where it localizes to the centrosomes to coordinate formation of the mitotic spindle and regulate centrosome separation during mitosis [219]. Kinesin-associate protein 3 (KAP3) is also a multifunctional protein that localizes to motor protein complexes that transport cargo along microtubules in interphase cells, and relocalizes to the mitotic spindle during cell division. Disruption of the KAP3/kinesin complex in HeLa cells resulted in abnormal numbers of centrosomes and formation of multiple mitotic spindles that resulted in aneuploidy, highlighting the importance of this protein in progression through mitosis [220].

Table 2: Identified TgAtg8 Interacting Proteins

Protein Name	Gene ID	Fold Change	SP	AIM	CRISPR Score
Atg8 Conjugation System					
TgAtg7	TGGT1_229690	126.27	1	Yes	-3.91
TgAtg8	TGGT1_254120	20.12	1		-2.75
Branched Chain Ketodehydrogenase (BCKDH) Complex					
TgBCKDH E2	TGGT1_319920	167.6	1		-1.92
TgBCKDH E1b	TGGT1_314400	21.82	1		-1.6
TgTPPK	TGGT1_215250	20.79	1		-3.28
TgBCKDH E1a	TGGT1_239490	21.95	0.85	Yes	n/a
Golgi vesicle trafficking					
TgDrpC	TGGT1_270690	214.21	1	Yes	-4.54
TgNSF	TGGT1_318510	76.11	1	Yes	-4.36
TgGAT	TGGT1_268430	32.49	1	Yes	-1.77
TgSNAPb	TGGT1_218760	15.98	1		-5.35
TgARP	TGGT1_247300	9.59	0.97		-0.08
Others					
TgPUS2	TGGT1_306660	25.19	1	Yes	-4.59
TgMFS	TGGT1_297245	8.9	0.97	Yes	-5.71

* For identified TgAtg8 interacting proteins that were previously uncharacterized or lacked clear homologues, gene names were assigned according to predicted function based on presence of functional domains or predicted structural homologues identified by HHpred. GAT, GGAs And TOM1; ARP, Armadillo Repeat containing Protein; PUS, Pseudouridine Synthetase; MFS, Major Facilitator Superfamily.

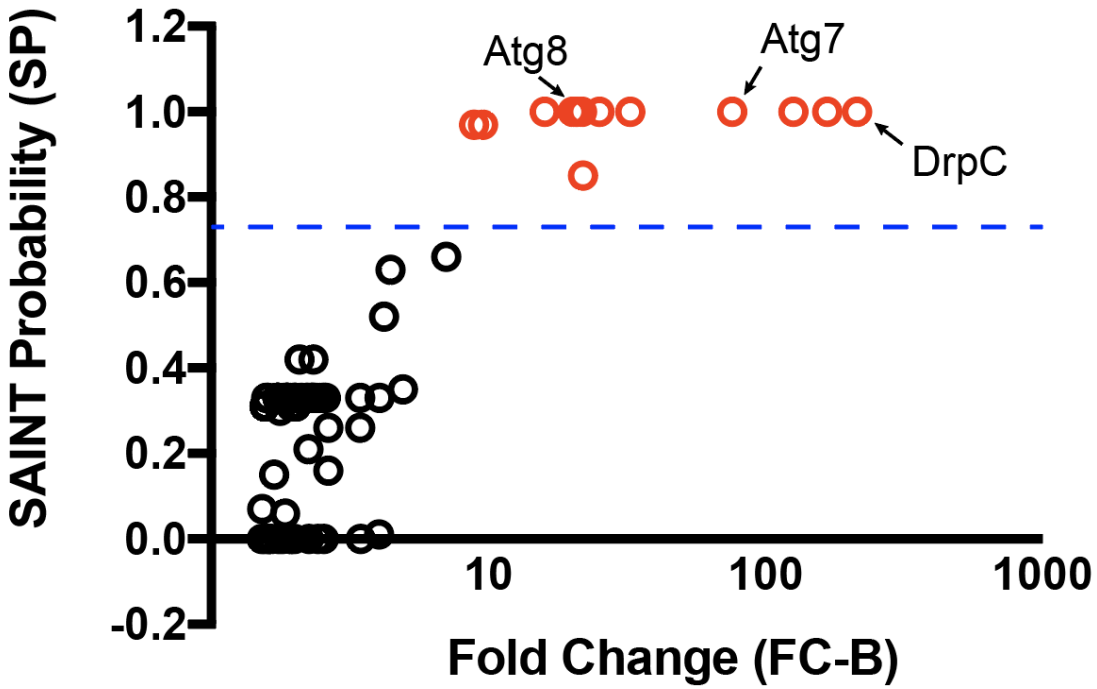

Figure 22: Proteins identified in TgAtg8 interactome.
Twelve proteins were identified as being enriched in TgAtg8 IPs with high confidence (SAINT Probability score >0.75). The SAINTExpress stringent fold-change (FC-B) and SP values are plotted, displaying high confidence hits colored in red. Dashed line represents SP cutoff (0.75).

Interestingly, TgAtg3 was not detected as an interactor in this analysis, despite our previous data suggesting that these two proteins do interact (**Figure 20**). However, proteomics analysis performed to identify TgAtg3 interacting proteins using the endogenously tagged TgAtg3-HA (**Figure 20**) identified both TgAtg7 and TgAtg8 as the top two TgAtg3 interacting proteins **(Table 3, Appendix 4)**

Table 3: Identified TgAtg3 interacting proteins

Protein Description	Gene ID	Fold Change	SP
TgAtg7	TGGT1_229690	187.86	1
TgAtg3	TGGT1_236110	42.94	1
TgAtg8	TGGT1_254120	67.65	1
hypothetical protein	TGGT1_305270	86.21	1
hypothetical protein	TGGT1_311830	13.96	0.99
hypothetical protein	TGGT1_203280	16.16	0.97

3.9 Localization of TgAtg8 interacting proteins

In *Toxoplasma,* TgAtg8 localizes predominantly to the outer membrane of the apicoplast. As none of the proteins identified in our TgAtg8 interactor list had never been characterized or localized, we hypothesized that our immunoprecipitation may simply be enriching for proteins that localize to the apicoplast due to pulling down apicoplast membrane. To address this, we tagged five of the interacting proteins, including representatives of the Golgi trafficking-related proteins, as well as components of the BCKDH complex and the dynamin-like protein TgDrpC. For all genes, a 3xHA epitope tag was introduced at the endogenous locus of the gene of interest in the RHΔ*hxgprt*Δ*ku80* background. Each tagged protein was analyzed by SDS-PAGE and immunoblotting, and all proteins migrated near their predicted molecular weight, with the exception of TgTPPK (predicted MW = 89 kD, observed MW = ~60 kD) (**Figure 23**). Transcriptomics data for TgTPPK does not predict alternative splice forms for this gene, however analysis of the TgTPPK mRNA sequence using the ATGpr webserver [221] identifies a putative alternative translation start site (starting at mRNA base pair 664) that would produce a protein with a predicted molecular weight of 64 kD, and in frame with the 3xHA epitope tag. Importantly, the protein produced from this alternative translation start site would include the functional TPP kinase domain.

Next, we localized each of the tagged TgAtg8 interacting proteins by IFA using an anti-HA antibody (**Figure 24**). All components of the BCKDH complex localized to the parasite mitochondrion, as shown by their co-localization with the mitochondrial matrix protein F1β ATPase. This localization is in agreement with the previous report suggesting their function in acetyl-CoA production in the mitochondrial matrix [214]. The putative TgNSF protein co-localized with the Golgi-localized sortilin-like receptor TgSORTLR, while the dynamin-related protein TgDrpC was found to localize to bright, cytosolic punctae that occasionally localized near regions of mitochondrial constriction (**Figure 25**). However, this localization at the mitochondrion did not increase following monensin treatment (which induces mitochondrial fragmentation), so the functional consequences of TgDrpC localization near regions of mitochondrial constriction remains unclear. These results show that the identified TgAtg8 interacting proteins localize to numerous and distinct sub-cellular regions and our immunoprecipitation was not simply enriching for apicoplast-localized proteins.

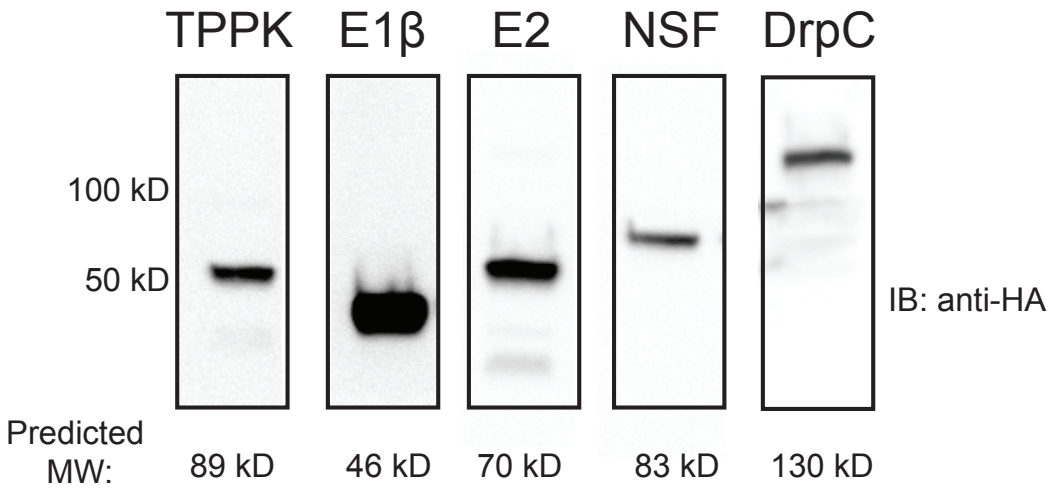

Figure 23: Confirmation of endogenously-tagged TgAtg8 interacting proteins by immunoblotting.
Immunoblots of TgAtg8 interacting proteins detected with anti-HA antibody. All proteins migrated near expected molecular weights, except for TgTPPK, which migrated at approximately 60 kD.

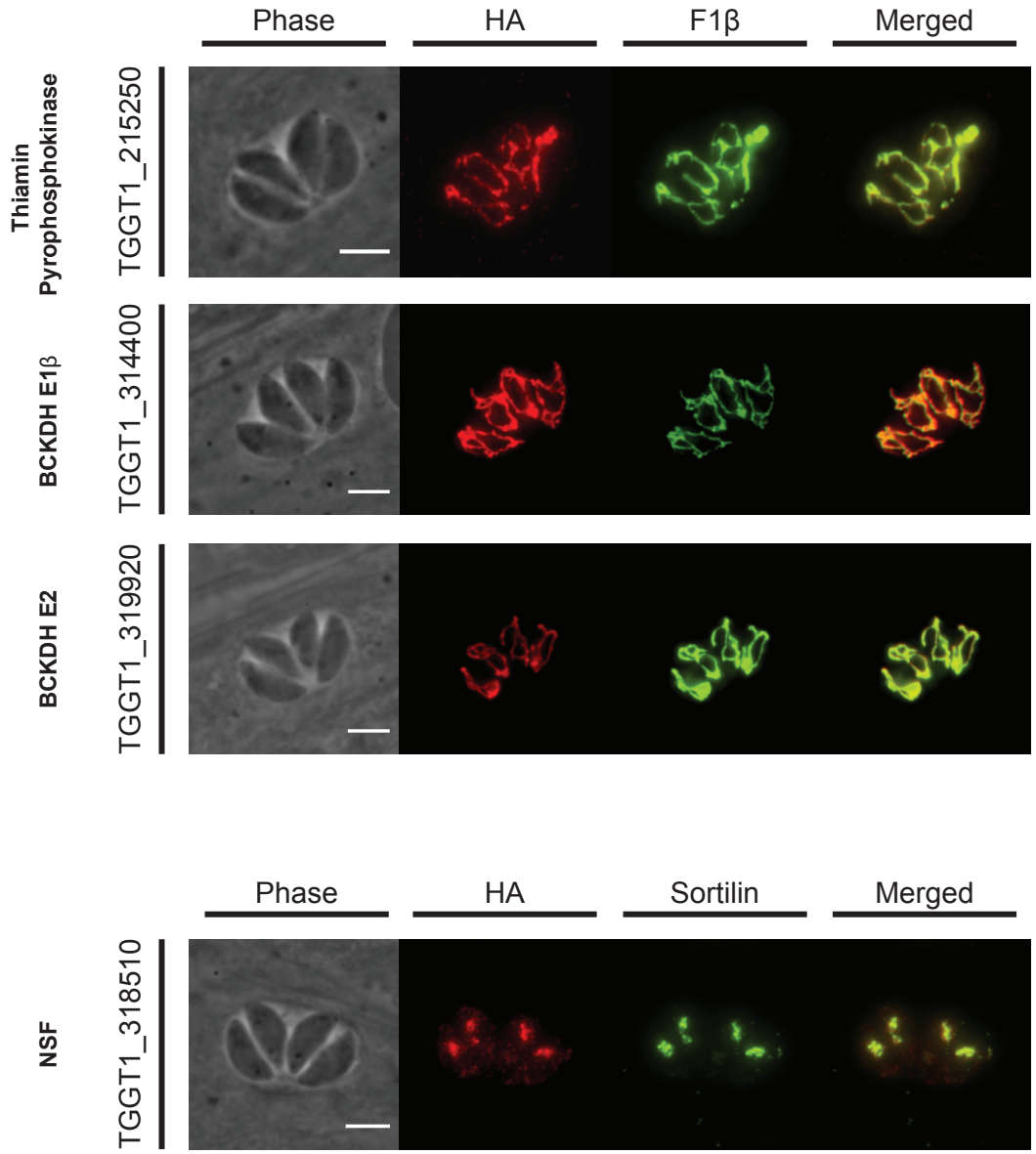

Figure 24: TgAtg8 interacting proteins localize to mitochondrion and Golgi organelles.
Representative IFA staining for endogenously-tagged TgAtg8 interacting proteins, as visualized by staining with anti-HA (red). All three components of the BCKDH complex localize to the parasite mitochondrion, as shown by co-localization with the mitochondrial matrix protein F1β ATPase (green). The putative TgNSF protein localizes to the Golgi apparatus as shown by co-localization with sortilin receptor-like protein TgSORTLR (green).

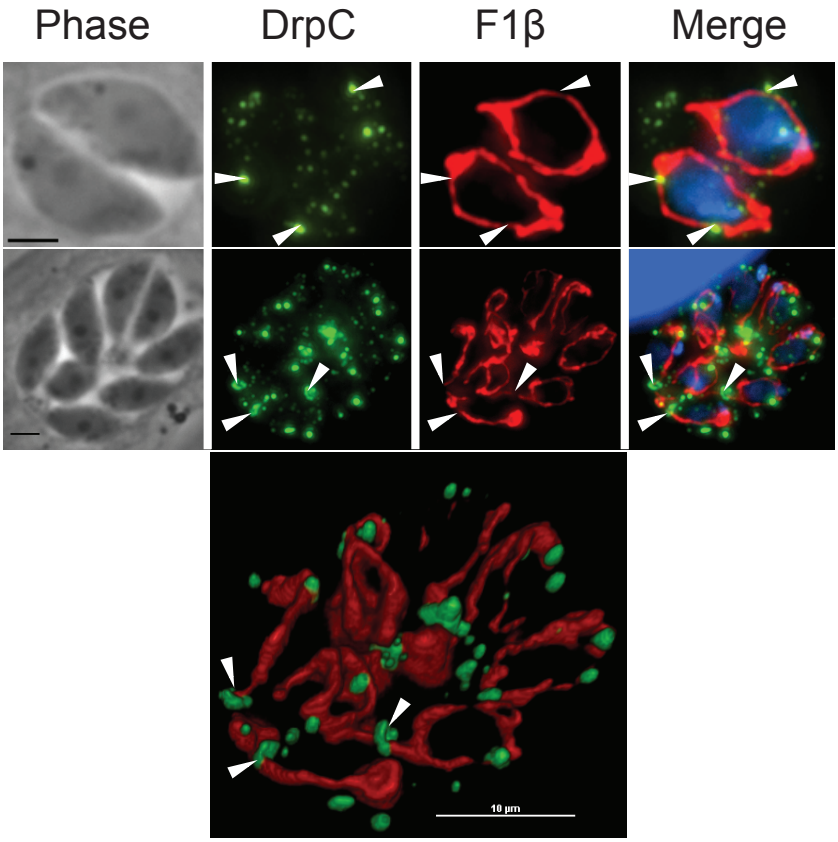

Figure 25: TgDrpC localizes to cytosolic punctae near regions of mitochondrial membrane constriction.
Representative IFA of TgDrpC (green), DAPI (blue) and F1β ATPase (red) showing partial co-localization of TgDrpC punctae with regions of mitochondrial membrane constriction (arrowheads). Scale bar = 3μm. Image by Robert Charvat.

3.10 TgDrpC relocates from cytoplasm to daughter buds during parasite replication

Of the identified TgAtg8 interacting proteins, we were particularly interested in TgDrpC, as the functions of dynamin and dynamin-like proteins in organelle division and Golgi trafficking aligned with functions associated with TgAtg8 [222]. Two dynamin-like proteins, TgDrpA and TgDrpB, have previously been characterized in *Toxoplasma* and were required for apicoplast and secretory organelle biogenesis, respectively [223,224]. However, unlike TgDrpA and TgDrpB, TgDrpC lacks a conserved GTPase Effector Domain (GED) that is typically required for efficient formation of dynamin oligomers and for stimulation of the GTPase domain activity [225]. In mammals, dynamin-like protein 1

is required for mitochondrial fission, and dynamin-related proteins are required for mitochondrial division in *Arabidopsis* spp. and *Trypanosoma brucei* [226–228]. We therefore sought to functionally characterize TgDrpC to determine the biological function of this divergent dynamin-like protein and to explore its role in Atg8/autophagy related processes in *Toxoplasma.*

To characterize TgDrpC and its interaction with TgAtg8, we tagged the endogenous TgDrpC gene in the cMyc-TgAtg8 background parasites. Immunofluorescence analyses showed that TgDrpC punctae did not co-localize with TgAtg8 in intracellular parasites (**Figure 26**). In contrast, TgDrpC and TgAtg8 were frequently found to co-localize at regions near the apicoplast or Golgi in extracellular parasites (**Figure 26**). This co-localization was observed in approximately 30% of parasites, and the frequency of co-localization did not increase following prolonged extracellular treatment (data not shown). Therefore, the TgAtg8-TgDrpC co-localization and interaction appears to occur in a sub-set of parasites, perhaps in response to certain conditions; however, the potential conditions that promote the interaction remain unknown. We also preformed reciprocal co-immunoprecipitation of TgDrpC-HA and cMyc-TgAtg8 and confirmed that these proteins can interact in extracellular parasites (**Figure 26C**).

While characterizing TgDrpC localization, we frequently observed that TgDrpC formed ring structures that appeared to localize to the leading edge of the elongating daughter parasite pellicle during mitosis (**Figure 27**). To explore this localization, we conducted immunofluorescence assays for TgDrpC and co-stained with antibodies that recognize two proteins commonly used to visualize daughter bud formation, IMC3 and MORN1. IMC3 is a component of the inner membrane complex that localizes underneath the plasma membrane and is used to visualize the entire daughter pellicle [229]. MORN1 is recruited to the apical complex of the nascent daughter cells early during division, and migrates with the growing daughter IMC through cytokinesis. During its migration MORN1 forms a ring structure at the leading edge of the growing IMC, and this ring is required for constriction of the daughter IMC to complete cell division [230,231]. These experiments revealed that TgDrpC co-localizes to MORN1-positive structures early during daughter bud formation and migrates with the MORN1 ring during mitosis, remaining localized to this structure until the late stages of cytokinesis (**Figure 27**).

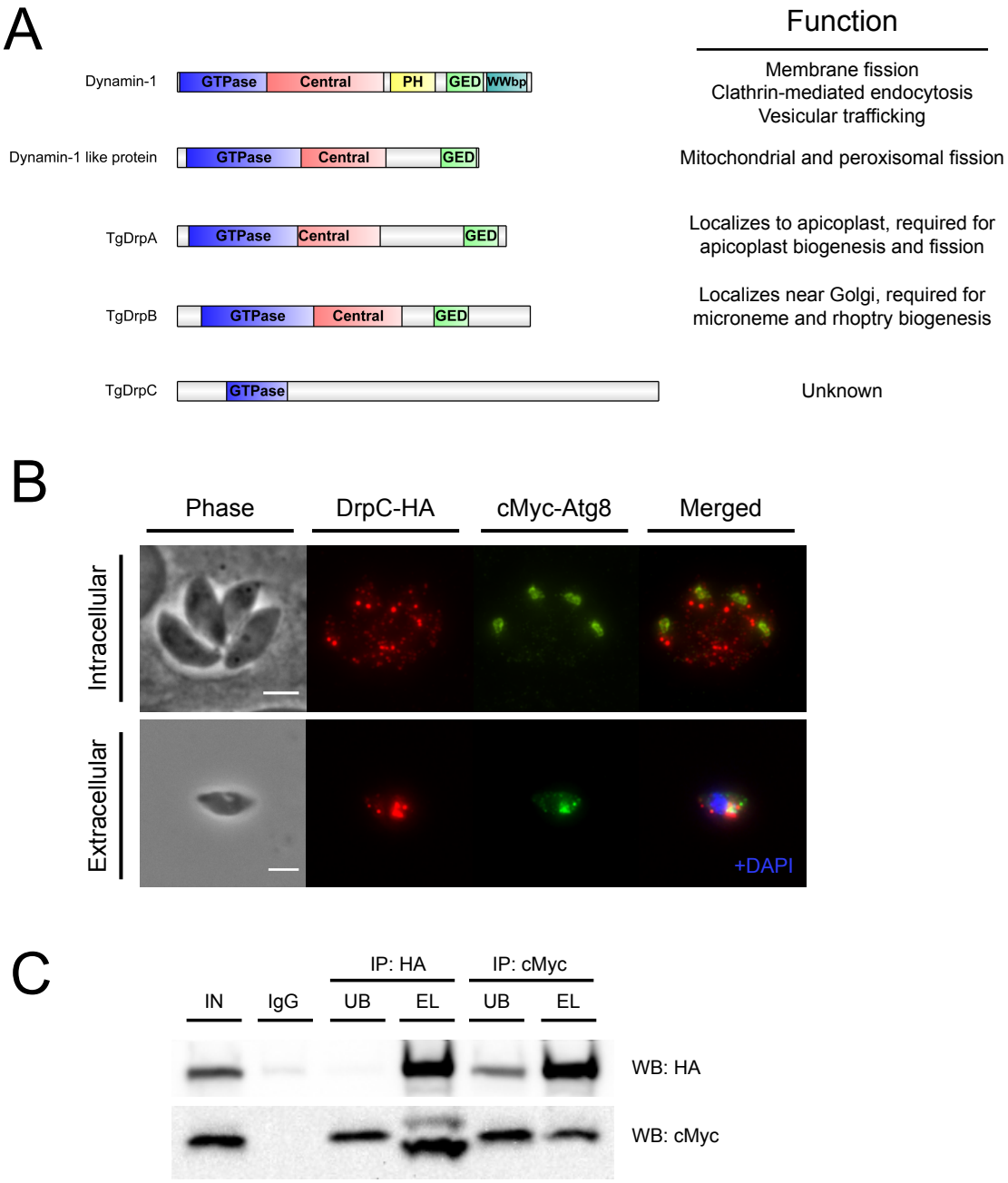

Figure 26: Characterization of TgDrpC interaction with TgAtg8.
A) Schematic diagram of mammalian dynamin-1 and dynamin-1 like proteins showing conservation of domains in *Toxoplasma* dynamin-related proteins. TgDrpA and TgDrpB both contain the GTPase, central domain, and GTPase Effector Domain (GED). In contrast, TgDrpC contains only the GTPase domain. Known functions of dynamin and dynamin-like proteins from *Toxoplasma* and mammalian systems are listed at right of domain diagram. B) Representative IFA images of TgDrpC-HA (red) and cMyc-TgAtg8 (green) co-tagged parasites. TgDrpC punctae were not found to co-localize with TgAtg8 in intracellular parasites, however co-localization was observed in ~30 percent of

extracellular parasites. C) Immunoblot showing reciprocal co-immunoprecipitation of TgAtg8 and TgDrpC from extracellular parasites. IN, soluble lysate input, IgG, IP with non-specific mouse IgG control, UB, unbound/flow-through, EL, elution in 2xSDS buffer. Scale bar = 3μm.

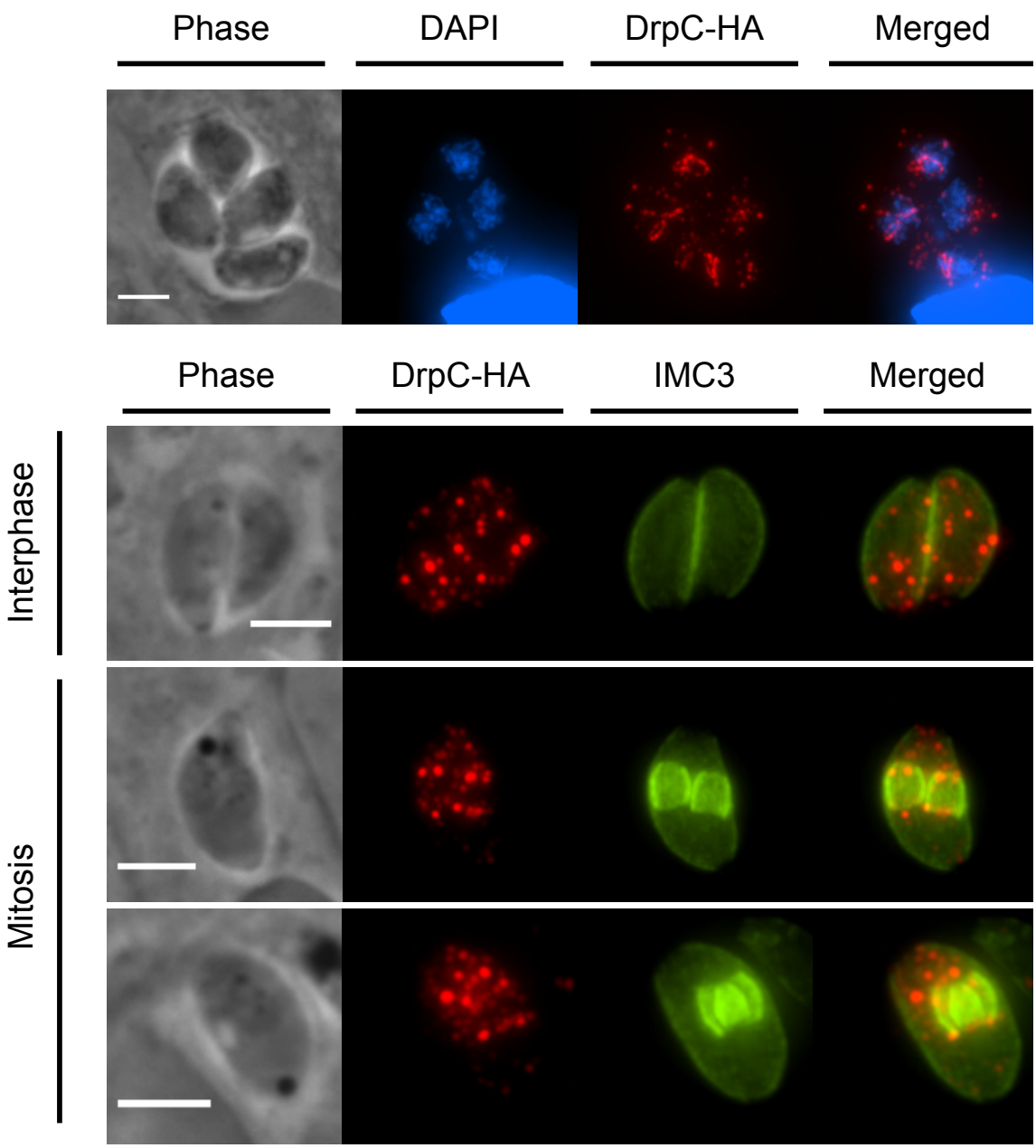

Figure 27: TgDrpC localizes to daughter buds during parasite replication.
Representative IFA of TgDrpC-HA (red) showing localization of TgDrpC to ring structures during mitosis. Co-staining with IMC3 (green) to visualize daughter bud formation revealed that TgDrpC localizes throughout the cytoplasm during interphase, but is only found in cytoplasmic punctae apical of the leading edge of the nascent daughter parasite during mitosis. Scale bar = 3μm.

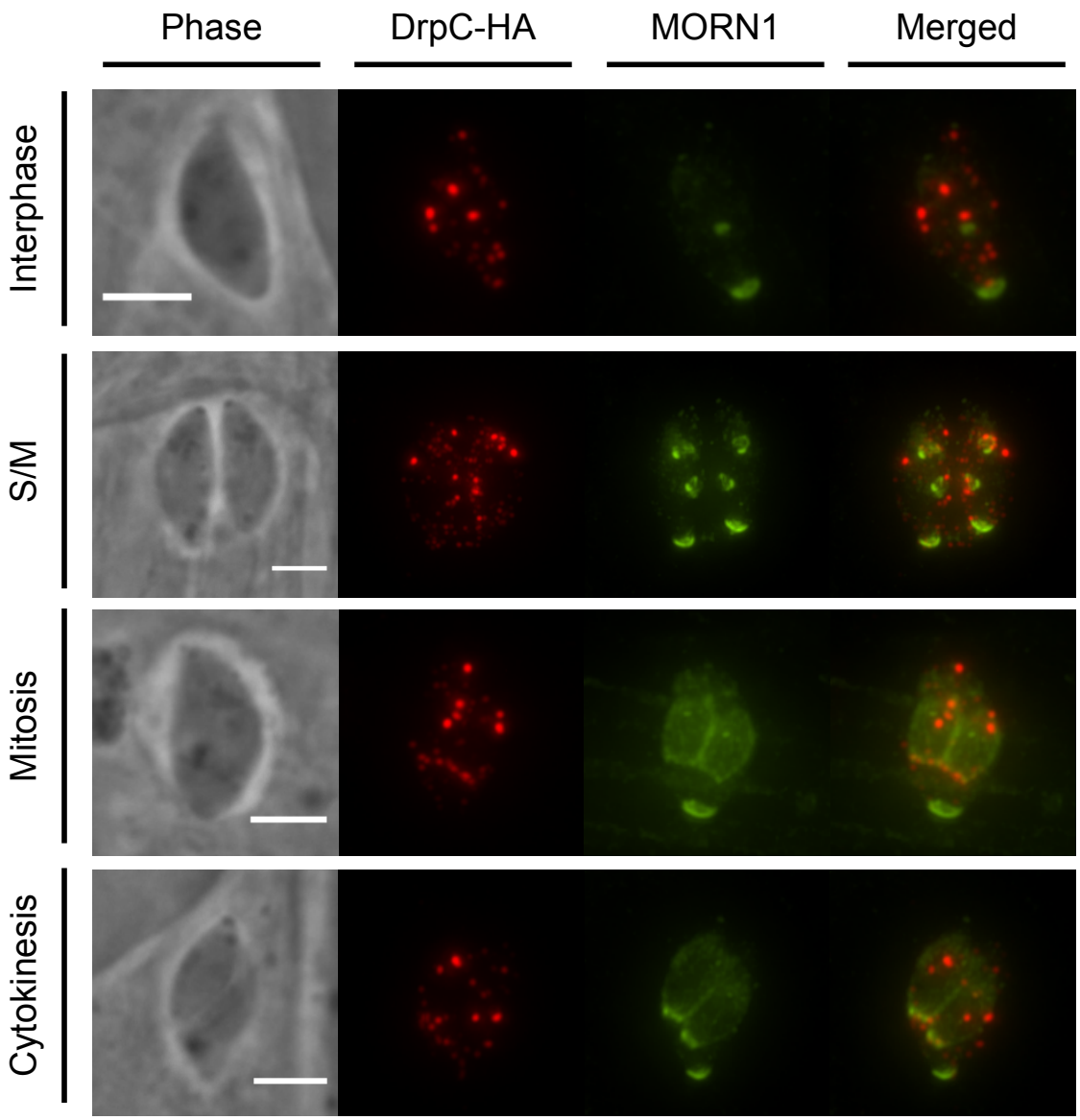

Figure 28: TgDrpC co-localizes with MORN1 structures during cell division.
IFA analysis of TgDrpC-HA (red) co-stained for MORN1 (green). TgDrpC does not co-localize with MORN1 at the basal complex during interphase, but is recruited to the daughter bud early during formation. TgDrpC co-migrates with MORN1 at the leading edge of the daughter parasite pellicle during mitosis until the final stages of cytokinesis. Scale bar = 3μm.

3.11 Conditional knock-down of TgDrpC impairs parasite replication

Given the dynamic localization of TgDrpC, we hypothesized that this protein may be involved in trafficking of membrane material to the inner membrane complex of the daughter parasites, which is thought to be derived from the ER/Golgi compartments [9].

We sought to determine the function of TgDrpC by assessing the effects of conditional TgDrpC knock-down on parasite replication and fitness. We used a conditional knock-down approach becuase previous studies showed that TgDrpC is essential for parasite viability [213,232]. We employed a similar cloning strategy utilized to introduce the 3xHA epitope tag at the endogenous TgDrpC locus in the RHΔ*hxgprt*Δ*ku80* background but included a destabilization domain (DD) tag in the tagging construct. For this system, proteins fused to the DD tag are constitutively degraded in the absence of a synthetic stabilizing compound called Shield-1 [233]. This allows for the reversible regulation of protein levels in *Toxoplasma* and for the functional characterization of essential genes [234].

Two independent TgDrpC-HA-DD parasite clones were isolated and the regulation of TgDrpC-HA-DD protein by Shield-1 was assessed. Plaque assays performed in the presence of a two-fold dilution series of Shield-1 showed a concentration-dependent reduction in the area of host cell lysis, suggesting that loss of TgDrpC impaired parasite replication (**Figure 29**). We next monitored the TgDrpC-HA-DD protein levels by immunoblotting to assess the kinetics and efficiency of TgDrpC knock-out (**Figure 30**). No reduction in TgDrpC-HA-DD protein levels was observed following 24 hours of culture in the absence of Shield-1. However, after 48 hours without Shield-1 we observed a nearly complete loss of TgDrpC-HA-DD protein levels (88.5% reduction, ± 7.4%, n=3, SEM). No decrease in endogenously tagged TgDrpC protein levels was observed in the TgDrpC-HA parasite strain, illustrating the specific degradation of DD-tagged TgDrpC.

We next assessed the effects of loss of TgDrpC on parasite replication by conducting doubling assays in the presence or absence of Shield-1. In agreement with our immunoblotting results, we observed no difference in number of parasites per vacuole after 24 hours without Shield-1. After 48 hours, TgDrpC-HA and TgDrpC-HA-DD parasites maintained in Shield-1 appeared to have undergone egress and reinvasion, as most vacuoles contained 4 or fewer parasites (**Figure 31**). In contrast, we observed that the majority of vacuoles in the TgDrpC-HA-DD parasites contained 16 or more parasites, suggesting that the loss of TgDrpC blocks parasite replication and prevents progression through the lytic cycle.

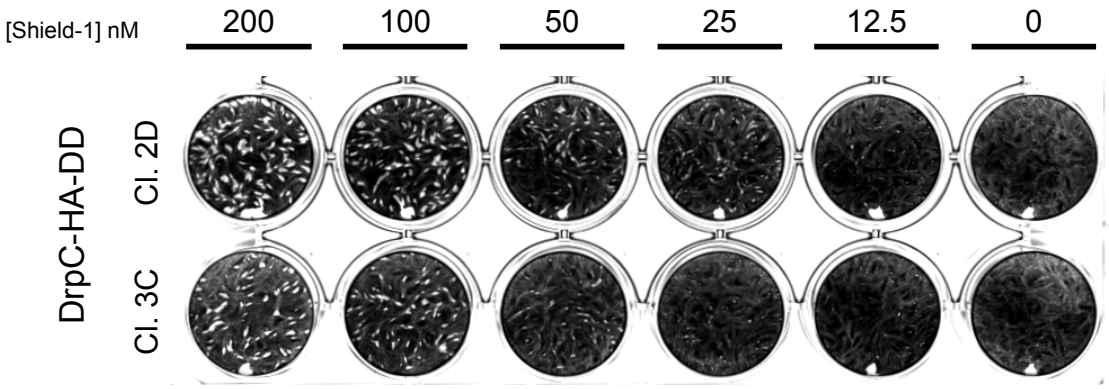

Figure 29: Conditional knock-down of TgDrpC using destabilization domain (DD) reveals essential role in parasite viability.
Plaque assay showing area of host cell lysis due to parasite replication over a five day period. Plaque size shows a positive correlation with concentration of Shield-1, indicating that stabilization of TgDrpC-HA-DD is required for parasite growth.

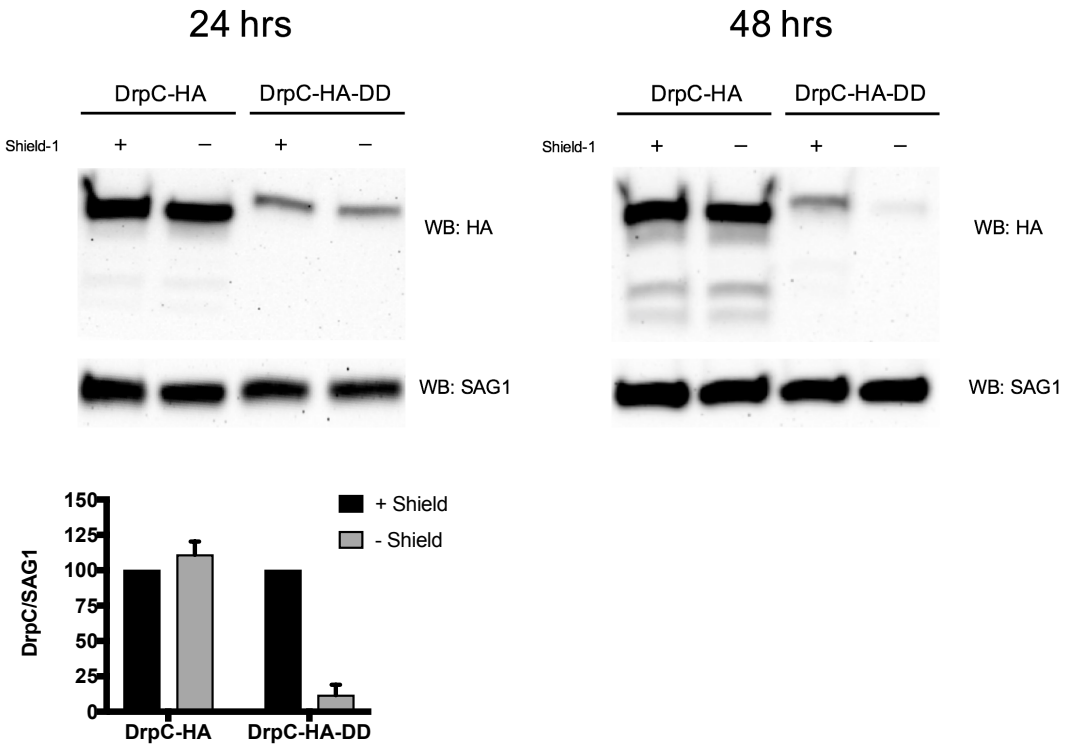

Figure 30: Assessment of TgDrpC-HA-DD regulation by Shield-1.
Immunoblots staining for TgDrpC-HA and TgDrpC-HA-DD proteins in the presence and absence of 200 nM Shield-1. A reduction of TgDrpC-HA-DD protein levels is observed 48 hours after the removal of Shield-1. Quantitation showing densitometry analysis of three biological replicates shown on right (n=3, ±SEM).

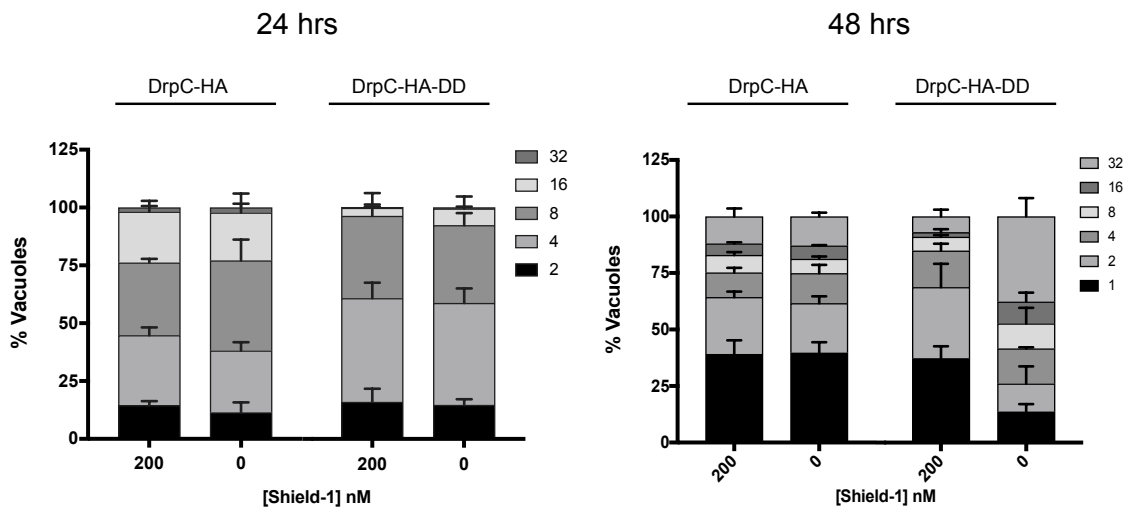

Figure 31: Loss of TgDrpC impairs parasite replication and progression through lytic cycle.
Doubling assays quantifying the number of parasites per vacuole following 24 and 48 hours of growth in the presence or absence of Shield-1 (n=3, ±SEM).

3.12 Conditional knock-down of TgDrpC impairs organelle maintenance and biogenesis

Having shown that TgDrpC is required for parasite replication, we next sought to determine whether the growth impairment was due to defects in organelle biogenesis or maintenance. We first assessed the effects of conditional TgDrpC knock-down on the inner membrane complex, which was visualized by IFA using antibodies against IMC3. The relocalization of TgDrpC to the daughter parasites during division suggested that TgDrpC may be involved in the trafficking of membrane or proteins to the newly forming daughter pellicle. In TgDrpC-HA-DD parasites maintained in the presence of Shield-1, we saw normal IMC3 staining delineating the entire parasite pellicle (**Figure 32**). Upon loss of TgDrpC by removal of Shield-1, parasites were highly vacuolarized with large, membranous blebs within the PV at the basal end of parasites (**Figure 32**, arrowheads). However, despite these irregularities in parasite morphology, staining for IMC3 showed that IMC3 was correctly localized and delineated each individual parasite pellicle. Additionally, we observed parasites undergoing mitosis with IMC3 recruited to the budding daughter parasites (**Figure 32**, arrows), suggesting that TgDrpC is not required for the formation of the inner membrane complex during division.

We next assessed the effects of TgDrpC knock-down on the mitochondrion and apicoplast organelles, which require TgAtg8 function for maintenance and division.

Conditional knock-down of TgDrpC resulted in mitochondrial fragmentation in approximately 35-45% of parasites (**Figure 33**). Additionally, we observed vacuoles containing parasites lacking a discernible apicoplast, which occurred at similar frequency as the observed mitochondrial phenotype (**Figure 33**). These phenotypes are similar to the ones observed following genetic manipulation of TgAtg8 and members of the TgAtg8 conjugation pathway, suggesting that TgAtg8's function in maintaining these organelles may be facilitated in part by its interaction with TgDrpC.

Given the enrichment of Golgi-trafficking related proteins identified in the TgATg8 interactome, we determined the effects of TgDrpC knock-down on the Golgi apparatus. Upon maintaining TgDrpC-HA-DD parasites in the absence of Shield-1, we found a significant number of vacuoles containing Golgi that appeared completely disrupted, as visualized by staining for TgSORTLR (**Figure 34**). A similar phenotype is observed when tachyzoites are exposed to Brefeldin A, which inhibits the association of COP-I coat proteins with the Golgi and results in the collapse of the Golgi due to fusion with the ER (**Figure 34**) [235].

Previous studies showed that disruption of Golgi-trafficking by overexpression of a dominant-negative version of TgSORTLR blocked the formation of rhoptries and micronemes [236]. Additionally, disruption of the Golgi with Brefeldin A blocks secretion of proteins from the dense granules [235]. Further, the biogenesis of the rhoptries and micronemes is dependent upon the dynamin-related protein TgDrpB [223]. Therefore, we hypothesized that conditional knock-down of TgDrpC may similarly effect the formation or function of these secretory organelles. To test this hypothesis, we preformed immunofluorescence assays to visualize the rhoptries and dense granules under the presence and absence of Shield-1. These assays showed that conditional knock-down of TgDrpC led to an accumulation of the rhoptry protein ROP1 in small cytoplasmic vesicles, and resulted in the failure to form mature rhoptry organelles (**Figure 35**). IFA analysis of the micronemal protein MIC5 did not reveal significant alterations in MIC5 localization following loss of TgDrpC, suggesting that biogenesis of the micronemes may not be dependent on TgDrpC (data not shown). Additionally, we visualized GRA7, a protein that localizes to the dense granules found in the cytoplasm that are constitutively secreted into the PV following invasion of host cells. While TgDrpC-HA-DD parasites maintained in the presence of Shield-1 displayed an enrichment of GRA7 signal in the PV with few cytoplasmic punctae, parasites grown in the absence of Shield-1 contained a significantly higher number of cytoplasmic GRA7

vesicles (**Figure 36**). Together, these results suggest that TgDrpC is required for rhoptry organelle biogenesis and for trafficking of GRA7 vesicles for secretion into the PV.

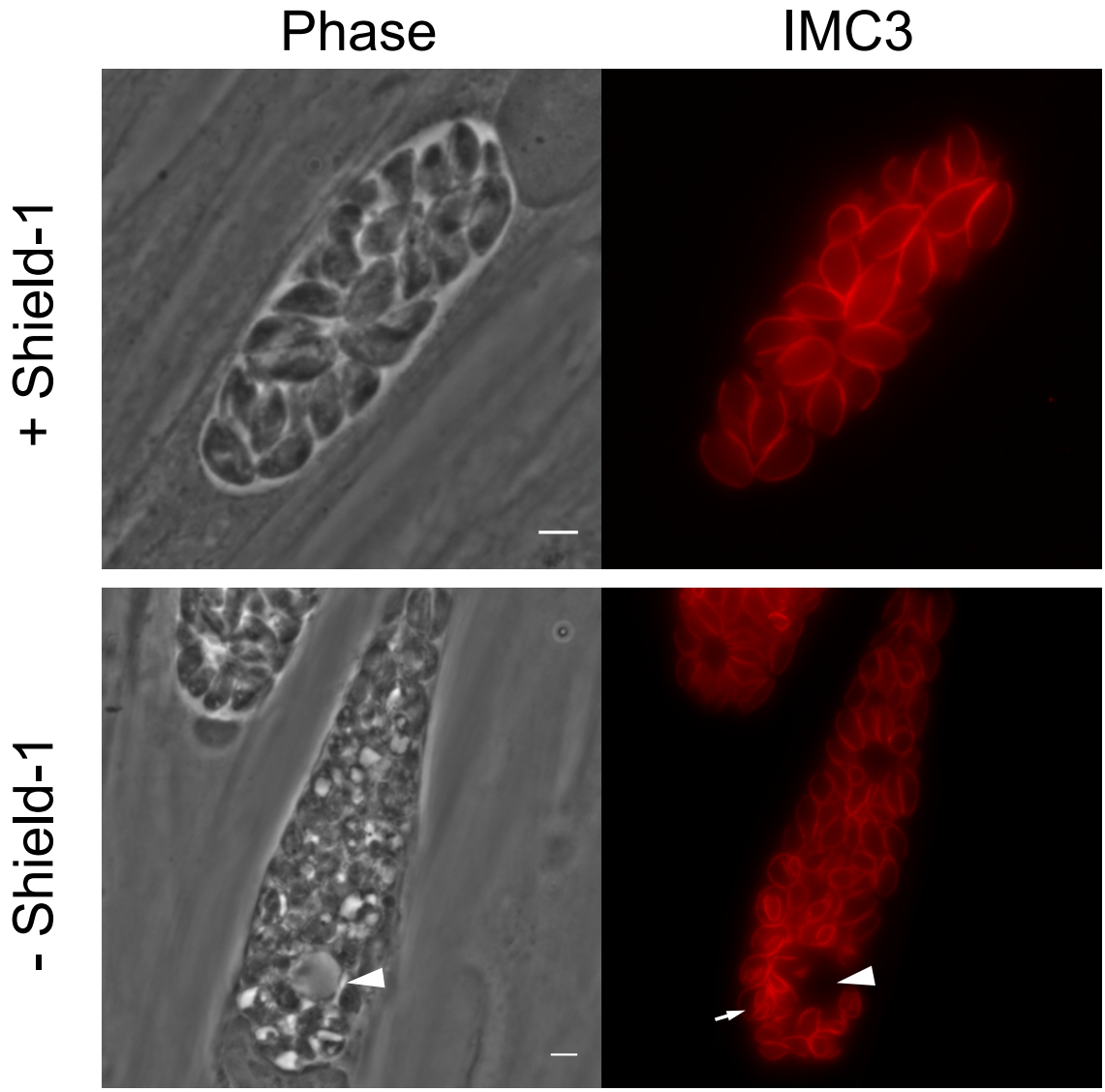

Figure 32: Loss of TgDrpC does not impair formation of IMC.
Representative IFAs of TgDrpC-HA-DD parasites maintained in the presence of 200 nM Shield-1 (+ Shield-1) or in the absence of Shield-1 (- Shield-1). Cells were fixed for IFA analysis 48 hours after the removal of Shield-1, and stained with anti-IMC3 to visualize the inner membrane complex (IMC). Parasites grown in the absence of Shield-1 are vacuolarized, and display large, intravacuolar membranous blebs (arrowheads). However, IMC3 appears to correctly localize to the IMC following removal of Shield-1, and is seen at daughter parasites (arrows), indicating that its recruitment during division is not impaired by loss of TgDrpC. Scale bar = 3μm.

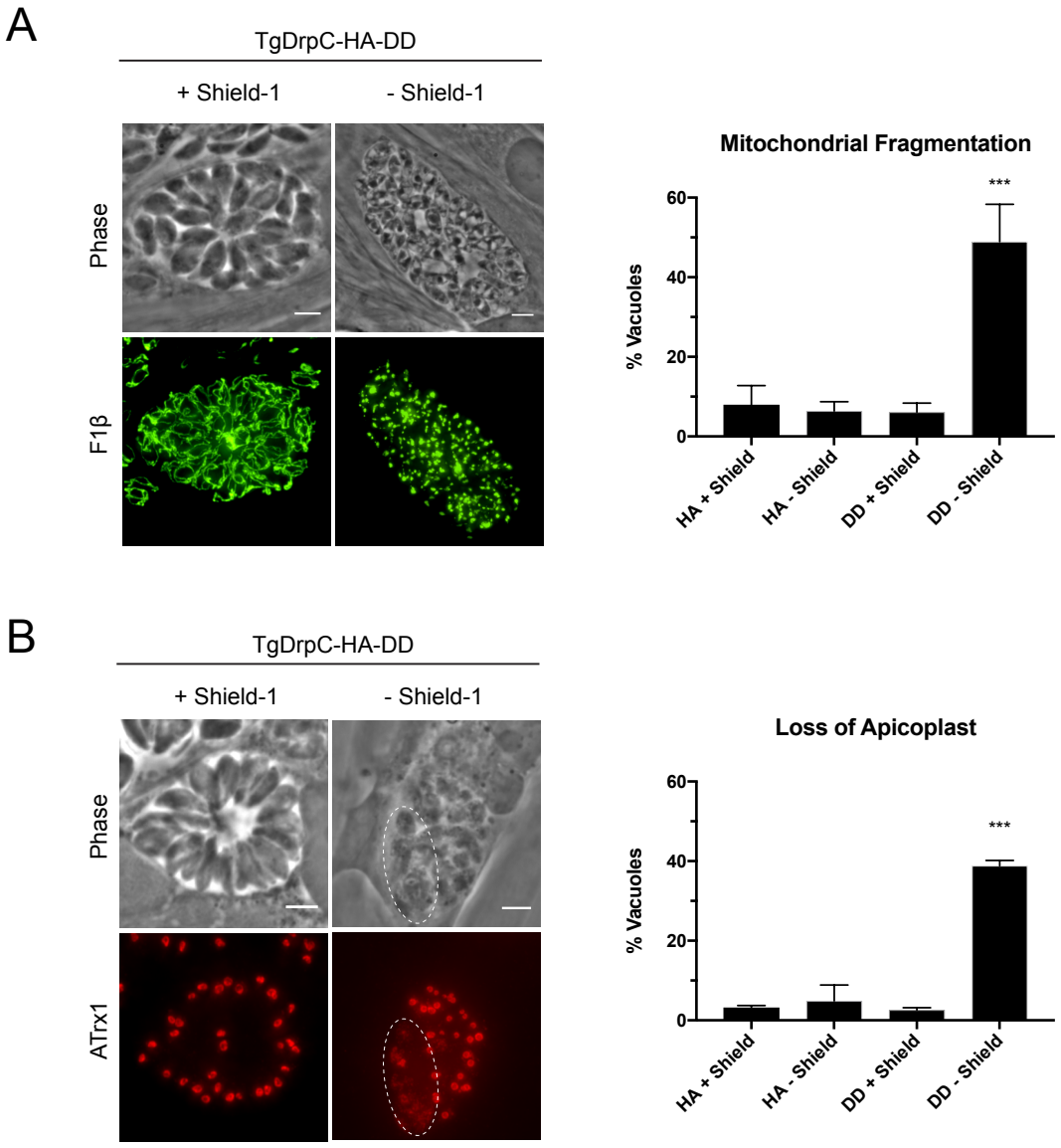

Figure 33: Loss of TgDrpC causes defects in mitochondrion and apicoplast organelles associated with TgAtg8 function.
A) Representative IFAs (left) and quantitation (right) of mitochondrial fragmentation observed upon conditional knock-down of TgDrpC. Parasites growth in that absence of Shield-1 for 48 hours showed fragmentation of the parasite mitochondrion, as observed by staining with an antibody against the mitochondrial matrix protein F1β-ATPase. Scale bar = 3μm. B) Representative IFAs of parasites grown in the presence or absence of 200 nM Shield-1 for 48 hours. Vacuoles containing parasites without apicoplasts or with disintegrated apicoplasts (highlighted with dashed line), were observed upon removal of Shield-1. Scale bar = 3μm. Quantitation for both A) and B) represent n=3, ± SEM, *** = $p < 0.0001$, one-way ANOVA with Sidak-corrected multiple comparisons.

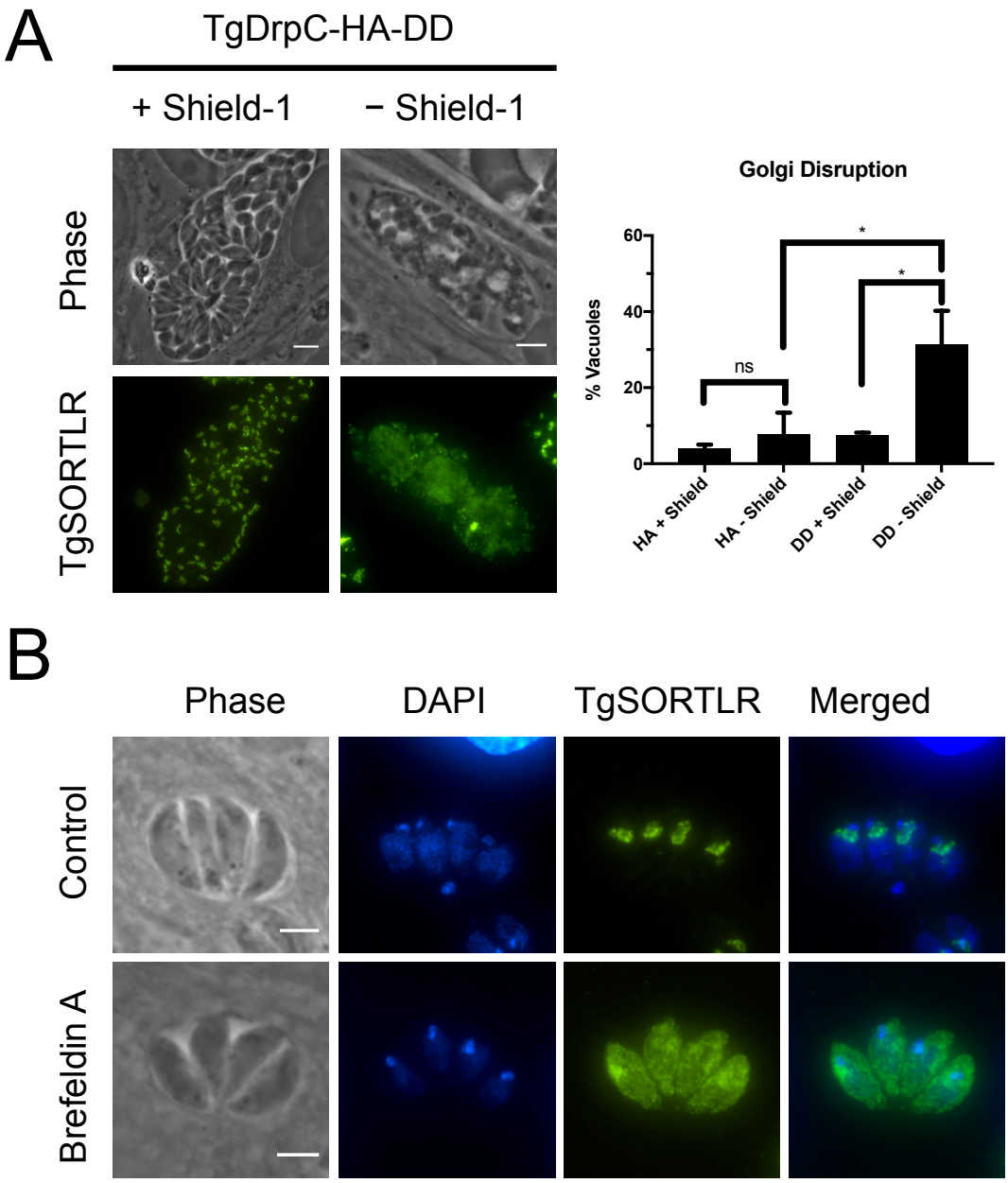

Figure 34: Loss of TgDrpC results in disruption of the Golgi apparatus.
A) Representative IFA of TgDrpC-HA-DD parasites grown in the presence or absence of 200 nM Shield-1 for 48 hours. In the absence of Shield-1, vacuoles contained parasites with disrupted Golgi, as visualized with staining for TgSORTLR (green). Quantitation represents n=3, ± SEM, * = $p < 0.05$, one-way ANOVA with Sidak-corrected multiple comparisons. B) Representative IFA of parasites treated for 2 hours with DMSO (control) or 5 µg/mL Brefeldin A, showing the redistribution of TgSORTLR (green) following disruption of the Golgi. Scale bar = 3µm

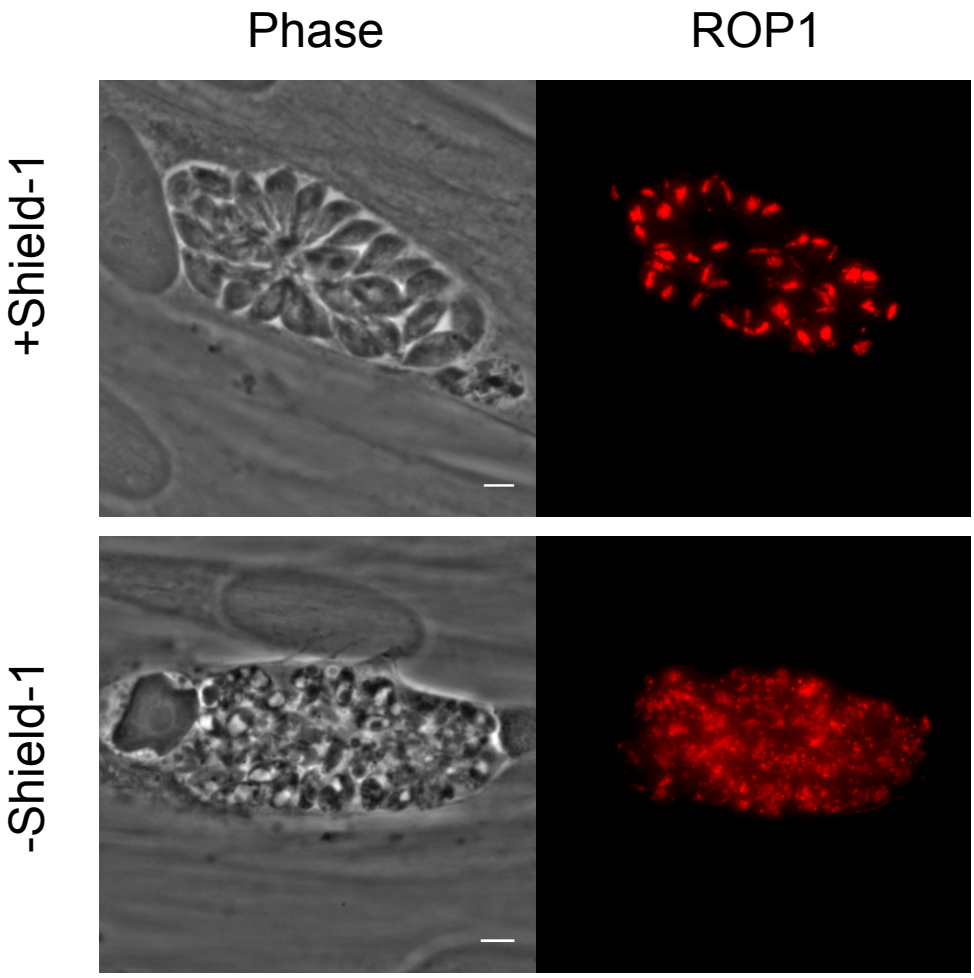

Figure 35: Loss of TgDrpC inhibits the formation of rhoptry organelles.
Representative IFAs of parasites maintained in the presence or absence of 200 nM Shield-1 for 48 hours. Staining for the rhoptry protein ROP1 (red) showing that in the absence of Shield-1, ROP1 is found to localize to small cytoplasmic vesicles rather than fully-formed, mature rhoptries. Scale bar = 3μm.

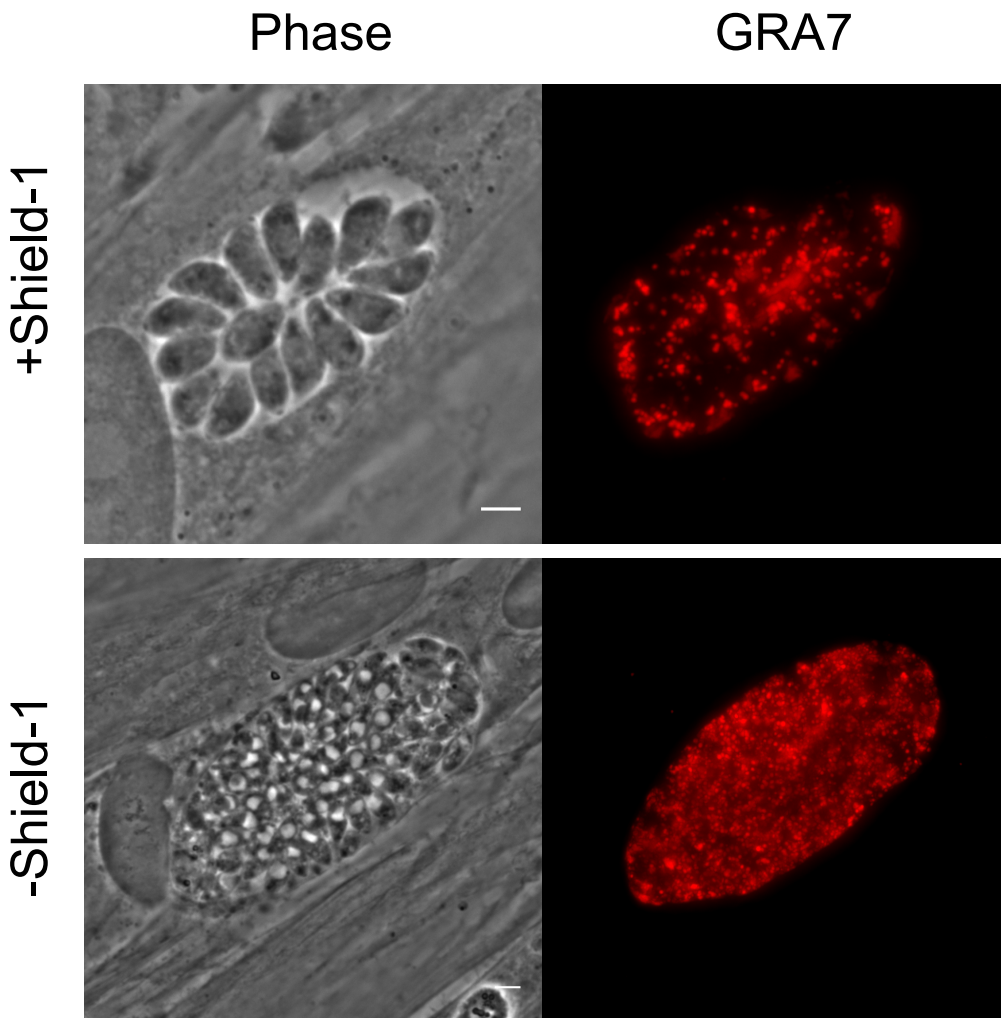

Figure 36: Loss of TgDrpC impairs secretion of the dense granules into the PV. Representative IFAs of parasites maintained in the presence or absence of 200 nM Shield-1 for 48 hours. Staining for the dense granule protein GRA7 (red) revealed an enrichment of GRA7 localization to vesicles in the parasite cytoplasm in the absence of Shield-1, suggesting an impairment of dense granule secretion upon loss of TgDrpC. Scale bar = 3μm.

Summary Aim 2:

With our second aim, we took advantage of reagents generated in our first aim (cMyc-TgAtg8) to identify TgAtg8 interacting proteins using a proteomics approach. This work is the first study to identify or characterize the interacting proteins for any member of the autophagy machinery in *Toxoplasma.* In addition to confirming the interaction between members of the TgAtg8 conjugation system, we discovered a potential role for TgAtg8 in trafficking of vesicles through the Golgi. Although this function of TgAtg8 has not previously been proposed in *Toxoplasma*, the identified TgAtg8 interacting proteins

are homologues of proteins that interact with the mammalian GATE-16 Atg8 family protein, which was originally identified for its role in Golgi trafficking. Our analysis of one of the identified TgAtg8 interacting proteins, TgDrpC, revealed that this divergent dynamin-like protein is essential for parasite viability. Conditional knock-down of TgDrpC indicates potential functional roles for TgDrpC in biogenesis of the rhoptry organelles and secretion of the dense granules. Additionally, loss of TgDrpC resulted in fragmentation of the parasite mitochondrion, disruption of the Golgi and loss of apicoplast. As these phenotypes are similar to those seen upon loss of TgAtg8, we believe that the interaction between TgAtg8 and TgDrpC may be required for the maintenance of these organelles, however the exact mechanism behind these phenotypes remains unresolved.

Aim 3: Determine whether TgAtg8 lipidation could be pharmacologically inhibited by treatment with recently identified *Plasmodium falciparum* Atg3-Atg8 interaction inhibitors.

Recent work characterizing the *Plasmodium falciparum* Atg3-Atg8 interaction has identified a group of small molecule inhibitors that bind to PfAtg8 W- and L-site pockets and prevent its association with PfAtg3's AIM region. Three inhibitor compounds were identified from the open-access Medicines for Malaria Venture box of Malaria compounds, and were effective against *P. falciparum* in culture. Importantly, these compounds also display activity against numerous other protozoan parasites, leading to the proposal that inhibition of parasitic Atg3-Atg8 interactions may be a conserved drug target for many protozoan pathogens. We hypothesized that these inhibitors would have utility in *Toxoplasma* as tools to study the function of the autophagy pathway in parasite biology and as potential new therapeutics. In our third aim we tested the hypothesis that these compounds would inhibit the Atg3-Atg8 interaction in *Toxoplasma* as they do in *Plasmodium.* In the following sections, we present data showing that although these compounds are effective at inhibiting *Toxoplasma in vitro*, these compounds do not prevent the TgAtg3-Atg8 interaction and instead display novel mechanisms of action relating to parasite replication and calcium-mediated egress.

3.13 Virtual docking suggests MMV compounds are unable to bind within TgAtg8 W- and L-site pockets

To assess whether the three compounds from the Malaria Box identified as PfAtg3-Atg8 inhibitors (referred to hereafter as MMVs 1-3, Table 4) have similar effects

against *Toxoplasma*, we first sought to compare the amino acid conservation of the W- and L-site residues between PfAtg8 and TgAtg8, as these are the regions of the protein targeted by these compounds [162]. Alignment of the PfAtg8 and TgAtg8 amino acid sequences showed a high level of conservation (66% identity, 83% similarity). Importantly, 17 out of the 19 residues comprising the PfAtg8 W- and L-site binding pockets are conserved in TgAtg8 (**Figure 37A**). This high level of conservation between the *P. falciparum* and *Toxoplasma* Atg8 suggests that the MMV compounds identified as PfAtg3-Atg8 inhibitors may act similarly on TgAtg8.

To test this hypothesis, we used the I-TASSER predicted TgAtg8 protein structure for *in silico* docking analyses with MMVs 1-3 (**Figure 37B**). In parallel, we performed docking of all three compounds with the solved PfAtg8 crystal structure to confirm that the predictions generated by the docking program used in our studies (SwissDock) were in agreement with the previous docking studies that used the OpenEye docking program [162]. Interestingly, while all three compounds were predicted to bind within the W- and L-site pockets in PfAtg8, only MMV1 was predicted to bind to this region in TgAtg8. Further, no binding sites involving the TgAtg8 W- and L-site pockets were found for MMV2 and 3 (**Figure 37B**) even though our docking studies successfully reproduced the previously reported binding predictions for these two compounds in PfAtg8. Together, these results suggest that the ability of the PfAtg3-Atg8 inhibitors to bind within the TgAtg8 W- and L-site pockets may not be conserved, despite high levels of similarity between PfAtg8 and TgAtg8 in both amino acid sequence and predicted protein structure.

Table 4: Effects of *Plasmodium falciparum* Atg3-Atg8 inhibitors on protozoan pathogens

Compound	MMV1	MMV2	MMV3	Reference
MMV Number	MMV007907	MMV001246	MMV665909	
ZINC ID	ZINC190251	ZINC06823436	ZINC12547067	
CHEMBLE ID	CHEMBL470514	CHEMBL591637	CHEMBL591362	
Structure	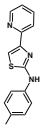	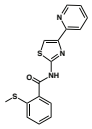	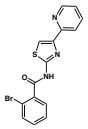	
Toxoplasma gondii				
RhΔhx, EC_{50}	597 nM	203 nM	275 nM	This publication
TS-4, EC_{50}	>30 µM	>30 µM	>30 µM	Boyom et al., 2014
Plasmodium falciparum				
Blood Stage, EC_{50}	82-2374 nM	1206-4375 nM	1360-3741 nM	Van Voorhis et al., 2016
Life Cycle Stages[a] Inhibition at 10µM No effect				Van Voorhis et al., 2016
Gametocytes, EC_{50}	231-2678 nM	781-4651 nM	2019 nM	Duffy and Avery, 2013, Lucantoni et al., 2016, Van Voorhis et al., 2016
Plasmodium berghei				
Liver Stage % Inhibition at 5 µM	91%	97%	95%	Van Voorhis et al., 2016
Cryptosporidium parvum, EC_{50}	N/A	1780 nM	3470 nM	Van Voorhis et al., 2016
Neospora caninum % Inhibition at 1 µM	N/A	>50%	>50%	Van Voorhis et al., 2016
Babesia				
B. bovis, EC_{50}	15190 nM	6600 nM	4600 nM	Van Voorhis et al., 2016
B. bigemina, EC_{50}	12900 nM	680 nM	1000 nM	Van Voorhis et al., 2016
B. caballi, EC_{50}	5620 nM	3350 nM	1000 nM	Van Voorhis et al., 2016
Trypanosoma				
T. brucei rhodesiense, EC_{50}	14814 nM	272 nM	376 nM	Kaiser et al., 2015
T. brucei brucei, EC_{50}	13423 nM	931 nM	1037 nM	Kaiser et al., 2015
T. cruzi, EC_{50}	281 nM	250 nM	260 nM	Kaiser et al., 2015
Leishmania				
L. infantum, EC_{50}	5384 nM	336 nM	1587 nM	Kaiser et al., 2015
L. donovani (axenic), % Inhibition at 5 µM	98%	96%	85%	Van Voorhis et al., 2016

[a] ER, early ring, LR, late ring, T, trophozoite, S, schizont, M, merozoite

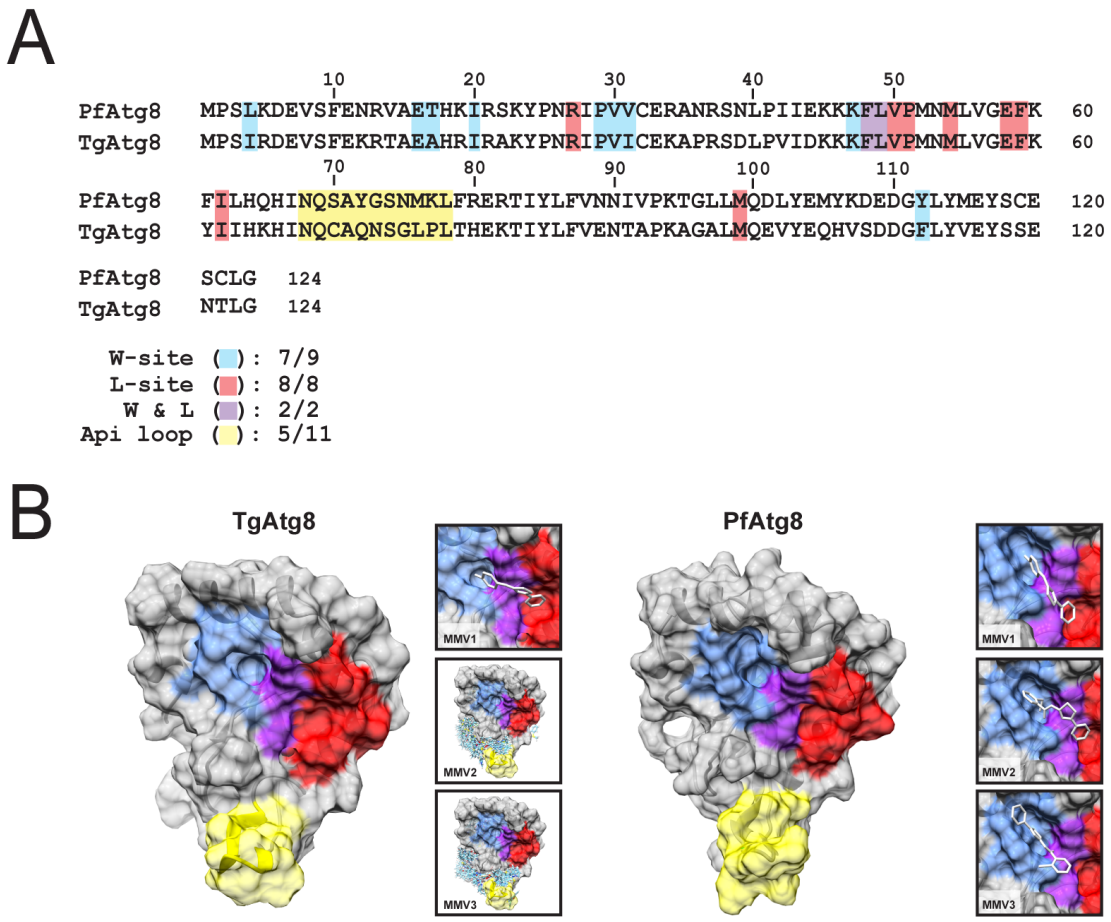

Figure 37: *P. falciparum* Atg3-Atg8 inhibitors are not predicted to bind to TgAtg8 despite conservation of residues comprising the W- and L-site pockets.
A) Comparative analysis of the PfAtg8 and TgAtg8 amino acid sequences, highlighting the conservation of residues in the W-site (blue) L-site (red), and apicomplexan-specific loop (yellow). Two residues (F48/L49) contributing to both W- and L-sites are highlighted in purple. Numbers below sequence alignments indicate number of conserved residues in each region. B) The TgAtg8 protein structure was predicted using the I-TASSER server and was used for *in silico* docking studies for MMVs 1-3. Insets illustrate predicted binding sites for each of the MMV compounds. The residues located in the W- and L-site binding pockets, as well as the apicomplexan loop, are highlighted on the protein surface using the coloring scheme as described above.

3.14 *Plasmodium* Atg8-Atg3 inhibitors impair *Toxoplasma* replication *in vitro*

Despite these potential differences in binding, we next sought to determine whether MMVs 1-3 inhibited *Toxoplasma* growth. Parasites were inoculated onto HFF monolayers and allowed to replicate for five days in the presence of either 10 μM drug or DMSO vehicle. Treatment with all three MMVs showed a significant reduction in the area of host cell lysis, suggesting that *Toxoplasma* progression through the lytic cycle was

impaired by drug treatment (**Figure 38A**). This growth inhibition was further confirmed using an established colorimetric assay [190] that utilizes a *Toxoplasma* strain stably expressing the *E. coli* β-galactosidase enzyme to generate quantitative inhibition curves for MMVs 1-3 (**Figure 38B**). All three compounds exhibited sub-micromolar EC_{50} values, in agreement with the range of EC_{50} values reported for these compounds in *P. falciparum* and other protozoan parasites (Table 4) [237–241]. Together, our results show that all three PfAtg3-Atg8 interaction inhibitors are active against *Toxoplasma* in a dose-dependent manner, despite not being identified in a previous screen of the Malaria Box compounds against *Toxoplasma* [237].

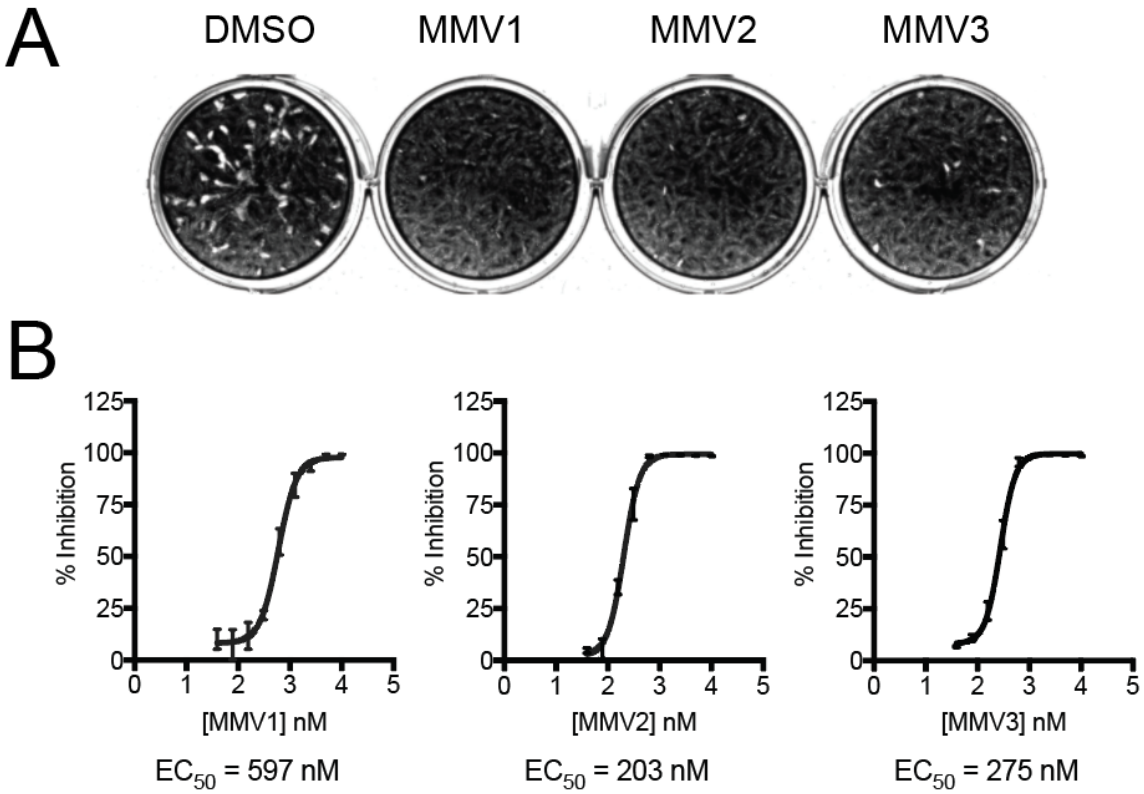

Figure 38: PfAtg3-Atg8 inhibitors block *Toxoplasma* growth *in vitro*.
A) Representative plaque assay showing impaired parasite growth over a five-day period in the presence of MMV compounds at 10 μM, as compared to DMSO vehicle treated controls. B) Growth inhibition curves were generated to determine of EC50 concentrations for each of the three MMV compounds. Parasites expressing β-galactosidase were cultured in the presence of drug or DMSO for 4 days. Parasite growth was assessed by colorimetric assay following a 24-hour incubation with the β-galactosidase substrate CPRG. Percent inhibition was calculated by normalizing to uninfected HFFs (100% inhibition) and DMSO vehicle treated infected wells (0% inhibition). Curves represent the average of three independent experiments, and are plotted with error bars representing ± standard error of the mean (SEM). EC_{50} values were calculated by non-linear regression using Prism and are included for each compound below their respective curves. C) Treatment with MMVs 1-3 showed a

concentration-dependent decrease in the number of parasites per vacuole after 24 hours of treatment as compared to DMSO vehicle treated controls (n=3, ± SEM).

3.15 Effects of MMV1-3 on Atg8-related organelles

Having identified that the MMV compounds could effectively inhibit *Toxoplasma* growth, we next sought to assess whether this inhibition was associated with their reported mechanism of action in inhibiting PfAtg3-Atg8 interaction and thus preventing Atg8 lipidation. Genetic manipulation of TgAtg8 lipidation by conditional knock-down of TgAtg3 [94] and TgAtg4 [104] resulted in defects in the maintenance of the mitochondrion and apicoplast organelles. We therefore hypothesized that treatment with the MMV compounds might similarly effect these organelles. Interestingly, while conducting these assays, we noted that treatment with MMV1 at concentrations greater than 1 μM caused parasite egress from the host cell. This effect was unique to MMV1, as MMV2 and MMV3 did not induce egress at any concentrations tested. Therefore, in the case of MMV1, our characterization of the effects of drug treatment on the mitochondrion and apicoplast was limited to concentrations below 1 μM.

Treatment with MMV1 at concentrations that did not induce parasite egress had no effect on apicoplast division or mitochondrial integrity (**Figure 39 and Figure 40**). However, upon treating intracellular parasites with 10 μM MMV2 and MMV3, we observed significant mitochondrial fragmentation within the first 6 hours of treatment (MMV2 = 65.0±13.0%, MMV3 = 84.7±8.2%, SEM, n=3), with nearly all vacuoles containing parasites with fragmented mitochondria after 24 hours of treatment (MMV2 = 94.4±3.2%, MMV3 = 97.7±0.7%, SEM, n=3) (**Figure 39**). Unlike the mitochondrion, the apicoplast remained intact under all treatment conditions, although defects in positioning and segregation of this organelle into dividing parasites were frequently observed (**Figure 40,** arrowheads).

As MMV2 and MMV3 were found to inhibit *Toxoplasma* growth with sub-micromolar EC_{50} values, we next assessed whether mitochondrial fragmentation also occurred at lower concentrations of drug treatment. Interestingly, no alterations in mitochondrial morphology were observed in parasites treated with 1 μM MMV2 or MMV3 (**Figure 41**), a concentration at which both compounds significantly inhibit parasite growth (**Figure 38B**). Additionally, whereas the effects of monensin treatment and starvation on mitochondrial fragmentation were prevented by co-treatment with the autophagy inhibitor 3-methyladenine (3-MA) [93,154], no such protection was observed

upon co-treatment of MMV2 or MMV3 with 3-MA (**Figure 41**). These results suggest that the inhibition of parasite growth by MMV2 and MMV3 is independent of their ability to induce mitochondrial fragmentation at higher concentrations.

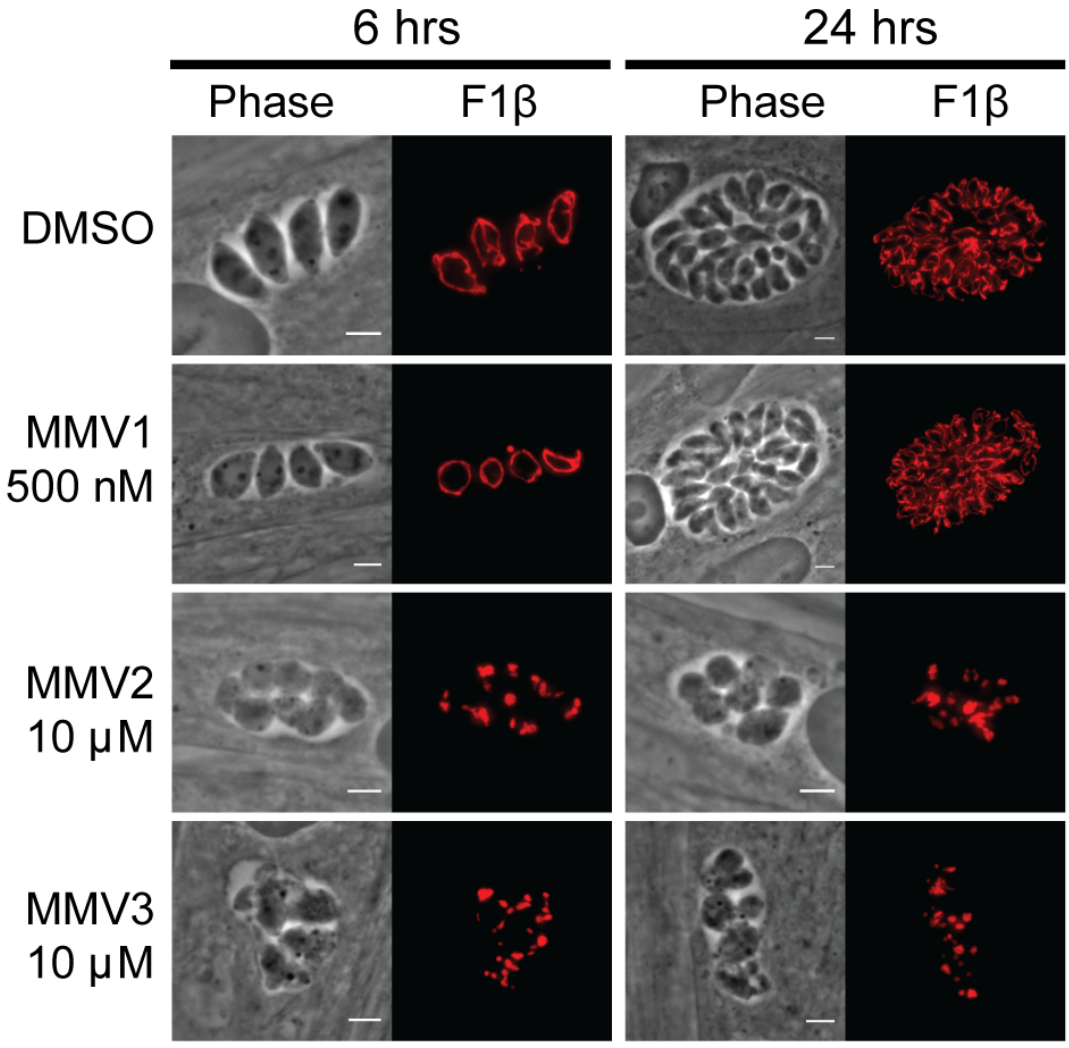

Figure 39: Treatment with MMV2 and MMV3 causes fragmentation of the parasite mitochondrion.
A) Representative IFA images following 6 and 24 hours of treatment with DMSO vehicle or MMVs, stained for F1β-ATPase (red) to visualize the mitochondrion. B) IFAs of DMSO or MMV treated parasites stained for ATrx1 (red) to visualize the apicoplast and DAPI (blue). The apicoplast remains intact during MMV treatment, however organelle-positioning defects are observed at 24 hours (arrowheads), likely due to the observed defects in cytokinesis. Scale bar = 3µm.

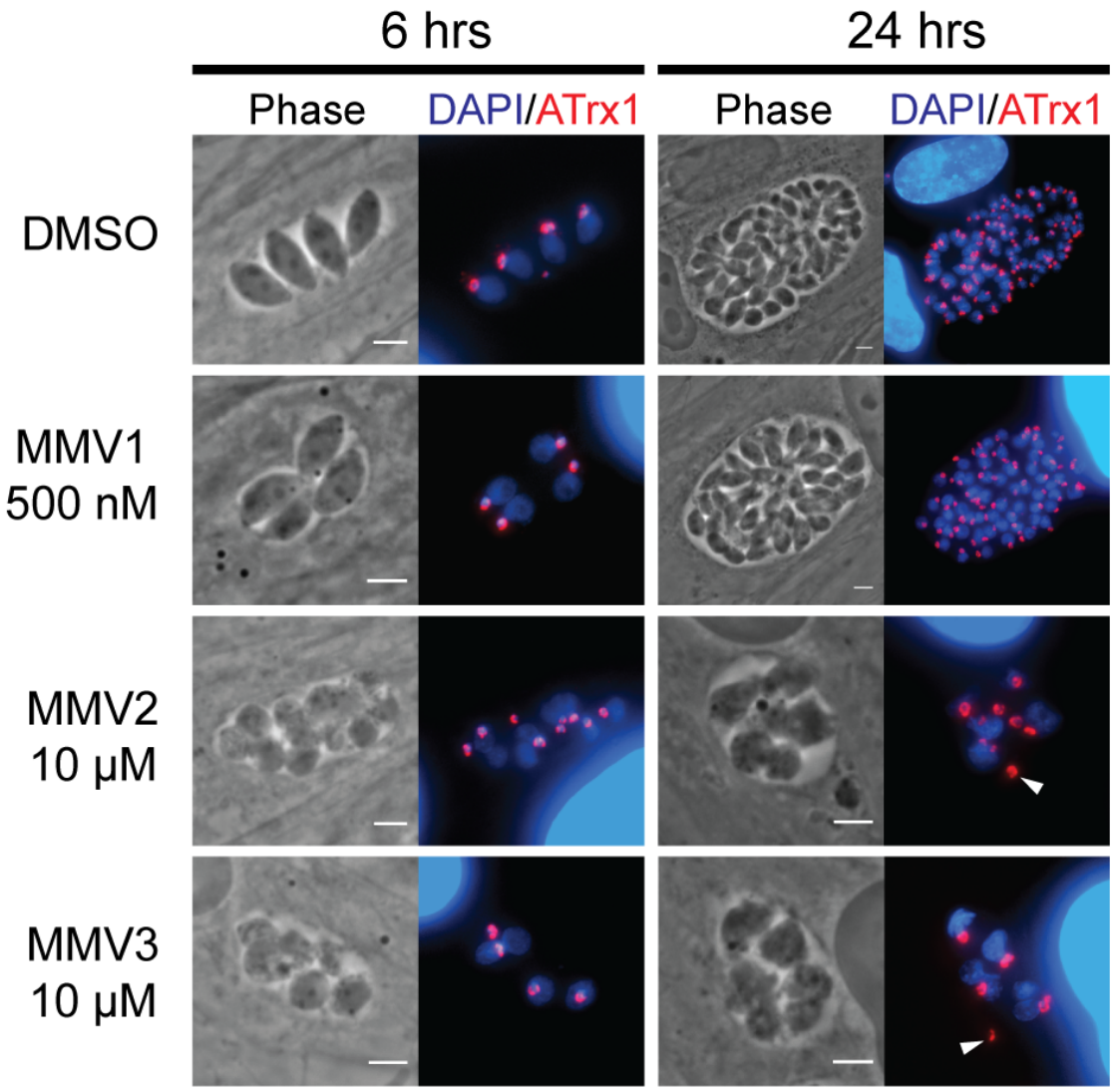

Figure 40: MMV treatment does not result in loss of apicoplast.
Representative IFAs of DMSO or MMV treated parasites stained for ATrx1 (red) to visualize the apicoplast and DAPI (blue). The apicoplast remains intact during MMV treatment, however organelle-positioning defects are observed at 24 hours (arrowheads), likely due to the observed defects in cytokinesis.

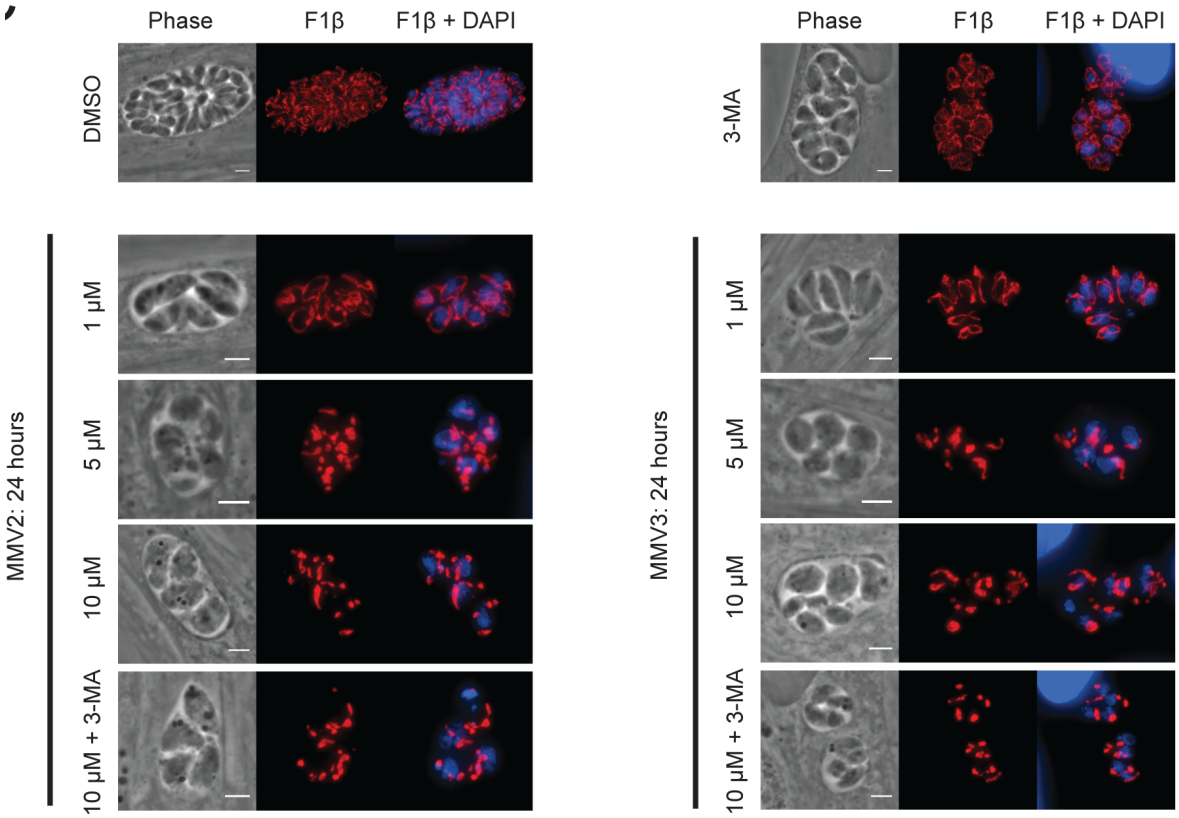

Figure 41: Mitochondrial fragmentation caused by MMV2 and MMV3 not protected by autophagy inhibitor 3-MA.
Representative IFA images of parasites treated with DMSO, 10 mM 3-MA, or MMV2-3 for 24 hours, stained for the mitochondrial matrix protein F1β-ATPase (red) and DAPI (blue). Mitochondrial fragmentation was observed with 5 and 10 μM treatment, and was not protected by co-treatment with 3-MA. Scale bar = 3μm.

3.16 MMV1-3 do not prevent Atg8 lipidation

To further characterize the effects of MMV treatment on the autophagy pathway in *Toxoplasma,* we next sought to directly assess how these compounds altered TgAtg8 lipidation status. In yeast and mammalian systems, Atg8 lipidation is routinely monitored by visualization of a GFP-Atg8 fusion protein, which relocalizes to cytosolic punctae representing autophagosomes following autophagy induction [242]. A similar approach has been used to monitor the induction of TgAtg8 lipidation in *Toxoplasma* in response to drug treatment and starvation [94,154]. However, TgAtg8 also localizes to the outer membrane of the apicoplast in a lipidation-dependent manner [104] . Given the predicted function of MMV1-3 as Atg3-Atg8 interaction inhibitors, we hypothesized that treatment of intracellular parasites with MMV1-3 would result in a loss of TgAtg8 localization to the apicoplast, as was observed in TgAtg8 mutants lacking the C-terminal glycine required

for lipidation [104]. However, we experienced difficulties in testing this hypothesis due to the high levels of GFP-TgAtg8 present in the cytosol as the result of its overexpression [94]. Thus, to facilitate the monitoring of TgAtg8 lipidation and localization in response to intracellular MMV treatment, we utilized the endogenously tagged cMyc-TgAtg8 parasites described in Section 3.4 (**Figure 12**).

We hypothesized that treatment with the MMV compounds would result in a shift in TgAtg8 localization from the apicoplast to the cytosol. However, following 6 and 24 hours of treatment with all three MMVs tested, TgAtg8 retained its punctate staining pattern and remained predominantly localized to the apicoplast (**Figure 42A**). Further, immunoblotting revealed that rather than inhibiting TgAtg8 lipidation, treatment with 10 μM MMV2 and MMV3 for 6 hours resulted in an increase in the lipidated form of TgAtg8, similar to the effects of autophagy induction by starvation and monensin treatment on endogenous TgAtg8 (**Figure 42B**).

As before, the induction of egress by MMV1 treatment limited the concentrations of this compound that we were able to assess to concentrations well below those reported to effect Atg8 lipidation in *Plasmodium falciparum* [162]. Therefore, we could not determine whether MMV1 could block TgAtg8 lipidation in intracellular parasites. To overcome this limitation, we used established methods to monitor GFP-TgAtg8 lipidation following induction of autophagy by extracellular starvation and tested whether MMV1 could prevent the lipidation-dependent relocalization from the cytosol to punctate structures [94]. As shown in **Figure 42C**, no reduction of GFP-TgAtg8 punctae formation was observed by co-treatment with either 1 or 10 μM MMV1. Together, these findings show that the MMV compounds do not inhibit Atg8 lipidation in *Toxoplasma* and are unlikely to act as TgAtg3-TgAtg8 interaction inhibitors as reported for *Plasmodium*.

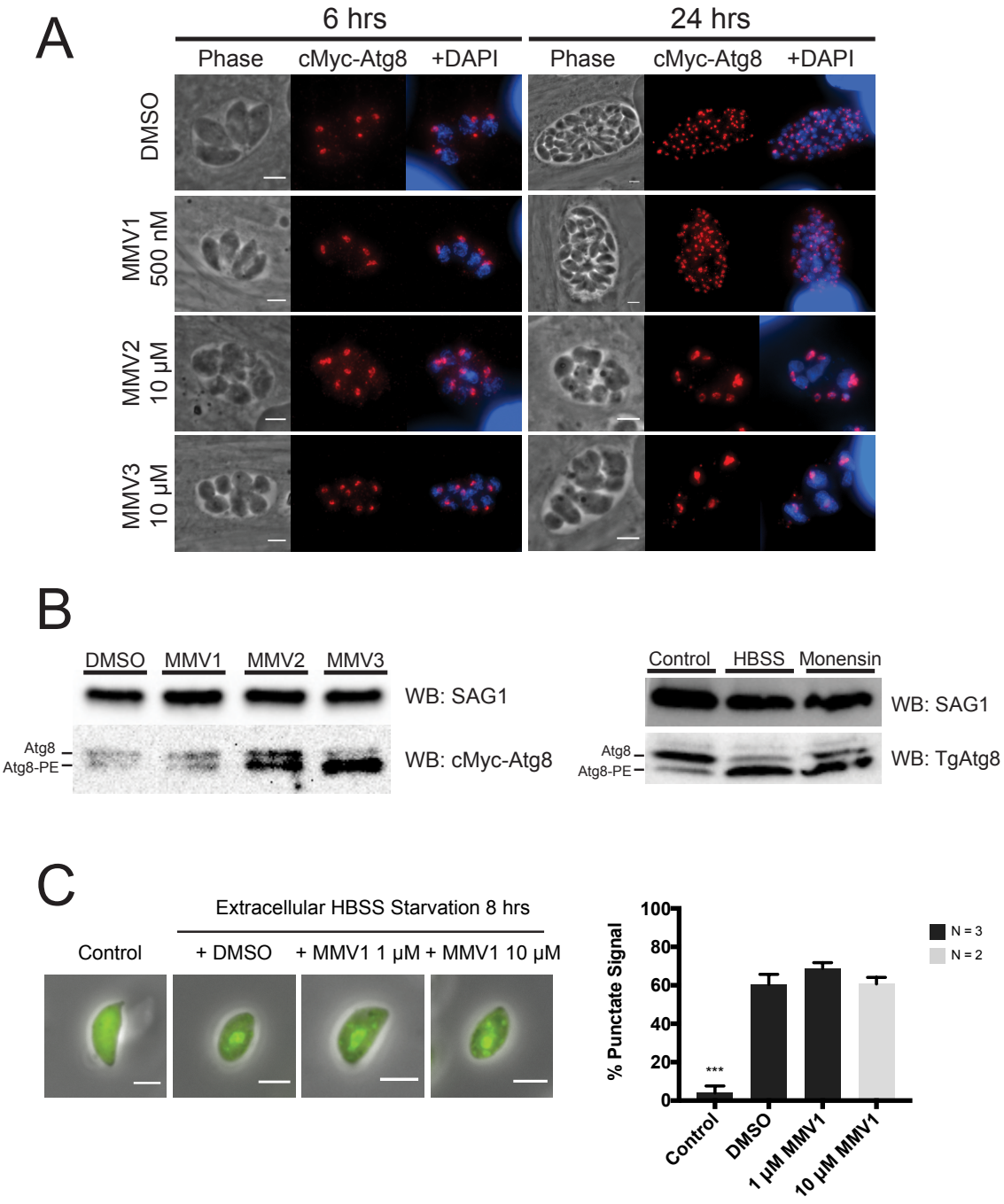

Figure 42: Treatment with MMVs does not alter Atg8 localization at the apicoplast or prevent Atg8 lipidation.

A) Representative IFAs of cMyc-TgAtg8 parasites after 6 and 24 hours of treatment with DMSO or MMVs, stained with DAPI (blue) and for cMyc (red). cMyc-TgAtg8 retains its apicoplast localization following MMV treatment. Scale bar = 3µm. B) Representative immunoblots of lysates from cMyc-Atg8 parasites treated for 6 hours with DMSO or MMVs. Treatment with 10 µM MMV2 and MMV3 increased the ratio of lipidated TgAtg8 (Atg8-PE) to unlipidated TgAtg8 (Atg8). No change in lipidation state was observed by treatment with 500 nM MMV1. The increased levels of Atg8-PE were similar to the

increase in endogenous TgAtg8 lipidation in RHΔ*hxgprt* parasites starved extracellularly (HBSS) or treated with 1 ng/mL monensin for 6 hours, as compared to DMSO treated controls. Blots were probed with anti-cMyc or anti-TgAtg8, and with anti-SAG1 as a loading control. C) Representative IFA images of GFP-Atg8 parasites before (Control) or after 8 hours of extracellular starvation in HBSS. Co-treatment with MMV1 failed to reduce the number of parasites with GFP-Atg8 punctae, *** = $p<0.001$, ± SEM. Scale bar = 3μm.

3.17 MMV2 and MMV3 inhibit *Toxoplasma* cytokinesis

Our initial characterization of MMV1-3 showed that they blocked parasite growth, as shown by the decreased area of lysis of the host cell monolayer. However, a reduction in the area of host cell lysis can be attributed to impairment of one or more steps of the *Toxoplasma* lytic cycle, including parasite replication, egress, and host cell invasion [39]. We therefore sought to determine which step or steps of this cycle were affected by treatment with MMV1-3.

All three compounds were first assessed for their effects on parasite replication by quantifying the number of rounds of parasite replication during 24 hours of drug treatment. Despite the effects of MMV1 on parasite egress, we did observe a concentration-dependent delay in parasite growth at concentrations that did not induce egress (**Figure 43A**). Additionally, treatment with MMV2 or MMV3 at 2.5 μM completely blocked parasite replication, as all vacuoles contained two or fewer parasites after 24 hours of treatment while ~50% of DMSO vehicle treated vacuoles contained 8 or more parasites (**Figure 43A**).

While characterizing the effects of the MMV compounds on parasite replication we observed that parasites treated with 2.5 μM or higher concentrations of MMV2 and MMV3 exhibited an abnormal, rounded morphology with a loss of uniform parasite size and shape **(Figure 43 A-B).** Immunofluorescence staining with DAPI to visualize the parasite nuclei revealed that parasites within these abnormal vacuoles appeared to have nuclei that had duplicated but failed to properly divide. Together, these changes suggested that parasite cytokinesis may be impaired by treatment with MMV2 and MMV3, as the phenotypes are similar to those observed in parasites with defects in the late stages of cell division [200,243].

Quantification of abnormal vacuoles showed that approximately 40% of vacuoles displayed these morphological abnormalities, and the percentage of abnormal vacuoles did not increase between 6 and 24 hours of treatment. These replication defects were further characterized by staining with an antibody against the protein inner membrane

complex 3 (IMC3), a component of the parasite cytoskeleton that together with the plasma membrane comprises the parasite pellicle [244]. While the nuclei in DMSO-treated parasites appeared uniform in size and shape, and were correctly segregated into a single IMC3-stained pellicle, parasites treated with MMV2 and MMV3 contained duplicated nuclei surrounded by a single cytoskeleton, as well as IMC3 structures containing no nucleus or apicoplast (**Figure 44**). Together, these results suggest that the growth inhibitory effects of MMV2 and MMV3 are a result of a rapid block of *Toxoplasma* replication involving disruption of cell division due to impaired daughter bud formation and nuclear division.

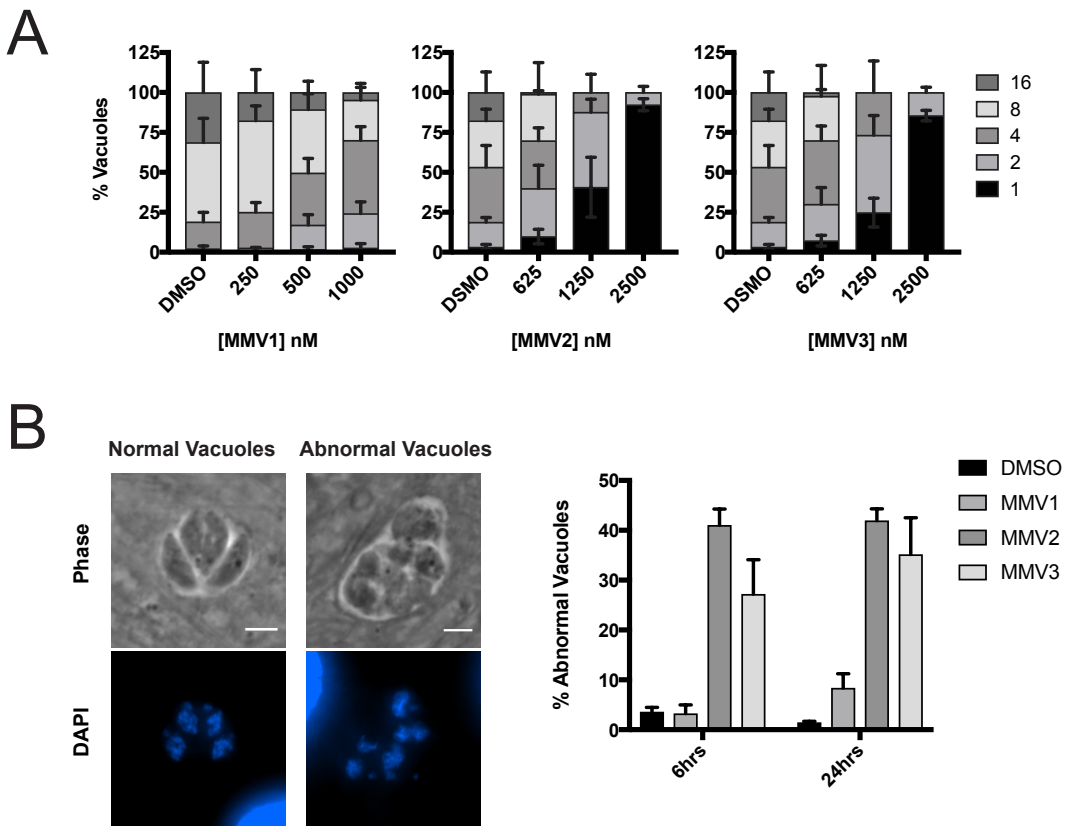

Figure 43: MMV2 and MMV3 block *Toxoplasma* replication and impair division.
A) Treatment with MMVs 1-3 showed a concentration-dependent decrease in the number of parasites per vacuole after 24 hours of treatment as compared to DMSO vehicle treated controls (n=3, ± SEM). B) IFAs of parasites treated with 10 μM MMV2 and MMV3 for 6 hours showing representative images of normal vacuoles (DMSO) and abnormal vacuoles observed with MMV2 and MMV3 treatment. Visualization of the nuclei by staining with DAPI revealed that MMV2 and MMV3 treated parasites contained distorted parasites with apparent defects in nuclear division. The percentage of abnormal vacuoles does not increase between 6 and 24 hours of treatment, n=3, ± SEM. Scale bar = 3μm.

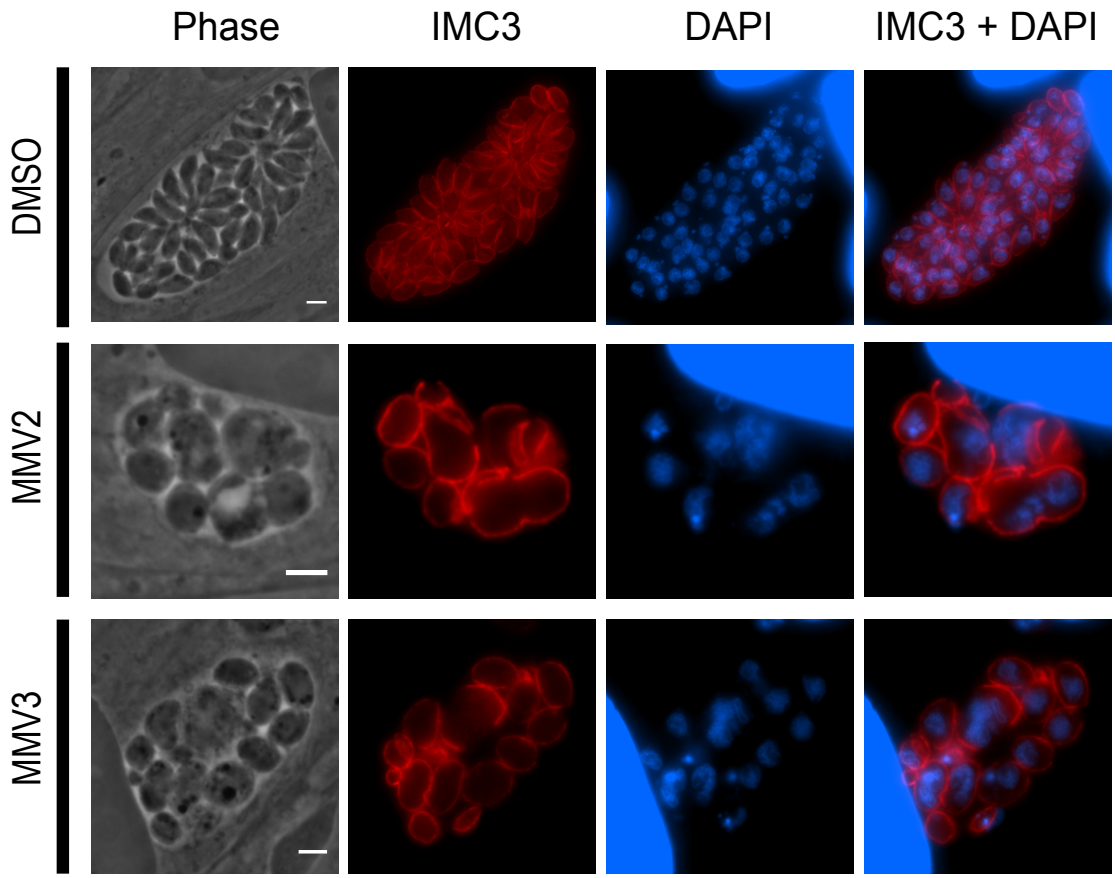

Figure 44: MMV2 and MMV3 impair cytokinesis.
Representative IFAs of normal (DMSO) and abnormal vacuoles (MMV2/3) stained for IMC3 (red), to visualized the inner membrane complex of daughter cells, and DAPI (blue). MMV treated parasites display nuclei that are not surrounded by an IMC3-positive cytoskeleton, and IMC3 structures that do not contain nuclei or apicoplasts as observed by DAPI staining. Scale bar = 3μm.

3.18 Assessing the role of calcium in MMV1 induced egress

We next sought to characterize the mechanism by which MMV1 induced parasite egress from the host cells. The induction of egress by MMV1 followed similar kinetics as those observed upon treatment with 1 μM calcium ionophore A23187, which induces nearly 100% egress within 2 minutes (**Figure 45A**). To quantitatively assess MMV1-induced egress we utilized an established assay to measure the release of lactate dehydrogenase caused by lysis of the host cells upon parasite egress [173]. The induction of egress by MMV1 was concentration dependent, with an egress EC_{50} of ~1150 nM (**Figure 45B**).

We next examined whether MMV1 induces egress by a similar mechanism as calcium ionophores, which depends on the calcium dependent protein kinase TgCDPK3 [245,246]. Interestingly, MMV1 failed to induce egress in parasites lacking TgCDPK3 (**Figure 45C**), indicating that MMV1 induces egress by a similar mechanism as calcium ionophores. We therefore hypothesized that treatment of extracellular parasites with MMV1 would result in the release of intracellular calcium as has been shown for ionophores [247]. To test this, freshly egressed parasites were loaded with the calcium indicator dye Fluo-4 AM and the fluorescence intensities were monitored prior to and immediately following treatment with MMV1, A23187, or DMSO vehicle. Treatment with MMV1 resulted in increased Fluo-4 AM fluorescence, with similar kinetics and peak intensities as treatment with A23187 (**Figure 45D**). Treatment with the cell-permeant calcium chelator BAPTA-AM completely blocked the increase in Fluo-4 AM fluorescence in response to MMV1 treatment (**Figure 45E**). Lastly, we assessed whether prolonged treatment with MMV1 recapitulates the loss of parasite viability observed with extracellular ionophore treatment, termed ionophore-induced death [248]. Indeed, treatment of extracellular parasites with MMV1 for 2 hours dramatically reduced parasite viability as illustrated by the reduction in growth compared to DMSO controls, as measured by plaque assay (**Figure 45F**). Together, our results suggest that MMV1-induced egress involves the release of calcium from intracellular stores and activation of calcium-mediated signaling pathways that have previously been implicated in parasite egress.

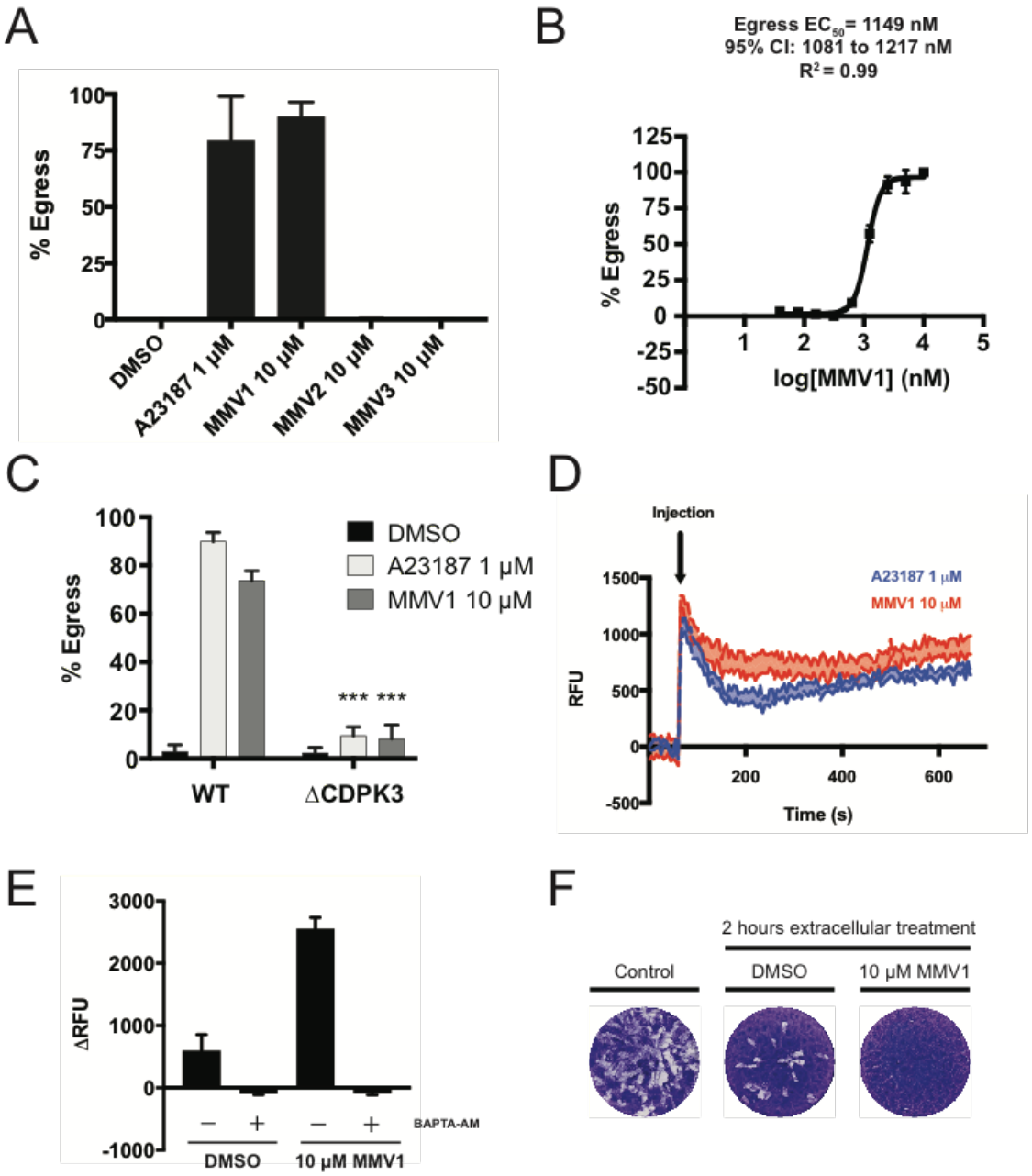

Figure 45: MMV1 induces parasite egress by increasing intracellular calcium levels.

A) Infected HFF monolayers were treated for two minutes with 10 µM MMVs, DMSO vehicle, or 1 µM calcium ionophore A23187. The percentage of egressed vacuoles was calculated by scoring at least 100 vacuoles as intracellular or egressed (n=3, + SEM). B) Induction of egress by MMV1 was quantitatively assessed to determine an egress EC50 value by measuring the amount of lactate dehydrogenase (LDH) released from the host cells upon parasite egress. Percent egress was normalized to DMSO treated (0%) and 10 µM MMV1 (100%) treated wells, n=3, + SEM. C) Parasites lacking the calcium dependent protein kinase TgCDPK3 fail to egress following two-minute treatment with

MMV1, n=3, + SEM, *** = p <0.0001. D) Kinetic traces of Fluo-4 AM fluorescence (relative fluorescence units, RFU) in response to A23187 or MMV1. Extracellular parasites were loaded with the calcium indicator dye Fluor-4 AM to measure changes in intracellular calcium concentrations following drug treatment. Baseline fluorescence was measured for 60 s, at which time compounds were injected into the wells (shown by arrow). Traces represent the average of three technical replicates with the shaded area representing the standard error of the mean. E) Change in fluorescence intensity between the final baseline RFU measurement (60 s) and the first measurement following injection of compounds (67 s). Parasites treated with the calcium chelator BAPTA-AM show no change in intracellular calcium levels following treatment with MMV1, n=3, + SEM. F) Representative plaque assay used to assess parasite viability following treatment of extracellular parasites for 2 hours with DMSO or MMV1. Control parasites were added to HFF monolayer immediately following manual release from host cells and prior to 2-hour treatment.

Summary Aim 3:

In our third aim we explored the conservation of activity and mechanism of action for three small molecules recently identified as Atg3-Atg8 interaction inhibitors in *Plasmodium falciparum*. Our results showed that all three compounds were active against *Toxoplasma* at sub-micromolar concentrations, despite not being identified in a high-throughput screen of MMV compounds against *Toxoplasma*. Two of these compounds blocked parasite replication by disrupting cytokinesis, and were found to induce mitochondrial fragmentation and TgAtg8 lipidation at high concentrations. The third compound was found to stimulate parasite egress from the host cells in a calcium-signaling dependent manner. Additionally, none of the three compounds appeared to prevent the lipidation of TgAtg8 or its localization to the apicoplast. Together, these results show a lack of conservation for the mechanism of action for these three compounds between *Plasmodium* and *Toxoplasma*. Further, our studies provide important groundwork characterizing the effects of these compounds on *Toxoplasma* biology, and identified novel activities for these compounds in replication and egress. Further studies identifying specific drug targets for each of the compounds will be required and will inform the assessment of their potential for further optimization and development as novel broad-spectrum antiparasitics.

Chapter 4: Discussion

Aim 1: Determine the functional consequences of TgAtg8 lysine-23 acetylation on the TgAtg3-TgAtg8 interaction

In our first aim, we examined the effects of TgAtg8 K23 acetylation on TgAtg3-Atg8 interaction, TgAtg8 localization and function, and parasite fitness. As acetylation of mammalian Atg8 protein LC3B has recently been shown to regulate its localization and function, we hypothesized that K23 acetylation may act in a similar fashion to regulate TgAtg8 function. Structural modeling of the TgAtg8 protein revealed that this lysine residue localized to the second N-terminal alpha-helix, which is involved in coordinating interactions with proteins and membranes for Atg8 proteins in higher eukaryotes. Additionally, this residue was adjacent to the W- and L-site binding pockets that facilitate interactions between Atg8 proteins and interactors that contain the conserved WXXL Atg8 Interacting Motif (**Figure 7**). Based on these findings, we hypothesized that K23 acetylation regulates the interaction between TgAtg8 and AIM containing proteins. We chose to test this hypothesis by examining the interaction between TgAtg8 and TgAtg3, which was, at the time, the only putative AIM-containing protein that had been proposed in *Toxoplasma*.

To address this hypothesis, we developed numerous parasite strains and reagents to utilize genetic, biochemical, and biophysical techniques to assess the effects of K23 acetylation on TgAtg8 function. We first attempted to ectopically express GFP-TgAtg8 K23 mutant proteins containing amino acid substitutions routinely used to mimic lysine in its acetylated (K23Q) or non-acetylated (K23R) state. We hypothesized that if K23 acetylation was important for TgAtg8 function, overexpression of these mutant GFP fusion proteins may act in a dominant-negative manner by competing with endogenous TgAtg8 for interaction with components of the Atg8 conjugation system. However, parasites expressing GFP-TgAtg8 K23 mutant proteins did not display any defects in parasite replication or fitness (**Figure 8**). It is important to note that ectopic expression of a lipidation-deficient GFP-TgAtg8G124A mutant is equally well tolerated by the parasite [94]. This may indicate that the GFP-TgAtg8 fusion protein is not capable of interacting with the same set of proteins as the endogenous TgAtg8 protein and is thus unable to act in a dominant-negative fashion. Although GFP-Atg8 fusion proteins are routinely used to monitor autophagy in many systems and are capable of being lipidated, it is possible that the addition of a 27 kD GFP tag to the 15 kD TgAtg8 protein could prevent a subset of protein-protein interactions from occurring. Future studies comparing the

interactomes of GFP-TgAtg8 and cMyc-TgAtg8 proteins may reveal differences that explain the lack of phenotype in these mutants.

While examining the localization for each of these GFP-TgAtg8 fusion proteins, we discovered that in addition to its localization at the apicoplast, GFP-TgAtg8 localizes to the daughter parasite pellicle during cell division (**Figure 9**). GPF-TgAtg8 was observed at daughter buds early during mitosis and remained associated with the pellicle through the completion of cytokinesis. In higher eukaryotes, the N-terminal alpha-helices of Atg8 proteins facilitate their direct interactions with membranes and microtubules [112]. The localization of TgAtg8 to the daughter buds could therefore be the result of its interaction with the membrane of the IMC or with the subpellicular microtubules. However, the subpellicular microtubules only extend along the apical two-thirds of the parasite [10], and we observe GFP-TgAtg8 localization along the entire length of the parasite. This suggests that localization of GFP-TgAtg8 to the daughter buds is not due to interactions with the microtubules. Interestingly, the results of our TgAtg8 interactome studies revealed a potential role for TgAtg8 in vesicle trafficking through the Golgi (**Figure 22).** As the IMC is thought to be derived from the Golgi/ER, it is possible that TgAtg8 is present on vesicles trafficked from the Golgi to the nascent daughter IMC. In this capacity, TgAtg8 could be used to direct specific proteins to the IMC by recruiting cargo proteins to the appropriate vesicles. Alternatively, TgAtg8 could be used to facilitate the homotypic fusion events required to expand the membrane of the IMC during daughter parasite growth. Further studies are required to determine the functional significance of this novel localization for TgAtg8, and may provide insight into the proteins localized at the IMC and their route of delivery to this organelle during division. However, this novel localization was observed in all K23 mutants, suggesting that the association with the pellicle is not dependent on the K23 acetylation status.

Although we encountered difficulties in directly assessing the effects of K23 mutations on TgAtg8 protein lipidation in the parasite, we were able to determine that ablation of K23 acetylation by endogenous mutation of K23 to arginine did not prevent lipidation or localization to the apicoplast (**Figure 13**). As lipidation of TgAtg8 requires its interaction with components of the Atg8 conjugation system, this suggests that K23 acetylation is not required for interaction with TgAtg7 or TgAtg3. To confirm these results, we used a complementary approach to assess the ability of K23 mutant proteins to bind with a peptide containing the putative Atg3 AIM motif (**Figure 18**). Our results suggest that K23 acetylation status is unlikely to significantly alter the interaction

between TgAtg8 and TgAtg3, as all mutants were able to similarly bind to the TgAtg3 AIM peptide. Additionally, assessment of the TgAtg3-Atg8 by co-immunoprecipitation from a dual-tagged parasite strain further confirmed that acetylation of K23 is not required for this interaction to occur (**Figure 20**). Together, these results suggest that any potential effect of K23 acetylation on TgAtg8 function is unlikely to be related to regulating its interaction with components of the Atg8 conjugation system.

Our studies using ectopic and endogenous K23 mutant proteins revealed two potential phenotypes associated with K23 acetylation. First, we observed that ectopically expressed K23Q mutant proteins from multiple, independently generated parasite strains had higher protein levels compared to K23K controls, as measured by immunoblotting (**Figure 8**). Additionally, both ectopic and endogenous K23R mutant proteins appeared to have slightly lower protein levels as compared to K23K controls (**Figure 13**). We hypothesized that this may indicate a role of K23 acetylation in promoting TgAtg8 protein stability. Our thermal shift assays suggested a minor effect of both K23Q and K23R mutations on TgAtg8 protein thermal stability that followed the trends observed at the protein level (**Figure 19**). However, the shift in thermal stability was small compared to other reports of mutations shown to alter protein stability [212], and therefore the biological significance of the observed thermal stability effects are likely minimal. This suggests that any stabilizing effects of K23 acetylation are not directly due to increased intrinsic protein stabilization.

In addition to directly stabilizing proteins, acetylation can promote protein stability by protecting lysine residues from ubiquitination and subsequent degradation [197,201,249]. Although TgAtg8 was found to be ubiquitinated at two lysine residues in a global assessment of ubiquitination in *Toxoplasma*, K23 was not identified in this study [250]. In contrast, the analogous lysine in HsGABARAPL2/GATE-16 (K24) that was reported to be acetylated is also ubiquitinylated [194,251,252]. It is possible that although it wasn't detected in the global assessment of ubiquitination in *Toxoplasma*, TgAtg8 K23 may also be the target of ubiquitinylation, and acetylation of K23 protects TgAtg8 from being targeted for degradation by the proteasome. However, protection from ubiquitination is unlikely to be the major reason behind the observed stabilizing effect in K23Q mutants, as mutation to arginine (K23R) would similarly protect against ubiquitnation, and yet we do not observe the same increase in protein levels with the K23 mutation. Together, these results led us to hypothesize that the differences in stability observed in K23 mutants may be due to altered protein-protein interactions.

The second and more significant phenotype that we observed in our K23 mutational analyses was the severe impairment of replication and spontaneous differentiation to bradyzoite tissue cysts following endogenous mutation of K23 to arginine (**Figure 15**). This phenotype was particularly remarkable given that the mutation was introduced into an RH type I backgrounds strain that is generally regarded to have lost its ability to form tissue cysts [29], and that the K23R parasites differentiated in the absence of exogenous stressors typically required for *in vitro* differentiation. The molecular mechanism behind the observed conversion of K23R parasites to bradyzoites remains unclear. Attempts at further studies to address this question were prevented by adaptation of these parasites during passage in tissue culture. However, the differentiation from tachyzoites to bradyzoites is known to be closely associated with progression through the cell cycle [41,253,254]. For example, the conversion of tachyzoites to bradyzoites has previously been shown to be preceded by a lengthening of the parasite doubling time, followed by upregulation of BAG1 [255]. It is therefore possible that the severe slow-growth phenotype we observed in the K23R mutant parasites "pre-disposed" these parasites to enter into a differentiation program that is cell-cycle regulated. However, other parasite strains generated in our lab that exhibit similar slow growth rates do not similarly undergo conversion to bradyzoites. Therefore, it is not clear how the K23R mutation promotes the parasites to enter into the differentiation process. It is possible that the observed phenotype could be directly caused by the K23R mutation. It also could have been the result of an adaptation made by the parasite to tolerate the K23R mutation. Given the difficulty in obtaining independent K23R mutant clones, confirmation and characterization of this phenotype will likely require the use of an inducible system to regulate the expression of the endogenous and K23R mutant proteins. Preliminary work has been done to establish these reagents and will be discussed in the **Future Directions** section below.

Aim 2: Characterize the TgAtg8 interactome to identify novel TgAtg8 interacting proteins

With our second aim, we sought to expand the current knowledge regarding the function of TgAtg8 in parasite biology by performing the first proteomic characterization of Atg8 interacting proteins in *Toxoplasma*. We took advantage of the cMyc-TgAtg8 endogenously-tagged parasite strain developed in our first aim to immunoprecipitate TgAtg8 from parasite lysate for the identification of interacting proteins. In addition to identifying homologues of components of the Atg8 conjugation system (TgAtg7), our

study revealed a novel role of TgAtg8 in vesicle trafficking through the Golgi (**Figure 22**). Our list of TgAtg8 interacting proteins was enriched for proteins known to specifically interact with the GABARAP/GATE-16 family of Atg8 proteins (NSF/Sec18p, SNAP/Sec17p), building confidence in the validity of our data set and supporting a role of TgAtg8 in GATE-16 like processes.

In addition to homologues of NSF and SNAP proteins, we also identified parasite-specific "hypothetical proteins" that may represent novel proteins involved in Golgi trafficking in *Toxoplasma*. For example, we identified proteins with predicted function as clathrin adaptors (TgGAT, (TGGT1_268430)) and in transport of vesicles along microtubules (TgARP, (TGGT1_247300)). Proteins containing the GGA1/GAT domain found in TgGAT have structural homology to SNARE proteins and are implicated in membrane fusion [218,256]. Additionally, the GAT domain can bind directly to ubiquitin. Although an interaction between the GAT domain and Atg8 family proteins has not been reported, it is possible that the GAT domain could bind to the ubiquitin-like fold present in Atg8 proteins. We also identified a protein with predicted structural homology to kinesin-associated protein 3 (KAP3) (TgARP), which further suggests a connection between TgAtg8 and vesicle trafficking. KAP3 associates with kinesin motor proteins and facilitates the transportation of cargo along microtubules [257]. It is possible that TgAtg8-decorated vesicles, representing either autophagosomes or vesicles transiting the Golgi network, could interact with KAP3 to direct their movement along microtubules. Further studies assessing these proteins are required to determine their function in *Toxoplasma* and to determine the regions responsible for interaction with TgAtg8.

In addition to TgGAT and TgARP, we were particularly interested in the dynamin-like protein TgDrpC, which was the most significantly enriched protein in all three of our immunoprecipitations (**Figure 22**). Characterization of the dynamin-like proteins TgDrpA and TgDrpB revealed that these proteins are required for division of the apicoplast and biogenesis of the secretory organelles, respectively [223,224]. Given the known role of TgAtg8 in apicoplast division, as well as the novel role in Golgi-trafficking identified by our interactome studies, we hypothesized that TgDrpC participates with TgAtg8 to coordinate either or both of these processes. We therefore sought to characterize this novel dynamin-like protein to determine its localization and function in *Toxoplasma.*

Characterization of TgDrpC revealed that it localizes to cytoplasmic punctae in interphase tachyzoites. However, TgDrpC undergoes a dramatic relocalization following the initiation of daughter parasite formation, where it co-localizes to the MORN1 ring

structure at the leading edge of the forming daughter pellicle (**Figure 28**). The functional importance of this localization is unclear. MORN1 localizes to this ring structure where it is required for the constriction of the daughter pellicle to facilitate the pinching-off of daughter parasites at the completion of cytokinesis [231]. Dynamin and dynamin-like proteins are known to oligomerize and form contractile rings, providing GTPase activity for membrane fission during endocytosis or during organelle fission [225]. However, the oligomerization and stimulation of the GTPase activity typically require interaction between the GTPase and GED domains, of which TgDrpC only contains the GTPase domain (**Figure 26**). Therefore, it is unclear whether TgDrpC is capable of performing its canonical function in membrane fission, and as such its function at the MORN1 ring remains unknown.

This data suggests that the relocalization of TgDrpC to the daughter pellicle may represent a function in the trafficking of membrane material or proteins to the IMC during replication. This was particularly intriguing given our discovery that TgAtg8 also localizes to the daughter pellicle during division (**Figure 9**). However, the loss of TgDrpC following conditional knock-down did not appear to alter the formation of the IMC as visualized by IFA for IMC3 (**Figure 32**). Additionally, conditional knock-down of TgDrpC did not result in parasites that failed to complete cytokinesis, as was observed upon loss of MORN1 [231]. Also, whereas TgAtg8 localized to the entire daughter pellicle, TgDrpC demonstrated a specific localization at the MORN1 contractile ring. Therefore, while the localization of TgDrpC and TgAtg8 to the daughter parasite during division is intriguing, further work is required to determine the function each of these proteins has at this location.

Although no defects in IMC formation or cytokinesis were observed in TgDrpC knock-down parasites, we did observe that loss of TgDrpC blocked parasite replication and progression through the lytic cycle (**Figure 31**). Assessment of various organelles revealed defects in the formation of rhoptries (**Figure 35**), disruption of the Golgi (**Figure 34**) and fragmentation of the mitochondrion (**Figure 33**) following loss of TgDrpC. Additionally, we observed an increase in vacuoles containing parasites lacking apicoplasts. However, we note that the disruption of apicoplast division and biogenesis was not as penetrant as was observed following knock-down of TgDrpA, TgAtg8 or members of the Atg8 conjugation system [94,103,223]. In addition to these defects, we also observed an apparent defect in the secretion of the dense granules, which were found to accumulate in cytoplasmic vesicles within the parasites upon loss of TgDrpC

(**Figure 36**). Together, these phenotypes suggest that TgDrpC, and potentially TgAtg8, may be required for vesicle trafficking through the Golgi required for secretory organelle biogenesis and maturation.

A potential role for TgDrpC and/or TgAtg8 in vesicle trafficking related to the formation of the secretory organelles is particularly intriguing. Formation of the secretory organelles, including the rhoptries, micronemes and dense granules, is dependent on the coordinated function of proteins involved in sorting and trafficking of proteins from the ER to the appropriate vesicles that ultimately form the mature secretory organelles. For example, TgSORTLR contains an N-terminal lumenal domain that directly interacts with rhoptry and microneme proteins to recruit them to specific vesicles for transit through the Golgi and endosome like compartment [236]. Similarly, the *Toxoplasma* AP-1 adaptin complex recognizes specific sequence motifs in rhoptry proteins and facilitates their transit from post-Golgi vesicles to mature rhoptries [258]. Disruption of both TgSORTLR and AP-1 resulted in accumulation of rhoptry and microneme proteins in endosomal compartment and a failure to form mature secretory organelles. Additionally, chemical disruption of the Golgi network by Brefeldin A resulted in the inhibition of dense granule secretion [235]. Therefore, the defects observed upon TgDrpC, namely the disruption of the Golgi network, could explain the downstream defects observed in rhoptry biogenesis and dense granule secretion. Additional studies defining which region of the Golgi/endosome like compartment TgDrpC and TgAtg8 localize to, as well as determining whether conditional knock-down of TgAtg8 also results in similar phenotypes, will clarify the function of both of these proteins on Golgi trafficking and organelle biogenesis in *Toxoplasma*.

One of the most striking phenotypes we observed following TgDrpC knock-down is fragmentation of the single parasite mitochondrion. Dynamin-like proteins are known to be involved in mitochondrial fission and division in other species [226–228]. However, this activity requires contractile function of dynamin-like proteins. The ability of TgDrpC to act in this manner is questionable given the absence of functional domains. Despite these missing domains, we do observe occasional localization of TgDrpC near the mitochondrion in regions of mitochondrial membrane constriction (**Figure 25**). It is possible that TgDrpC exerts its constrictive force through interactions with other proteins. Characterization of TgDrpC interacting proteins may shed light on potential proteins that could participate in this function, but remain unknown at this time.

While the identification of proteins involved in Golgi trafficking agreed with known functions of Atg8 family proteins, the interaction of TgAtg8 with multiple members of the BCKDH complex in of TgAtg8 interactome is not as readily explained. All components of the BCKDH complex identified in our study were found to localize to the mitochondrion (**Figure 24**). As in higher eukaryotes, *Toxoplasma* mitochondrial proteins are posttranslationally imported into the mitochondrion through the recognition of a conserved, N-terminal targeting sequence [259]. Two of the identified BCKDH complex proteins in our interactome contain targeting sequences. Thus, it is unlikely that their interaction with TgAtg8 is the result of TgAtg8-mediated trafficking of these proteins to the mitochondrion. One possibility is that the identification of these complex members is due to their targeted degradation by mitophagy. Mitophagy is known to be induced in response to misfolding of proteins in the mitochondrial matrix [260]. The BCKDH is a particularly large complex, made up of over 40 subunits with a total size of ~10 million Daltons [261] (for comparison, the mammalian ATP synthase complex is ~ 650 kD [262]). As a result, the BCKDH complex may be more susceptible to errors in folding or complex formation and may be targeted for degradation by mitophagy. If this is the case, the mechanism by which these proteins are specifically targeted for degradation, as well as the adaptor protein at the outer mitochondrial membrane that interacts with TgAtg8 (i.e., functional homologue of p62/SQSTM1) to target specific regions of the mitochondrion for degradation are of great interest and should be the subject of future studies.

Another point of interest regarding the BCKDH is the identification of both subunits of the mitochondrial trifunctional protein complex (HADHA and HADHB) in multiple, independent proteomic studies characterizing Atg8 protein interactions in mammalian systems [263,264]. The functional connection between Atg8 proteins and HADHA/B in mammalian cells remains poorly characterized, however they have been found to co-localize in cytoplasmic punctae following induction of autophagy by treatment with palmitic acid [263]. This complex typically localizes to the inner mitochondrial membrane and is used for beta-oxidation of long-chain fatty acids to generate acetyl-CoA in the mitochondrial matrix [265]. This is similar to the activity of the BCKDH identified in our interactome, which catabolizes short-chain alpha-ketoacids and pyruvate to generate acetyl-CoA in the mitochondrion [214]. Therefore, there appears to be a conserved connection between Atg8 and complexes involved in generation of

mitochondrial acetyl-CoA, and this connection deserves further exploration in *Toxoplasma*.

In summary, our characterization of the TgAtg8 revealed previously unreported functions of TgAtg8 in vesicle trafficking through the Golgi network. Characterization of the TgAtg8 interacting protein TgDrpC revealed that this divergent dynamin-like protein is essential for *Toxoplasma* tachyzoite viability. Conditional knock-down revealed that loss of TgDrpC impairs the biogenesis and maintenance of numerous organelles, including the Golgi apparatus, rhoptries and mitochondrion. Whether the loss of TgAtg8 results in similar organelle defects remains to be seen and will be the subject of future experiments. Additionally, the characterization of TgAtg8 interacting proteins provides a reference dataset that can be used in future studies assessing the effects of TgAtg8 mutations or small molecule inhibitors for the targeted disruption of TgAtg8 protein-protein interactions.

Our interactome data shows that TgAtg8 interacts with a variety of proteins and likely has functions in multiple, distinct protein complexes with important roles in numerous aspects of *Toxoplasma* biology. Accordingly, it is possible that disruption of TgAtg8 protein interactions by small molecules targeting a single region of TgAtg8 could disrupt numerous pathways and processes in the parasite. Whether these interactions are facilitated through a common binding site on TgAtg8, such as the W- and L-site pockets, remains to be determined and requires further study.

Aim 3: Determine whether TgAtg8 lipidation could be pharmacologically inhibited by treatment with Atg3-Atg8 interaction inhibitors recently identified in *Plasmodium*

In our third aim we assessed three inhibitors of the interaction between Atg3 and Atg8 in *P. falciparum* to determine whether they acted in a similar manner in *Toxoplasma gondii*. Our results show that despite high levels of conservation of the proposed binding sites for these compounds on TgAtg8, these compounds do not block TgAtg8 lipidation. Despite the lack of a conserved mechanism of action, all three compounds were found to inhibit *Toxoplasma* growth in a dose-dependent manner, with EC_{50} values in the sub-micromolar range. We have identified that two of these compounds (MMV001246 (MMV2) and MMV665909 (MMV3)) inhibit *Toxoplasma* replication by disrupting daughter bud formation and cytokinesis during parasite replication. Additionally, we found that treatment with the third compound (MMV007907

(MMV1)) results in the release of calcium from the intracellular stores resulting in parasite egress from the host cell.

Numerous inhibitors of the PfAtg3-Atg8 interaction have been identified using biophysical approaches [107,162,163], however we chose to focus on MMV1-3 for the following reasons. First, MMV1 is one of the few PfAtg3-Atg8 inhibitors that has been found to alter PfAtg8 lipidation status when parasites were treated in culture [162]. Second, all three of the compounds tested herein were identified from the Medicines for Malaria Venture Malaria Box, a collection of 200 drug-like and 200 probe-like molecules that is available for researchers free of charge. Importantly, MMV1-3 are also active against other important human pathogens including *Cryptosporidium* spp., *Babesia* spp., *Trypanosoma* spp., and *Leishmania* spp. (**Table 4**). Collectively, these pathogens represent a significant disease burden in humans, and treatment of these infections is threatened by the development of drug resistance to the limited number of therapeutics currently available. Therefore, the activity of MMV1-3 against multiple protozoans suggested that disruption of the Atg3-Atg8 interaction in these parasites may represent a potential avenue for development of novel broad-spectrum antiparasitics.

To address the possibility for a conserved mechanism of action for MMV1-3 outside of *Plasmodium*, we evaluated these compounds for their ability to similarly disrupt the Atg3-Atg8 interaction in the closely related apicomplexan *Toxoplasma*. We hypothesized that the similarity between *P. falciparum* and *Toxoplasma* Atg8 proteins may allow for the mechanism of action to be conserved between the two species. However, our *in silico* docking experiments suggest that MMV2 and MMV3 are unlikely to bind to TgAtg8 in a similar fashion as described in *P. falciparum* (**Figure 37**). Although the residues that comprise the W- and L-site binding pockets are highly conserved between PfAtg8 and TgAtg8, it is possible that amino acid substitutions in the residues proximal to these binding pockets could prevent the binding of these compounds to TgAtg8, as shown for *P. yoelli* Atg8 [162]. The PfAtg8 W- and L-site pockets were proposed as ideal targets for small molecule inhibitors due to their differences in structure and electrostatic potential from human Atg8 homologues [107]. However, an additional set of compounds has recently been identified that inhibits the PfAtg3-Atg8 interaction by binding to the apicomplexan-loop [163]. As this structure is unique to apicomplexan Atg8 proteins, it also provides an additional avenue for targeted disruption of the parasite Atg3-Atg8 interaction while avoiding effects on the host. Whether any of the compounds that target the PfAtg8 apicomplexan loop have activity against

Toxoplasma or other apicomplexans remains untested. However, given the differences in amino acid sequence present in this loop in *Toxoplasma* (**Figure 37**), identification of bona fide TgAtg3-Atg8 inhibitors may require structural resolution of the TgAtg3-Atg8 interaction and/or development of biophysical screening approaches such as those used in *P. falciparum*.

Our characterization of MMV1-3 showed that all three compounds inhibited *Toxoplasma* at sub-micromolar concentrations. This is in contrast to a previous high-throughput screen that failed to identify any of the three MMVs as having activity against *Toxoplasma* [237]. However, as noted by the authors in [237], the EC_{50} values they observed for certain 2,4-diamino-quinazoline-based compounds were significantly higher than values reported in a separate study in *Toxoplasma* [266]. The authors attribute these differences to their use of the TS-4 mutant derived from the standard RH strain, which could also explain the differences between their study and our observed activities for MMV1-3. Additionally, as shown in **Table 4**, EC_{50} values obtained from high-throughput screens are highly variable, likely due to differences in the methods used to assess compound efficacy between studies. In contrast, our study characterized the effects of MMV1-3 on multiple aspects of *Toxoplasma* biology using standard *Toxoplasma* strains and assays. Our findings illustrate the importance of using multiple, independent methodologies for screening and validating the activity of the Malaria Box compounds across species.

Our studies revealed that the effects of MMV2 and MMV3 on *Toxoplasma* replication involve impairments of daughter parasite formation and cytokinesis (**Figure 43**). Additionally, at higher concentrations, MMV2 and MMV3 induce fragmentation of the mitochondrion and increased lipidation of TgAtg8 (**Figure 39, Figure 42**), similar to the effects of monensin treatment and starvation [93,94,154]. However, unlike monensin and starvation, the autophagy inhibitor 3-MA does not block the effects of MMV2 and MMV3 on the mitochondrion. One possible explanation for this observation is that the induction of autophagy may occur downstream of mitochondrial fragmentation. In this scenario, mitochondrial disruption could be induced by several stimuli, including some that are blocked by 3-MA's inhibition of phosphoinositide 3-kinase (PI3K) (including starvation and monensin), as well as others that target the mitochondrial through alternative, PI3k-independent mechanisms (like MMV2 and MMV3). We propose that in the case of MMV2 and MMV3, autophagy is likely induced following mitochondrial fragmentation, and the subsequent induction of TgAtg8 lipidation may represent cell

death *with* autophagy rather than cell death *by* autophagy [267]. In either case, given that the effects of MMV2 and MMV3 on the mitochondrion and TgAtg8 lipidation are only observed at concentrations significantly higher than the identified EC_{50} values, these effects are likely an indirect response occurring down stream of MMV2-3's effects on cell cycle inhibition, or are off target effects resulting from use of such high concentrations.

In addition to novel mechanisms of action identified for MMV2 and MMV3, we also found that MMV1 can induce parasite egress from the host cells. This effect is comparable to the activity of the calcium ionophore A23187. Like A23187, MMV1-induced egress is dependent on signaling through TgCDPK3. As shown in (**Figure 45**), MMV1 triggers the release of calcium from intracellular stores; however, the exact mechanism by which this occurs remains unclear. The chemical structure of MMV1 precludes it from coordinating with calcium ions and transporting them across membranes in a manner similar to A23187. Instead, MMV1 my bind directly to receptors or ion channels to trigger calcium release, although such receptors and channels remain to be identified in *Toxoplasma*. Alternatively, MMV1 may act similar to other small molecules that stimulate calcium release and parasite egress through activation of the cGMP-dependent protein kinase PKG signaling pathway [268,269]. Further studies are needed to determine whether the effects of MMV1 are dependent on PKG signaling, and to determine which intracellular stores release calcium in response to MMV1 treatment.

Together, our studies revealed that MMV1-3 inhibit *Toxoplasma* at therapeutically relevant concentrations. The EC_{50} values we observe *in vitro* are well below concentrations reported to have cytotoxic effects in mammalian cells [238]. However, preliminary pharmacokinetic studies in mice suggest that MMV1-3 are highly bound to plasma proteins (>95%) [238]. Additionally, mice given an oral dose of 140 μg/kg failed to show plasma concentrations greater than 1 μM within 9 hours of administration, suggesting that the efficacy of these compounds *in vivo* may be limited due to poor bioavailability [238]. Whether these compounds can be administered at dosages that are efficacious in an *in vivo* model of toxoplasmosis remains untested. While MMV1-3 may currently be limited to use *in vitro* towards target identification, future structure-activity relationship studies may lead to the development of derivatives of these compounds with better pharmacological properties. As MMV1-3 already display activity against a variety of protozoan pathogens, further characterization of their mechanisms of action holds promise towards the development of compounds with broad-spectrum use as antiparasitics.

Chapter 5: Future Directions and Closing Remarks

Future directions for Aim 1:

Given our inability to generate endogenous K23 mutants, and the lack of a phenotype in ectopically expressed K23 mutants, further dissection of the role of K23 mutations will require development of additional methods to express these proteins in a conditional system. We have designed constructs expressing TgAtg8 under the constitutive tubulin promoter and containing an N-terminal HA-epitope tag. These constructs integrate by double homologous recombination at the non-essential uracil phosphoribosyltransferase (UPRT) gene locus, and include a chloramphenicol acetyltransferase minigene selection cassette. These have been designed to be transfected into a parasite background in which the endogenous TgAtg8 gene is under the regulation of a Tetracycline-regulatable (TET-Off) promoter [103]. In this system, parasites harboring the HA-TgAtg8 ectopic protein could be isolated in the absence of tetracycline. After isolating these clones, the endogenous TgAtg8 gene could be conditionally repressed using anhydrous tetracycline treatment. This would allow for assessment of the phenotypes observed in various TgAtg8 mutant proteins in a conditional system that would avoid the limitations encountered by our previous two approaches; namely the lack of a dominant-negative phenotype in ectopically expressed GFP-Atg8 mutants, and the inability to recover certain TgAtg8 mutants potentially due to their negative effects on parasite viability.

This system would not only be useful for assessing the effects of K23 acetylation mutants, but could be used to introduce various mutations in TgAtg8 to identify specific residues required for lipidation or localization at the apicoplast, and to characterize their impacts on parasite fitness. This approach would also allow for confirmation of the K23R phenotype observed in the endogenous K23R mutant parasites. To compliment these studies, we have generated various mutations of TgAtg8 residues shown to facilitate the Atg3-Atg8 interaction in *Plasmodium* and have introduced these mutations in both the conditional expression constructs described above, as well as in pET19b plasmids for the purification of recombinant proteins harboring these mutations. This would allow these mutations to be studied side-by-side, assessing their effects on protein localization, lipidation and parasite fitness, as well as using the thermal shift assays developed in this thesis to monitor interaction with TgAtg3 AIM peptide. Together, these approaches would allow for identification of residues required for TgAtg3-TgAtg8

interaction and would allow for the assessment of the effects of their mutation and loss of interaction on parasite biological processes.

The thermal shift assays developed in this thesis may also be of utility for the screening of putative AIM motifs identified in TgAtg8 interacting proteins. Although TgAtg3 contained a single putative AIM sequence, many of the TgAtg8 interacting proteins identified in our proteomics analysis contain multiple potential AIMs that could facilitate their interaction with TgAtg8. The thermal shift assay could be a useful method to screen potential AIM motifs *in vitro* to identify candidates for additional mutational studies in the parasite.

Additionally, the recombinant TgAtg8 protein generated in these studies could be used to resolve the crystal structure of TgAtg8. This would provide important information regarding the exact structure of the W- and L-site binding pockets and may allow for more accurate *in silico* docking studies to identify potential inhibitors targeting this binding pocket. Alternatively, the recombinant TgAtg8 could be used for high-throughput screening of compounds using techniques similar to those used to identify PfAtg3-Atg8 inhibitors, including surface plasmon resonance. Lastly, recombinant TgAtg8 could be used as a substrate for *in vitro* KAT assays using acetyltransferases purified from *Toxoplasma* to identify which KAT(s) are capable of acetylating TgAtg8 at K23. These approaches could all be undertaken using the reagents developed in this thesis, and could provide valuable information for the development of novel therapeutics targeting the TgAtg8 interactome.

Future directions for Aim 2:

Our results from Aim 2 suggest that TgAtg8 interacts with components of the Golgi trafficking machinery. We also identified potential new *Toxoplasma* proteins involved in vesicle trafficking, including TgDrpC. Initial follow up studies based on the findings in Aim 2 should focus on confirmation of the role of TgAtg8 in the phenotypes associated with TgDrpC knock-down. For example, we plan to assess the effects of loss of TgAtg8 on the Golgi and secretory organelles using the TET-Off TgAtg8 parasite strain described above. These experiments will help delineate which phenotypes are associated with both TgAtg8 and TgDrpC, and which may be due solely to the function of each protein individually. Additional studies examining the co-localization of these proteins are also needed to determine the conditions that promote the interaction between TgAtg8 and TgDrpC, as we only observe their co-localization in extracellular parasites. We are currently in the process of conducting immuno-electron microscopy

studies using the dual-tagged TgDrpC-HA/cMycTgAtg8 parasite strain to determine where TgDrpC and TgAtg8 localize in the parasite in both intracellular and extracellular conditions. Previous studies examining TgAtg8 localization by immuno-EM were conducted only in parasites that had been subjected to extracellular HBSS starvation, and were done using the GFP-TgAtg8 parasite strain. Thus, the localization of TgAtg8 in intracellular or non-stressed parasites remains unknown. Additionally, none of the studies examining TgAtg8 localization have reported its localization at the Golgi or at the daughter parasite pellicle, two places that our studies suggest TgAtg8 localizes to. Therefore, our immuno-EM studies will allow us to examine TgAtg8 localization to confirm its localization in vesicles near the Golgi or associated with the daughter pellicle and to determine whether TgDrpC is found at these locations.

Another important question that could be addressed using the techniques developed in our second aim is the identification of proteins connecting TgAtg8 to the centrosomes during division. The TgARP protein identified in the interactome is a potential candidate connecting TgAtg8 to centrosome division. Although the armadillo repeat domain has homology to kinesin-associated protein 3 and thus may have function in vesicle trafficking on microtubules, it was also predicted by HHpred to have homology to beta-catenin. As introduced previously, beta-catenin is a multifunctional protein that localizes to centrosomes during mitosis and coordinates their separation during division. Accordingly, TgARP may be the link between TgAtg8 at the apicoplast and the centrosomes. As TgARP remains completely uncharacterized, future studies tagging this protein and characterizing its localization through the cell cycle will provide insight into whether TgARP has similar functions in centrosome duplication.

An additional future direction would be to optimize the immunoprecipitation methods to allow for characterization of TgAtg8 interactome following autophagy induction. Our studies revealed that induction of autophagy by extracellular starvation prevented TgAtg8 from being liberated from the membrane into the soluble fraction. Although harsher lysis buffer conditions may allow for solublization of TgAtg8 following autophagy starvation, these conditions will also likely disrupt protein-protein interactions. This could be prevented by the use of a cell-permeable cross-linking reagent such as dithiobis(succcinimidyl propionate) (DSP), an amine-reactive crosslinker containing a cleavable disulfide bond in the spacer arm to allow for reversal of crosslinking following immunoprecipitation. In addition to allowing the characterization of TgAtg8 interacting proteins following starvation, this approach may also allow for the identification of

TgAtg8 interactors that were missed in our initial study due to their presence at the membrane. For example, our TgAtg8 interactome did not identify any known apicoplast localized proteins, and none of the hypothetical proteins that we have since localized were found at the apicoplast. This is despite the fact that TgAtg8 localizes predominantly to the apicoplast in both intracellular and extracellular parasites. Therefore, development of these additional methods may also allow for a more thorough investigation of the TgAtg8 interactome even under non-autophagy inducing conditions.

Our characterization of TgDrpC has revealed an exciting potential function for this protein in organelle biogenesis, specifically related to the ER/Golgi and the Golgi-derived secretory organelles. Further studies are required to ensure that the defects that we observe upon loss of TgDrpC are not indirect effects due to parasite death. Although we do not observe depletion of TgDrpC within the first 24 hours following removal of Shield-1, we have not done a thorough time-course experiment to assess TgDrpC regulation between 24 and 48 hours. These experiments will help inform the kinetics of TgDrpC loss with greater resolution and will provide insight into the time-points that we could assess the organelle phenotypes at in future studies. These additional experiments may allow us to observe the defects in organelles prior to the 48 hour time-point, when the parasites may simply be displaying the organelle defects due to parasite death.

In addition to these proposed studies, it would be interesting to conditionally express a dominant-negative TgDrpC in which the conserved lysine residue in the GTPase domain has been mutated to alanine to ablate GTPase activity. Similar approaches were taken to characterize the functions of TgDrpA and TgDrpB, and would be informative to determine whether the GTPase activity of TgDrpC is required for its function in *Toxoplasma.* Other studies could be used to determine which regions of TgDrpC are required for function, and potentially to determine the region of TgDrpC that interacts with TgAtg8. These studies could be performed by Shield-1 regulatable expression of a series of TgDrpC trunctation proteins harboring the DD tag and examining the phenotypes following stabilization of these proteins by addition of Shield-1. Alternatively, these conditional mutants could be ectopically expressed in the TgDrpC-HA-DD parasite background to assess their ability to rescue the loss of full-length TgDrpC protein following the removal of Shield-1. These experiments would allow for determination of which portions of TgDrpC are required for proper localization and

function in the parasite, and may identify functionally important regions of the TgDrpC C-terminus that lacks predicted functional domains.

Future directions for Aim 3:

Our studies on MMV1-3 revealed that all three of these compounds are active against *Toxoplasma*. The initial characterization of these compounds revealed that MMV2-3 block parasite replication, and result in impairments of cytokinesis. Additionally, MMV1 is a potent inducer of parasite egress from the host cell. Despite these novel findings, the molecular target for each of these compounds is still unknown and requires further studies. For all three of these compounds, identification of their targets could be assessed using a forward genetics approach to mutagenize a population of parasites with ethylnitrosourea (ENU) followed by selection with each MMV compound to isolate resistant mutant parasites. Our group has extensive experience preforming these types of assays and has used this approach to identify targets of multiple compounds [245,270]. These studies would likely provide insight into the target of these molecules or the pathways that these compounds target to elicit their effects on the parasite.

In addition to taking a forward genetics approach, the mechanism of action for each drug could be further explored to expand upon our initial observations reported in this thesis. For example, parasites treated with MMV2 or MMV3 could be analyzed by flow cytometry to determine whether these compounds result in inhibition of parasite replication at a specific stage of the cell cycle. Additionally, the effects of each compound on cell division and cytokinesis could be further examined by IFA for additional markers of cell division, such as those used to characterize the defects in cell-cycle upon loss of alpha-tubulin acetylation [200]. These could provide insight into which specific step of division is impaired by treatment with these compounds.

The mechanism of action for MMV1 could also be better defined by further characterization of the signaling pathways involved in its induction of egress. For example, given that MMV1 is unlikely to act as an ionophore to transport ions across membranes, it is possible that MMV1 is activating signaling pathways known to be involved with parasite egress, such as the PKG pathway. Parasite egress can be triggered by PKG activation, while treatment with PKG inhibitors can block the induction of egress in response to calcium ionophores [173]. Therefore, the ability for MMV1 to induce egress could be assessed in the presence and absence of inhibition of PKG by Compound 1 [173,271]. In addition, characterization of the effects of MMV1 on host cell calcium levels would help determine whether MMV1 stimulates egress by acting directly

upon the parasite or if this effect is mediated at least in part by the host cell. Completion of these assays will help determine whether MMV1 induces parasite egress through established signaling pathways, or may reveal that MMV1 acts through alternative signaling pathways that have not previously been implicated in parasite egress.

Additionally, the effects of MMV1 on calcium release could be further characterized by identification of the specific intracellular store that MMV1 treatment releases calcium from, as well as by quantitatively measuring calcium levels with the indicator Fura-2 AM. Determining the source of the calcium liberated by MMV1 treatment could be examined by assessing calcium fluxes before and after treatment with compounds known to liberate calcium from specific intracellular stores. For example, calcium stored in neutral compartments can be specifically mobilized by treatment with ionomycin, while calcium in acidic compartments can be mobilized by treatment with glycyl-L-phenylalanine-napthylamide (GPN). Treatment with thapsigargin, an inhibitor of the ER-localized SERCA pumps, inhibits reuptake of calcium into the ER and can be used to assess the role of ER-derived calcium in cytosolic calcium fluxes following drug treatment [269]. These compounds could be used to identify which compartment MMV1 releases calcium from, providing additional insight into the mechanism of action for MMV1 and potential subcellular location of the target of MMV1.

Lastly, each of the three MMV compounds could be used for preliminary experiments to determine their *in vivo* efficacy using a mouse model for acute toxoplasmosis. Preliminary PK/PD studies suggest that these compounds are highly bound to plasma proteins, and they may have poor availability. However, we have also observed that they display EC_{50} values in the sub-micromolar range, and do not appear to have cytotoxic effects in cell culture at concentrations as high as 30 μM [238]. Therefore, it is possible that despite the poor bioavailability these compounds may be able to reach concentrations *in vivo* that have therapeutic effects. These preliminary studies would provide a baseline with which future studies using structural derivatives of these compounds could be tested against and could provide proof-of-concept for the potential of these compounds for future development as therapeutics.

Future questions for the field:

In addition to the future studies mentioned above, there are a number of broader questions regarding the function of autophagy proteins in *Toxoplasma* and other apicomplexans that are of interest to the field. Although these questions do not directly relate to the studies presented herein, we have developed a number of reagents and

techniques that could be applied to address these following questions relating to autophagy in *Toxoplasma:*

Is there a functional Atg5-Atg12 E3-like complex in *Toxoplasma*?

Homologues to the E1-like (Atg7), E2-like (Atg3) and Atg4 peptidase have been identified and characterized in *Toxoplasma.* However, there have been no studies exploring the putative homologues of the E3-like Atg5-Atg12 complex, and therefore whether these proteins are functional homologues remains unclear. Bioinformatics analysis casts doubt on their ability to function as canonical Atg5 or Atg12 proteins, due to the absence of conserved residues and sequence features that are found in higher eukaryotes (see **Section 1.4**). Therefore, it is likely that these proteins do not have a function in coordinating TgAtg8 lipidation to PE. If this is the case, does TgAtg8 undergo conjugation to PE in the absence of an E3 complex? To date there are no reports of Atg8 proteins undergoing lipidation in the absence of an E3 complex. Therefore it is possible that *Toxoplasma* may rely on the function of an uncharacterized protein to coordinate this activity. Although not discussed in this thesis, we have generated parasites in which both TgAtg5 and TgAtg12 are endogenously tagged. These reagents will be useful for determining whether these proteins form a complex similar to that observed in other systems, and to determine whether genetic disruption of these genes impacts TgAtg8 lipidation.

Is autophagy a general cell death response in the parasite?

The autophagy pathway has been proposed to have numerous functions in *Toxoplasma*. In addition to its proposed role in response to starvation and drug treatment, autophagy has been suggested as a potential cell death mechanism in *Toxoplasma*. This is further supported by the lack of homologues to canonical apoptosis genes in the *Toxoplasma* genome. In higher eukaryotes, autophagy is recognized as a form of regulated cell death, however it is generally thought that autophagy plays both cytoprotective roles as well as cytotoxic roles. Indeed, in *Toxoplasma* it is possible that autophagy is induced in an attempt to alleviate stress caused by nutrient deprivation or drug treatment, and that prolonged autophagy can ultimately result in parasite death. This makes autophagy a particularly attractive drug target, as either inhibition or activation of the parasite autophagy pathway may result in parasite death. Recent studies showing that the autophagy pathway is active and essential for bradyzoites [272] suggests that this pathway may be a viable target for both acute and chronic stages of toxoplasmosis. However, it remains unclear how general of a response autophagy

induction is in *Toxoplasma.* Preliminary data collected during the completion of this thesis revealed that TgAtg8 lipidation was induced by treatment with EC_{50} concentrations of multiple antiparasitics with diverse mechanisms of action (pyrimethamine, folate synthesis inhibitor; trichostatin A and apicidin, HDAC inhibitors). Importantly the ability of these compounds to induce TgAtg8 lipidation did not correlate with their ability to cause mitochondrial fragmentation. Previous methods to induce autophagy have also resulted in mitochondrial fragmentation, and as a result, it was unclear whether induction of autophagy was the cause or effect of mitochondrial fragmentation. Our observation suggests that numerous stresses can induce autophagy in the parasite, and that the induction of TgAtg8 can occur in the absence of mitochondrial fragmentation. The cMycTgAtg8 parasite strain should be a useful reagent to assess in TgAtg8 lipidation status in response to a wider variety of stressors or treatments, and will provide further insight into the potential role of autophagy as a general stress response in *Toxoplasma.*

If canonical autophagy occurs in the parasite, to what organelle or location are autophagosomes trafficked and fused to for degradation of cargo?

One of the major outstanding questions relating to *Toxoplasma* autophagy is the identity of the lysosome or vacuole-like organelle that putative autophagosomes are trafficked to for degradation. *Toxoplasma* lacks a definitive lysosomal vacuole, however does contain an acidic vaucuolar compartment (VAC, also referred to as the plant-like vacuole (PLV)). This compartment contains cathepsin proteases that were first implicated in maturation of micronemal proteins in the endosomal compartment but have more recently been shown to degrade ingested material acquired through endocytosis [273]. Inhibition of proteases localized to the VAC/PLV blocked the degradation of TgAtg8-containing autophagosomes, providing the first support for the VAC/PLV as the site for autophagosome fusion and autophagic degradation [272]. However, the fusion of autophagosomes with the VAC/PLV has only been observed in bradyzoite stage parasites. Further studies are required to identify whether the VAC/PLV is also utilized by tachyzoites for autophagy, or, alternatively, whether TgAtg8 is utilized by the parasite in distinct, stage-specific functions. Additionally, identification of specific cargo proteins targeted for clearance by autophagy will provide powerful tools to monitor autophagic flux in *Toxoplasma* and confirm the role of this pathway in canonical autophagy processes.

Does *Toxoplasma* have functional homologues of ATG proteins outside of the Atg8 conjugation system?

The majority of studies of autophagy in *Toxoplasma* have focused on the components of the Atg8 conjugation system. A recent study has characterized the *Toxoplasma* homologue of Atg9, and found that the loss of this protein resulted in a decreased ability of the parasite to survive extracellular stress and a decreased virulence in mice [95]. However, this study did not definitively show that it was a functional homologue of Atg9 with respect to its role in delivery of membrane to the nascent autophagosomes. Additionally, other putative *Toxoplasma* ATG homologues including TgAtg1, TgAtg5, TgAtg6, TgAtg7, TgVps34, TgVps15, or TgAtg12 have not been characterized. We have endogenously tagged a number of these putative autophagy genes (including TgAtg5, TgAtg6, TgAtg7 and TgAtg12) and have begun to characterize their localization and expression levels under basal and autophagy-inducing conditions. Studies are now underway to characterize their interactomes using the methods developed for TgAtg8, and should provide insight into the biological functions of these putative ATG homologues in *Toxoplasma*.

Closing Remarks:

In this thesis work we explored the Atg8 conjugation system in *Toxoplasma* to gain insight into how TgAtg8 function was regulated in the hopes of identifying potential avenues for therapeutic intervention. *We hypothesized that in addition to interacting with homologues of the canonical eukaryotic Atg8 conjugation machinery, TgAtg8 interacts with novel proteins to facilitate its functions in parasite-specific processes. Additionally, we hypothesized that these protein interactions were subject to regulation by post-translational modifications, and that they could be pharmacologically disrupted by the recently identified PfAtg3-Atg8 interaction inhibitors.*

Our studies were motivated by our previous findings that TgAtg8 was acetylated in extracellular parasites, and that autophagy/TgAtg8 lipidation was induced by treatment with the ionophore drug monensin. As acetylation of ATG proteins is emerging as a major mechanism by which autophagy is regulated in other eukaryotes, we examined whether acetylation of TgAtg8 could provide a similar regulatory function in *Toxoplasma*. Our first aim sought to characterize the effects of this PTM on TgAtg8's ability to interact with TgAtg3, and thus its ability to undergo lipidation and localization to the apicoplast. Our results show that acetylation of TgAtg8 at lysine-23 is not required for the TgAtg3-Atg8 interaction or its lipidation and apicoplast localization. Additionally,

these experiments revealed a new localization for TgAtg8 at the daughter parasite pellicle during division that could represent a novel function of this protein during daughter parasite formation.

We next characterized the TgAtg8 interactome to identify proteins that might coordinate TgAtg8's functions in canonical autophagy and parasite-specific biological processes. While conducting these experiments, we discovered that TgAtg8 is significantly upregulated at the mRNA and protein levels following egress from the host cell. Our proteomics studies also identified a potential role for TgAtg8 in Golgi trafficking, suggesting that TgAtg8 may have similar biological functions as the GABARAP/GATE-16 family of Atg8 proteins in addition to its previously characterized LC3-like function in autophagosome formation in *Toxoplasma.* These studies identified numerous proteins that are unique to *Toxoplasma* and may assist TgAtg8 in parasite-specific functions, such as apicoplast division. Our characterization of one of the TgAtg8 interacting proteins, TgDrpC, provides additional evidence for TgAtg8 involvement in trafficking through the Golgi and the biogenesis of post-Golgi secretory organelles. These preliminary findings set the stage for future studies exploring the role of TgAtg8 in these processes that may identify specific protein-protein interactions that could be the targets of future therapeutics.

In our third aim, we examined three Atg3-Atg8 interaction inhibitors recently identified in *Plasmodium falciparum* to determine their utility as therapeutics and as tools to study the autophagy pathway in *Toxoplasma*. Our studies are the first to show that these three compounds have activity against *Toxoplasma*, and revealed that the conservation of activity is not likely due to a conserved mechanism of action for these compounds in *Toxoplasma.* Although these compounds do not inhibit the TgAtg3-TgAtg8 interaction, they do represent three novel compounds with potential for future development as antiparasitics. Future studies identifying their targets and mechanisms of action in *Toxoplasma* may provide valuable insight into the rationale behind their activity against other protozoan parasites, and could aid in the development of novel, broad spectrum antiparasitics.

Collectively, this work addresses previously unexplored aspects of TgAtg8 function, and the results will help guide future studies of autophagy and TgAtg8 function both in our laboratories and in the field. We believe that characterization of TgAtg8 and other components of the *Toxoplasma* autophagy pathway will identify potential new drug

targets, and will uncover new and exciting aspects of *Toxoplasma* biology relating to autophagy and beyond.

Appendices

Appendix 1: Primers used in this study

Primer Name	Sequence (5' - 3')	Use
Atg8 CDS Fw	CCATCGATTCGCGACGAAGTG	Amplification of Atg8 CDS
Atg8 CDS Rev	TTACCCCAGAGTGTTCTCTGAAGAGTATTCC	
Atg8 CDS Add cMyc Fw	AAAATGGAGCAGAAGCTCATCTCCGAGGAGGACCTGCCATCGATTCGCGACGAAGT	Add N-terminal cMyc tag to amplified Atg8 CDS
Atg8 3' Amp EcoRV-GS Fw	CGCGCCGGCGCCGATATCGGGAGTGTCGCGGCC	Amplification of Atg8 3' homology arm for homologous recombination
Atg8 3' Amp EcoRV-GS Rev	GAGCTCCCCGGGGATATCGCATACCACACTGGGACGC	
Atg8 5' Amp ApaI-GS Fw	GCGAATTGGGTACCGGGCCCGTAGGGGACCACCGAACAGC	Amplification of Atg8 5' homology arm for homologous recombination
Atg8 5' Amp ApaI-GS Rev	TCCATTTTGTTTTTCAAGACGGCGAATATCTGGT	
cMyc-Atg8 XbaI-GS Fw	GAAAAACAAAATGGAGCAGAAGCTCATCTCC	Add Infusion cloning 15bp homology to Atg8 CDS
cMyc-Atg8 XbaI-GS Rev	GCAGCTCGAGTCTAGATTACCCCAGAGTGTTCTCTGAAGAGT	
Atg8 Intron 2 Rev	TCCCAGGGCACCTATGGAAGA	Screening of endogenous Atg8 locus for replacement
Atg8 5' HR Upstream Fw	GCGTCTTTGGAGCCATTCGG	
Atg8 3'HR Downstream Rev	TGCGAATGGCTAATGGGACATTATTCG	
Atg8 CDS pET19b Fw	ACGACGACAAGCATATGCCATCGATTCGCGACG	Infusion cloning of Atg8 CDS into pET19b for recombinant protein expression
Atg8 CDS pET19b Rev	CAGCCGGATCCTCGAGTTACCCCAGAGTGTTCTCTGAAGAGTATTCC	
TgAtg3 GT1 Infusion 600bp Fw	TACTTCCAATCCAATTTAATTAAGAGACTTCCTCAATACATGCAAGTACACAT	Amplification of 3' end of genes for cloning into pLIC vectors for endogenous tagging, all cloning into PacI site that allows for use in pLIC-3xHA-DHFR, pLIC-HA-DD and pLIC-StrepTY-HXGPRT vectors
TgAtg3 GT1 Infusion 600bp Rev	CCTCCACTTCCAATTTTAATTAACTTCTCGTTTTTTGTACTGCGGT	
TgAtg6 GT1 Fw Infusion	TACTTCCAATCCAATTTAATTAATGGGTGTTGTGCGTGGG	
TgAtg6 GT1 Rev Infusion	CCTCCACTTCCAATTTTAATTAAGGAGGCAGGCGGGC	
TgAtg9 gDNA Infusion Fw	TTCCAATCCAATTTAATTAAAGGGTCCTTTTCTTCCAAGAAGC	
TgAtg9 gDNA Infusion Rev	CCACTTCCAATTTTAATTAAGTTGACGTCTCCTCGAGTCAC	
TgULK1 gDNA Infusion Fw	TTCCAATCCAATTTAATTAAGAGCGAGCAGAGGCGAG	

TgULK1 gDNA Infusion Rev	CCACTTCCAATTTTAATTAACACTCCCATCCAAAATGAGGG	
TgTOR Infusion PacI Fw	TTCCAATCCAATTTAATTAAGGTCTATGTGGCTTTGTGCGA	
TgTOR Infusion PacI Rev	CCACTTCCAATTTTAATTAATCACCAAAACGGGCACCAG	
pLIC-Atg12 StrepTY Infusion Fw	TTCCAATCCAATTTAATTAAGTACTGTGTAACGAATTTCATTACACTTCATGC	
pLIC-Atg12 StrepTY Infusion Rev	CCACTTCCAATTTTAATTAAATAAGCGGGAGTGTAGCAGTACG	
pLIC-Atg4 StrepTY Infusion Fw	TTCCAATCCAATTTAATTAAACGGTGTGCTGCAGATGG	
pLIC-Atg4 StrepTY Infusion Fw	TTCCAATCCAATTTAATTAAACGGTGTGCTGCAGATGG	
pLIC-Atg4 StrepTY Infusion Rev	CCACTTCCAATTTTAATTAACCGGTCTGTGCCGC	
pLIC-Atg7 StrepTY Infusion Fw	TTCCAATCCAATTTAATTAAATGGGAGCCACGCCT	
pLIC-Atg7 StrepTY Infusion Rev	CCACTTCCAATTTTAATTAACTTGGTCTCTGCTGCATCCT	
pLIC-Atg5 StrepTY Infusion Fw	CCACTTCCAATTTTAATTAAAGTGCGGTTGCCGC	
pLIC-Atg5 StrepTY Infusion Rev	TTCCAATCCAATTTAATTAACGGTCTTCGCGGAGACG	
TGGT1_318510 LIC-HA-DD Fw	TTCCAATCCAATTTAATTAAGTCTGCGAGTCTGGCAAGG	
TGGT1_318510 LIC-HA-DD Rev	CCACTTCCAATTTTAATTAAGAAGGGCATTGGGTCATAACT	
TGGT1_218760 LIC-HA-DD Fw	TTCCAATCCAATTTAATTAACTCCAAATAAGCATTTGGCCATT	
TGGT1_218760 LIC-HA-DD Rev	CCACTTCCAATTTTAATTAAAGAGAGGTCGACTTCTCCGT	
TGGT1_319920 LIC-HA Fw	TTCCAATCCAATTTAATTAAGGTAAGAACAACGACCGACG	
TGGT1_319920 LIC-HA Rev	CCACTTCCAATTTTAATTAATCGGAGATGAAGCAGCATCAT	
TGGT1_215250 LIC-HA Fw	TTCCAATCCAATTTAATTAAGGATATCCGTACGTTCACACAGTCAAG	
TGGT1_215250 LIC-HA Rev	CCACTTCCAATTTTAATTAAAGACTCATGCGACTTTTCAAGAGG	
TGGT1_314400 LIC-HA Fw	TTCCAATCCAATTTAATTAACGTAAACAAGACCTCCCGCT	

TGGT1_314400 LIC-HA Rev	CCACTTCCAATTTTAATTAACGCCTGCTTCAGTTCACG	
pLIC-DrpC-HA Fw	TTCCAATCCAATTTAATTAATGTCTGGCGCGGAGAAAC	
pLIC-DrpC-HA Rev	CCACTTCCAATTTTAATTAAAGCCCCATTCAACGGTGAC	
StrepTY Tag sequencing Rev	CCACTTCTCGTACTATGGCCGGTC	Sequencing primer used to confirm insertion of gene fragment into the pLIC-StrepTY vector
HA-Lic-DHFR Sequencing.REV	GACAGAACAATACCGGCACCACTT	Sequencing primer used to confirm insertion of gene fragment into the pLIC-3xHA-DHFR vector
HA-Atg8 G124A Q5 Fw	GAACACTCTGGCATAAGATATCCTAGGG	Site-directed mutagenesis primers used to mutate residues in Atg8. Primers used for mutation of residues in both pET19b-Atg8 CDS vector to make mutant recombinant Atg8 proteins, as well as to mutate residues in pTub-HA-Atg8-CAT-UPRT vector for mutating Atg8 residues used for targeted expression of Atg8 mutants in conditional knock-down approaches
HA-Atg8 G124A Q5 Rev	TCTGAAGAGTATTCCACG	
HA-Atg8 R27E Fw Q5	GTATCCCAACGAAATTCCGGTCATCTGC	
HA-Atg8 R27E Rev Q5	TTTGCCCGAATGCGGTGT	
HA-Atg8 K47E Fw Q5	TGACAAGAAGGAATTCCTCGTGC	
HA-Atg8 K47E Rev Q5	ATCACTGGCAGGTCCGAC	
HA-Atg8 R19Q Fw Q5	GGAGGCACACCAGATTCGGGCAA	
HA-Atg8 R19Q Rev Q5	GCTGTCCTCTTTTCGAAGG	
HA-Atg8 R19A Fw Q5	GGAGGCACACGCAATTCGGGCAAAG	
HA-Atg8 R19A Rev Q5	GCTGTCCTCTTTTCGAAG	
GFP-Atg8 G/A Q5 Fw	GAACACTCTGGCATAATTAATTAATCACCG	Site-directed mutagenesis primers used to mutate G124 to alanine in pTUB-GFP-cMyc-Atg8 plasmid used for ectopic overexpression.
GFP-Atg8 G/A Q5 Rev	TCTGAAGAGTATTCCACG	
5' Flank UPRT Fw	CCCTGGTACACTCGGAAATG	Amplification of UPRT 5' homology for targeting of pTUB-HA-Atg8-CAT constructs to UPRT locus
5' Flank UPRT Rev	CCAATGGCATCACTTGACAG	
3' Flank UPRT Fw	GCCACGGGGTATATCTTTGG	Amplification of UPRT 3' homology for targeting of pTUB-HA-Atg8-CAT constructs to UPRT locus
3' Flank UPRT Rev	CAGACAGTTTTTCGGCAACC	
5' UPRT Infusion PciI Fw	CCTTTTGCTCACATGTGGATCCCCCTGGTACACTCGGAAATG	Addition of Infusion overhangs for cloning of 5'UPRT
5' UPRT Infusion PciI Rev	GCAGGAAAGAACATGTCCAATGGCATCACTTGACAGCG	

3' UPRT Infusion NotI Fw	AGTTCTAGAGCGGCCGCGCCACGGGGTATATCTTTGGT	Addition of Infusion overhangs for cloning of 3'UPRT
3' UPRT Infusion NotI Rev	ACCGCGGTGGCGGCCGCGGATCCCAGACAGTTTTTCGGCAACC	
UPRT Screen US Fw	GCGAAAATGGTGGGAGCAGC	Primer for screening for disruption of UPRT locus by targeting of GOI; Fw primer upstream of 5'UPRT homology sequence used for targeting
UPRT Screen CTRL Rev	CAACAGGCAGAGTCACGGAAAGC	Reverse primer for screening of UPRT locus; will only amplify if UPRT locus is intact. If GOI has been inserted, will not amplify
pTUB Screen Rev	GCAGGAACACATTCCTGCACC	Reverse primer in tubulin promoter used to drive GOI targeted to UPRT locus. Will only amplify if recombination occurs, no amplification with UPRT screen US Fw primer if GOI at UPRT locus
CAT SAG1 3'UTR int screen Fw	GGAGTGTTTCGCAGCAAGCAG	Fw primer in heterologous Sag1 3'UTR used for Chloramphenicol selection cassette used in pTUB-HA targeting to the UPRT locus. Primer used with UPRT 3'DS Rev will only amplify if recombination occurred
UPRT 3' DS Screen Rev	TTCGATCGACCGAAGCAACACTGG	Reverse primer downstream of UPRT 3' region used for targeting GOI to UPRT locus.
PCR Lin UPRT Fw	AGGATGGAATTCCTGCAGCCC	Primers to linearize pTUB-HA-Atg8-DHFR vector to replace DHFR selection cassette with Chloramphenicol selection cassette
PCR Lin UPRT Rev	CGCGGCTTATCTAGTTAAGGGAGC	
CAT UPRT Infusion Fw	CAGGAATTCCATCCTCCCCTCGGGGGGGC	Infusion cloning of Chloramphenicol selection cassette into linearized pTUB-HA-Atg8-DHFR
CAT UPRT Infusion Rev	TTGGCACGTGCATATCGCGATC	
pTUB-HA-CAT-UPRT EcoRV Del Fw	TTGGCACGTGcATATCGCGATC	Used to delete EcoRV site in UPRT 5' Flank to allow for digestion with EcoRV to remove CDS and be able to clone in GOI into EcoRV site for targeted expression at UPRT locus under pTUB-HA
pTUB-HA-CAT-UPRT EcoRV Del Rev	CGTGCAGAAAATCAGTCAC	

ML1771	CTGCTTTCGTCTGTCTTC	Primers from Bestiero et al, used to confirm TATi-Atg8 parasite strain used for conditional knock-down of Atg8 and rescue with WT or mutant Atg8s at UPRT locus
ML1772	CAAATGGCTATGTTCGCC	
ML1773	CCAAACCAGATATTCGCC	
ML1774	TACGACTCACTATAGGGC	
Atg1 qPCR Fw CT	TCTTCTCCTCTGCCTTCTGC	qRT-PCR Primers
Atg1 qPCR Rev CT	CGAAAAGTCACTCCAGCACA	
Atg3 qPCR Fw CT	AGAAGGTGGTGGACAGTTGG	
Atg3 qPCR Rev CT	CCATGGTGAAGTCGTACTCG	
Atg4 qPCR Fw CT	ACGGAGAAGAGGCTGAGACA	
Atg4 qPCR Rev CT	TGAGGTCCTTCTCCACAACC	
Atg5 qPCR Fw CT	CTGGAAGCGAAGAAGCTGAT	
Atg5 qPCR Rev CT	GCGACGATCTCTCTCGTTGT	
Atg6 qPCR CT Fw	CGTCTCCAGGTGTCCAGACT	
Atg6 qPCR CT Rev	CAGCCACTTCAGATCGATGA	
Atg7 qPCR Fw CT	GGAGACAAGACCAAGCGAAG	
Atg7 qPCR Rev CT	GCTTCTCTCCGACACCAAAG	
Atg8 qPCR FW CT	TTGTTTGTTGAAAATACGGCACCGAAG	
Atg8 qPCR Rev CT	TTACCCCAGAGTGTTCTCTGAAGAGTATTC	
Atg9 qPCR Fw CT	AGACGAAGAAGAGCGAGACG	
Atg9 qPCR Rev CT	GTCTCCCTCGACTGATCGAA	
Atg12 qPCR CT Fw	ACATTTCCCTGTCGAACGTC	
Atg12 qPCR CT Rev	TACGAAACCATGAGGCTTCC	
qGFP Fw	GAGGGATACGTGCAGGAGAG	
qGFP Rev	ATCCTGTTGACGAGGGTGTC	
qTubA1 Ct Fw	GCATGATCAGCAACAGCACT	
qTubA1 Ct Rev	GAGAGCAGCCAAATCCTCAC	

Appendix 2: Primary antibodies used in this study

Antibody	Species	Reference/Supplier
Tg β-tubulin	Rabbit	Morrissette & Sibley, 2002 JCS
TgCentrin-1	Rabbit	Sanders & Salisbury, 1994, JCB
TgMORN1	Rabbit	Gubbels & Striepen, 2006, JCS
TgAtrx1 (apicoplast)	Mouse	DeRocher & Parsons, 2008, Eukaryotic Cell
TgNHE3 (PLV)	Guinea Pig	Arrizabalaga et al 2011, Exp Cell Research
TgSAG1	Mouse	Genway (GWB-9894D)
TgROP1 (Tg49)	Mouse	Ossorio & Boothroyd, 1992, MBP
TgGRA7	Mouse	Peter Bradley (unpublished)
TgMIC5	Rabbit	Carruthers et al, 2000, MBP
TgIMC3	Rat	Gubbels & Striepen, 2004, MBP
TgF1β-ATPase	Mouse	Peter Bradley (unpublished)
anti-acetyl-tubulin	Mouse	Sigma (6-11-B-1)
anti-cMyc	Mouse	CST (9B11)
anti-HA	Rabbit	CST (C29F4)
anti-HA	Rat	Roche (3F10)
anti-GFP	Rabbit	Sigma (G1544)

Appendix 3: TgAtg8 Interactome SAINTExpress Results (FC-B > 2, detected in at least 2 of 3 IPs)

[Product Description]	GENE ID	MYC_FC_A	MYC_FC_B	MYC_SP	cMyc IP 1	cMyc IP 2	cMyc IP 3	IgG IP 1	IgG IP 2	IgG IP 3
arginyl-tRNA synthetase	TGGT1_270690	233.28	214.21	1	77	84	92	0	0	0
2-oxo acid dehydrogenases acyltransferase (catalytic domain) domain-containing protein	TGGT1_319920	178.21	167.6	1	90	96	85	0	0	1
putative autophagy-related protein 7 atg7	TGGT1_229690	132.5	126.27	1	59	62	33	0	0	0
putative N-ethylmaleimide-sensitive fusion protein	TGGT1_318510	84.15	76.11	1	30	27	32	0	0	0
hypothetical protein	TGGT1_268430	35.76	32.49	1	7	17	16	0	0	0
RNA pseudouridine synthase superfamily protein	TGGT1_306660	25.78	25.19	1	17	23	10	0	1	1
dehydrogenase E1 component family protein	TGGT1_239490	32.03	21.95	0.85	12	59	2	0	0	1
putative pyruvate dehydrogenase E1 component, beta subunit	TGGT1_314400	26.87	21.82	1	5	36	3	0	0	0
thiamin pyrophosphokinase, catalytic domain-containing protein	TGGT1_215250	21.28	20.79	1	5	19	5	0	0	0
putative autophagy-related protein 8 atg8	TGGT1_254120	23.03	20.12	1	12	7	5	0	0	0
putative SNAP protein (soluble N-ethylmaleimide-sensitive factor Attachment Protein)	TGGT1_218760	20.31	15.98	1	3	6	11	0	0	0
hypothetical protein	TGGT1_247300	10.87	9.59	0.97	8	5	3	1	0	0
transporter, major facilitator family protein	TGGT1_297245	9.1	8.9	0.97	2	5	3	0	0	0
acetyl-CoA acetyltransferase	TGGT1_301120	14.15	7.06	0.66	9	0	3	0	0	0
transmembrane protein	TGGT1_313930	6.43	4.93	0.35	7	4	12	2	5	2
putative gamma-soluble NSF attachment protein	TGGT1_320690	6.74	4.44	0.63	2	0	3	0	0	0
ATPase, AAA family protein	TGGT1_234420	7.9	4.21	0.52	7	0	2	0	0	1

leucyl aminopeptidase LAP	TGGT1_290670	4.35	4.06	0.33	4	14	2	1	0	5
actin	TGGT1_411760	4.4	4.04	0.01	7	11	12	3	6	7
putative U1 snRNP-associated protein Usp106	TGGT1_262960	4.53	3.47	0	18	13	35	10	4	24
heat shock protein HSP90	TGGT1_288380	3.64	3.45	0.26	4	21	5	0	0	13
dense granule protein GRA1	TGGT1_270250	3.04	2.65	0.26	7	21	2	5	0	10
glyceraldehyde-3-phosphate dehydrogenase GAPDH1	TGGT1_289690	2.99	2.65	0.16	10	27	3	4	0	18
heat shock protein HSP70	TGGT1_273760	2.58	2.55	0	19	29	16	12	12	32
actin ACT1	TGGT1_209030	2.47	2.43	0	9	24	6	8	3	18
profilin PRF	TGGT1_293690	3.67	2.34	0.42	3	8	0	1	0	2
microneme protein MIC3	TGGT1_319560	2.69	2.25	0	16	15	3	10	14	5
ribosomal-ubiquitin protein RPL40	TGGT1_289750	3.54	2.24	0.21	4	0	2	1	0	2
serine-threonine phosophatase 2C (PP2C)	TGGT1_231850	3.8	2.08	0.42	6	12	0	4	0	2

Appendix 4: TgAtg3 Interactome SAINTExpress Results (FC-B > 2, detected in at least 2 of 3 IPs)

[Product Description]	GENE	ATG3_FC_A	ATG3_FC_B	ATG3_SP	Atg3 IP 1	Atg3 IP 2	Atg3 IP3	IgG 1	IgG 2	IgG 3
putative autophagy-related protein 3 atg3	TGGT1_236110	221.81	187.86	1	91	59	58	0	0	0
hypothetical protein	TGGT1_305270	100.08	86.21	1	29	39	26	0	0	0
putative autophagy-related protein 7 atg7	TGGT1_229690	78.34	67.65	1	26	27	20	0	0	0
putative autophagy-related protein 8 atg8	TGGT1_254120	49.27	42.94	1	28	24	21	0	0	2
hypothetical protein	TGGT1_203280	20.04	16.16	0.97	11	12	6	1	0	1
hypothetical protein	TGGT1_311830	15.71	13.96	0.99	5	5	4	0	0	0
S1 RNA binding domain-containing protein	TGGT1_211670	14.58	10.99	0.61	9	7	3	0	0	2
hypothetical protein	TGGT1_258850	13.84	10.73	0.46	7	11	4	0	0	3
ribosomal-ubiquitin protein RPS27A	TGGT1_245620	9.27	7.44	0.45	7	5	3	0	1	2
hypothetical protein	TGGT1_226050	12.58	6.92	0.66	5	4	0	0	0	0
putative U1 snRNP-associated protein Usp106	TGGT1_262960	5.31	4.66	0	38	52	38	26	29	15
hypothetical protein	TGGT1_241170	5.53	4.65	0	13	15	9	6	7	6
peptidyl-prolyl cis-trans isomerase, cyclophilin-type domain-containing protein	TGGT1_305940	7.52	4.3	0.33	4	1	0	0	0	0
zinc knuckle domain-containing protein	TGGT1_244840	4.13	3.83	0.01	5	3	5	2	2	3
hypothetical protein	TGGT1_261620	6.17	3.71	0.17	8	9	1	4	2	2
hypothetical protein	TGGT1_249570	4.17	3.55	0	8	10	6	8	7	0
putative rRNA-processing protein FCF1	TGGT1_319950	3.85	3.49	0	7	8	7	4	7	4

ribosomal protein RPL34	TGGT1_227600	4.81	3.48	0.22	1	2	0	0	0	0
hypothetical protein	TGGT1_230160	3.7	3.38	0	6	8	7	2	8	5
ribosomal protein RPL38	TGGT1_231080	3.69	3.2	0	14	15	11	10	11	11
ribosomal protein RPL44	TGGT1_203630	3.84	3.05	0	9	8	4	6	5	5
hypothetical protein	TGGT1_266470	3.34	3.03	0	6	7	6	5	6	4
hypothetical protein	TGGT1_315570	3.37	3.02	0	8	8	7	8	8	2
ribosomal protein RPS25	TGGT1_231140	3.1	2.84	0	6	9	8	6	7	7
ribosomal protein RPL27A	TGGT1_310490	3.42	2.75	0	6	2	3	3	3	2
ribosomal protein RPS18	TGGT1_225080	2.81	2.69	0	6	9	11	7	8	9
ribosomal protein RPL37	TGGT1_239330	3.48	2.64	0	7	9	3	7	6	3
ribosomal protein RPS17	TGGT1_207840	2.71	2.55	0	13	19	21	16	19	19
mRNA turnover 4 (MRT4) family protein	TGGT1_255320	3.01	2.54	0	5	5	3	5	3	4
ribosomal protein RPL17	TGGT1_299050	2.72	2.45	0	16	13	14	14	17	15
hypothetical protein	TGGT1_311000	3.56	2.45	0.03	2	2	0	1	1	0
ribosomal protein RPL37A	TGGT1_300190	2.69	2.44	0	7	8	7	8	7	8
ribosomal protein RPL26	TGGT1_248390	2.66	2.38	0	18	15	15	20	16	17
hypothetical protein	TGGT1_315610	2.74	2.37	0	8	11	7	7	12	9
chaperonin protein BiP	TGGT1_311720	2.54	2.35	0	38	37	42	41	52	40
ribosomal protein RPL31	TGGT1_266070	2.53	2.32	0	7	7	7	8	8	7
ribosomal protein RPL8	TGGT1_204020	2.31	2.29	0	4	6	13	5	4	15
ribosomal protein RPL22	TGGT1_239760	2.43	2.29	0	5	5	6	6	7	4
ribosomal protein RPS8	TGGT1_245460	2.61	2.27	0	16	15	12	17	15	18
ribosomal protein RPL18	TGGT1_300000	2.42	2.2	0	3	8	8	6	7	7
histone H2Ba	TGGT1_305160	2.3	2.16	0	9	11	12	13	15	10
ribosomal-ubiquitin protein RPL40	TGGT1_289750	2.19	2.14	0	2	2	3	2	4	1
ribosomal protein RPL14	TGGT1_267060	2.22	2.13	0	3	3	4	4	4	3
ribosomal protein RPL28	TGGT1_229250A	2.29	2.11	0	5	5	5	6	6	6

putative bud site selection protein	TGGT1_226240	2.75	2.09	0	16	18	7	16	19	13
3'5'-cyclic nucleotide phosphodiesterase domain-containing protein	TGGT1_280410	2.87	2.05	0.02	2	1	0	0	2	0

Bibliography

1. Adl SM, Leander BS, Simpson AGB, Archibald JM, Anderson OR, Bass D, et al. Diversity, nomenclature, and taxonomy of protists. Syst Biol. 2007;56: 684–689. doi:10.1080/10635150701494127

2. Tenter AM, Heckeroth AR, Weiss LM. Toxoplasma gondii: from animals to humans. Int J Parasitol. 2000;30: 1217–1258.

3. Katris NJ, Dooren GG van, McMillan PJ, Hanssen E, Tilley L, Waller RF. The Apical Complex Provides a Regulated Gateway for Secretion of Invasion Factors in Toxoplasma. PLOS Pathog. 2014;10: e1004074. doi:10.1371/journal.ppat.1004074

4. Hu K, Johnson J, Florens L, Fraunholz M, Suravajjala S, DiLullo C, et al. Cytoskeletal Components of an Invasion Machine—The Apical Complex of Toxoplasma gondii. PLOS Pathog. 2006;2: e13. doi:10.1371/journal.ppat.0020013

5. Köhler S, Delwiche CF, Denny PW, Tilney LG, Webster P, Wilson RJ, et al. A plastid of probable green algal origin in Apicomplexan parasites. Science. 1997;275: 1485–1489.

6. Zhu G, Marchewka MJ, Keithly JS. Cryptosporidium parvum appears to lack a plastid genome. Microbiol Read Engl. 2000;146 (Pt 2): 315–321. doi:10.1099/00221287-146-2-315

7. Fleige T, Fischer K, Ferguson DJP, Gross U, Bohne W. Carbohydrate Metabolism in the Toxoplasma gondii Apicoplast: Localization of Three Glycolytic Isoenzymes, the Single Pyruvate Dehydrogenase Complex, and a Plastid Phosphate Translocator. Eukaryot Cell. 2007;6: 984–996. doi:10.1128/EC.00061-07

8. Waller RF, McFadden GI. The apicoplast: a review of the derived plastid of apicomplexan parasites. Curr Issues Mol Biol. 2005;7: 57–79.

9. Gordon JL, Beatty WL, Sibley LD. A Novel Actin-Related Protein Is Associated with Daughter Cell Formation in Toxoplasma gondii. Eukaryot Cell. 2008;7: 1500–1512. doi:10.1128/EC.00064-08

10. Morrissette NS, Sibley LD. Cytoskeleton of Apicomplexan Parasites. Microbiol Mol Biol Rev. 2002;66: 21–38. doi:10.1128/MMBR.66.1.21-38.2002

11. Splendore A. Un nuovo protozoa parassita deconigli incontrato nelle lesioni anatomiche d'une malattia che ricorda in molti punti il Kala-azar dell'uoma. Rev Soci Sci Sao Paulo. 1908;3: 109–112.

12. Nicolle C, Manceaux L. Sure une infection a corps de Leishman (ou organismes voisons) du gondi. C R Acad Sci. 1908;147: 763.

13. Dubey JP. The History of Toxoplasma gondii—The First 100 Years. J Eukaryot Microbiol. 2008;55: 467–475. doi:10.1111/j.1550-7408.2008.00345.x

14. Nicolle C, Manceaux L. Sur un Protozoaire nouveau du Gondi. C R Acad Sci. 1909;

15. Sibley LD, Boothroyd JC. Virulent strains of Toxoplasma gondii comprise a single clonal lineage. Nature. 1992;359: 82–85. doi:10.1038/359082a0

16. Howe DK, Sibley LD. Toxoplasma gondii comprises three clonal lineages: correlation of parasite genotype with human disease. J Infect Dis. 1995;172: 1561–1566.

17. Howe DK, Honoré S, Derouin F, Sibley LD. Determination of genotypes of Toxoplasma gondii strains isolated from patients with toxoplasmosis. J Clin Microbiol. 1997;35: 1411–1414.

18. Su C, Evans D, Cole RH, Kissinger JC, Ajioka JW, Sibley LD. Recent expansion of Toxoplasma through enhanced oral transmission. Science. 2003;299: 414–416. doi:10.1126/science.1078035

19. Sibley LD, Khan A, Ajioka JW, Rosenthal BM. Genetic diversity of Toxoplasma gondii in animals and humans. Philos Trans R Soc B Biol Sci. 2009;364: 2749–2761. doi:10.1098/rstb.2009.0087

20. Dardé ML. Toxoplasma gondii, “new” genotypes and virulence. Parasite Paris Fr. 2008;15: 366–371. doi:10.1051/parasite/2008153366

21. Pena HFJ, Gennari SM, Dubey JP, Su C. Population structure and mouse-virulence of Toxoplasma gondii in Brazil. Int J Parasitol. 2008;38: 561–569. doi:10.1016/j.ijpara.2007.09.004

22. Dubey JP, Sundar N, Gennari SM, Minervino AHH, Farias NA da R, Ruas JL, et al. Biologic and genetic comparison of Toxoplasma gondii isolates in free-range chickens from the northern Pará state and the southern state Rio Grande do Sul, Brazil revealed highly diverse and distinct parasite populations. Vet Parasitol. 2007;143: 182–188. doi:10.1016/j.vetpar.2006.08.024

23. Dubey JP, Zhu XQ, Sundar N, Zhang H, Kwok OCH, Su C. Genetic and biologic characterization of Toxoplasma gondii isolates of cats from China. Vet Parasitol. 2007;145: 352–356. doi:10.1016/j.vetpar.2006.12.016

24. Carme B, Bissuel F, Ajzenberg D, Bouyne R, Aznar C, Demar M, et al. Severe acquired toxoplasmosis in immunocompetent adult patients in French Guiana. J Clin Microbiol. 2002;40: 4037–4044.

25. Saeij JPJ, Boyle JP, Boothroyd JC. Differences among the three major strains of Toxoplasma gondii and their specific interactions with the infected host. Trends Parasitol. 2005;21: 476–481. doi:10.1016/j.pt.2005.08.001

26. Saeij JPJ, Boyle JP, Coller S, Taylor S, Sibley LD, Brooke-Powell ET, et al. Polymorphic Secreted Kinases Are Key Virulence Factors in Toxoplasmosis. Science. 2006;314: 1780–1783. doi:10.1126/science.1133690

27. Taylor S, Barragan A, Su C, Fux B, Fentress SJ, Tang K, et al. A secreted serine-threonine kinase determines virulence in the eukaryotic pathogen Toxoplasma gondii. Science. 2006;314: 1776–1780. doi:10.1126/science.1133643

28. Yang N, Farrell A, Niedelman W, Melo M, Lu D, Julien L, et al. Genetic basis for phenotypic differences between different Toxoplasma gondii type I strains. BMC Genomics. 2013;14: 467. doi:10.1186/1471-2164-14-467

29. Villard O, Candolfi E, Ferguson DJ, Marcellin L, Kien T. Loss of oral infectivity of tissue cysts of Toxoplasma gondii RH strain to outbred Swiss Webster mice. Int J Parasitol. 1997;27: 1555–1559.

30. Wang J-L, Huang S-Y, Behnke MS, Chen K, Shen B, Zhu X-Q. The Past, Present, and Future of Genetic Manipulation in Toxoplasma gondii. Trends Parasitol. 2016;32: 542–553. doi:10.1016/j.pt.2016.04.013

31. Striepen B. Parasitic infections: Time to tackle cryptosporidiosis. Nat News. 2013;503: 189. doi:10.1038/503189a

32. Vinayak S, Pawlowic MC, Sateriale A, Brooks CF, Studstill CJ, Bar-Peled Y, et al. Genetic modification of the diarrhoeal pathogen Cryptosporidium parvum. Nature. 2015;523: 477–480. doi:10.1038/nature14651

33. Kim K, Weiss LM. Toxoplasma gondii: the model apicomplexan. Int J Parasitol. 2004;34: 423–432. doi:10.1016/j.ijpara.2003.12.009

34. Dubey JP, Lindsay DS, Speer CA. Structures of Toxoplasma gondii Tachyzoites, Bradyzoites, and Sporozoites and Biology and Development of Tissue Cysts. Clin Microbiol Rev. 1998;11: 267–299.

35. Robert-Gangneux F, Dardé M-L. Epidemiology of and diagnostic strategies for toxoplasmosis. Clin Microbiol Rev. 2012;25: 264–296. doi:10.1128/CMR.05013-11

36. Jones TC, Hirsch JG. The interaction between Toxoplasma gondii and mammalian cells. II. The absence of lysosomal fusion with phagocytic vacuoles containing living parasites. J Exp Med. 1972;136: 1173–1194.

37. Blader I, Coleman B, Chen C-T, Gubbels M-J. The lytic cycle of Toxoplasma gondii: 15 years later. Annu Rev Microbiol. 2015;69: 463–485. doi:10.1146/annurev-micro-091014-104100

38. Nishi M, Hu K, Murray JM, Roos DS. Organellar dynamics during the cell cycle of Toxoplasma gondii. J Cell Sci. 2008;121: 1559–1568. doi:10.1242/jcs.021089

39. Black MW, Boothroyd JC. Lytic Cycle of Toxoplasma gondii. Microbiol Mol Biol Rev. 2000;64: 607–623. doi:10.1128/MMBR.64.3.607-623.2000

40. Dubey JP. Bradyzoite-induced murine toxoplasmosis: stage conversion, pathogenesis, and tissue cyst formation in mice fed bradyzoites of different strains of Toxoplasma gondii. J Eukaryot Microbiol. 1997;44: 592–602.

41. Skariah S, McIntyre MK, Mordue DG. Toxoplasma gondii: determinants of tachyzoite to bradyzoite conversion. Parasitol Res. 2010;107: 253–260. doi:10.1007/s00436-010-1899-6

42. Weiss LM, Kim K, editors. Toxoplasma gondii: the model apicomplexan: perspectives and methods. 1st ed. Amsterdam ; Boston: Elsevier/Academic Press; 2007.

43. Wainwright KE, Miller MA, Barr BC, Gardner IA, Melli AC, Essert T, et al. Chemical inactivation of Toxoplasma gondii oocysts in water. J Parasitol. 2007;93: 925–931. doi:10.1645/GE-1063R.1

44. Wainwright KE, Lagunas-Solar M, Miller MA, Barr BC, Gardner IA, Pina C, et al. Physical inactivation of Toxoplasma gondii oocysts in water. Appl Environ Microbiol. 2007;73: 5663–5666. doi:10.1128/AEM.00504-07

45. Dumètre A, Le Bras C, Baffet M, Meneceur P, Dubey JP, Derouin F, et al. Effects of ozone and ultraviolet radiation treatments on the infectivity of Toxoplasma gondii oocysts. Vet Parasitol. 2008;153: 209–213. doi:10.1016/j.vetpar.2008.02.004

46. Lélu M, Villena I, Dardé M-L, Aubert D, Geers R, Dupuis E, et al. Quantitative Estimation of the Viability of Toxoplasma gondii Oocysts in Soil. Appl Environ Microbiol. 2012;78: 5127–5132. doi:10.1128/AEM.00246-12

47. Dumètre A, Dardé M-L. How to detect Toxoplasma gondii oocysts in environmental samples? FEMS Microbiol Rev. 2003;27: 651–661. doi:10.1016/S0168-6445(03)00071-8

48. Economic Research Service (ERS), U.S. Department of Agriculture (USDA). Cost Estimates of Foodborne Illnesses [Internet]. Available: http://ers.usda.gov/data-products/cost-estimates-of-foodborne-illnesses.aspx (2014).

49. FAO, editor. Livestock in the balance. Rome: FAO; 2009.

50. Hide G, Morley EK, Hughes JM, Gerwash O, Elmahaishi MS, Elmahaishi KH, et al. Evidence for high levels of vertical transmission in Toxoplasma gondii. Parasitology. 2009;136: 1877–1885. doi:10.1017/S0031182009990941

51. Silva MG da, Vinaud MC, Castro AM de. Prevalence of toxoplasmosis in pregnant women and vertical transmission of Toxoplasma gondii in patients from basic units of health from Gurupi, Tocantins, Brazil, from 2012 to 2014. PLOS ONE. 2015;10: e0141700. doi:10.1371/journal.pone.0141700

52. CDC. Toxoplasmosis - General Information - Frequently Asked Questions [Internet]. [cited 27 May 2017]. Available: http://www.cdc.gov/parasites/toxoplasmosis/gen_info/faqs.html

53. Luft BJ, Remington JS. Toxoplasmic encephalitis in AIDS. Clin Infect Dis Off Publ Infect Dis Soc Am. 1992;15: 211–222.

54. Nissapatorn V. Toxoplasmosis in HIV/AIDS: a living legacy. Southeast Asian J Trop Med Public Health. 2009;40: 1158–1178.

55. Nissapatorn V, Lee C, Quek KF, Leong CL, Mahmud R, Abdullah KA. Toxoplasmosis in HIV/AIDS patients: a current situation. Jpn J Infect Dis. 2004;57: 160–165.

56. Gallino A, Maggiorini M, Kiowski W, Martin X, Wunderli W, Schneider J, et al. Toxoplasmosis in heart transplant recipients. Eur J Clin Microbiol Infect Dis Off Publ Eur Soc Clin Microbiol. 1996;15: 389–393.

57. Derouin F, Pelloux H, ESCMID Study Group on Clinical Parasitology. Prevention of toxoplasmosis in transplant patients. Clin Microbiol Infect Off Publ Eur Soc Clin Microbiol Infect Dis. 2008;14: 1089–1101. doi:10.1111/j.1469-0691.2008.02091.x

58. Chintakuntlawar A, Kidd M, Al-Kali A, Wilson W, Thompson CA. Toxoplasmosis in patients with hematologic malignancies. Leuk Lymphoma. 2015;56: 536–538. doi:10.3109/10428194.2014.926348

59. Kodjikian L, Hoigne I, Adam O, Jacquier P, Aebi-Ochsner C, Aebi C, et al. Vertical transmission of toxoplasmosis from a chronically infected immunocompetent woman. Pediatr Infect Dis J. 2004;23: 272–274.

60. Wilson CB, Nizet V, Maldonado YA, Remington JS, Klein JO, editors. Remington and Klein's infectious diseases of the fetus and newborn infant. Eighth edition. Philadelphia, PA: Elsevier, Saunders; 2016.

61. Park Y-H, Nam H-W. Clinical Features and Treatment of Ocular Toxoplasmosis. Korean J Parasitol. 2013;51: 393–399. doi:10.3347/kjp.2013.51.4.393

62. McCannel CA, Holland GN, Helm CJ, Cornell PJ, Winston JV, Rimmer TG. Causes of uveitis in the general practice of ophthalmology. UCLA Community-Based Uveitis Study Group. Am J Ophthalmol. 1996;121: 35–46.

63. Perkins ES. Ocular toxoplasmosis. Br J Ophthalmol. 1973;57: 1–17.

64. Goldstein EJC, Montoya JG, Remington JS. Management of Toxoplasma gondii Infection during Pregnancy. Clin Infect Dis. 2008;47: 554–566. doi:10.1086/590149

65. Gratzl R, Sodeck G, Platzer P, Jäger W, Graf J, Pollak A, et al. Treatment of toxoplasmosis in pregnancy: concentrations of spiramycin and neospiramycin in maternal serum and amniotic fluid. Eur J Clin Microbiol Infect Dis Off Publ Eur Soc Clin Microbiol. 2002;21: 12–16.

66. Gupta A, Shah P, Haider A, Gupta K, Siddiqi MI, Ralph SA, et al. Reduced ribosomes of the apicoplast and mitochondrion of Plasmodium spp. and predicted interactions with antibiotics. Open Biol. 2014;4. doi:10.1098/rsob.140045

67. McFadden GI, Roos DS. Apicomplexan plastids as drug targets. Trends Microbiol. 1999;7: 328–333. doi:10.1016/S0966-842X(99)01547-4

68. Gatton ML, Martin LB, Cheng Q. Evolution of Resistance to Sulfadoxine-Pyrimethamine in Plasmodium falciparum. Antimicrob Agents Chemother. 2004;48: 2116–2123. doi:10.1128/AAC.48.6.2116-2123.2004

69. Feng Y, He D, Yao Z, Klionsky DJ. The machinery of macroautophagy. Cell Res. 2014;24: 24–41. doi:10.1038/cr.2013.168

70. Mizushima N, Klionsky DJ. Protein turnover via autophagy: implications for metabolism. Annu Rev Nutr. 2007;27: 19–40. doi:10.1146/annurev.nutr.27.061406.093749

71. Russell RC, Yuan H-X, Guan K-L. Autophagy regulation by nutrient signaling. Cell Res. 2014;24: 42–57. doi:10.1038/cr.2013.166

72. Mizushima N, Levine B. Autophagy in mammalian development and differentiation. Nat Cell Biol. 2010;12: 823–830. doi:10.1038/ncb0910-823

73. Kaushik S, Cuervo AM. Proteostasis and aging. Nat Med. 2015;21: 1406–1415. doi:10.1038/nm.4001

74. Choi J, Park S, Biering SB, Selleck E, Liu CY, Zhang X, et al. The parasitophorous vacuole membrane of Toxoplasma gondii is targeted for disruption by ubiquitin-like conjugation systems of autophagy. Immunity. 2014;40: 924–935. doi:10.1016/j.immuni.2014.05.006

75. Colombo MI. Pathogens and autophagy: subverting to survive. Cell Death Differ. 2005;12: 1481–1483. doi:10.1038/sj.cdd.4401767

76. Jin M, Klionsky DJ. The Core Molecular Machinery of Autophagosome Formation. In: Wang H-G, editor. Autophagy and Cancer. New York, NY: Springer New York; 2013. pp. 25–45. doi:10.1007/978-1-4614-6561-4_2

77. Yang Z, Klionsky DJ. Mammalian autophagy: core molecular machinery and signaling regulation. Curr Opin Cell Biol. 2010;22: 124–131. doi:10.1016/j.ceb.2009.11.014

78. Rao Y, Perna MG, Hofmann B, Beier V, Wollert T. The Atg1–kinase complex tethers Atg9-vesicles to initiate autophagy. Nat Commun. 2016;7: 10338. doi:10.1038/ncomms10338

79. Nakatogawa H, Suzuki K, Kamada Y, Ohsumi Y. Dynamics and diversity in autophagy mechanisms: lessons from yeast. Nat Rev Mol Cell Biol. 2009;10: 458–467. doi:10.1038/nrm2708

80. Kamada Y. Prime-numbered Atg proteins act at the primary step in autophagy, Unphosphorylatable Atg13 can induce autophagy without TOR inactivation. Autophagy. 2010;6: 415–416. doi:10.4161/auto.6.3.11390

81. Papinski D, Schuschnig M, Reiter W, Wilhelm L, Barnes CA, Maiolica A, et al. Early steps in autophagy depend on direct phosphorylation of Atg9 by the Atg1 kinase. Mol Cell. 2014;53: 471–483. doi:10.1016/j.molcel.2013.12.011

82. Rieter E, Vinke F, Bakula D, Cebollero E, Ungermann C, Proikas-Cezanne T, et al. Atg18 function in autophagy is regulated by specific sites within its β-propeller. J Cell Sci. 2013;126: 593–604. doi:10.1242/jcs.115725

83. Longatti A, Tooze SA. Vesicular trafficking and autophagosome formation. Cell Death Differ. 2009;16: 956–965. doi:10.1038/cdd.2009.39

84. Stack JH, Herman PK, Schu PV, Emr SD. A membrane-associated complex containing the Vps15 protein kinase and the Vps34 PI 3-kinase is essential for protein sorting to the yeast lysosome-like vacuole. EMBO J. 1993;12: 2195–2204.

85. Dall'Armi C, Devereaux KA, Di Paolo G. The role of lipids in the control of autophagy. Curr Biol CB. 2013;23: R33-45. doi:10.1016/j.cub.2012.10.041

86. Fogel AI, Dlouhy BJ, Wang C, Ryu S-W, Neutzner A, Hasson SA, et al. Role of membrane association and Atg14-dependent phosphorylation in beclin-1-mediated autophagy. Mol Cell Biol. 2013;33: 3675–3688. doi:10.1128/MCB.00079-13

87. Geng J, Klionsky DJ. The Atg8 and Atg12 ubiquitin-like conjugation systems in macroautophagy. "Protein Modifications: Beyond the Usual Suspects" Review Series. EMBO Rep. 2008;9: 859–864. doi:10.1038/embor.2008.163

88. The Role of Atg Proteins in Autophagosome Formation. Annu Rev Cell Dev Biol. 2011;27: 107–132. doi:10.1146/annurev-cellbio-092910-154005

89. Weidberg H, Shpilka T, Shvets E, Abada A, Shimron F, Elazar Z. LC3 and GATE-16 N Termini Mediate Membrane Fusion Processes Required for Autophagosome Biogenesis. Dev Cell. 2011;20: 444–454. doi:10.1016/j.devcel.2011.02.006

90. Kirisako T, Ichimura Y, Okada H, Kabeya Y, Mizushima N, Yoshimori T, et al. The Reversible Modification Regulates the Membrane-Binding State of Apg8/Aut7 Essential for Autophagy and the Cytoplasm to Vacuole Targeting Pathway. J Cell Biol. 2000;151: 263–276. doi:10.1083/jcb.151.2.263

91. Sakoh-Nakatogawa M, Matoba K, Asai E, Kirisako H, Ishii J, Noda NN, et al. Atg12–Atg5 conjugate enhances E2 activity of Atg3 by rearranging its catalytic site. Nat Struct Mol Biol. 2013;20: 433–439. doi:10.1038/nsmb.2527

92. Suzuki K, Ohsumi Y. Molecular machinery of autophagosome formation in yeast, Saccharomyces cerevisiae. FEBS Lett. 2007;581: 2156–2161. doi:10.1016/j.febslet.2007.01.096

93. Ghosh D, Walton JL, Roepe PD, Sinai AP. Autophagy is a cell death mechanism in Toxoplasma gondii. Cell Microbiol. 2012;14: 589–607. doi:10.1111/j.1462-5822.2011.01745.x

94. Besteiro S, Brooks CF, Striepen B, Dubremetz J-F. Autophagy Protein Atg3 is Essential for Maintaining Mitochondrial Integrity and for Normal Intracellular Development of Toxoplasma gondii Tachyzoites. PLoS Pathog. 2011;7. doi:10.1371/journal.ppat.1002416

95. Nguyen HM, El Hajj H, El Hajj R, Tawil N, Berry L, Lebrun M, et al. Toxoplasma gondii autophagy-related protein ATG9 is crucial for the survival of parasites in their host. Cell Microbiol. 2017;19. doi:10.1111/cmi.12712

96. Daher W, Morlon-Guyot J, Sheiner L, Lentini G, Berry L, Tawk L, et al. Lipid kinases are essential for apicoplast homeostasis in Toxoplasma gondii. Cell Microbiol. 2015;17: 559–578. doi:10.1111/cmi.12383

97. Parussini F, Coppens I, Shah PP, Diamond SL, Carruthers VB. Cathepsin L occupies a vacuolar compartment and is a protein maturase within the endo/exocytic system of Toxoplasma gondii. Mol Microbiol. 2010;76: 1340–1357. doi:10.1111/j.1365-2958.2010.07181.x

98. Dou Z, Coppens I, Carruthers VB. Non-canonical maturation of two papain-family proteases in Toxoplasma gondii. J Biol Chem. 2013;288: 3523–3534. doi:10.1074/jbc.M112.443697

99. Walker DM, Mahfooz N, Kemme KA, Patel VC, Spangler M, Drew ME. Plasmodium falciparum Erythrocytic Stage Parasites Require the Putative Autophagy Protein PfAtg7 for Normal Growth. Snounou G, editor. PLoS ONE. 2013;8: e67047. doi:10.1371/journal.pone.0067047

100. Tanida I, Mizushima N, Kiyooka M, Ohsumi M, Ueno T, Ohsumi Y, et al. Apg7p/Cvt2p: A novel protein-activating enzyme essential for autophagy. Mol Biol Cell. 1999;10: 1367–1379.

101. Mizushima N, Noda T, Yoshimori T, Tanaka Y, Ishii T, George MD, et al. A protein conjugation system essential for autophagy. Nature. 1998;395: 395–398. doi:10.1038/26506

102. Williams RAM, Smith TK, Cull B, Mottram JC, Coombs GH. ATG5 Is Essential for ATG8-Dependent Autophagy and Mitochondrial Homeostasis in Leishmania major. PLOS Pathog. 2012;8: e1002695. doi:10.1371/journal.ppat.1002695

103. Lévêque MF, Berry L, Cipriano MJ, Nguyen H-M, Striepen B, Besteiro S. Autophagy-Related Protein ATG8 Has a Noncanonical Function for Apicoplast Inheritance in Toxoplasma gondii. mBio. 2015;6. doi:10.1128/mBio.01446-15

104. Kong-Hap MA, Mouammine A, Daher W, Berry L, Lebrun M, Dubremetz J-F, et al. Regulation of ATG8 membrane association by ATG4 in the parasitic protist Toxoplasma gondii. Autophagy. 2013;9: 1334–1348. doi:10.4161/auto.25189

105. Eickel N, Kaiser G, Prado M, Burda P-C, Roelli M, Stanway RR, et al. Features of autophagic cell death in Plasmodium liver-stage parasites. Autophagy. 2013;9: 568–580. doi:10.4161/auto.23689

106. Tomlins AM, Ben-Rached F, Williams RA, Proto WR, Coppens I, Ruch U, et al. Plasmodium falciparum ATG8 implicated in both autophagy and apicoplast formation. Autophagy. 2013;9: 1540–1552. doi:10.4161/auto.25832

107. Hain AUP, Weltzer RR, Hammond H, Jayabalasingham B, Dinglasan RR, Graham DRM, et al. Structural characterization and inhibition of the Plasmodium Atg8-Atg3 interaction. J Struct Biol. 2012;180: 551–562. doi:10.1016/j.jsb.2012.09.001

108. Tsukada M, Ohsumi Y. Isolation and characterization of autophagy-defective mutants of Saccharomyces cerevisiae. FEBS Lett. 1993;333: 169–174.

109. Duszenko M, Ginger ML, Brennand A, Gualdrón-López M, Colombo M-I, Coombs GH, et al. Autophagy in protists. Autophagy. 2011;7: 127–158. doi:10.4161/auto.7.2.13310

110. Paz Y, Elazar Z, Fass D. Structure of GATE-16, membrane transport modulator and mammalian ortholog of autophagocytosis factor Aut7p. J Biol Chem. 2000;275: 25445–25450. doi:10.1074/jbc.C000307200

111. Noda NN, Ohsumi Y, Inagaki F. ATG systems from the protein structural point of view. Chem Rev. 2009;109: 1587–1598. doi:10.1021/cr800459r

112. Kouno T, Mizuguchi M, Tanida I, Ueno T, Kanematsu T, Mori Y, et al. Solution structure of microtubule-associated protein light chain 3 and identification of its functional subdomains. J Biol Chem. 2005;280: 24610–24617. doi:10.1074/jbc.M413565200

113. Schwarten M, Stoldt M, Mohrlüder J, Willbold D. Solution structure of Atg8 reveals conformational polymorphism of the N-terminal domain. Biochem Biophys Res Commun. 2010;395: 426–431. doi:10.1016/j.bbrc.2010.04.043

114. Coyle JE, Qamar S, Rajashankar KR, Nikolov DB. Structure of GABARAP in two conformations: implications for GABA(A) receptor localization and tubulin binding. Neuron. 2002;33: 63–74.

115. Shpilka T, Weidberg H, Pietrokovski S, Elazar Z. Atg8: an autophagy-related ubiquitin-like protein family. Genome Biol. 2011;12: 226. doi:10.1186/gb-2011-12-7-226

116. Nemos C, Mansuy V, Vernier-Magnin S, Fraichard A, Jouvenot M, Delage-Mourroux R. Expression of gec1/GABARAPL1 versus GABARAP mRNAs in human: predominance of gec1/GABARAPL1 in the central nervous system. Brain Res Mol Brain Res. 2003;119: 216–219.

117. Legesse-Miller A, Sagiv Y, Porat A, Elazar Z. Isolation and Characterization of a Novel Low Molecular Weight Protein Involved in Intra-Golgi Traffic. J Biol Chem. 1998;273: 3105–3109. doi:10.1074/jbc.273.5.3105

118. Sagiv Y, Legesse-Miller A, Porat A, Elazar Z. GATE-16, a membrane transport modulator, interacts with NSF and the Golgi v-SNARE GOS-28. EMBO J. 2000;19: 1494–1504. doi:10.1093/emboj/19.7.1494

119. Tachikawa M, Mochizuki A. Golgi apparatus self-organizes into the characteristic shape via postmitotic reassembly dynamics. Proc Natl Acad Sci. 2017;114: 5177–5182. doi:10.1073/pnas.1619264114

120. Rabouille C, Levine TP, Peters JM, Warren G. An NSF-like ATPase, p97, and NSF mediate cisternal regrowth from mitotic Golgi fragments. Cell. 1995;82: 905–914.

121. Müller JM, Rabouille C, Newman R, Shorter J, Freemont P, Schiavo G, et al. An NSF function distinct from ATPase-dependent SNARE disassembly is essential for Golgi membrane fusion. Nat Cell Biol. 1999;1: 335–340. doi:10.1038/14025

122. Müller JMM, Shorter J, Newman R, Deinhardt K, Sagiv Y, Elazar Z, et al. Sequential SNARE disassembly and GATE-16–GOS-28 complex assembly mediated by distinct NSF activities drives Golgi membrane fusion. J Cell Biol. 2002;157: 1161–1173. doi:10.1083/jcb.200202082

123. Koike M, Tanida I, Nanao T, Tada N, Iwata J, Ueno T, et al. Enrichment of GABARAP Relative to LC3 in the Axonal Initial Segments of Neurons. PLoS ONE. 2013;8. doi:10.1371/journal.pone.0063568

124. Jacob TC, Moss SJ, Jurd R. GABAA receptor trafficking and its role in the dynamic modulation of neuronal inhibition. Nat Rev Neurosci. 2008;9: 331–343. doi:10.1038/nrn2370

125. Cook JL, Re RN, deHaro DL, Abadie JM, Peters M, Alam J. The trafficking protein, GABARAP, binds to and enhances plasma membrane expression and function of the angiotensin AT1 receptor. Circ Res. 2008;102: 1539–1547. doi:10.1161/CIRCRESAHA.108.176594

126. Chen C, Wang Y, Huang P, Liu-Chen L-Y. Effects of C-terminal Modifications of GEC1 Protein and γ-Aminobutyric Acid Type A (GABAA) Receptor-associated Protein (GABARAP), Two Microtubule-associated Proteins, on κ Opioid Receptor Expression. J Biol Chem. 2011;286: 15106–15115. doi:10.1074/jbc.M111.230896

127. Laínez S, Valente P, Ontoria-Oviedo I, Estévez-Herrera J, Camprubí-Robles M, Ferrer-Montiel A, et al. GABAA receptor associated protein (GABARAP) modulates TRPV1 expression and channel function and desensitization. FASEB J Off Publ Fed Am Soc Exp Biol. 2010;24: 1958–1970. doi:10.1096/fj.09-151472

128. Labonté D, Thies E, Kneussel M. The kinesin KIF21B participates in the cell surface delivery of γ2 subunit-containing GABAA receptors. Eur J Cell Biol. 2014;93: 338–346. doi:10.1016/j.ejcb.2014.07.007

129. Nakajima K, Yin X, Takei Y, Seog D-H, Homma N, Hirokawa N. Molecular Motor KIF5A Is Essential for GABAA Receptor Transport, and KIF5A Deletion Causes Epilepsy. Neuron. 2012;76: 945–961. doi:10.1016/j.neuron.2012.10.012

130. Monastyrska I, Rieter E, Klionsky DJ, Reggiori F. Multiple roles of the cytoskeleton in autophagy. Biol Rev Camb Philos Soc. 2009;84: 431–448. doi:10.1111/j.1469-185X.2009.00082.x

131. Mansuy V, Boireau W, Fraichard A, Schlick J-L, Jouvenot M, Delage-Mourroux R. GEC1, a protein related to GABARAP, interacts with tubulin and GABAA receptor. Biochem Biophys Res Commun. 2004;325: 639–648. doi:10.1016/j.bbrc.2004.10.072

132. Mohrlüder J, Hoffmann Y, Stangler T, Hänel K, Willbold D. Identification of clathrin heavy chain as a direct interaction partner for the gamma-aminobutyric acid type A receptor associated protein. Biochemistry (Mosc). 2007;46: 14537–14543. doi:10.1021/bi7018145

133. Mann SS, Hammarback JA. Molecular characterization of light chain 3. A microtubule binding subunit of MAP1A and MAP1B. J Biol Chem. 1994;269: 11492–11497.

134. Halpain S, Dehmelt L. The MAP1 family of microtubule-associated proteins. Genome Biol. 2006;7: 224. doi:10.1186/gb-2006-7-6-224

135. Pedrotti B, Islam K. Purification of microtubule associated protein MAP1B from bovine brain: MAP1B binds to microtubules but not to microfilaments. Cell Motil Cytoskeleton. 1995;30: 301–309. doi:10.1002/cm.970300407

136. He H, Dang Y, Dai F, Guo Z, Wu J, She X, et al. Post-translational Modifications of Three Members of the Human MAP1LC3 Family and Detection of a Novel Type of Modification for MAP1LC3B. J Biol Chem. 2003;278: 29278–29287. doi:10.1074/jbc.M303800200

137. Schaaf MBE, Keulers TG, Vooijs MA, Rouschop KMA. LC3/GABARAP family proteins: autophagy-(un)related functions. FASEB J. 2016; fj.201600698R. doi:10.1096/fj.201600698R

138. Weidberg H, Shvets E, Shpilka T, Shimron F, Shinder V, Elazar Z. LC3 and GATE-16/GABARAP subfamilies are both essential yet act differently in autophagosome biogenesis. EMBO J. 2010;29: 1792–1802. doi:10.1038/emboj.2010.74

139. Shvets E, Abada A, Weidberg H, Elazar Z. Dissecting the involvement of LC3B and GATE-16 in p62 recruitment into autophagosomes. Autophagy. 2011;7: 683–688.

140. Pankiv S, Clausen TH, Lamark T, Brech A, Bruun J-A, Outzen H, et al. p62/SQSTM1 binds directly to Atg8/LC3 to facilitate degradation of ubiquitinated protein aggregates by autophagy. J Biol Chem. 2007;282: 24131–24145. doi:10.1074/jbc.M702824200

141. Kirkin V, Lamark T, Sou Y-S, Bjørkøy G, Nunn JL, Bruun J-A, et al. A role for NBR1 in autophagosomal degradation of ubiquitinated substrates. Mol Cell. 2009;33: 505–516. doi:10.1016/j.molcel.2009.01.020

142. Novak I, Kirkin V, McEwan DG, Zhang J, Wild P, Rozenknop A, et al. Nix is a selective autophagy receptor for mitochondrial clearance. EMBO Rep. 2010;11: 45–51. doi:10.1038/embor.2009.256

143. Schwarten M, Mohrlüder J, Ma P, Stoldt M, Thielmann Y, Stangler T, et al. Nix directly binds to GABARAP: a possible crosstalk between apoptosis and autophagy. Autophagy. 2009;5: 690–698.

144. Zhu Y, Massen S, Terenzio M, Lang V, Chen-Lindner S, Eils R, et al. Modulation of Serines 17 and 24 in the LC3-interacting Region of Bnip3 Determines Pro-survival

Mitophagy versus Apoptosis. J Biol Chem. 2013;288: 1099–1113. doi:10.1074/jbc.M112.399345

145. Clausen TH, Lamark T, Isakson P, Finley K, Larsen KB, Brech A, et al. p62/SQSTM1 and ALFY interact to facilitate the formation of p62 bodies/ALIS and their degradation by autophagy. Autophagy. 2010;6: 330–344.

146. Filimonenko M, Isakson P, Finley KD, Anderson M, Jeong H, Melia TJ, et al. The selective macroautophagic degradation of aggregated proteins requires the PI3P-binding protein Alfy. Mol Cell. 2010;38: 265–279. doi:10.1016/j.molcel.2010.04.007

147. Brennand A, Gualdrón-López M, Coppens I, Rigden DJ, Ginger ML, Michels PAM. Autophagy in parasitic protists: unique features and drug targets. Mol Biochem Parasitol. 2011;177: 83–99. doi:10.1016/j.molbiopara.2011.02.003

148. de Souza W, Sant'Anna C, Cunha-e-Silva NL. Electron microscopy and cytochemistry analysis of the endocytic pathway of pathogenic protozoa. Prog Histochem Cytochem. 2009;44: 67–124. doi:10.1016/j.proghi.2009.01.001

149. Alvarez VE, Kosec G, Sant'Anna C, Turk V, Cazzulo JJ, Turk B. Autophagy Is Involved in Nutritional Stress Response and Differentiation in Trypanosoma cruzi. J Biol Chem. 2008;283: 3454–3464. doi:10.1074/jbc.M708474200

150. Herman M, Pérez-Morga D, Schtickzelle N, Michels PAM. Turnover of glycosomes during life-cycle differentiation of Trypanosoma brucei. Autophagy. 2008;4: 294–308.

151. Besteiro S, Williams RAM, Morrison LS, Coombs GH, Mottram JC. Endosome sorting and autophagy are essential for differentiation and virulence of Leishmania major. J Biol Chem. 2006;281: 11384–11396. doi:10.1074/jbc.M512307200

152. Kitamura K, Kishi-Itakura C, Tsuboi T, Sato S, Kita K, Ohta N, et al. Autophagy-related Atg8 localizes to the apicoplast of the human malaria parasite Plasmodium falciparum. PloS One. 2012;7: e42977. doi:10.1371/journal.pone.0042977

153. Sheiner L, Vaidya AB, McFadden GI. The metabolic roles of the endosymbiotic organelles of Toxoplasma and Plasmodium spp. Curr Opin Microbiol. 2013;16: 452–458. doi:10.1016/j.mib.2013.07.003

154. Lavine MD, Arrizabalaga G. Analysis of Monensin Sensitivity in Toxoplasma gondii Reveals Autophagy as a Mechanism for Drug Induced Death. PLOS ONE. 2012;7: e42107. doi:10.1371/journal.pone.0042107

155. Gaviria D, Paguio MF, Turnbull LB, Tan A, Siriwardana A, Ghosh D, et al. A Process Similar to Autophagy Is Associated with Cytocidal Chloroquine Resistance in Plasmodium falciparum. PLOS ONE. 2013;8: e79059. doi:10.1371/journal.pone.0079059

156. He C, Klionsky DJ. Regulation Mechanisms and Signaling Pathways of Autophagy. Annu Rev Genet. 2009;43: 67–93. doi:10.1146/annurev-genet-102808-114910

157. Bánréti A, Sass M, Graba Y. The emerging role of acetylation in the regulation of autophagy. Autophagy. 2013;9: 819–829. doi:10.4161/auto.23908

158. Li Y-T, Yi C, Chen C-C, Lan H, Pan M, Zhang S-J, et al. A semisynthetic Atg3 reveals that acetylation promotes Atg3 membrane binding and Atg8 lipidation. Nat Commun. 2017;8: 14846. doi:10.1038/ncomms14846

159. Yi C, Ma M, Ran L, Zheng J, Tong J, Zhu J, et al. Function and molecular mechanism of acetylation in autophagy regulation. Science. 2012;336: 474–477. doi:10.1126/science.1216990

160. Huang R, Xu Y, Wan W, Shou X, Qian J, You Z, et al. Deacetylation of Nuclear LC3 Drives Autophagy Initiation under Starvation. Mol Cell. 2015;57: 456–466. doi:10.1016/j.molcel.2014.12.013

161. Jeffers V, Sullivan WJ. Lysine Acetylation Is Widespread on Proteins of Diverse Function and Localization in the Protozoan Parasite Toxoplasma gondii. Eukaryot Cell. 2012;11: 735–742. doi:10.1128/EC.00088-12

162. Hain AUP, Bartee D, Sanders NG, Miller AS, Sullivan DJ, Levitskaya J, et al. Identification of an Atg8-Atg3 Protein–Protein Interaction Inhibitor from the Medicines for Malaria Venture Malaria Box Active in Blood and Liver Stage Plasmodium falciparum Parasites. J Med Chem. 2014;57: 4521–4531. doi:10.1021/jm401675a

163. Hain AUP, Miller AS, Levitskaya J, Bosch J. Virtual Screening and Experimental Validation Identify Novel Inhibitors of the Plasmodium falciparum Atg8-Atg3 Protein-Protein Interaction. ChemMedChem. 2016;11: 900–910. doi:10.1002/cmdc.201500515

164. Miller AS, Bosch J. Targeting the Atg8 Conjugation Pathway for Novel Anti-Apicomplexan Drug Discovery. Comprehensive Analysis of Parasite Biology: From Metabolism to Drug Discovery. Wiley-VCH Verlag GmbH & Co. KGaA; 2016. pp. 213–229. doi:10.1002/9783527694082.ch9

165. Donald RG, Roos DS. Gene knock-outs and allelic replacements in Toxoplasma gondii: HXGPRT as a selectable marker for hit-and-run mutagenesis. Mol Biochem Parasitol. 1998;91: 295–305.

166. Huynh M-H, Carruthers VB. Tagging of Endogenous Genes in a Toxoplasma gondii Strain Lacking Ku80. Eukaryot Cell. 2009;8: 530–539. doi:10.1128/EC.00358-08

167. Suvorova ES, Radke JB, Ting L-M, Vinayak S, Alvarez CA, Kratzer S, et al. A nucleolar AAA-NTPase is required for parasite division. Mol Microbiol. 2013;90: 338–355. doi:10.1111/mmi.12367

168. Sambrook J, Russell DW. Purification of Nucleic Acids by Extraction with Phenol:Chloroform. Cold Spring Harb Protoc. 2006;2006: pdb.prot4455. doi:10.1101/pdb.prot4455

169. Sambrook J, Russell DW. Standard Ethanol Precipitation of DNA in Microcentrifuge Tubes. Cold Spring Harb Protoc. 2006;2006: pdb.prot4456. doi:10.1101/pdb.prot4456

170. Donald RG, Carter D, Ullman B, Roos DS. Insertional tagging, cloning, and expression of the Toxoplasma gondii hypoxanthine-xanthine-guanine phosphoribosyltransferase gene. Use as a selectable marker for stable transformation. J Biol Chem. 1996;271: 14010–14019.

171. Donald RG, Roos DS. Stable molecular transformation of Toxoplasma gondii: a selectable dihydrofolate reductase-thymidylate synthase marker based on drug-resistance mutations in malaria. Proc Natl Acad Sci U S A. 1993;90: 11703–11707.

172. Guzmán C, Bagga M, Kaur A, Westermarck J, Abankwa D. ColonyArea: an ImageJ plugin to automatically quantify colony formation in clonogenic assays. PloS One. 2014;9: e92444. doi:10.1371/journal.pone.0092444

173. Lourido S, Tang K, Sibley LD. Distinct signalling pathways control Toxoplasma egress and host-cell invasion. EMBO J. 2012;31: 4524–4534. doi:10.1038/emboj.2012.299

174. Gajria B, Bahl A, Brestelli J, Dommer J, Fischer S, Gao X, et al. ToxoDB: an integrated Toxoplasma gondii database resource. Nucleic Acids Res. 2008;36: D553–D556. doi:10.1093/nar/gkm981

175. NCBI Resource Coordinators. Database Resources of the National Center for Biotechnology Information. Nucleic Acids Res. 2017;45: D12–D17. doi:10.1093/nar/gkw1071

176. Johnson M, Zaretskaya I, Raytselis Y, Merezhuk Y, McGinnis S, Madden TL. NCBI BLAST: a better web interface. Nucleic Acids Res. 2008;36: W5-9. doi:10.1093/nar/gkn201

177. Altschul SF, Gish W, Miller W, Myers EW, Lipman DJ. Basic local alignment search tool. J Mol Biol. 1990;215: 403–410. doi:10.1016/S0022-2836(05)80360-2

178. Aurrecoechea C, Barreto A, Basenko EY, Brestelli J, Brunk BP, Cade S, et al. EuPathDB: the eukaryotic pathogen genomics database resource. Nucleic Acids Res. 2017;45: D581–D591. doi:10.1093/nar/gkw1105

179. Sievers F, Wilm A, Dineen D, Gibson TJ, Karplus K, Li W, et al. Fast, scalable generation of high-quality protein multiple sequence alignments using Clustal Omega. Mol Syst Biol. 2011;7: 539. doi:10.1038/msb.2011.75

180. Guindon S, Lethiec F, Duroux P, Gascuel O. PHYML Online—a web server for fast maximum likelihood-based phylogenetic inference. Nucleic Acids Res. 2005;33: W557–W559. doi:10.1093/nar/gki352

181. Roy A, Kucukural A, Zhang Y. I-TASSER: a unified platform for automated protein structure and function prediction. Nat Protoc. 2010;5: 725–738. doi:10.1038/nprot.2010.5

182. Grosdidier A, Zoete V, Michielin O. SwissDock, a protein-small molecule docking web service based on EADock DSS. Nucleic Acids Res. 2011;39: W270-277. doi:10.1093/nar/gkr366

183. Meng EC, Pettersen EF, Couch GS, Huang CC, Ferrin TE. Tools for integrated sequence-structure analysis with UCSF Chimera. BMC Bioinformatics. 2006;7: 339. doi:10.1186/1471-2105-7-339

184. Pettersen EF, Goddard TD, Huang CC, Couch GS, Greenblatt DM, Meng EC, et al. UCSF Chimera--a visualization system for exploratory research and analysis. J Comput Chem. 2004;25: 1605–1612. doi:10.1002/jcc.20084

185. Guex N, Peitsch MC. SWISS-MODEL and the Swiss-PdbViewer: an environment for comparative protein modeling. Electrophoresis. 1997;18: 2714–2723. doi:10.1002/elps.1150181505

186. Livak KJ, Schmittgen TD. Analysis of relative gene expression data using real-time quantitative PCR and the 2(-Delta Delta C(T)) Method. Methods San Diego Calif. 2001;25: 402–408. doi:10.1006/meth.2001.1262

187. Untergasser A, Cutcutache I, Koressaar T, Ye J, Faircloth BC, Remm M, et al. Primer3--new capabilities and interfaces. Nucleic Acids Res. 2012;40: e115–e115. doi:10.1093/nar/gks596

188. Schneider CA, Rasband WS, Eliceiri KW. NIH Image to ImageJ: 25 years of image analysis. Nat Methods. 2012;9: 671–675.

189. lukemiller.org» Blog Archive » Analyzing gels and western blots with ImageJ [Internet]. [cited 10 Apr 2017]. Available: http://lukemiller.org/index.php/2010/11/analyzing-gels-and-western-blots-with-image-j/

190. McFadden DC, Seeber F, Boothroyd JC. Use of Toxoplasma gondii expressing beta-galactosidase for colorimetric assessment of drug activity in vitro. Antimicrob Agents Chemother. 1997;41: 1849–1853.

191. Nettleship JE, Brown J, Groves MR, Geerlof A. Methods for protein characterization by mass spectrometry, thermal shift (ThermoFluor) assay, and multiangle or static light scattering. Methods Mol Biol Clifton NJ. 2008;426: 299–318. doi:10.1007/978-1-60327-058-8_19

192. Teo G, Liu G, Zhang J, Nesvizhskii AI, Gingras A-C, Choi H. SAINTexpress: improvements and additional features in Significance Analysis of Interactome software. J Proteomics. 2014;100: 37–43. doi:10.1016/j.jprot.2013.10.023

193. Choi H, Larsen B, Lin Z-Y, Breitkreutz A, Mellacheruvu D, Fermin D, et al. SAINT: Probabilistic Scoring of Affinity Purification - Mass Spectrometry Data. Nat Methods. 2011;8: 70–73. doi:10.1038/nmeth.1541

194. Mertins P, Qiao JW, Patel J, Udeshi ND, Clauser KR, Mani DR, et al. Integrated proteomic analysis of post-translational modifications by serial enrichment. Nat Methods. 2013;10: 634–637. doi:10.1038/nmeth.2518

195. Choudhary C, Kumar C, Gnad F, Nielsen ML, Rehman M, Walther TC, et al. Lysine acetylation targets protein complexes and co-regulates major cellular functions. Science. 2009;325: 834–840. doi:10.1126/science.1175371

196. Drazic A, Myklebust LM, Ree R, Arnesen T. The world of protein acetylation. Biochim Biophys Acta BBA - Proteins Proteomics. 2016;1864: 1372–1401. doi:10.1016/j.bbapap.2016.06.007

197. Caron C, Boyault C, Khochbin S. Regulatory cross-talk between lysine acetylation and ubiquitination: role in the control of protein stability. BioEssays. 2005;27: 408–415. doi:10.1002/bies.20210

198. Noda NN, Ohsumi Y, Inagaki F. Atg8-family interacting motif crucial for selective autophagy. FEBS Lett. 2010;584: 1379–1385. doi:10.1016/j.febslet.2010.01.018

199. Birgisdottir ÅB, Lamark T, Johansen T. The LIR motif – crucial for selective autophagy. J Cell Sci. 2013;126: 3237–3247. doi:10.1242/jcs.126128

200. Varberg JM, Padgett LR, Arrizabalaga G, Sullivan WJ. TgATAT-Mediated α-Tubulin Acetylation Is Required for Division of the Protozoan Parasite Toxoplasma gondii. mSphere. 2016;1: e00088-15. doi:10.1128/mSphere.00088-15

201. Li M, Luo J, Brooks CL, Gu W. Acetylation of p53 inhibits its ubiquitination by Mdm2. J Biol Chem. 2002;277: 50607–50611. doi:10.1074/jbc.C200578200

202. Wang X, Hayes JJ. Acetylation Mimics within Individual Core Histone Tail Domains Indicate Distinct Roles in Regulating the Stability of Higher-Order Chromatin Structure. Mol Cell Biol. 2008;28: 227–236. doi:10.1128/MCB.01245-07

203. He M, Zhang L, Wang X, Huo L, Sun L, Feng C, et al. Systematic Analysis of the Functions of Lysine Acetylation in the Regulation of Tat Activity. PLOS ONE. 2013;8: e67186. doi:10.1371/journal.pone.0067186

204. Klionsky DJ, Abdelmohsen K, Abe A, Abedin MJ, Abeliovich H, Acevedo Arozena A, et al. Guidelines for the use and interpretation of assays for monitoring autophagy (3rd edition). Autophagy. 2016;12: 1–222. doi:10.1080/15548627.2015.1100356

205. Zhang YW, Halonen SK, Ma YF, Wittner M, Weiss LM. Initial Characterization of CST1, a Toxoplasma gondii Cyst Wall Glycoprotein. Infect Immun. 2001;69: 501–507. doi:10.1128/IAI.69.1.501-507.2001

206. Bohne W, Gross U, Ferguson DJ, Heesemann J. Cloning and characterization of a bradyzoite-specifically expressed gene (hsp30/bag1) of Toxoplasma gondii, related to genes encoding small heat-shock proteins of plants. Mol Microbiol. 1995;16: 1221–1230.

207. Sullivan WJ, Jeffers V. Mechanisms of Toxoplasma gondii persistence and latency. FEMS Microbiol Rev. 2012;36: 717–733. doi:10.1111/j.1574-6976.2011.00305.x

208. Soête M, Camus D, Dubremetz JF. Experimental induction of bradyzoite-specific antigen expression and cyst formation by the RH strain of Toxoplasma gondii in vitro. Exp Parasitol. 1994;78: 361–370.

209. Lo M-C, Aulabaugh A, Jin G, Cowling R, Bard J, Malamas M, et al. Evaluation of fluorescence-based thermal shift assays for hit identification in drug discovery. Anal Biochem. 2004;332: 153–159. doi:10.1016/j.ab.2004.04.031

210. Huynh K, Partch CL. Current Protocols in Protein Science. Curr Protoc Protein Sci Editor Board John E Coligan Al. 2015;79: 28.9.1-28.9.14. doi:10.1002/0471140864.ps2809s79

211. Layton CJ, Hellinga HW. Quantitation of protein–protein interactions by thermal stability shift analysis. Protein Sci Publ Protein Soc. 2011;20: 1439–1450. doi:10.1002/pro.674

212. Bultema JB, Kuipers BJH, Dijkhuizen L. Biochemical characterization of mutants in the active site residues of the β-galactosidase enzyme of Bacillus circulans ATCC 31382. FEBS Open Bio. 2014;4: 1015–1020. doi:10.1016/j.fob.2014.11.002

213. Sidik SM, Huet D, Ganesan SM, Huynh M-H, Wang T, Nasamu AS, et al. A Genome-wide CRISPR Screen in Toxoplasma Identifies Essential Apicomplexan Genes. Cell. 2016;166: 1423–1435.e12. doi:10.1016/j.cell.2016.08.019

214. Oppenheim RD, Creek DJ, Macrae JI, Modrzynska KK, Pino P, Limenitakis J, et al. BCKDH: The Missing Link in Apicomplexan Mitochondrial Metabolism Is Required for Full Virulence of Toxoplasma gondii and Plasmodium berghei. PLOS Pathog. 2014;10: e1004263. doi:10.1371/journal.ppat.1004263

215. Liu J-Y, Timm DE, Hurley TD. Pyrithiamine as a Substrate for Thiamine Pyrophosphokinase. J Biol Chem. 2006;281: 6601–6607. doi:10.1074/jbc.M510951200

216. Patel MS, Nemeria NS, Furey W, Jordan F. The pyruvate dehydrogenase complexes: structure-based function and regulation. J Biol Chem. 2014;289: 16615–16623. doi:10.1074/jbc.R114.563148

217. Söding J, Biegert A, Lupas AN. The HHpred interactive server for protein homology detection and structure prediction. Nucleic Acids Res. 2005;33: W244–W248. doi:10.1093/nar/gki408

218. Collins BM, Watson PJ, Owen DJ. The structure of the GGA1-GAT domain reveals the molecular basis for ARF binding and membrane association of GGAs. Dev Cell. 2003;4: 321–332.

219. Mbom BC, Nelson WJ, Barth A. β-catenin: A multi-functional protein's role at the centrosome and implications for a broader role in cell division. BioEssays News Rev Mol Cell Dev Biol. 2013;35: 804–809. doi:10.1002/bies.201300045

220. Haraguchi K, Hayashi T, Jimbo T, Yamamoto T, Akiyama T. Role of the kinesin-2 family protein, KIF3, during mitosis. J Biol Chem. 2006;281: 4094–4099. doi:10.1074/jbc.M507028200

221. Nishikawa T, Ota T, Isogai T. Prediction whether a human cDNA sequence contains initiation codon by combining statistical information and similarity with protein sequences. Bioinforma Oxf Engl. 2000;16: 960–967.

222. Goud Gadila SK, Williams M, Saimani U, Delgado Cruz M, Makaraci P, Woodman S, et al. Yeast dynamin Vps1 associates with clathrin to facilitate vesicular trafficking and controls Golgi homeostasis. Eur J Cell Biol. 2017;96: 182–197. doi:10.1016/j.ejcb.2017.02.004

223. van Dooren GG, Reiff SB, Tomova C, Meissner M, Humbel BM, Striepen B. An novel dynamin-related protein has been recruited for apicoplast fission in Toxoplasma gondii. Curr Biol CB. 2009;19: 267–276. doi:10.1016/j.cub.2008.12.048

224. Breinich MS, Ferguson DJP, Foth BJ, van Dooren GG, Lebrun M, Quon DV, et al. An alveolate specific dynamin is required for the biogenesis of specialised secretory organelles in Toxoplasma gondii. Curr Biol CB. 2009;19: 277–286. doi:10.1016/j.cub.2009.01.039

225. Hinshaw JE. Dynamin and its Role in Membrane Fission [Internet]. National Center for Biotechnology Information (US); 2002. Available: https://www.ncbi.nlm.nih.gov/books/NBK2233/

226. Arimura S, Tsutsumi N. A dynamin-like protein (ADL2b), rather than FtsZ, is involved in Arabidopsis mitochondrial division. Proc Natl Acad Sci U S A. 2002;99: 5727–5731. doi:10.1073/pnas.082663299

227. Smirnova E, Griparic L, Shurland DL, van der Bliek AM. Dynamin-related protein Drp1 is required for mitochondrial division in mammalian cells. Mol Biol Cell. 2001;12: 2245–2256.

228. Morgan GW, Goulding D, Field MC. The Single Dynamin-like Protein of Trypanosoma brucei Regulates Mitochondrial Division and Is Not Required for Endocytosis. J Biol Chem. 2004;279: 10692–10701. doi:10.1074/jbc.M312178200

229. Gubbels M-J, Wieffer M, Striepen B. Fluorescent protein tagging in Toxoplasma gondii: identification of a novel inner membrane complex component conserved among Apicomplexa. Mol Biochem Parasitol. 2004;137: 99–110. doi:10.1016/j.molbiopara.2004.05.007

230. Gubbels M-J, Vaishnava S, Boot N, Dubremetz J-F, Striepen B. A MORN-repeat protein is a dynamic component of the Toxoplasma gondii cell division apparatus. J Cell Sci. 2006;119: 2236–2245. doi:10.1242/jcs.02949

231. Lorestani A, Sheiner L, Yang K, Robertson SD, Sahoo N, Brooks CF, et al. A Toxoplasma MORN1 null mutant undergoes repeated divisions but is defective in basal assembly, apicoplast division and cytokinesis. PloS One. 2010;5: e12302. doi:10.1371/journal.pone.0012302

232. Pieperhoff MS, Pall GS, Jiménez-Ruiz E, Das S, Melatti C, Gow M, et al. Conditional U1 Gene Silencing in Toxoplasma gondii. PLOS ONE. 2015;10: e0130356. doi:10.1371/journal.pone.0130356

233. Banaszynski LA, Chen L-C, Maynard-Smith LA, Ooi AGL, Wandless TJ. A rapid, reversible, and tunable method to regulate protein function in living cells using synthetic small molecules. Cell. 2006;126: 995–1004. doi:10.1016/j.cell.2006.07.025

234. Herm-Götz A, Agop-Nersesian C, Münter S, Grimley JS, Wandless TJ, Frischknecht F, et al. Rapid control of protein level in the apicomplexan Toxoplasma gondii. Nat Methods. 2007;4: 1003–1005. doi:10.1038/nmeth1134

235. Coppens I, Andries M, Liu JL, Cesbron-Delauw MF. Intracellular trafficking of dense granule proteins in Toxoplasma gondii and experimental evidences for a regulated exocytosis. Eur J Cell Biol. 1999;78: 463–472. doi:10.1016/S0171-9335(99)80073-9

236. Sloves P-J, Delhaye S, Mouveaux T, Werkmeister E, Slomianny C, Hovasse A, et al. Toxoplasma Sortilin-like Receptor Regulates Protein Transport and Is Essential for Apical Secretory Organelle Biogenesis and Host Infection. Cell Host Microbe. 2012;11: 515–527. doi:10.1016/j.chom.2012.03.006

237. Boyom FF, Fokou PVT, Tchokouaha LRY, Spangenberg T, Mfopa AN, Kouipou RMT, et al. Repurposing the Open Access Malaria Box To Discover Potent Inhibitors of Toxoplasma gondii and Entamoeba histolytica. Antimicrob Agents Chemother. 2014;58: 5848–5854. doi:10.1128/AAC.02541-14

238. Van Voorhis WC, Adams JH, Adelfio R, Ahyong V, Akabas MH, Alano P, et al. Open Source Drug Discovery with the Malaria Box Compound Collection for Neglected Diseases and Beyond. PLoS Pathog. 2016;12: e1005763. doi:10.1371/journal.ppat.1005763

239. Duffy S, Avery VM. Identification of inhibitors of Plasmodium falciparum gametocyte development. Malar J. 2013;12: 408. doi:10.1186/1475-2875-12-408

240. Lucantoni L, Fidock DA, Avery VM. Luciferase-Based, High-Throughput Assay for Screening and Profiling Transmission-Blocking Compounds against Plasmodium falciparum Gametocytes. Antimicrob Agents Chemother. 2016;60: 2097–2107. doi:10.1128/AAC.01949-15

241. Kaiser M, Maes L, Tadoori LP, Spangenberg T, Ioset J-R. Repurposing of the Open Access Malaria Box for Kinetoplastid Diseases Identifies Novel Active Scaffolds against Trypanosomatids. J Biomol Screen. 2015;20: 634–645. doi:10.1177/1087057115569155

242. Mizushima N, Yoshimorim T, Levine B. Methods in Mammalian Autophagy Research. Cell. 2010;140: 313–326. doi:10.1016/j.cell.2010.01.028

243. Morrissette NS, Sibley LD. Disruption of microtubules uncouples budding and nuclear division in Toxoplasma gondii. J Cell Sci. 2002;115: 1017–1025.

244. Gubbels M-J, Wieffer M, Striepen B. Fluorescent protein tagging in Toxoplasma gondii: identification of a novel inner membrane complex component conserved among Apicomplexa. Mol Biochem Parasitol. 2004;137: 99–110. doi:10.1016/j.molbiopara.2004.05.007

245. Garrison E, Treeck M, Ehret E, Butz H, Garbuz T, Oswald BP, et al. A Forward Genetic Screen Reveals that Calcium-dependent Protein Kinase 3 Regulates Egress in Toxoplasma. PLOS Pathog. 2012;8: e1003049. doi:10.1371/journal.ppat.1003049

246. Treeck M, Sanders JL, Gaji RY, LaFavers KA, Child MA, Arrizabalaga G, et al. The Calcium-Dependent Protein Kinase 3 of Toxoplasma Influences Basal Calcium Levels and Functions beyond Egress as Revealed by Quantitative Phosphoproteome Analysis. PLOS Pathog. 2014;10: e1004197. doi:10.1371/journal.ppat.1004197

247. Carruthers VB, Sibley LD. Mobilization of intracellular calcium stimulates microneme discharge in Toxoplasma gondii. Mol Microbiol. 1999;31: 421–428.

248. Black MW, Arrizabalaga G, Boothroyd JC. Ionophore-Resistant Mutants of Toxoplasma gondii Reveal Host Cell Permeabilization as an Early Event in Egress. Mol Cell Biol. 2000;20: 9399–9408. doi:10.1128/MCB.20.24.9399-9408.2000

249. Li K, Wang R, Lozada E, Fan W, Orren DK, Luo J. Acetylation of WRN Protein Regulates Its Stability by Inhibiting Ubiquitination. PLOS ONE. 2010;5: e10341. doi:10.1371/journal.pone.0010341

250. Silmon de Monerri NC, Yakubu RR, Chen AL, Bradley PJ, Nieves E, Weiss LM, et al. The Ubiquitin Proteome of Toxoplasma gondii Reveals Roles for Protein Ubiquitination in Cell-Cycle Transitions. Cell Host Microbe. 2015;18: 621–633. doi:10.1016/j.chom.2015.10.014

251. Wagner SA, Beli P, Weinert BT, Schölz C, Kelstrup CD, Young C, et al. Proteomic analyses reveal divergent ubiquitylation site patterns in murine tissues. Mol Cell Proteomics MCP. 2012;11: 1578–1585. doi:10.1074/mcp.M112.017905

252. Wagner SA, Beli P, Weinert BT, Nielsen ML, Cox J, Mann M, et al. A proteome-wide, quantitative survey of in vivo ubiquitylation sites reveals widespread

regulatory roles. Mol Cell Proteomics MCP. 2011;10: M111.013284. doi:10.1074/mcp.M111.013284

253. Dzierszinski F, Nishi M, Ouko L, Roos DS. Dynamics of Toxoplasma gondii Differentiation. Eukaryot Cell. 2004;3: 992–1003. doi:10.1128/EC.3.4.992-1003.2004

254. Radke JR, Guerini MN, Jerome M, White MW. A change in the premitotic period of the cell cycle is associated with bradyzoite differentiation in Toxoplasma gondii. Mol Biochem Parasitol. 2003;131: 119–127.

255. Jerome ME, Radke JR, Bohne W, Roos DS, White MW. Toxoplasma Gondii Bradyzoites Form Spontaneously during Sporozoite-Initiated Development. Infect Immun. 1998;66: 4838–4844.

256. Suer S, Misra S, Saidi LF, Hurley JH. Structure of the GAT domain of human GGA1: A syntaxin amino-terminal domain fold in an endosomal trafficking adaptor. Proc Natl Acad Sci. 2003;100: 4451–4456. doi:10.1073/pnas.0831133100

257. Doodhi H, Ghosal D, Krishnamurthy M, Jana SC, Shamala D, Bhaduri A, et al. KAP, the accessory subunit of kinesin-2, binds the predicted coiled-coil stalk of the motor subunits. Biochemistry (Mosc). 2009;48: 2248–2260. doi:10.1021/bi8018338

258. Ngô HM, Yang M, Paprotka K, Pypaert M, Hoppe H, Joiner KA. AP-1 in Toxoplasma gondii mediates biogenesis of the rhoptry secretory organelle from a post-Golgi compartment. J Biol Chem. 2003;278: 5343–5352. doi:10.1074/jbc.M208291200

259. Sheiner L, Soldati-Favre D. Protein Trafficking inside Toxoplasma gondii. Traffic. 2008;9: 636–646. doi:10.1111/j.1600-0854.2008.00713.x

260. Jin SM, Youle RJ. The accumulation of misfolded proteins in the mitochondrial matrix is sensed by PINK1 to induce PARK2/Parkin-mediated mitophagy of polarized mitochondria. Autophagy. 2013;9: 1750–1757. doi:10.4161/auto.26122

261. Ævarsson A, Chuang JL, Max Wynn R, Turley S, Chuang DT, Hol WG. Crystal structure of human branched-chain α-ketoacid dehydrogenase and the molecular basis of multienzyme complex deficiency in maple syrup urine disease. Structure. 2000;8: 277–291. doi:10.1016/S0969-2126(00)00105-2

262. Bason JV, Montgomery MG, Leslie AGW, Walker JE. How release of phosphate from mammalian F1-ATPase generates a rotary substep. Proc Natl Acad Sci. 2015;112: 6009–6014. doi:10.1073/pnas.1506465112

263. Maeyashiki C, Oshima S, Otsubo K, Kobayashi M, Nibe Y, Matsuzawa Y, et al. HADHA, the alpha subunit of the mitochondrial trifunctional protein, is involved in long-chain fatty acid-induced autophagy in intestinal epithelial cells. Biochem Biophys Res Commun. 2017;484: 636–641. doi:10.1016/j.bbrc.2017.01.159

264. Behrends C, Sowa ME, Gygi SP, Harper JW. Network organization of the human autophagy system. Nature. 2010;466: 68–76. doi:10.1038/nature09204

265. Rector RS, Payne RM, Ibdah JA. Mitochondrial Trifunctional Protein Defects: Clinical Implications and Therapeutic Approaches. Adv Drug Deliv Rev. 2008;60: 1488–1496. doi:10.1016/j.addr.2008.04.014

266. Bessoff K, Spangenberg T, Foderaro JE, Jumani RS, Ward GE, Huston CD. Identification of Cryptosporidium parvum Active Chemical Series by Repurposing the Open Access Malaria Box. Antimicrob Agents Chemother. 2014;58: 2731–2739. doi:10.1128/AAC.02641-13

267. Kroemer G, Levine B. Autophagic cell death: the story of a misnomer. Nat Rev Mol Cell Biol. 2008;9: 1004–1010. doi:10.1038/nrm2527

268. Brown KM, Lourido S, Sibley LD. Serum Albumin Stimulates Protein Kinase G-dependent Microneme Secretion in Toxoplasma gondii. J Biol Chem. 2016;291: 9554–9565. doi:10.1074/jbc.M115.700518

269. Sidik SM, Triana MAH, Paul AS, Bakkouri ME, Hackett CG, Tran F, et al. Using a Genetically Encoded Sensor to Identify Inhibitors of Toxoplasma gondii Ca2+ Signalling. J Biol Chem. 2016; jbc.M115.703546. doi:10.1074/jbc.M115.703546

270. Jeffers V, Kamau ET, Srinivasan AR, Harper J, Sankaran P, Post SE, et al. TgPRELID, a Mitochondrial Protein Linked to Multidrug Resistance in the Parasite Toxoplasma gondii. mSphere. 2017;2: e00229-16. doi:10.1128/mSphere.00229-16

271. Donald RGK, Allocco J, Singh SB, Nare B, Salowe SP, Wiltsie J, et al. Toxoplasma gondii Cyclic GMP-Dependent Kinase: Chemotherapeutic Targeting of an Essential Parasite Protein Kinase. Eukaryot Cell. 2002;1: 317–328. doi:10.1128/EC.1.3.317-328.2002

272. Cristina MD, Dou Z, Lunghi M, Kannan G, Huynh M-H, McGovern OL, et al. Toxoplasma depends on lysosomal consumption of autophagosomes for persistent infection. Nat Microbiol. 2017;2: nmicrobiol201796. doi:10.1038/nmicrobiol.2017.96

273. Dou Z, McGovern OL, Cristina MD, Carruthers VB. Toxoplasma gondii Ingests and Digests Host Cytosolic Proteins. mBio. 2014;5: e01188-14. doi:10.1128/mBio.01188-14

Curriculum Vitae

Joseph M. Varberg

Education

Indiana University — Indianapolis, IN
PhD, Pharmacology — October 2017

Rockhurst University — Kansas City, MO
BS, Chemistry, *magna cum laude* — August 2011

Research Experience

PhD Student — August 2012 – October 2017
Indiana University School of Medicine
Mentors: Gustavo Arrizabalaga, PhD, and William J. Sullivan, Jr., PhD
Thesis: Biochemical and pharmacological characterization of the Atg8 conjugation system in *Toxoplasma gondii*.

Research Technician — April 2011-July 2012
Stowers Institute for Medical Research, Kansas City, MO
Mentor: Ali Shilatifard, PhD
Project: Assisted in the characterization of the Little Elongation Complex (LEC) and its role in transcriptional regulation of snRNA genes.

NSF Research Experience for Undergraduates — Summer 2010
Department of Chemistry, University of Kansas, Lawrence, KS
Mentor: Christopher G. Elles, PhD
Project: Used ultrafast laser spectroscopy to probe the excited state dynamics of a diarylethene-type molecular photochromic switch

Undergraduate Research — 2009-2011
Rockhurst University, Kansas City, MO
Mentor: Petia Bobadova-Parvanova, PhD
Project: Performed first-principle calculations to assist in the design of novel carborane-containing conducting polymers for application in next generation photovoltaic devices

Funding

PhRMA Foundation Pre-Doctoral Fellowship (Pharmacology) — 2015-2016
Pharmaceutical Research and Manufacturers of America
Title: “Regulators of parasite autophagy as novel drug targets for infectious disease”

Honors and Awards

Paradise Travel Award — January 2015
Indiana University School of Medicine

University Fellowship — 2012-2014
Indiana University School of Medicine

Rockhurst University Outstanding Research Seminar — May 2011
Rockhurst University

Award for Excellence in Chemistry — May 2011
American Institute of Chemists

REU Chemistry Leadership Group Travel Award — March 2011
National Science Foundation

Don E. Gibbs Memorial Research Scholarship — 2010-2011
Rockhurst University

Best Undergraduate Poster, Physical Chemistry — October 2010
American Chemical Society, Midwest Regional Meeting

Knipscher Chemistry Scholarship — 2010-2011
Rockhurst University

Peer Reviewed Publications

Varberg JM, Heredero Bermejo, I, Garbuz T, Charvat R, Jacobs K, Sullivan, Jr. WJ., Arrizabalaga G. Identification of *Toxoplasma gondii* Atg8 interacting proteins reveals role in membrane trafficking. *In preparation.*

Varberg JM, LaFavers KA, Arrizabalaga G, Sullivan, Jr. WJ. "Characterization of *Plasmodium* Atg3-Atg8 inhibitors identifies novel alternative mechanisms of action in *Toxoplasma*". *In submission.*

Jeffers V, Kamau E, Srinivasan A, Harper J, Sankaran P, Post S, **Varberg JM,** Sullivan, Jr. WJ, Boyle J. "TgPRELID, a novel mitochondrial protein linked to multi-drug resistance in the parasite *Toxoplasma gondii*. mSphere. 2017 Feb 1. **Featured on cover**

Saraf A, Cervantes S, Bunnik EM., Ponts N, Sardiu ME, Chung DD, Prudhomme J, Wen Z, **Varberg JM**, Washburn MP, Florens L, Le Roch KG. "Dynamic and combinatorial landscape of histone modifications during the intra-erythrocitic developmental cycle of the malaria parasite". J. Proteome Res. 2016 Aug 5.

Varberg JM*, Padgett LR*, Arrizabalaga G, Sullivan, Jr. WJ. "TgATAT-mediated α-tubulin acetylation is required for division of the protozoan parasite *Toxoplasma gondii"*. mSphere. 2016 Jan 20. **Featured on cover,** *co-first author

Hu D, Smith ER, Garruss AS, Mohaghegh N, **Varberg JM**, Lin C, Jackson J, Gao X, Saraf A, Florens L, Washburn MP, Eissenberg JC, Shilatifard A. "The Little Elongation Complex Functions at Initiation and Elongation Phases of snRNA Gene Transcription". Mol Cell. 2013 Aug 22.

Conference Presentations

Varberg JM, Arrizabalaga G, Sullivan WJ, Jr. "Mutation of lysine-23 on *Toxoplasma gondii* autophagy protein TgAtg8 impairs parasite replication". Midwest Neglected Infectious Diseases Meeting, Notre Dame, IN, August 2015, ***Poster***

Varberg JM, Arrizabalaga G, Sullivan WJ, Jr. "Mutation of lysine-23 on *Toxoplasma gondii* autophagy protein TgAtg8 impairs parasite replication". 13th International Congress on Toxoplasmosis and *T. gondii* Biology, Gettysburg, PA, June 2015, ***Poster***

Varberg JM, Arrizabalaga G, Sullivan WJ, Jr. "TgAtg8 acetylation: A role in regulating autophagy in *Toxoplasma gondii*?" Molecular Parasitology Meeting, Woods Hole, MA, September 2014, ***Poster***

Varberg JM, Arrizabalaga G, Sullivan WJ Jr. "Investigation of acetylation and autophagy in the protozoan parasite *Toxoplasma gondii*". ASBMB National Meeting, San Diego, CA, April 2014, ***Poster***

Varberg JM, Ward CL, Kern JL, Zheldakov IL, Elles CG. "Ultrafast dynamics of a photochromic molecular photoswitch: One- vs. two-photon excitation". 241st National meeting of the American Chemical Society, Anaheim, CA, March, 2011. ***Poster***

Varberg JM, Bobadova P, Vicente MGH. "Using first-principle calculations to design novel carboane-containing conducting polymers". 241st National meeting of the American Chemical Society, Anaheim, CA, March, 2011. ***Poster***

Varberg JM, Ward CL, Zheldakov IL, Elles CG. "Excited state dynamics of a diarylethene-type molecular photochromic switch". 45th Midwest regional meeting of the American Chemical Society, Wichita, KS, October, 2010. ***Poster***. *Chosen for Award

Varberg JM, Bobadova P, Vicente MGH. "Computational study of novel carborane-containing conjugated polypyroles". 45th Midwest regional meeting of the American Chemical Society, Wichita, KS, October, 2010. ***Talk***

Service

Grand Awards Judge, Senior Division — April 2017
Hoosier Science and Engineering Fair

IBMG Travel Grant Review Committee — Spring 2016
Indiana University School of Medicine

Student President, Department of Pharmacology and Toxicology — 2015-2016
Indiana University School of Medicine

Student Representative, IBMG Admissions Committee — 2015-2016
Indiana University School of Medicine

Student Mentoring and Teaching

Stephen Fakoyejo – Medical Student — Summer 2016
Indiana University School of Medicine

Austin Carroll – Undergraduate Student — Spring 2012
Stowers Institute for Medical Research

Supplemental Instructor — 2010-2011
General Chemistry I/II, Organic Chemistry I
Rockhurst University

Affiliations

American Chemical Society — 2010 – present
American Association for the Advancement of Science — 2011 – present
American Society for Biochemistry and Molecular Biology — 2014 - present